Doctoral Theses at NTNU 2004:145

Øyvind Sylta

Hydrocarbon migration modelling and exploration risk.

NTNU
Norwegian University of
Science and Technology
Doctoral thesis
for the degree of doctor philosophiae
Faculty of engineering science and technology
Department of geology and mineral resources
engineering

NTNU

Øyvind Sylta

Hydrocarbon migration modelling and exploration risk.

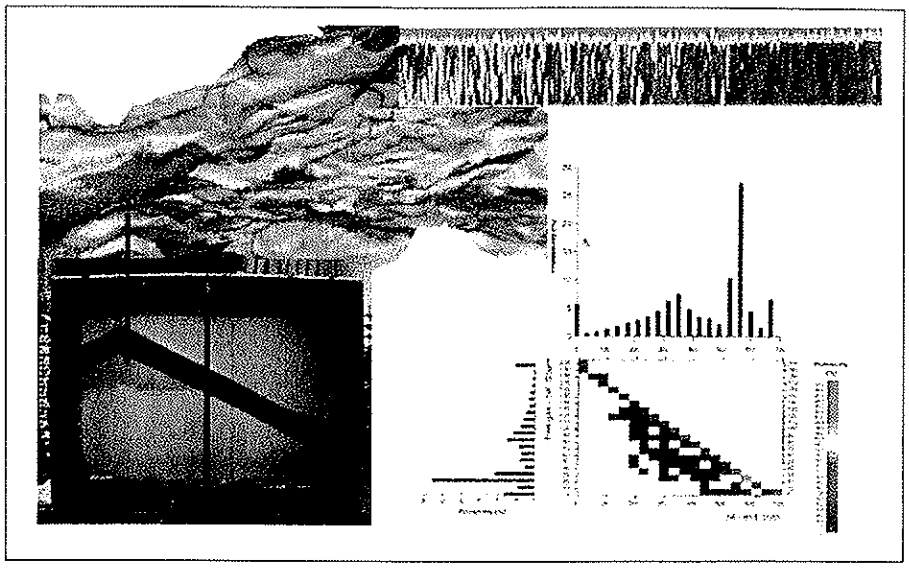

A thesis accepted by

The Norwegian University of Science and Technology (NTNU), Trondheim, Norway.

For the defence of the academic degree

Dr. philos.

2004

13.10.04

044108105

Preface

This dissertation is the result of my involvement in scientific investigations within the topics of basin modelling, hydrocarbon migration modelling and prospect risking for more than 10 years. It is a result of a long term fascination with trying to understand geology and geological processes by the use of quantitative methods. Modelling and the use of computerized numerical techniques have therefore become key elements in the work. During this work I have had the pleasure of cooperating with many geologists in different companies. These have always inspired me, and some of the most critical comments have turned out to be extremely helpful in helping to determine the direction of my research.

The topics covered in this dissertation are demanding in that several large research topics are touched upon. These include quantitative geology, numerical modelling, hydrocarbon generation and modelling, fluid flow modelling, reservoir technology and risking techniques. I am in no way an expert on all of these topics. Rather, it is the mixture of elements from all of these topics that I here try to combine into a contribution that it is hoped can influence the future success of petroleum exploration.

There are a great number of references that are relevant to the topics touched upon in this thesis. I have chosen to refer only to those papers that are most relevant for the work. Each chapter is a self-contained paper, except for Chapters 1 and 22 which tie together the work and concludes, respectively. Published papers are referred to by author(s) and chapter numbers to facilitate the navigation within the volume for the reader.

The work presented here would not have been possible without the support from Karl Oscar Sandvik during the early days, when the concept of modelling secondary migration was still new to the petroleum industry. Karl Oscar was always supportive and established contacts with many future clients in the oil companies. Atle Mørk provided the inspiration to write this dissertation. Wenche Krokstad, Olav Selle, Odd Steve Hustad, Hans Borge, Ane Lothe, Oddmund Frigård and Frode Vassenden have been important discussion partners in different research topics. I am grateful for the many discussions with all my co-authors. Berit Fossum has helped with the drafting of figures in many of the papers.

Early support from Conoco, and in particular Tony Dore, was extremely important for me. The cooperation with Arild Skjervøy and Kate Weissenburger was rewarding because of their excellent understanding of the petroleum exploration process and willingness to try new and unproven techniques in Norwegian licensing rounds. During recent years, Agip and Norsk Hydro are particularly thanked for their support of my work. The many discussions with Domenico Grigo, Nils Telnes, Christian Zwach and Stuart Burley (BG) have enabled me to further develop the concepts discussed in this dissertation.

The Norwegian Research Council (NFR) has played a key role as an enabler: The first version of the Semi secondary migration simulator was coded with basic funding from NFR, and the final compilation of the dissertation was funded through a grant from

NFR (Petroforsk). I am grateful for this funding. All the work included has been performed while I was an employee with IKU, which later became SINTEF Petroleumsforskning AS, and working on oil company funded research projects. SINTEF is thanked for making this possible.

My wife Wenche and our children Torstein and Inga have always been supportive. Without their support, I would not have been able to complete this work.

Abstract

Successful exploration for oil and gas require high quality risk assessments of prospects before drilling. The availability of accurate digital descriptions of the geological system, including structural depth maps, has facilitated the use of migration modelling in prospect risk assessment during recent years. The aims of this thesis include to assess the validity of the process descriptions used in the study of basin scale hydrocarbon migration, and to impose possible constraints on the use of these. The use of migration modelling techniques in the risking of prospect is studied, and new risking techniques using a combination of Monte Carlo and migration modelling are developed.

Laboratory experiments observe oil saturation during migration with a $\gamma - ray$ - technique, and show secondary migration be a focused process. Migration of oil and gas occurs in the uppermost parts of carrier systems, and flow-paths are typically less than 1 m thick. The hydrocarbon saturation and relative permeabilities are low, but migration velocities approach 1000 km/My in many carrier systems. Full Darcy fluid flow modelling using computational cells with vertical sizes of more than a few centimetres, and average hydrocarbon saturations within the computing nodes will, in general, not provide a good description of the secondary migration process, and can result in too large losses being modelled. Methods for quantifying secondary migration and computing resulting hydrocarbon saturations, velocities and losses are presented. These methods can be used for quick-look assessments, and can be utilized in ray-tracing simulation techniques.

Vertical leakage through a cap-rock has been studied in a visual laboratory experiment, and the results are interpreted to show that capillary leakage is a dynamic process that will typically build hydrocarbon columns that exceed the entry pressures of the cap-rocks. When supply from a source is stopped, the column will shrink. The column may shrink to a snap-off pressure that is less than the cap-rock entry pressure column height. The result is a dynamic trap that can continue to leak hydrocarbons millions of years after the filling has stopped. Leakage can therefore continue also during periods of uplift and erosion. Vertical capillary leakage will typically occur at low saturations and over a large area. Percolation modelling does not provide a good process description of this process, while multi-phase Darcy fluid flow modelling can provide an accurate description if the vertical resolution of the cap-rock is sufficient to accommodate the vertical flow property variability and hydrocarbon saturations.

The effects of faults as barriers and conduits to fluid flow are investigated. A pressure compartment technique is suggested for modelling the average single-phase flow properties of faults. The modelling is thereby simplified and speeded up to allow for sensitivity studies. This description has allowed for studying the time dependency of hydraulic cap-rock leakage and the influence on hydrocarbon trapping. Clay-smearing within fault planes is considered to be a good method for describing the fault seal

properties for the modelling of multi-phase oil and gas migration across and along fault planes. This approach is integrated into a ray-tracing secondary migration simulator.

Migration and trapping of hydrocarbons are affected by many geological processes. The effects of burial reconstruction techniques and palaeo-water depths on secondary migration are investigated. The results suggest that traps may be sensitive to these processes.

Case studies demonstrate that secondary migration modelling can be used to study the dynamic history of trap filling and changes in trapped hydrocarbon phases. The good matches of the migration models that are achieved to calibration data suggest, but cannot prove, that migration modelling is a valid method for providing input to prospect risk assessment in the exploration process.

A Monte Carlo simulation technique that uses (pseudo) 3D basin modelling and migration modelling to compute probability distributions of accumulated volumes of oil and gas in prospects is presented. Important input variables are described using probability distributions. The method uses existing (drilled) calibration wells to weight simulation runs by the difference between modelled and measured oil and gas volumes or column heights. The methods can be used to compute maps of oil and gas finding probabilities and maps of most likely oil and gas columns. Standard deviations can also be plotted to study the uncertainties of model predictions. The quality and accuracy of the geologic knowledge can be investigated by construction of a-posteriori probability distributions of the geologic variables used to define the hydrocarbon generation and migration system. This is possible when large amounts of simulations are compiled.

List of Content

CHAPTER 1

1. Introduction

Introduction and Discussion

Aims of study

The aims of this study are to deduce improved methods for modeling the migration of oil and gas at geologic time scales, and develop methods that can be used to advance the incorporation of process based 3D basin scale hydrocarbon migration simulation techniques in exploration risk assessments. Critical analyses of existing methods and descriptions of new algorithms that can be used effectively to model the migration processes are included. The methods are based upon laboratory experiments, and validation of models use basin scale case studies and the matching of existing field data to support the conclusions.

Background

The petroleum industry is increasingly relying on computerized methods to develop new oil and gas resources and exploit these resources. The use of seismic methods in combination with geological model building and fluid flow simulation techniques have allowed for significant increases in the amounts of oil and gas that can be produced from existing fields. During the last 10 years this increase in the producible oil and gas has contributed significantly to the ability to maintain a sufficient supply of petroleum for the continuously increasing demands of the world population. The increase in supply of petroleum has been one of the major requirements for the world economic growth, and a steady increase in the produced volumes is most likely needed to maintain the economic growth in the future.

The discovered hydrocarbon resources are a finite resource. Sooner or later each discovered field will be depleted, even when enhanced oil recovery (EOR) techniques are used. The EOR methods typically increase the ultimate recovery fraction of each oil field with in the order of 10-20%. Some fields, such as the Ekofisk Field in the North Sea, experience much higher EOR increases, and thus contribute to the reserves base for an extended period of time. But this can not change the overall trend of a limited potential for reserve growth due to EOR in existing fields.

During the last 10 years, the increased utilization of 3D seismic has helped in increasing the output from existing fields. The introduction of 3D seismic has, however, not been able to keep the exploration for oil and gas at a level where depleting reserves from the production of oil and gas can be replaced with resources from new discoveries. Therefore, most of the significant oil production increase in the 1990's has been from EOR techniques in combination with faster depletion of existing fields. The latter can be seen in NPD statistics that show a larger number of producing wells than planned being completed in existing Norwegian fields.

The trend of insufficient exploration success and a lack of replacing existing resources through efficient oil and gas exploration programs need to be reversed in order to keep up with the long-term world consumption of petroleum. Many oil companies and nations also face a depleting resource base from which to provide future revenue. Norway is a typical example: If exploration success is not increased, Norway will deplete most of their oil reserves during the next 30-40 years (Figure 1), while gas can be produced over a period of at least 100 years. The oil production from existing fields is planned to be reduced to 20% of the present day peak production rates as early as 2025 (Figure 1). This is a dramatic decrease in production and revenues for Norway. NPD has, however, estimated that Norway's reserve base can be increased significantly to delay the reduction in production (Stortingsmelding 38). Two development paths are outlined in Figure 2: "Forvitringsbanen" ("decline scenario"), which occurs if only the approved plans are followed, and a much more optimistic "langsiktig utviklingsbanen" ("long-term scenario") which can be achieved if all the resources are exploited and produced.

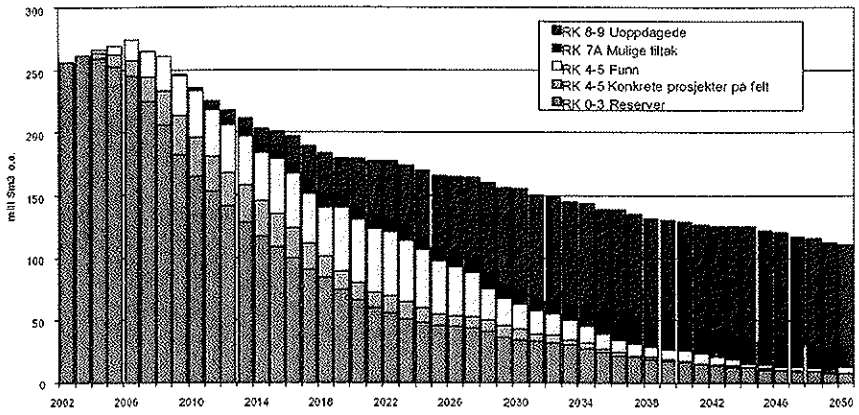

Figure 1 Estimates of future Norwegian oil production (Berge, 2003).

The undiscovered resources of Norway are estimated to be 40% of the remaining resources. During the years from 1998 to 2003, NPD reports an average of 18 wells drilled per year. NPD therefore believes that it will be very difficult to find and produce these undiscovered resources with the expected discovery rates (Berge, 2003). A total of 30 wells will be required per year with the present day discovery rate, to find sufficient amounts of oil. It can become a challenge to achieve this level of exploration activity when the prospects become smaller.

The most striking feature of Figure 1 may be the growth of the uppermost green bar, representing the undiscovered resources, after 2020. In the optimistic scenario, 50% of the Norwegian petroleum production will be from fields that have not yet been discovered! And these fields are not likely to be found with the exploration activity that is now taking place! Clearly, a dramatic increase in the exploration success is required for Norway to achieve their goals in future petroleum production.

Dramatic increases in exploration success can be achieved by tax incentives, geological break-through, or technology development. Reducing taxes could obviously increase the number of wells to the 30 wells NPD considers necessary to find sufficient amounts of undiscovered resources. A geological break-through could be that an oil-play was discovered in the Vøring basin, or that the key to the hydrocarbons in the Barents Sea were unlocked. Many oil companies may want to rely on this approach, but it is risky, in that the probability of success of any of these two events occurring is perhaps less than 50%. In fact, our estimates of the probabilities are highly subjective, and not published outside the risking teams of oil companies.

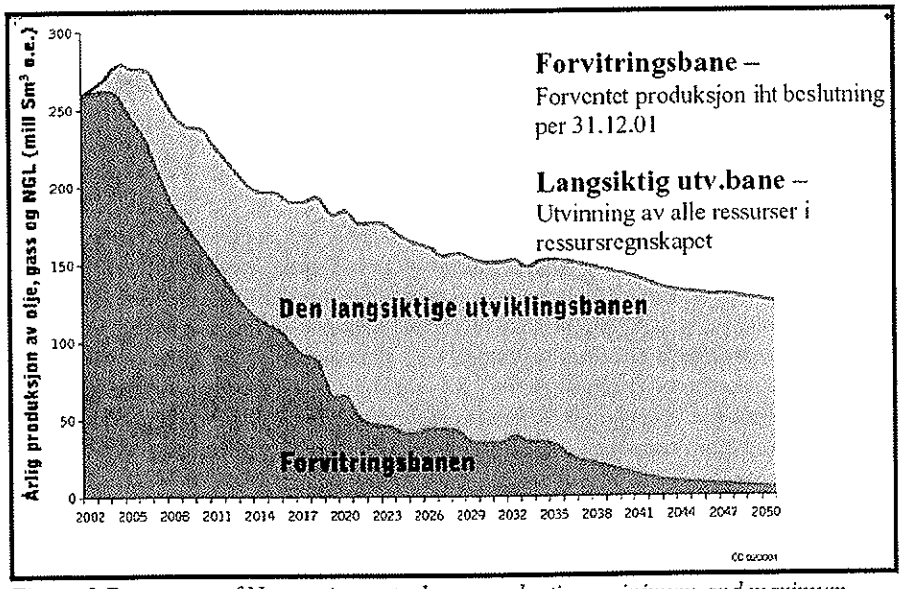

Figure 2 Prognoses of Norwegian petroleum production: minimum and maximum scenario (Berge, 2003).

Technology development can provide an important contribution to achieve a sufficient success in exploration activities. Much of the costs involved in petroleum exploration are related to the process of drilling wells. Making each well less expensive, or reducing the number of exploration wells that it takes to find and delineate a new field could therefore significantly improve the economics of exploration.

Petroleum exploration and risk assessments

Exploration wells are drilled to identify and describe new oil and gas fields from prospects that have been defined using well log or seismic data. The main purpose of exploration drilling is to confirm or reject a geologic model of the subsurface. Almost all exploration wells can be described as expenses for the oil companies. Only in rare cases where exploration wells are converted to production wells, will there be any

income directly resulting from an exploration well. Therefore, there is no economic downside to reducing the number of exploration wells, or eliminating them altogether, if the confirmation of the oil and gas fields could be achieved using other methods.

The implementation of new methods and techniques that have the potential for increasing the success rate of exploration wells is a natural first step for increasing the exploration efficiency. The worldwide exploration success ratio (the probability of finding oil or gas in an exploration well) is around 30%, and the Norwegian success ratio also has hovered around this value during the 1990's. An important aspect of this low probability value is that for each new exploration well, the most likely outcome will be that it is dry. This influences the planning of the strategy around the drilling of each exploration well. There is little use in making extensive plans for a positive outcome (a discovery) before the well has been drilled. Therefore each new exploration well tends to be followed by a period of analysis and further geological and/or geophysical modeling and assessment. This period can easily result in a year of no apparent activity within a licensed area. The result is that it takes many years to develop a license into a discovery and later a field for production.

If the methods that were applied in the exploration of oil and gas could increase the drilling success ratio to, say, 80%, then the entire setting of the exploration activity could be modified. The most likely outcome would then be a confirmation of the geological model, and the exploration teams could make more extensive and "firm" plans for the activities after each exploration well at an earlier stage in the ownership of a license. Still, contingency plans for the case of dry wells would have to be made, but in most cases one could speed up the entire exploration phase. The result would be a much faster and more economic exploration for oil and gas, in particular in offshore areas such as the North Sea, where drilling activities are expensive, and delays between the exploration (cost phase) and production (income phase) are costly.

The last 10 years have documented that the exploration success ratio can not be increased significantly by the use of 3D seismic alone. Seismic quality improvements during the last 10 years seem to have been instrumental in not decreasing the exploration success as prospects become harder to find, but not in increasing the success rate. This development should perhaps not come as a major surprise. Seismic reflections are influenced by the fluid and vapour properties of the media that the signal traverse, but the effects of the fluid and vapour are usually only minor compared to the effects of changes in lithology. Only in cases of gas-filled reservoirs can one expect to see clear effects with a fair degree of certainty. Even in these cases, a dry reservoir that resulted from an old gas accumulation that later leaked out may give almost the same seismic response as an existing gas accumulation.

Using seismic hydrocarbon indicators alone as decision criteria for drilling exploration wells can be a quite expensive methodology. If a model is built from e.g. seismic amplitude changes above crests of structures that may contain hydrocarbons, the first mistake (dry well) will not typically be sufficient to disprove the assumptions. Most likely the seismic indicators will have worked in another area, and therefore the a-priori mode of operation will be to "believe" in the seismic indicators. Only after the second dry well is there sufficient information to seriously doubt the seismic information. Still,

one will often find reasons why it did not work for one or both of the wells, and argue for a third exploration well. An oil company can therefore easily end up drilling 3 dry wells based on seismic information alone before the concept is downgraded as not working well in the area. This would then constitute a cost of up to $100 million (700 MNOK) in areas such as the North Sea.

Processed based modeling of geological processes can be used as fairly independent decision criteria for exploration campaigns. Most companies use thermal modeling and source rock generation modeling to demonstrate that prospects or plays have the potential for receiving sufficient quantities of oil and/or gas before they drill. This is not sufficient to increase the success ratio from their present level. Very few, if any, oil companies have so far tried successfully to systematically describe the migration into and leakage out of all prospects that they consider drilling using quantitative process based methods in three dimensions. The proper 3D mass-balance modeling of all fluids that are part of geological systems that contain prospects must therefore still be considered a new and untested technique in petroleum exploration.

There are many reasons why well calibrated 3D fluid flow models of the geological system are not extensively used in the exploration process. Some of these are:

- Lack of data of sufficient quality to construct a 3D geological model.
- Insufficient time to make all the required interpretations.
- The method has not been proven to add value to the exploration process.
- Assumed costs of the work involved.
- Lack of experienced personnel.
- Existing tools are extremely demanding to use.
- Parameters needed by existing models are not well constrained yet.
- Lack of long-term planning of exploration activities.
- Uncertainty as to how to use results of the analysis within the exploration workflow.

Existing commercial and research basin scale simulators aim to model subsidence and burial of the relevant sediments during geological time. The thermal evolution of source rocks, reservoirs and seals are computed using typically a heat flow history, surface temperatures and conductive and sometimes convective heat transport (Hermanrud, 1993). From the reconstructed temperature history, kinetic models are used to simulate the generation of oil and gas component groups through geologic time. Primary migration of hydrocarbons is modelled from the source to the nearest permeable carrier rock using Darcy flow. Secondary migration can be modelled using Darcy flow, percolation or ray-tracing methods, while attempts at modeling the capillary leakage out of traps use Darcy flow or percolation methods.

The most extensive simulators will take days or weeks to complete a full 3D basin scale simulation of all the above processes. The parameters of existing models are not sufficiently constrained to allow for the direct modeling of the hydrocarbon phases in existing fields. Therefore extensive calibration of the basin model is almost always required to find good matches to the observed data. Observed data include pressures and temperatures in drilled wells, maturity measurements from cores and cuttings, and

oil and gas saturations/contacts in drilled wells. The long simulation times have so far prevented the probabilistic use of basin scale simulators. Most uses of these techniques have been in deterministic modeling studies. In deterministic modeling, results from one or very few simulations runs are used as best case scenarios for the geological and economic risk assessments. Alternative cases are then not fully explored, and it is easy to forget (miss) the very low and high side potentials of a prospect. In other words, the risk of not including the correct geological scenario in the analysis increases with a deterministic approach to modeling.

The full potential of using 3D basin scale hydrocarbon generation and migration simulators in combination with modern seismic data can only be achieved if the algorithms incorporated into the simulators give a fair to excellent description of the processes involved. The algorithms used have to be sufficiently fast to allow for multiple realizations over hours or days. This is critical to allow for accurate and rapid risk assessment of prospects during the short decision times allowed for exploration work.

The hydrocarbon migration processes

The Darcy equation describes the relationship between fluid flow, permeability and pressures (potential differences) in porous media (discussed in e.g. Bear, 1972). Multi-phase flow can be described by including relative permeability and capillary pressures in the fluid flow equation(s). Basin modeling started off by adopting the methods that had been developed at the reservoir scale for basin scale simulations. The computing nodes were increased from e.g. 200*200*10m used in reservoir simulation to 1km*1km*100m for typical basin scale simulations (Johannesen et al. 2002). The size of the computing node was thus increased 250 times in order to keep simulations run times acceptable, with each simulation run taking a few days or weeks to complete.

The adoption of the reservoir simulation methodology, which often assumes constant hydrocarbon saturations within each computing node for each time step modelled, can be considered quite risky for simulating migration at basin scales. Selle et al. (1993 - Chapter 3), Sylta et al. (1998 - Chapter 4) and Sylta (2002 - Chapter 5) have shown that oil and gas migration in permeable carrier rocks occurs as focused, low saturation migration stringers. The vertical thickness of secondary migration stringers are typically less than 1m (Figure 3), and migration velocities can exceed 1000 km/My.

The hydrocarbon saturation varies vertically within even thin stringers (Figure 3), from zero at the base of the stringer, to typically 10-20% at the top of the stringer (Sylta et al., 1998 - Chapter 4). The average relative permeability within the migration stringer will be very low because of the low saturations, but the velocities of the oil and gas that migrate within the stringer are very high compared to the long geologic time periods modelled. One way of speeding up simulations can therefore be to assume that the hydrocarbons can migrate from the source rock to the traps within each time step used in the modeling of the process (Sylta, 1993 - Chapter 6). Time step lengths of basin scale fluid flow simulators will typically be in the range 0.1 Ma and with migration

velocities approaching 1000 km /My. This means that oil and gas can migrate distances that are longer than 100 km within a single time step in a basin scale fluid flow simulator. The ray-tracing method (Sylta, 1987, 1993 - Chapter 6) and the percolation method (Carruthers, 1996) assume such high hydrocarbon migration rates, and these process descriptions therefore make use of the above assumption (and others) to achieve simulation times for large datasets that do not exceed a few minutes, at least for simple (fluid phase) conditions.

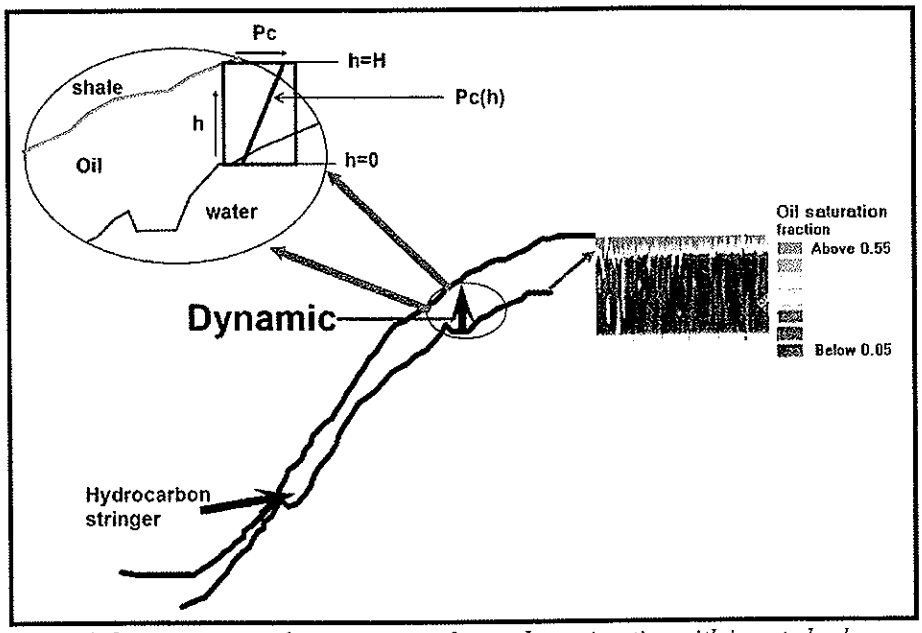

Figure 3 Cross-section outlining process of secondary migration with inserted colour-coded oil saturation distribution within carrier (modified from Sylta et al., 1998 and Selle et al., 1993).

In contrast, the classical Darcy basin scale fluid flow simulators will take days to run full 3D geologic models. Sylta (Chapter 10) discusses how this method can cause hydrocarbon saturations to be modelled to be too high, velocities too low, and therefore computed hydrocarbon losses to be too large. In an example taken from the literature, Sylta (Chapter 10) shows that oil volumes corresponding to a giant oil field are modelled to be lost in a spill route within the Tampen Spur area.

There are several possible approaches that can be used to modify the classical basin modelling (CBM) methods so that the hydrocarbon flow properties are treated more correct (Chapter 10). One way would be to use up-scaled permeability and capillary functions; another would be to use hybrid solutions for hydrocarbon migration within the carrier system. Hybrid systems (Hantschel et al., 2003) can make use of ray-tracing

or percolation techniques (Carruthers, 1996) to describe the migration within the carrier system, while the normal Darcy approach would handle the rest of the geological system (Hantschel et al.,, 2003).

Faults are important features that need to be accounted for in many geological systems, but are frequently ignored or treated very simplistic in CBM. Faults can act as barriers to flow or be "open" to flow at geologic scales. Faults may act as barriers at production scales (years), while being completely open to flow at geologic time scales. Here we only discuss the basin scale processes. During the 1980s, the modeling capabilities with respect to faults as barriers to hydrocarbon migration at basin scales were quite limited. Sylta (1987) introduced sealing faults and geometric (juxtaposition) faults into a ray-tracing approach. Later, attempts were made to use entry pressures and fault transmissibilities to describe flow properties (Sylta, 1996). Flow transmissibility multipliers have been shown to be useful for simulating flow at the reservoir (time) scale (Manzoochi et al., 1999).

The experience with using fault transmissibility formulation in hydrocarbon migration simulations led to a conclusion that there is insufficient data to constrain these fault properties for basin scale simulations at the present time. There is also quite some uncertainty as to whether fault permeability is an important parameter for basin scale hydrocarbon migration. The supply rate of oil and gas from the source rocks is generally considered very low compared to the flow that a low-permeability fault can accommodate over long geologic time spans. As a first order approach, entry pressures are considered the more important process property to describe for oil and gas migration modelling at basin scales. The formulation of Childs et al. (2002 - Chapter 13) was therefore used to describe the influence of shale-smear gouge (SGR) in faults on hydrocarbon migration and leakage out of traps that have a component of fault seal.

Early case studies involving fault seal simulations focused on developing scenarios that could be used in the risking process. Each scenario involved setting a number of fault segments to various combinations of open or closed. The simulation results were used to assess into which prospects oil and/or gas migrated and when. From this information a geologic risk profile could be developed for each prospect (Schroeder and Sylta, 1993 - Chapter 16). One limitation of the open/barrier/juxtaposition approach to fault seal modeling is that the outcomes are very much either/or. The result is often that either a trap is filled with hydrocarbons or it is dry. Monte Carlo simulation approaches are not so easy to apply to this fault seal definition, because each scenario has to be defined manually by geologist(s).

In contrast, the clay-smear modeling (Childs et al., 2002 - Chapter 13) can be made to behave more smoothly, through the setting of properties in the entry pressures relationship, Pe(SGR). Faults can therefore be modelled to change from sealing, to partly sealing to completely sealing by changing fault properties. These properties may also be obtained from laboratory investigations of core samples. Sperrevik et al. (2002) showed how a database of entry pressure and permeability could be developed and a resulting Pe(SGR) formula was defined. It is still not certain that this kind of formulation will apply for entire faults (Childs, pers. comm., 2003). Until the Sperrevik et al. (2002) type of formulation is proven effective, many geologists will prefer a cut-

off type formulation, where faults are open to flow when the computed SGR is lower than a limit value, and closed to flow when the SGR value is greater than this limit.

There is only one way to resolve these issues, and that is to apply the formulations to many case studies. Eventually one or the other (or both) formulation will fail, and a proper description can be deduced. Unfortunately, this process will take at least 5 to 10 years to complete, and we are therefore unable to conclude with respect to this problem in this work. At the very least, the incorporation of the various fault seal descriptions into a simulator (Childs et al., 2002, Sylta et al., 2003) has made it feasibly to resolve these issues in the future.

Vertical migration in mud-rocks has been modelled in both 2D (Ungerer et al. 1987) and 3D (Johannesen et al., 2002) by means of basin scale fluid flow simulators using the Darcy equation approach with relative permeability and capillary (entry) pressures. Sylta (2002 - Chapter 10) compared the Darcy approach to using the percolation method for mud-rocks and concluded that the percolation method could not provide a proper process description for oil and gas migration in low-permeability rocks. The reason for this conclusion is that the effective permeability for the hydrocarbon phases that leak out of traps is too low for migration to occur within the focused migration pathways that the percolation process requires. Vertical migration by capillary leakage from traps will tend to occur over larger, often several km^2, areas. The hydrocarbon saturations within the cap-rock flow-paths will be low, as will migration velocities (Chapters 9, 10). Still, large quantities can leak out of traps at geologic time scales.

The capillary pressures at the interface of the cap rock and the reservoir has to exceed the entry pressures of the cap-rock for leakage to be initiated. Vassenden et al. (Chapter 8) showed in the laboratory that the column supported by the seal can become greater than the one supported by the entry pressures of the seal. When the supply of oil was stopped, their experiment showed that the column within the trap decreased substantially below the entry pressure of the seal, until a snap-off pressure was reached. The snap-off pressure in the laboratory experiment was observed to be only 35% of the entry pressure, suggesting that the capillary seals of cap-rocks can be much more dynamic than is normally considered in exploration work. The entry pressures sealing column capacity calculation often used in exploration should therefore be replaced by a more dynamic assessment of the cap-rock seal (Chapter 9). The time-dependent supply of oil and gas into a trap in combination with the capacity down to the spill-point of the trap are critical inputs to this analysis. It is not yet evident that this type of cap-rock seal analysis can at all be done successfully without a proper 3D migration modeling study.

The process of expulsion and primary migration from a source rock to the nearest carrier or reservoir rock is not dealt with here. A critical review of this process with respect to applying the correct process description in the fluid flow simulations has not yet been done. Most simulators rely on a Darcy type description for primary migration. The primary migration process is, however, surprisingly efficient, with efficient vertical migration reported to be occurring through thick mud-rock sequences.

Risking

Basin scale hydrocarbon migration modeling is suited for use in the geological and economic risk assessment of petroleum prospects. The application of this coupling is limited by our ability to provide sufficient input data, such as regional depth maps and 3D lithology property descriptions. The outputs of basin scale 3D migration modeling studies include volumes of oil and gas in mapped prospects. The quality of predictions made from these volumetric estimates can be tested by how well the model explains existing discoveries and dry wells in a study area.

Results from the first 3D migration modelling studies were immediately used in the risking process. Schroeder and Sylta (1993 - Chapter 16) and Skjervøy and Sylta (1993 - Chapter 17) showed how risking tables could be developed from "best case" scenarios and used to rank prospects. Both papers also show modelled amounts of oil and gas trapped in prospects versus geological time, thus allowing for a risking not only of the present day trapped oil and gas volumes, but also a risking of the palaeo-trapping of the hydrocarbons. The importance of this is that geologic events that are known to affect the trapping of oil and gas can be accounted for in a rigorous manner.

Sylta (1993 - Chapter 6) cross-plotted results from several simulation runs to elucidate dependencies between the amounts of gas trapped in one field (the Troll Field) and the amount of oil in a prospect in Block 35/9. The amounts of oil in 35/9 could thereby be estimated with some confidence to be between 50 and 95 10^6 Sm^3. After the work was completed, well 35/9-1R discovered oil/gas in 1989. The details of the discovery could not be discussed in Sylta (Chapter 6) because of the 5 year confidentiality period for the drilling results.

Scenario modelling can be used as a term for the risking process described above. First, a "base case" that describes as many of the existing fields, discoveries and dry wells as possible is obtained. A match of the base case scenario to dry wells is not always required because mapping inaccuracies may have resulted in mapped traps that are not actually there. The best case simulation run defines a set of values for all input variables that has been obtained in the calibration process. Sensitivities are thereafter studied by varying important variables systematically, usually just one variable at a time, and each new set of values defines a separate case. Each case is simulated and the results are studied with respect to trapping of oil and gas in the prospects and calibration fields. Prospects that change little when variables are varied are considered to be robust, and therefore the risks are less. If most of the sensitivity cases result in dry prospects or small volume estimates, then the prospect should be risked accordingly.

The most important advantages of the scenario modelling approach to risking of prospects are that it is very flexible, only a small number of simulation runs are required, and the results are usually manageable for the geologist. A serious problem can arise when only small changes from the base case simulation run cause the calibration to become unacceptable (no hydrocarbons modelled into large fields etc). In this case, a recalibration of many of the sensitivity runs is needed, and this may take too much time in an exploration setting. Calibration is still, after all, very close to a manual

task as long as inversion methods have not been adopted for hydrocarbon migration modelling.

The scenario modeling technique may be well suited to deal with fault seal scenarios. Experience from clay-smear modelling in faults and the resulting secondary migration pathways (Childs et al., 2002 - Chapter 13) suggest that faults can sometimes be treated either completely sealing or completely open to hydrocarbon migration. This leads to a definition of yes/no scenarios in the definition of hydrocarbon migration of some study areas. A typical example would be a scenario that defined a nominal fault A to be sealing or open to migration, a fault B to be sealing or open and a fault C to be sealing only when both fault A and B are sealing. This would lead to 4 simulation cases that could be simulated and the outcome used in the risking of one or more prospects.

Monte Carlo simulation techniques are very popular to use in the risking of prospects. A well established method for using Monte Carlo techniques is in the calculation of risked trapped hydrocarbons. A probabilistic quantification of the in-place oil and gas prospect volumes is usually required (Irwin et al. 1993). This can be achieved by estimating probability distributions of such parameters as gross rock volume, porosity, net/gross etc. These properties are then multiplied together using the Monte Carlo scheme (Figure 4). A few thousand calculations are typically used to compile the resulting probability distributions. The geologists also estimate the risk of success and multiply these together to find the aggregated probability of success, which in this case means the chance of finding economic quantities of oil and/or gas in the prospect.

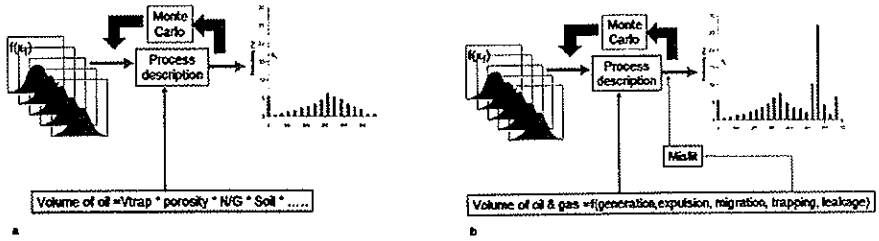

Figure 4 Principle of Monte Carlo simulation approach applied to prospect risking.
a: Properties are multiplied together to give volumes of oil and/or gas.
b: Processes are simulated and results are compiled into volumes of oil and gas.

In the methods proposed by Krokstad and Sylta (1996 - Chapter 20), the same procedure is in principle used, except that the multiplication of values is substituted by a full pseudo 3D migration simulator that simulates the amounts of oil and gas in all traps throughout the geological history until the present day (Figure 4). The resulting present day volumes (Chapter 20) or oil/gas column heights (Sylta and Krokstad, 2003 - Chapter 21) can then be compiled into probability distributions. The overall uncertainty of the predictions can be extracted from the probability distributions and plotted as

maps of e.g. most likely oil columns (Figure 5). This gives a good basis for understanding the spatial distribution of uncertainties, which is important for making decisions on where to drill the next exploration well in a study area.

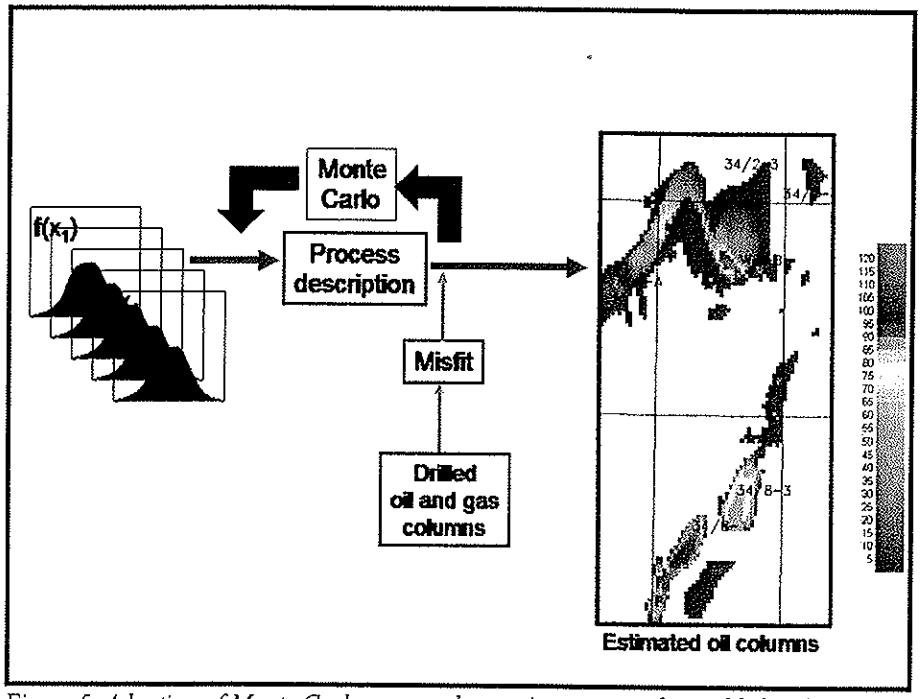

Figure 5. Adoption of Monte Carlo approach to estimate map of most likely oil columns (m). See Chapters 21 and 22 for detailed discussions.

When significant computing resources are made available, the Monte Carlo simulation techniques described above can be used to also compile probability distributions of the variables that have been used to calibrate the basin simulator (Sylta, 2004 - Chapter 22). This means that we can describe not only the a-posteriori uncertainties of the input variables, and thus our geological knowledge, but also how much we have improved this knowledge by providing more information to the analysis. The new information may be the results from drilling one exploration well.

The probabilistic description of the input variables is a valuable quantity for comparing results from one basin to another, and from one exploration play to another. Computed standard deviations of input variables such as oil expulsion factors (Chapter 22) can be used to build world-wide experience databases of geological knowledge, and thereby make it simpler to assess the exploration status of different areas, and compare risks in different areas to each other.

Case studies

Case studies play an extremely important role in the development of new exploration methodologies. The petroleum industry is conservative, and exploration risking techniques change slowly throughout the industry. This is one of the most important reasons that the included work has taken 10 years to complete.

Case studies are also the mechanism that has to be relied upon to show validity of the proposed process descriptions, methods and procedures. Geological processes can not be proven, as discussed by Oreskes et al. (1994). They argue that "*verification and validation of numerical models of natural systems is impossible. This is because natural systems are never closed and because model results are always non-unique. Models can be confirmed by the demonstration of agreement between observation and prediction, but confirmation is inherently partial.*" Therefore "*models can only be evaluated in relative terms, and their predictive value is always open to question.*" Oreskes el al. (1994) also discuss the practice of comparing numerical models with analytical solutions, and point out that the congruence between the analytical and the numerical solution does not mean that the numerical solution can be said to have been verified beyond the realm of the analytical solution.

The four included case studies (Chapters 16 to 19) demonstrate that the methods that have been introduced here based upon the process descriptions do demonstrate an agreement between observation and model results in these cases. This agreement is achieved by adjusting model variables until acceptable matches are found. The models are therefore not truly predictive. So far we have not documented any case where a modelling scenario could not be made to fit the data, except in cases where the input to the model was later considered wrong. Published documentation of such case studies is unfortunately difficult to achieve because of oil company confidentialities.

Included chapters and papers

Each chapter in this work represents a self-contained work. Most chapters correspond to papers that have been published in international journals with review or conference proceedings with review. These papers are listed with the year they were published below (Table 1). Chapters 1, 2 and 23 (Conclusions) have not been submitted for publication. Many of the papers have been presented at international conferences. Table 1 provides the title of each chapter, while full paper information is presented in References to the end of Chapter 1.

Chapter 1 (this chapter) is a summary chapter that describes the background of the work, introduces the topic of the work, states the objectives, and gives an overview of the work. Chapters 2 to 5 discuss the migration process and how it should be described and quantified. Chapters 6 to 10 deal with simulation techniques for secondary migration and leakage modelling. Chapters 11 to 15 discuss the simulation techniques in more details, with focus on the effects of special geologic features: pressure compartments, hydraulic leakage, faults, burial reconstruction and palaeo-water depths. Chapters 16 to 19 present 4 different case studies, while Chapters 20 to 22 outline

methods of risking using Monte Carlo methods. The risking methods make use of hydrocarbon migration simulators to build probability distributions of the results. Each chapter (paper) contains detailed discussion sections, while an overall discussion is included below. Chapter 23 presents the overall conclusions from the work.

Chapter 2 is a state-of-the-art discussion of processes and methods of evaluation relevant to hydrocarbon migration.

Chapter 3 presents experimental verification of the secondary migration process. This paper supports the use of focused migration stringers in the modelling of the secondary migration process.

Chapters 4 and 5 describe how the properties of migration stringers can be quantified using existing relative permeability and capillary pressures relationships. The results of this work includes graphs and equations that can be used to quickly assess migration losses, velocities etc, and equations that can be used to improve the calculations of secondary migration properties in 2D and 3D basin scale multiphase fluid flow simulators.

Chapters 6 and 7 discuss methods that can effectively be used to simulate the secondary migration of oil and gas from source to trap within carrier systems using computer technologies. The ray-tracing method is used for the simulation of the secondary migration. A multi-component hydrocarbon mixture can be simulated during migration and accumulation, although it is more time-consuming than using a gas-oil system.

Laboratory experiments described in Chapter 8 document the possible dynamic behaviour of traps during filling and leakage of hydrocarbons. The use of a simple entry pressure to describe capillary leakage out of traps may need to be revised and snap-off pressure concepts may have to be introduced.

Chapter 9 discusses the effects of dynamic hydrocarbon trapping on buried gas traps, with special emphasis on the delayed leakage that can result when trapped columns exceed the entry pressure capacities of the cap-rocks.

A review of the existing methods for simulating oil and gas secondary migration and leakage out of traps is performed in Chapter 10. There are limitations to the applicability of Darcy, ray-tracing and percolation type models. When the methods are applied outside the conditions where they are valid, erroneous conclusions and predictions most likely will result.

Chapters 11 to 13 discuss methods of handling faults as barriers to fluid flow, (water and hydrocarbons). Pressure modelling is discussed in Chapter 11 using a method that allows for the rapid modelling of fluid flow between pressure compartments. Lateral pressure differences are modelled to be controlled by averaged properties of the fault zones. Chapter 12 uses the pressure compartment methodology to assess vertical hydraulic leakage due to fracturing of the cap-rock seals. Chapter 13 introduces a method for using clay-smearing in faults to characterize the secondary migration properties of the faults and model migration with these properties.

Chapter 14 shows how advanced structural reconstruction techniques can replace the standard vertical subsidence and compaction modelling and thereby provide a more accurate geometry for use in hydrocarbon migration modelling at time steps before the present day. Chapter 15 also investigates effects of geometry on hydrocarbon migration, but this time the effects of reconstructing the bathymetry through time are studied. Comparisons are achieved by simulating migration for two cases, one with and one without the palaeo-water reconstruction effects.

Chapters 16 and 17 describe published case studies that use ray-tracing techniques to simulate hydrocarbon migration at basin scales. These are the first published case studies where hydrocarbon migration was simulated to yield volumetric estimates of the amounts of trapped oil and gas in un-drilled prospects for use in the risking process. Chapter 18 summarizes lessons learned during a number of North Sea migration case studies, including the one described in Chapter 17.

Chapter 19 contains a description of a basin modelling and secondary migration case study using ray-tracing techniques from a non-Norwegian basin, the East Irish Sea. The case study shows that a single simulation scenario can be created to explain the oil and gas distribution in a large number of fields. There is a complex hydrocarbon phase distribution in the traps within this basin.

Chapter 20 introduces the application of Monte Carlo simulation techniques in combination with hydrocarbon migration simulation techniques to provide uncertainty estimates and estimates of risked in-place oil and gas volumes for un-drilled traps. The probability distributions of the trapped volumes of oil and gas are here derived from probability distributions of the most important input variables, as defined by a user. Chapter 21 enhances the effort to provide improved risking tools by creating maps of estimates of probabilities, most likely oil and gas columns, and standard deviations of these columns. These maps can be used to choose the most optimum drilling location for the next well, and to plan drilling campaigns in an area.

Chapter 22 uses the established Monte Carlo simulation technique with more than 30.000 simulation runs to analyze the input variables. The results of each simulation run are weighted by how close the modelled column heights match observed hydrocarbon columns in drilled wells, and provide a-posteriori probability distributions of the geologic input variables. Geological uncertainties and estimates of measured improvements in geological knowledge are thus quantified

The conclusions from the work are listed in Chapter 23.

Table 1 Chapters & papers (*)

1. Sylta, Ø.: Introduction (with aims, background) and discussion.

2. Sylta, Ø.: Hydrocarbon migration, entrapment and preservation: Processes and Evaluation.
3. Selle, et al., 1993: Experimental verification of low-dip, low-rate two-phase (secondary) migration by means of gamma-ray absorption.
4. Sylta, Ø., Pedersen, J.I., Hamborg, M., 1998: On the vertical and lateral distribution of hydrocarbon migration velocities during secondary migration.
5. Sylta, Ø., 2002: Quantifying secondary migration efficiencies.
6. Sylta, Ø., 1993: New techniques and their application in the analysis of secondary migration.
7. Sylta, Ø., 1991: Modelling of secondary migration and entrapment of a multicomponent hydrocarbon mixture using equation-of-state modelling techniques.
8. Vassenden, F., Sylta, Ø., Zwach, C.: Secondary migration in a 2D visual laboratory model.
9. Sylta, Ø.: On the dynamics of capillary gas trapping: implications for the charging and leakage of gas reservoirs.
10. Sylta, Ø.: On the use of modelling techniques for hydrocarbon migration in carriers and seals.

11. Borge, H., Sylta, Ø., 1998: 3D Modelling of fault bounded pressure compartments in the North Viking Graben.
12. Lothe, A., Borge, H., Sylta, Ø.: Evaluation of late cap-rock failure and hydrocarbon trapping using a linked pressure and stress simulator.
13. Childs, C., et al., 2002: A method for including the capillary properties of faults in hydrocarbon migration models.
14. Huggins, P., et al.: Structural restoration techniques in 3D basin modelling: Implications for hydrocarbon migration and accumulation.
15. Kjennerud, T., Sylta, Ø., 2001: Application of quantitative palaeobathymetry in basin modelling, with reference to the northern North Sea.

16. Schroeder, F.W., Sylta, Ø., 1993: Modelling the hydrocarbon system of the North Viking Graben: a case study.
17. Skjervøy, A., Sylta, Ø., 1993: Modelling of expulsion and secondary migration along the southwestern margin of the Horda Platform.
18. Skjervøy, A., Sylta, Ø., Weissenburger, S., 2000: From basin modelling to basin management: reuse of basin-scale simulations.
19. Cowan, G., et al., 1999: Oil and gas migration in the Sherwood sandstone of the East Irish Sea Basin.

20. Krokstad, W., Sylta, Ø., 1996: Risk assessment using volumetrics from secondary migration modelling: assessing uncertainties in source rock yields and trapped hydrocarbons.
21. Sylta, Ø., Krokstad, 2003: Estimation of Oil and Gas Column Heights in Prospects Using Probabilistic Basin Modelling Methods.
22. Sylta, Ø., 2004: A probabilistic approach to improved geological knowledge and reduced exploration risks using hydrocarbon migration modeling.

23. Conclusions.

(*) Years are publication years for published papers. See also publication list at the end of Chapter 1.

Contributions to papers

There are a number of authors that have been involved in the work presented here. Much of the work presented involves simulation techniques that have been applied to data sets which have been worked up by others, in particular seismic interpretations, depth conversions, geological model constructions and geochemical and reservoir laboratory work. The thesis would not have been possible to complete without these contributions. Each chapter (paper) outlines the work done by the authors.

All the work described in the 9 single author chapters (1, 2, 5, 6, 7, 9, 10, 22 and 23) and which include 3 papers submitted for publication and 3 published papers, has been done by Sylta. Approximately 50% of the work of the 6 two-author papers has been done by Sylta. The first authors in these 6 papers (chapters 11, 15, 16, 17, 20 and 21) have done from 50% to 70% of the writing of the papers. The hydrocarbon migration simulations in these chapters were set up and run by Sylta.

There are eight multi-author papers included in the work (Chapters 3, 4, 8, 12, 13, 14, 18 and 19). My involvement in chapter 3 included proposing the concept of doing the experimental work, discussions during the planning stages, and participating in discussing the results and writing the published extended abstract. Most of the work in Chapter 4 was done by Sylta, including the method development, incorporating the numerical solution into the simulator and writing most of paper. The numerical solution of the loss equation was implemented by Pedersen.

Vassenden is the principal scientist behind the work in Chapter 8. My contribution has been in early discussions of the experimental set-up and in discussions of the experimental results and in contributing to the writing of the paper.

Lothe was the principal scientist in Chapter 12 and wrote most of the paper with continuous discussions with Sylta. The interpretation of the results was done jointly.

In Chapter 13 the method was first developed in joint discussions between Walsh, Childs and Sylta. The method was thereafter designed for Semi and implemented in the simulator by Sylta. My contribution to the paper also included participation in the writing of the paper.

Huggins was the coordinator and principal author of Chapter 14. My contribution included making the design of the 3DMove-Semi interface that allows for dynamic structural grids to be imported in Semi and used in the simulation of hydrocarbon generation, expulsion and migration. The migration modelling was done jointly by Tømmerås and Sylta. I also contributed to the writing of the paper itself and in the editing of the revised manuscript.

The inputs to Chapter 18 were taken from a number of case studies where I had been in charge of and/or performed the hydrocarbon migration modelling for Conoco. I also participated in the discussions and contributed to the writing, although the first author did most of the writing in this case.

Chapter 19 was based upon migration modelling work done by Hamborg and Sylta in a case study for BG, and where migration modelling was introduced to the BG staff. Most of the paper was therefore written by the BG staff with input from Hamborg and Sylta.

Discussion

Petroleum migration can be modelled as a simple multi-phase fluid flow process in three dimensions. The complexity of the subsurface does, however, make this simple model description extremely challenging to solve. Subsurface sediments exhibit flow properties that are extremely dissimilar. Sandstones are permeable, and cause oil and gas to migrate almost instantly from source to reservoir at geological times. Mud-rocks have orders of magnitude lower permeabilities when at relevant burial depths and cause hydrocarbons to migrate at low velocities. It has therefore not been possible (nor attempted by the author) to arrive at a unified method that can be applied to hydrocarbon migration in all types of sediments. This does not, however, mean that such a method does not exist. One logical aim of further investigations may be to arrive at a method that can properly describe migration both in low and high permeability rocks. For such a method to be useful, it will also have to be fast, and account for special geologic features such as faults and fractures.

The influence of faults on pressures (mostly water flow) and hydrocarbon migration has been dealt with using somewhat different formulations in this thesis. This is partly because of the intention to focus on the compartmentalization properties of the pressure system in the earlier work, but also because of a lack of fault flow property descriptions during the late 1980's and early 1990's, when the pressure compartment modelling concept was developed. Presently, more accurate formulations of the fault flow properties have been suggested (Manzoochi et al., 1999), and these can be used. It is, however, important to note that the SGR formulations that are used for fault transmissibility calculations in reservoir simulators will not work well if they are used unmodified in basin scale simulators. The work of Borge and Sylta (1998) clearly shows that there has to be a depth (or temperature) dependent element in the fault transmissibility models. The fact that this has not been considered a requirement for reservoir simulation purposes may be because a producible reservoir will typically only span a few hundred meters in depth from top to base. Basin depths range over many kilometers. Permeability and entry pressure formulations such as the ones proposed by Sperrevik et al. (2002) and used in Sylta et al. (2003) may provide a better description of the process results. Still, the fact that pressures are controlled by fault permeabilities whereas entry pressures are the most important properties for the hydrocarbon system remains. Making predictions of hydrocarbon trapping by assessing pressure barriers (size and locations) are therefore inherently difficult and may sometimes be impossible.

The ultimate aim of the hydrocarbon migration modelling in this thesis has been to make use of improved process descriptions in an improved risking methodology for undrilled oil and gas prospects. The fact that many different geological features have to be accounted for in the simulations does make the implementation of an improved strategy to an extremely demanding task. One challenge is for instance that changes in

the modelled sea bottom through the history of a basin may not be important to consider in many cases. But Chapter 15 shows that it can be very important in *some* cases: Migration spill routes from traps can be modified and modelled present day trapped hydrocarbon phases may change dramatically. One question to address in the future will therefore be: when do we need to consider this effect? If the answer is always, then the workflow has to be built accordingly. If we are able to create methods that can show when it is needed, then an overall less demanding, and therefore more efficient, risk assessment strategy may be devised.

The oil and gas migration effects of most of the geological processes that have been considered in this thesis show very non-linear behaviour. This leads to difficulties when trying to calibrate the migration models in different study areas. A large amount of freedom is given to the geologic modeller because there is generally a lack of data to calibrate the models to. This often makes it possible to come up with plausible migration scenarios to explain observations even when the input data are wrong. A typical case might be the tendency of some oil companies to use constant source rock properties within entire basins. The calibrated migration model may still provide an acceptable explanation of the discoveries that have been made even when later drilling shows that the source rock thicknesses change dramatically towards the basin depositional centres. When mismatches between the hydrocarbon migration model and the observed oil and gas pools are impossible, or very difficult, to remove by model calibration, then this may sometimes indicate that there is something wrong with the input data.

Frequently there will be insufficient data to make a reliable model of the carrier and source rocks at the time of running a migration case study. It may then be better to attempt to make alternative descriptions and use the migration simulator to study the sensitivity of the system. The Monte Carlo simulation approaches discussed in Chapters 20 to 22 can also provide important constraints on the geological system. There is still an additional need to develop more objective calibration methods. Many possible input parameter combinations can yield similar misfit results (see Chapter 22). Misfit is here defined as the error in calibration of the migration model (average difference between modelled and observed value). Using a single manually calibrated migration model may therefore lead to less accurate prospectivity assessments because the uncertainties in the modelling is not properly accounted for. Therefore, one future development of basin scale hydrocarbon migration simulators should be to develop inversion methods. These are methods that use the forward model iteratively to arrive at model parameters by minimizing a cost function. Inversion modelling can be combined with Monte Carlo simulation techniques to provide more accurate uncertainty predictions of amounts and locations of oil and gas in undrilled prospects.

With the many remaining challenges in the topic of hydrocarbon migration modelling and risk assessment, it may be tempting for oil companies to simply not consider using these methods in their exploration for oil and gas. It may indeed be possible to do this over the next few years. The main benefit would be that one can rely on old and tested methods, and simply hope to get slightly better at applying them than other oil companies. In the long run this strategy may be questioned: Modelling techniques will become better. Software will become easier to use, but more importantly: computers

will become faster and faster, allowing for more and more accurate migration models to be used. Therefore companies that introduce these techniques into their risking workflow have the upside potential of significantly improving their predictions and becoming more and more efficient, possibly gradually becoming superior to companies that resist the use of these tools.

Whether this future scenario becomes a reality, remains to be seen. There are of course several future scenarios where this will not be the case, the most notable one being if determination of hydrocarbon phases can be made directly from seismic data. In the meantime, the conclusions listed in Chapter 23 can be utilized.

Changes in printed version

The paper in Chapter 22 was published in the Petroleum Geoscience in October 2004. The draft version, which was submitted to the committee, was therefore replaced with the printed version here. Only minor changes were made in the review of the paper, including a couple of paragraphs added in the discussions.

References

Berge, G., 2003. Norsk Petroleumsnæring – har den noen fremtid. *Presented at Teknologiforum Rogaland 16 June, 2003. Presentation downloaded from NPD web-pages.*

Bear, J., 1972. Dynamics of Fluids in Porous Media. *Elsevier, New York.*

Borge, H., Sylta, Ø., 1998. 3D Modelling of fault bounded pressure compartments in the North Viking Graben. *Energy Exploration & Exploitation* **16**, 301-323.

Childs , C., Sylta, Ø., Moriya, S., Walsh, J.J., Manzocchi, T., 2002. A method for including the capillary properties of faults in hydrocarbon migration models. In: *Koestler, A.G., Hunsdale, R. (eds): Hydrocarbon seal quantification.* NPF special publication **11**, 127-139.

Cowan, G., Burley, D., Hoey, N., Holloway, P., Bermingham, P., Beveridge, N., Hamborg, M., Sylta, Ø., 1999. Oil and gas migration in the Sherwood sandstone of the East Irish Sea Basin. In: *Fleet, A.J., Boldy, S.A.R. (eds) Petroleum Geology of Northwest Europe: Proceedings of the 5th Conference*, 1383-1398.

Hantschel, T., Kauerauf, A., Wygrala, B., 2003. Modelling capillary sealing and flow barriers in basin scale simulations. *Presented at EAGE "Fault and Top Seals" conference in Montpellier*, 8-11 September. Abstract p 21.

Irwin, H., Hermanrud, C., Carlsen, E.M., Vollset, J., Nordvall, I., 1993. Basin modelling of hydrocarbon charge in the Egersund basin, Norwegian North Sea, pre- and

post-drilling assessments. In: *Dore et al. (eds): Basin Modelling: Advances and Applications*. NPF, Special Publications 3. Elsevier, Amsterdam, pp 539-548

Johannesen, J., Hay, J., Milne, J.K., Jebsen, C., Gunnesdal, S.C., Vayssaire, A., 2002. 3D oil migration modelling of the Jurassic petroleum system of the Statfjord area, Norwegian North Sea. *Petroleum Geoscience*, Vol **8**, 37-50.

Kjennerud, T., Sylta, Ø., 2001. Application of quantitative palaeobathymetry in basin modelling, with reference to the northern North Sea. *Petroleum Geoscience*, 2001, vol. 7, no. 4, 331-341.

Krokstad, W., Sylta, Ø., 1996. Risk assessment using volumetrics from secondary migration modelling: assessing uncertainties in source rock yields and trapped hydrocarbons. In: *Dore, A.G., Sinding-Larsen (eds.). Quantification and Prediction of Petroleum Resources*, NPF Special Publication **6**, 219-235.

Manzoochi, T., Walsh, J.J., Nell, P., Yielding, G., 1999. Fault transmissibility multipliers for flow simulation models. *Petroleum Geoscience*, **5**, 53-63.

Oreskes, N., Shrader-Frechette, K., Belitz, K., 1994. Verification, validation, and confirmation of numerical models in the earth geosciences. *Science*, Vol. **263**, 641-646.

Schroeder, F.W., Sylta, Ø., 1993. Modelling the hydrocarbon system of the North Viking Graben: a case study. In: *Dore et al. (eds): Basin Modelling: Advances and Applications*. NPF, Special Publications **3**, 469-484.

Selle, O.M., Jensen, J.I., Sylta, Ø., Andersen, T., Nyland, B., Broks, T.M., 1993. Experimental verification of low-dip, low-rate two-phase (secondary) migration by means of gamma-ray absorption. In: *Parnell, J. et al. (eds.). Geofluids'93. Contributions to an International Conference on Fluid Evolution, Migration and Interaction in Rocks*, 72-75.

Skjervøy, A., Sylta, Ø., 1993. Modelling of expulsion and secondary migration along the southwestern margin of the Horda Platform; In: *Dore A.G. et al. (eds.). Basin Modelling: Advances and Applications*. Norwegian Petroleum Society Special Publication 3. Elsevier, Amsterdam, 499-537.

Skjervøy, A., Sylta, Ø., Weissenburger, S., 2000. From basin modelling to basin management: reuse of basin-scale simulations. In: *Ofstad et al. (Eds). Improving the Exploration Process by Learning from the Past*. NPF Special Publication **9**, 141-157.

Sperrevik, S., Gillespie, P. A., Fisher, Q. J., Halvorsen, T., Knipe, R. J., 2002. Empirical estimation of fault rock properties. In: *Koestler, A.G. and Hunsdale, R., Hydrocarbon Seal Quantification*. NPF Special publication **11**, 109-125.

Stortingsmelding nr. 38 (2001-2002) Om olje- og gassvirksomheten. Tilråding fra Olje- og energidepartemtentet av 28. juni 2002.

Sylta, Ø., 1987. SEMI - A program for the modelling of buoyancy driven, SEcondary MIgration of oil and gas by means of a ray-tracing technique. *IKU Report 25.2403.00/01/87*, 51p. Open.

Sylta, Ø., 1991. Modelling of secondary migration and entrapment of a multicomponent hydrocarbon mixture using equation-of-state modelling techniques. In: *England, W.A., Fleet, A.J. (eds), Petroleum Migration*. Geol. Soc. London, Spec Publication **59**, 111-122.

Sylta, Ø., 1993. New techniques and their application in the analysis of secondary migration. In: *Dore et al. (eds): Basin Modelling: Advances and Applications*. NPF, Special Publications **3**, 385-398.

Sylta, Ø., 2001. Quantifying secondary migration efficiencies. Geofluids (2002) **2**, 285-298.

Sylta, Ø., 2004. A probabilistic approach to improved geological knowledge and reduced exploration risks using hydrocarbon migration modelling. *Petroleum Geoscience*, Vol. **10, no3**, 187–198.

Sylta, Ø, Krokstad, W., 2003. Estimation of Oil and Gas Column Heights in Prospects Using Probabilistic Basin Modelling Methods. *Petroleum Geoscience*, Vol. **9**, 243–254.

Sylta, Ø., Pedersen, J.I., Hamborg, M., 1998. On the vertical and lateral distribution of hydrocarbon migration velocities during secondary migration. In: *Parnell, J. (ed.). Dating and Duration of Fluid Flow and Fluid-Rock Interaction*. Geological Society London, Special Publication **144**, 221-232.

Sylta, Ø., Childs, C., Sperrevik, S, Tømmerås, A. 2003. On the use of multi-carrier hydrocarbon migration modelling with clay-smearing in faults. *Poster presented at the EAGE "Fault and Top Seals" conference in Montpellier*, September 2003. Abstract only, p 83.

Ungerer, P., Doligez, B., Chenet, P.Y., Burrus, J., Bessis, F., Lafargue, F., Giroir, G., Heum, O., Eggen, S., 1987. A 2-D model of basin scale petroleum migration by two-phase fluid flow. Application to some case studies. In: *B. Doligez (editor), Migration of hydrocarbons in sedimentary basins.* Technip, Paris, 415-456.

Draft of papers not yet in print but included as chapters:

Huggins, P., Burley, D., Sylta, Ø., Tømmerås, A. Bland, S., Kape, S., Kusznir, N., Structural restoration techniques in 3D basin modelling: Implications for hydrocarbon migration and accumulation. Chapter 14.

Lothe, A., Borge, H., Sylta, Ø. Evaluation of late caprock failure and hydrocarbon entrapment using a linked pressure and stress simulator (in press). Chapter 12.

Vassenden, F. Sylta, Ø. Zwach, C., Secondary migration in a 2D visual laboratory model (in press). Chapter 8.

Sylta, Ø.: On the dynamics of capillary gas trapping: implications for the charging and leakage of gas reservoirs (in press) Chapter 9.

Sylta, Ø., On the use of modelling techniques for hydrocarbon migration in carriers and seals. Chapter 10.

CHAPTER 2

2. Hydrocarbon migration, entrapment and preservation: Processes and Evaluation.

Hydrocarbon Migration, Entrapment and Preservation: Processes and Evaluation.

Øyvind Sylta, SINTEF Petroleum Research, 7465 Trondheim, Norway

Summary:

Hydrocarbon migration occurs at basin scale in tight mud-rocks and permeable carrier rocks. Hydrocarbons migrate from a source rock, through low permeable mud-rocks into carrier rocks. Hydrocarbons migrate laterally along the carrier rocks, just beneath a seal, until they are entrapped in traps that prevent further upward movement. Faults can act as both seals and migration conduits. Capillary leakage of gas and oil from the traps occurs when the capillary pressure within the hydrocarbon phase exceeds the cap rock entry pressures, while hydraulic leakage occurs when the pressures exceed the cap-rock leakoff pressures. Hydrocarbon components experience thermal alteration processes while being trapped, including cracking of heavy components into lighter components at high temperatures and biodegradation at low temperatures. The properties may also be changed by water washing and deasphalting.

The processes that control hydrocarbon migration include buoyancy, hydrodynamics and molecular diffusion. Sedimentary rocks exhibit a significant degree of heterogeneity, and the hydrocarbon migration process can be modelled using percolation theory concepts or Darcy flow using finite element and control volume techniques. The primary, secondary and tertiary migration processes may be modelled with different techniques.

Evaluation of migration often aims at describing the "source risk" by assessing the probabilities for different outcomes, e.g. trapped oil, gas or condensates in a trap. Expert opinions from experienced exploration geologists that rely on analogue systems have traditionally played an important role in describing the risks. Modern techniques have added the use of hydrocarbon migration simulations to provide estimates of oil and gas volume probabilities for traps. Future research should give improved estimates of risks by using, for example, Monte Carlo simulation techniques together with 3D basin scale fluid flow simulators.

Keywords:

Hydrocarbons, source rock, carrier rock, primary migration, trap, secondary migration, tertiary migration, buoyancy, hydrodynamics, compaction, permeability, overpressures, mud-rocks, adsorption, kerogen network, non-wetting phase, invasion percolation, faults, capillary seals, shale gouge ratio, diagenetic processes, hydraulic fractures, entry pressures, biomarkers, oil populations, diffusion, cracking, biodegradation, bacteria, thermal alteration, economic risk, basin simulators, risk factors, numerical modelling.

Glossary:

Capillary pressure: Pressure difference between the invading and the defending phases in a multi-phase porous system.

Capillary seal: Hydrocarbon seal caused by differences in entry pressures of different lithologies.

Carrier rock: A permeable rock horizon through which oil and gas migrate after leaving the source rock.

Compaction: Reduction of the bulk volume, or reduction of the pore spaces within, of a body of sediment in response to increasing weight of the overburden.

Diagenesis: All chemical, physical and biological changes undergone by a sediment after initial deposition and before final lithification.

Entry pressure: The minimum capillary pressure required to force a non-wetting fluid into capillary openings in a porous medium saturated with a wetting fluid.

Fault: A rock fracture or zone of fractures along which there has been displacement of the sides relative to one another.

Hydraulic seal: Low-permeability rocks seal for single and/or two-phase migration when total pore pressures are not sufficiently large to cause hydraulic fracturing. Fractures result in very high rates of migration, and therefore breach of the seal.

Invasion percolation: Migration is viewed as the invasion of a non-wetting hydrocarbon phase through a network of opposing capillary pressures. Hydrocarbons need to exceed (a) breakthrough pressure to migrate in stringers.

Mud-rocks: General term for fine grained sedimentary rocks; includes mudstone, claystone, shale and siltstone.

Primary migration: Migration of hydrocarbons out of the source rock and into the carrier rock.

Seal (rock): Impermeable rock preventing the upward migration of oil and gas from a trap.

Secondary migration: Migration of hydrocarbons in the carrier rock to the trap.

Shows: Hydrocarbons that are found in the pore space of porous rocks but cannot be produced by standard techniques during e.g. testing of wells.

Source rock: Sedimentary rock containing organic material that under appropriate conditions can be transformed into liquid or gaseous hydrocarbons.

Tertiary migration: Migration or leakage of hydrocarbons out of the trap.

Introduction

Hydrocarbons that have been generated in an organic rich source rock can be expelled from that source rock and then migrate within fine-grained (mud-) rocks until some of them reach a porous

and permeable carrier rock. Migration within the fine-grained source rocks is referred to as primary migration. Migration then continues, usually up-dip, within the permeable carrier rock until a trap is reached and the hydrocarbons are trapped in the reservoir rock. This process is referred to as secondary migration. The hydrocarbons are retained in the trap by sealing rocks that act as barriers to further migration. Long and short-term processes that act upon the hydrocarbons trapped in reservoirs will frequently cause leakage of oil and/or gas. The leakage, referred to as tertiary migration, may be slow, i.e. occur over more than 50 million years, or very fast, i.e. during a time span of less than a million years.

The different processes that control hydrocarbon migration are in general fairly well understood. Several processes tend to act concurrently, and the various processes may be active in different types of sedimentary basins and hydrocarbon plays. The quantification of migration processes is still at an immature stage, but the large scale adoption of basin simulators with integrated fluid flow modelling into exploration settings and decision making teams holds the promise of quantifying the ranges of flow saturations and velocities and hydrocarbon migration directions under different geologic conditions.

Hydrocarbon migration evaluations have relied strongly on organic geochemical techniques. Laboratory measurements of source rock material and samples from oil and gas pools have allowed for the creation of one or more migration scenarios that can explain existing results and also make predictions about future drilling possibilities. In the future such techniques may be complemented by more quantitative approaches using fluid flow simulators in combination with high-resolution mapping of basins and traps from 3D reflection seismic data. However, the success of these techniques will rely on a proper and quantitative description of hydrocarbon migration processes.

A. Processes

1. Buoyancy and Hydrodynamics

The most important processes that influence hydrocarbon migration are buoyancy and hydrodynamics (Hubbert, 1953). Hydrodynamic conditions in sedimentary basins are associated with overpressures and barriers. Diffusion processes may also influence migration in some geologic settings. To some extent, hydrocarbon phase conditions and thermal processes also influence migration, not so much in migration direction as in the type of hydrocarbons that can be found in the reservoirs today. While temperature is the most important factor in the hydrocarbon generation process, pressure is definitely the most important for the migration process.

Buoyancy influences hydrocarbon migration because water is heavier than oil and gas at subsurface conditions. Only in extremely rare cases can "oil" become as dense as water, and therefore buoyancy will generally cause hydrocarbons to flow upwards. Buoyancy is very important for the secondary migration process, the entrapment of oil into traps, and for tertiary leakage out of traps (Fig. 1). There is always a significant upward component in the direction of migration for these processes. The rates of migration are high for the secondary migration process, while slower migration rates are more normal during primary and tertiary migration.

Migration distances are generally less for primary and tertiary migration than for secondary migration in most basins.

Hydrodynamics is an important control on hydrocarbon migration in many sedimentary basins. During increased burial, sediments and faults become gradually less permeable due to mechanical and chemical compaction processes. Faults will often start to act as barriers as burial depth increases. Compaction is a result of increased loading on top of sediments during continuous sedimentation. When the permeability of fine-grained mud-rocks becomes very low, water is not able to escape from the low permeability formations sufficiently fast and, as a result, compaction is reduced and more of the sediment load is transferred from the grains to the interstitial liquid. This increased load on the water phase causes the pressure to increase in the pore-space, and overpressures result. Overpressures will be gradually reduced if the sedimentation rate decreases sufficiently, or a period of non-deposition or uplift follows. When the permeability of the mud-rocks is sufficiently low, pressure depletion may take millions of years. This will often be the case in passive margin basins at depths of e.g. 3500 to 5000 m.

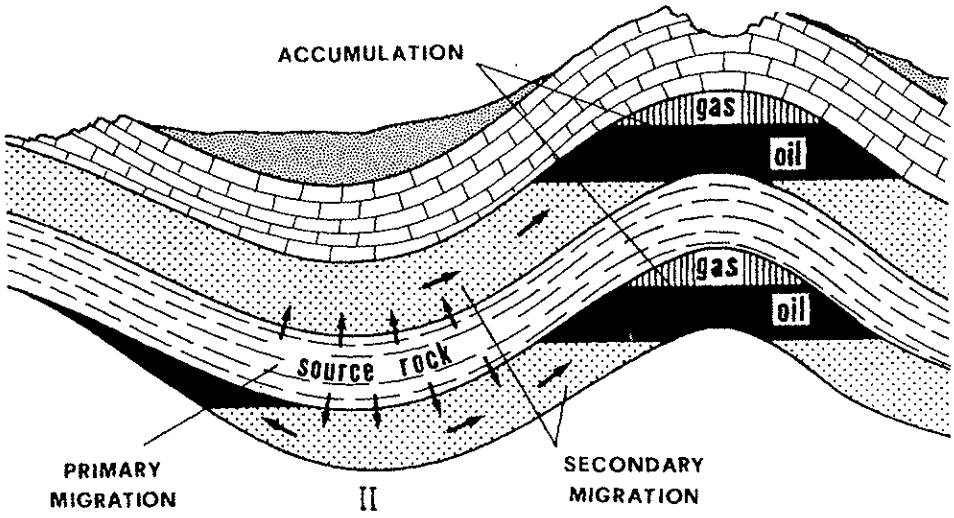

Fig. 1 Formation of oil and gas accumulations. Hydrocarbons move (primary and secondary migration until they are trapped in accumulations (from Tissot and Welte, 1978).

As overpressures increase in mud-rocks, flow from the fine-grained rocks into the permeable carrier rocks will be maintained. In cases where carrier rocks communicate with very large aquifers or the surface/sea, no overpressure increase will occur in the carriers. This is because the supply of fluids from the mud-rocks is low, while the permeability of the carriers is many orders of magnitude greater than that of the mud-rocks (Schøn, 1996). In this case, an overpressures gradient will be maintained within the mud-rocks, and hydrocarbons that are expelled from source rocks within the mud-rocks will experience a push from this overpressure gradient towards the carrier system.

Expulsion

Before the hydrocarbons that are generated within the source rock units can start to migrate, they have to overcome a resistance to flow from the source rock organic matter. The surface of the organic matter has an affinity for the hydrocarbons, and adsorption causes some of the oil and gas to be retained at the organic matter surface (Pepper and Corvi, 1995). It can also be argued that primary migration cannot start until some of the pore space is saturated (e.g. Skjervøy and Sylta, 1993), leading to a saturation dependent expulsion. A third process description of the expulsion process assumes migration of hydrocarbons within a kerogen network (Stainforth and Reinders, 1990). This latter description combines the expulsion and primary migration into one single process.

Primary migration

The primary migration of hydrocarbons in mud-rich sequences (Fig.1) is often a very efficient process, with relatively low losses of hydrocarbons. Any losses are due to retention of hydrocarbons in the pore-space. Observations of hydrocarbon saturations in shales that hydrocarbons must have migrated through to get from a source to a trap (e.g. the Heather Formation of the North Sea) show low values, except very close to the source rock units (MacKenzie et al., 1987). Many authors have studied the effects of primary migration using geochemical methods, e.g. Leythaeuser et al. (1984). Leythaeuser et al. (1982) and Krooss et al. (1993) investigated molecular diffusion as a primary migration process, but Darcy flow now seems to be the most commonly assumed process for primary migration. Darcy flow for hydrocarbons in tight shales will occur at very low migration rates, because these rocks have very low permeabilities. Laboratory measurements of permeability in shales show permeabilities in the nano-Darcy range ($1D=10^{-12}$ m^2), with a spread over at least two orders of magnitude (Ingram et al., 1997).

At very low permeabilities, the flow conditions are such that the hydrocarbon migration may occur at higher saturations, but through extremely focused flow-paths, while higher permeabilities in the mud-rocks may result in two or even three phase flow (oil, gas and water through the same pore-space). In tight shales, the generation of the hydrocarbons may lead to very localized pressure increases around the kerogen. This increase in the pressure is a result of density changes from converting organic matter to gases and liquids (and coke), and the relative increase in liquids to solid material within the rock. The removal of solid matter effectively increases the porosity and thereby load is transferred from the matrix to the liquids, thus increasing overpressures. When permeabilities are very low, the increased overpressures can result in localized fracturing of the source rock, and hydrocarbons would preferentially flow through these fractures because the highest overpressures would be where the oil is generated. The highest overpressure gradients would also be associated with where the hydrocarbons have been generated, and therefore hydrocarbon migration would increase more than the average water flow in the mud-rocks.

Secondary migration

Secondary migration, the flow of hydrocarbons within a permeable carrier system and into traps (Fig.1), occurs in a more open system than primary migration (Schowalter, 1979). The conditions of flow are more similar to the flow that occurs in oil fields during production

because of the good permeabilities in many carrier systems. Frequently, the carrier system consists of the same type of rocks as the producing fields, or traps, and rock properties are therefore available through laboratory measurements. Because of the high permeabilities, attempts have been made to study the secondary migration flow in laboratories. Dembicki and Andersen (1989) published an experiment where oil was injected into a vertical cylinder of sand. The resulting flow was observed by slicing the sand after the experiment was completed. Flow was observed to occur within a single oil stringer only a few mm in thickness, and the saturation was very high within the stringer, although a quantitative estimate was not made.

Selle et al. (1992) measured the oil migration within a 60 cm long sub-horizontal core at 5° dip, and measured the oil saturations during the experiment using a gammy-ray methodology. They observed that migration occurred at relatively low hydrocarbon saturations (10-20%), and for a high permeability carrier the flow was focused to the upper 1-2 cm of the core. For a lower permeability carrier the flow occurred over the entire core and at hydrocarbon saturations that were consistent with a two-phase Darcy flow, as verified by using a commercial multiphase flow simulator. The experiment took weeks to complete, which suggests that secondary migration velocities can be expected to exceed 1000 km/My in sedimentary basins. The very focused migration and not so high saturations within the pathways result in quite low secondary migration losses. It is only when secondary hydrocarbon migration passes through very low permeability units, e.g. siltstones, and/or when the hydrocarbon generation occurs over very short time spans, e.g. less than 1 million years, that secondary migration losses in the migration pathways can become so large that the traps may be insufficiently filled. Effective secondary migration is possible over long distances, and some oil fields may have been sourced from kitchens that lie more than 1000 km from the traps (Sylta et al., 1998). This is possible if the carrier system is continuous, the dip is very low, and no disturbances cause migration pathways to be intercepted by vertical leakage to the surface.

Frette et al. (1992) performed experiments of slow upward migration due to buoyancy, of a non-wetting phase in a 3D medium and used a modified invasion percolation algorithm to help explain the process as quasi-static at the pore scale. Carruthers and Ringrose (1998) suggested that invasion percolation could be used to describe the (secondary) migration at the basin scale because feeding rates from the source rocks are very low and the migration will occur with hydrocarbon saturations at or very near a percolation threshold.

During secondary migration, hydrocarbons also have to saturate the pore space in dead-ends and micro-traps (Fig. 2). These are tiny accumulations that are too small to produce (at least until now). The size of a micro-trap could be in the range of a few tens of m^3. However, when the carrier system is complex, with lots of lithology changes and/or small structurations, e.g. faults, the number of micro-traps and dead-ends can be very large, and therefore the volumes trapped in them may become significant in some geologic systems. The hydrocarbon phases trapped within dead-ends and micro-traps can be both oil and gas. Structural micro-traps may preferentially be filled with gas, because they are small and oil therefore tends to be spilled. Stratigraphic micro-traps may leak gas through the top, or laterally along a preferred flow-path because gases tend to migrate more easily through seals than oil due to their lower densities and viscosities.

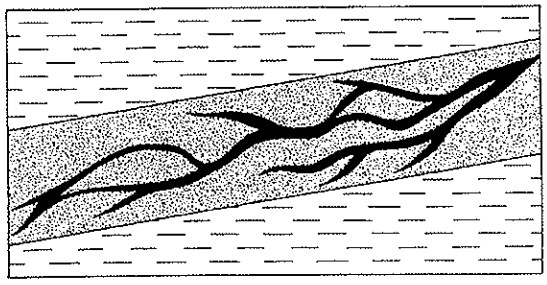

Fig. 2 Conceptual view of secondary migration of oil in a carrier surrounded by mud-rocks. Oil stringers are thin black "ganglions" (from England et al., 1991).

Faults and barriers

Faults may act as barriers to hydrocarbon migration or as conduits for hydrocarbons. When sand/shale sequences are faulted, some of the sand and shale is often dragged into the fault plane. Large fault juxtapositions often lead to more drag into the fault zone. Clay or shale that is dragged (smeared) into the fault plane will act as capillary seals to the hydrocarbons that try to get through. For across-fault migration from the hanging to the footwall side of a fault, hydrocarbons can migrate through very small holes in the fault plane. Hence, across-fault migration will be controlled by the minimum entry pressures of the part of the fault plane that is in contact with hydrocarbons. When fault throws are large, hydrocarbons may have to look for migration pathways up along the fault plane, and then they have to overcome the maximum entry pressure of the fault plane to get through. It is therefore often much more difficult to get migration up fault planes than across fault planes. The smearing of clay/shale within the fault plane can be expressed quantitatively by a shale gouge ratio, SGR (Knipe, 1997; Yielding et al., 1997). This factor can be used in assessing which faults are sealing. When faults act as barriers, hydrocarbons may flow along the fault until a trap is reached, or until the hydrocarbons are able to migrate around the fault.

Diagenetic processes will also help in sealing faults to hydrocarbon migration (and water flow). Sands that are dragged into the fault plane may undergo compaction and diagenesis by, for example, pressure solution and kinetic reactions. The permeability of the conduits within the fault plane will then be reduced and the entry pressures will increase. There is often, therefore, a correlation between faults that seal for overpressures and hydrocarbon migration (and trapping). It should be noted, however, that overpressures result from the total fluid flow across faults, and the water phase flow is the more important phase. By comparison, hydrocarbons only migrate through a small fraction of the fault plane. The correlation between overpressures and hydrocarbon seal across faults is therefore highly variable.

Carrier systems that are highly over-pressured can cause hydraulic fracturing of faults. Faults often form the boundaries of pressure cells, and therefore the shallowest point of a pressure cell can in many cases be found at a bounding fault. Hydraulic fractures are most likely to start off from the shallowest point of each pressure cell. Hydraulic leakage up fault planes is extremely difficult to prove, because we have no direct access to the fault plane, and therefore cannot take measurements within it. The effects of hydraulic leakage can be that a trap has been emptied by leakage of all or some of the hydrocarbons in it. One can then observe the retained oil in the

palaeo-trap and interpret the case as evidence of hydraulic leakage if the pressures are close to the leak-off pressures measured in the cap-rock. However, it is not possible to determine if the fault or the cap-rock contains the actual hydraulic leakage flow paths. It is therefore possible that hydraulic leakage up fault planes is a much more common process than it has so far been considered to be.

2. Entrapment

Trap types

Hydrocarbon accumulation in traps requires four-way closure by one or several seals to prevent hydrocarbons escaping to shallower levels. Traps are divided into structural, stratigraphic and combination types. Movements of the subsurface have formed structural traps after the deposition of the reservoir rock and the seal was completed, while stratigraphic traps are results of depositional changes that juxtapose reservoir and sealing rocks in a favorable position to trap hydrocarbons. The seals of the traps are usually not efficient until sufficient burial has reduced the permeability and increased the entry pressures to prevent hydrocarbons to leak out (see discussion later). Berg (1975) discussed the trapping potential of a trap and outlined equations for computing the oil column that could be trapped below a seal.

Numerous trap types have been defined. Salt is a nearly perfect seal, and a number of different trap types have therefore been defined around salt domes, along the flanks, over the top and within rim synclines. Combined stratigraphic and structural traps are fairly common. These traps rely on both a stratigraphic seal, for example a pinch out in one direction, and a structural seal, for example a structural ridge, may provide the closure in the other three directions. Early workers on hydrocarbon migration and trapping spent a significant time on defining trapping styles (see Watts, 1987 and Sales, 1993), and used these to correlate the sealing potential of different trap types between different basins. Later research has gone in different directions: (1) depositional and structural modelling to understand and predict how and where traps are formed; (2) fluid flow modelling to understand the filling and sealing of the traps, and (3) measurements of cap-rock sealing properties .

Trap filling

Basin modellers tend to view traps as being dynamic, where filling of a trap is a continuous process that continues frequently over more than 50 million years. This process starts immediately when a source rock in the catchments area of a trap has reached a thermal maturity sufficient to start expulsion and migration of hydrocarbons. The seal above the trap may not be efficient when hydrocarbons migrate into the trap, and hydrocarbons may then migrate through the trap and the seal above to the surface, only leaving a thin migration stringer saturated with hydrocarbons behind. Upon burial, the seal of the trap will become at least partially effective, and hydrocarbons start to fill it. In sedimentary basins with oil generating source rocks, an early phase of oil filling is quite normal. However, many source rocks will also contain some organic material, for example type III kerogen, with quite broad kinetics for the transformation of kerogen to oil and gas. The gas generating part of the kerogen can then start to expel hydrocarbons before the oil-generating fraction, and lead to a very early phase of gas filling of the trap. Often this filling will occur at a time when the seal is starting to become effective, and

only a small gas cap may form within the trap. Increased burial of the source rocks causes effective oil expulsion to start and fills of the trap with liquid hydrocarbons. More and more of the gas cap will be dissolved in the liquid oil as the trap subsides to greater burial depths, and the trap may change from a very small under-filled gas cap to an under-saturated oil filled trap. Further burial of the source below the "oil window" starts to feed the trap with more gas than oil and a gas cap re-develops in the trap. As more and more gas migrates into the trap, oil will start to be pushed out of the trap by the lighter gas, and eventually all the oil is spilled out of the trap into shallower traps. Deep burial also frequently leads to excessive overpressure development, with resulting hydraulic leakage of some or all of the hydrocarbons in the trap. The end result may then be a trap with only oil and gas shows remaining. The above is a typical filling history of a generic, deeply buried trap. Traps that are not buried too deep can be stopped at any stage in the history, and consequently any type of hydrocarbons can be found.

The trap filling process has been studied extensively by geochemical methods. England et al. (1991) discuss the trap filling and mixing of hydrocarbons. Horstad and Larter (1997) applied geochemical investigations to explain the filling history of the Troll Field. Typical of this approach is the difficulty in arriving at unique explanations of the trap filling histories and processes. Biomarkers are typically used to group oil populations. Many geochemical parameters can be interpreted in different ways. It is by combining different parameters and measurement types that workers are able to differentiate oil populations, and suggesf several migration phases for the filling of the traps. Using these techniques, suggestions on whether oil or gas first filled the traps can also be made (e.g. Horstad and Larter, 1997). Oil populations can be mapped in one or several traps and fields, and they can be used to split an oil province into several oil migration systems. There is no significant progress yet, however, in using the indicators in a more quantitative manner, for example as indicators of migration distances. A simple grouping into the prominent source rock types that source the trap (e.g. type I, II, III kerogen) is often attempted.

3. Preservation & destruction.

Sealing & leakage

Entry pressures obtained from laboratory measurements can characterize the sealing potential of cap-rocks. Cores are not easily obtained from exploration wells, and investigations of samples taken from the field will always be affected by their unloading history. Investigations of sealing potential by measuring entry pressures from cuttings have shown some potential, but are not yet performed on a large scale in the industry. Investigations into cap-rock processes rely on good geochemical data and a good understanding of fluid flow in mud-rocks. Leakage of hydrocarbons from traps is attributed to: (1) capillary leakage; (2) hydraulic leakage, and (3) molecular diffusion.

Krooss and Leythaeuser (1988) investigated molecular diffusion extensively by laboratory experiments. Molecular diffusion is today not considered the most important leakage mechanism because it takes too long time to leak out large quantities of hydrocarbons from a trap by this process, in particular for large (fluid phase) molecules. In some cases, with very diffusive and high entry pressure rocks, cap-rock diffusion can be more important. Molecular diffusion may also be an important process when leakage starts, to increase the content of hydrocarbons in the

cap-rock just above the trap, and thereby modify the hydrocarbon saturation profile within the cap-rock.

Capillary pressure leakage (Watts, 1987) can in many cases be demonstrated above fields by estimating the hydrocarbon saturations and mapping out which parts of the cap-rock are saturated with hydrocarbons. One may find that the cap-rock is saturated with hydrocarbons to a certain level (e.g. Leith et al., 1993). The hydrocarbon saturation in the cap-rock can be correlated roughly to measured or inferred entry pressures of the cap-rock sequence, suggesting that capillary leakage may have occurred. The correlation is not straightforward, however, because of the dynamic change of both the filling of the trap and the change of cap-rock properties through time.

The question as to whether hydrocarbon migration through cap-rocks occurs at capillary pressures very close to the entry pressures, and through preferred pathways defined by the entry pressure distribution within the cap rocks, or through two-phase Darcy flow has not been resolved yet in the literature. With the former process description, the rates of leakage are not important. Time becomes unimportant as such and percolation theory can be used to simulate the process. In a Darcy flow process description, flow-rates control the capillary pressures in the pores through which hydrocarbons migrate. The saturation is therefore flow-rate dependent, and the volume of rocks saturated during leakage will therefore be larger for a high flow-rate leakage scenario than for a low leakage rate scenario. A Darcy flow approach to leakage will therefore be more dynamic in the calculations of migration losses, and the maximum leakage rates may have to be determined to estimate how much oil and gas can be lost within the cap-rock. The assumed direction of hydrocarbon migration through the cap-rock will often be very similar in both process descriptions. The Darcy flow may, however, become more spread out, and several small traps can be sourced from the same deeper structure. With percolation, ganglions form to create an oil stringer backbone through which all hydrocarbons later pass (Fig. 3). This leads to an extremely efficient leakage once the threshold pressure has been exceeded by the non-wetting phase (Carruthers and Ringrose, 1998).

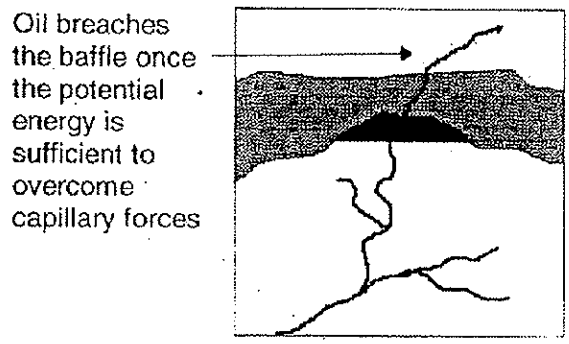

Fig. 3 Generalized view of oil migration using invasion percolation concepts (from Carruthers and Ringrose, 1998).

Hydraulic leakage results when the pore pressures are so large that the effective stress reaches zero. Effective stress, the pressure that is acting on the solid rock framework (Terzaghi and Peck, 1968), is the difference between the weight of the overburden and the pore pressure. Hydraulic leakage is very efficient because the resulting flow occurs through open fractures that

have high permeabilities. These fractures will close when the effective pressure starts to increase, effectively resealing the cap-rock for leakage. Once a fracture has been created in a cap-rock, it will be easier to reopen it at low effective stresses, because the tensile strength has been reduced to zero in the fracture, and resealing, even by diagenetic processes, may not restore the tensile strength. Hydraulic fracturing may be influenced also by tectonic stresses, but these stresses have been very difficult to predict at a prospect level. Traps that have leaked oil through hydraulic fractures tend to have significant volumes of oil remaining within the cap-rock, even though the trap itself may be dry or contain only residual hydrocarbons. Gas chimneys are sometimes associated with hydraulically leaking traps (Løseth et al., 2000).

While the process of hydraulic leakage is well understood, it is extremely difficult to predict prior to the drilling of an exploration well whether hydraulic leakage has occurred. Methods that can be used to predict the pore pressures are very important to assess the risk of hydraulic leakage. New generations of 3D basin fluid flow simulators (Grigo et al., 1991; Borge, 2000) may aid in increasing the predictability of hydraulic leakage occurrence.

Thermal alteration

Hydrocarbons that are exposed to high temperatures may undergo kinetic alteration (cracking) reactions. These reactions crack heavier components into lighter reactions and a residue (coke). Thermal alteration starts already in the source rock, but is also very effective in deep traps. Hydrocarbons in traps with temperatures that exceed 150°C are likely to be affected by thermal alteration. The cracking reactions are slower than those in source rocks because the source rock kerogen contains many catalysts that speed up the kinetic reactions. Artificial maturation experiments in the laboratory are used to quantify oil to gas cracking reactions (Schenk et al., 1997). In order to speed up the kinetic reactions that take millions of years to complete at natural conditions, laboratory temperatures used are much higher than those of the natural system. There are therefore some uncertainties whether the correct reactions occur in the laboratory. The kinetic models that result from artificial maturation experiments of oils do, however, give realistic conversion temperatures when applied to geologic heating rates.

At the resolution of existing experiments, different oil types only play a minor role on the results from laboratory experiments. Recent findings may suggest that the thermal stability of oils is greater than proposed by earlier workers (Tissot and Welte, 1978).

Biodegradation

Biodegradation occurs at relatively low temperatures by organic bacteria that use hydrocarbons as nutrients. The most important control is temperature, and biodegradation is observed at temperatures less than 80°C. A good supply of oxygen enhances the activity. The process is usually so fast that time does not seem to be a first-order constraint for the biodegradation process. Biodegradation can be classified into light, moderate and heavy biodegradation. Heavy biodegradation can result in major problems in producing oil fields, and some discoveries may not be possible to produce at all. Palaeo-biodegradation can be observed in some discoveries, and old biodegraded oil may partly have been flushed out by a new "fresh" oil phase that migrated into the trap at temperatures above the maximum temperatures for biodegradation. The biodegradation process causes oil to be converted to heavier and longer component groups together with light gas components.

Heavy biodegraded oil has a low API and is therefore easy to detect. Lower degrees of biodegradation can be observed from biomarkers in the oils. Although biodegradation has been demonstrated in the laboratory (both aerobic and anaerobic), the process has traditionally been described from an empirical viewpoint because access to biodegraded oil samples has been relatively easy (e.g. Horstad and Larter, 1992). Ranking schemes therefore dominate over mathematical/numerical models in the analysis of this process. Carpentier (2002) proposes a model for biodegradation based upon number of bacteria, hydrocarbon type preference, temperature, porosity, water saturation and water fluxes. The process is considered to contain a post-filling and in-filling part, where post-filling biodegradation acts on uplifted fields, while in-filling biodegradation occurs when hydrocarbons migrate into low-temperature traps. Okui and Tamura (2001) used basin-modelling techniques to elucidate on the biodegradation effects in some fields in the North Sea. This is an approach that is likely to be used extensively, particularly as 3D modelling of fluid flow at basin scales becomes more common.

Water washing and deasphalting

Trapped hydrocarbons can be affected by a number of processes in addition to thermal alteration and biodegradation. Water washing occurs when water flushes the reservoir without removing all the hydrocarbons, but stripping only some of the components from the oil. The most water-soluble components are the ones being removed. Tissot and Welte (1978) defined deasphalting as the precipitation of asphaltenes from heavy to medium crude oil by the dissolution in the oil of large amounts of gas and/or other lighter hydrocarbons in the range from C1 to C6. While these processes are relatively easy to understand conceptually, successful attempts to make detailed models that can be used for prediction of properties away from existing wells have not yet been made. This may in part be because of the complexity of the problem, but also because of a general lack of tools available to make quantitative predictions of hydrocarbon component (groups) in traps. The earlier works of Tissot and Welte (1978) and Palmer (1991) are therefore still state of the art.

B. Evaluation

The main objectives of an evaluation of hydrocarbon migration and entrapment in oil companies are to constrain and reduce economic risk in the exploration for oil and gas. Migration is often considered a part of the "source risk" or "hydrocarbon charge" topic. One of the main tasks of the assessment will be to arrive at a probability that a prospect contains an economic quantity of oil and/or gas. Modern techniques of risk assessment often use Monte Carlo simulation techniques to compile overall probabilities for prospects and licenses before a possible drilling is decided upon. The risk for migration can vary from 0 to 100%, and therefore the chosen risk can be extremely important for the ranking of prospects.

Traditionally, the assessment of migration has been performed through the use of expert opinions. Over the last 10 years, more quantitative methods have been introduced into the exploration phase, but still today (2002), many prospects will be drilled completely without any quantitative assessment of migration.

1. Primary and secondary migration

With the introduction of 1D basin modelling, it has been possible to model the thermal maturity of kerogen quickly and with some degree of confidence in an exploration setting, where time for analysis will always be a constraint. During the 1990's many of the 1D basin simulators have added expulsion modelling and also some limited functionality for primary migration efficiency calculations have been achieved (Okui and Waples, 1993). The 1D type of simulators have mostly avoided fluid flow modelling, e.g. pressure modelling, and have therefore been extremely quick to use and have not required exceptional skills to learn. Therefore 1D simulators are used by many (more than 1000) geologists.

The 2D basin simulators have also been introduced into the oil industry during the 1990's. These simulators have been used to study flow patterns, both pressures and hydrocarbon migration. Typically, the 2D simulators model the process in depth and along a profile, and vertical burial with limited fault functionality has been the norm. Quantitative estimates of trapped hydrocarbon volumes could not be calculated, but predictions of phases in traps have been made with some success. The compositional simulators have also attempted to predict more accurately the history of phases and hydrocarbon components in traps, increasing the probability of predicting e.g. condensate traps.

Map migration techniques use a 2D approach where the two lateral spatial coordinates are used and hydrocarbon migration is simulated along a single carrier through time (Skjervøy and Sylta, 1993; Symington et al., 1998). Also these tools have used only vertical burial of the sediments, but the capability of handling lateral fault seal has been incorporated into many of the tools (e.g. Sylta, 1993).

Full 3D hydrocarbon secondary migration using, for example, Darcy flow, relative permeabilities and related numerical techniques, are starting to be used. These techniques have problems in retaining a sufficient resolution of the geologic model if simulation times are to be kept reasonable. Use of 3D percolation simulation techniques, based upon the methods of Carruthers and Ringrose (1998), has been proposed as a fast approach to modelling secondary migration. This approach can be combined with Monte Carlo simulation techniques even for very large numerical models.

2. Entrapment

The analysis of hydrocarbon entrapment typically makes extensive use of organic geochemical methods. Different types of investigations may be employed to group trapped hydrocarbons into "families", which again allows for assessments on how the trap was filled with hydrocarbons. Future analyses will most likely combine these methods with input from (secondary) migration modelling. The tracing of different oils from their sources to their traps may be done in new computer simulators that can support already established organic geochemistry methods of source-oil fingerprinting.

The analysis of entrapment today uses elements from fault seal analysis, such as clay smear modelling of important faults. This analysis can indicate whether a particular fault has been sealing or open, where the sealing characteristics change, and therefore if or where hydrocarbons may have entered a particular trap. This information can be crucial as to whether the trap will be

filled with oil or gas. This type of analysis results in information that is considered quite sensitive by the oil companies, and publication of results from applications can be expected to be few.

PVT modelling can be used to improve phase predictions in entrapment analysis. Component distribution of trapped hydrocarbons can be taken from oil samples from nearby wells and phase diagrams may be constructed. The difference in behavior of different hydrocarbon families can be elucidated, and used to assess the condensate concentration in traps (di Primio et al., 1998). Seismic AVO modelling techniques are starting to be used for assessing possible hydrocarbon fill in undrilled prospects directly from seismic (Davies et al., 2002).

3. Preservation & destruction

The analysis of preservation and destruction of hydrocarbons includes quantifying and risking the processes of: (1) hydrocarbon leakage; (2) thermal cracking of oil; (3) biodegradation, and (4) water washing and deasphalting . The most important process to quantify will often be the hydrocarbon leakage, while the cracking and biodegradation problems are often converted to simple depth ranges for the traps and prospects. The prospect risk is then considered much higher outside the favourable depth ranges. Water washing and deasphalting are problems that are studied when they are encountered, while generally little emphasis is put on these processes before exploration drilling.

Hydrocarbon leakage assessments can be based on a quantification of overpressures for determining hydraulic leakage. It has been common to create overpressure maps using a geological expert who interpolates overpressures from well data and using assumed fault seal to delineate pressures compartments with similar pressures. Borge and Sylta (1998) suggested using a modelling technique to facilitate the same, but using a quantitative model for fault transmissibilities. The use of 2D pressure modelling has been employed quite extensively during the 1990's as an aid in making predictive models of overpressure distributions along transects. The transects are typically located along the steepest gradient of the basin, where rapid changes in overpressures are likely to be modeled.

The 2D transect modelling technique has also been used to quantify leakage rates due to hydraulic fracturing and capillary leakage. Because both pressures and temperatures can be fairly well constrained in a 2D simulator, all the processes involved in the preservation and destruction of hydrocarbons in traps can be accounted for. This gives perhaps the best approach to the analysis of these processes today.

The preservation and destruction of pore space in traps is not strictly a migration problem. Nevertheless, it is important to note that the compaction and diagenetic processes affecting porosities are crucial to the analysis of hydrocarbon preservation and destruction. Methods for modelling these diagenetic processes were introduced in 1990's (Walderhaug, 1996).

The major challenge for the evaluation methods is to become more predictive. Many of the processes that involve the preservation and destructions of hydrocarbons in traps are highly non-linear, and all aspects of the processes are not understood, e.g. biodegradation and water washing. Future research into these topics may benefit from advances in other research fields.

4. Risk & Economics

Oil companies aim to determine risk factors for hydrocarbon migration (sourcing) before they decide whether they want to pursue the licensing and/or drilling of traps and prospects. Traditionally, the geological and geophysical experts have been able to determine this risk factor by expert opinions based upon existing basin specific knowledge. One disadvantage of this approach has been that surprises (dry wells) are quite common because geological conditions change from trap to trap. Even small changes may cause a seal to leak in one trap while being effective in another.

Regional geological studies have traditionally been used as risk constraints. Recently, the use of regional migration modelling studies has also helped in the description of prospect risk. The use of full 3D hydrocarbon migration simulations is now being introduced to the oil industry. A few commercial packages are being marketed. The advantages of these packages are many. One of the most important facilities of 3D simulators is that they encourage geologists to create integrated models that explain not only a few but nearly all of the observations. Extensive calibration of the system to geologic observations allows for building complex models that consistently explain the observed temperatures, pressures, maturity indicators and hydrocarbon trapping. It is then simpler to arrive at consistent risking of prospects within that particular study area. One may still be too optimistic or pessimistic within one particular study area, but consistency between traps is maintained, and the ranking of prospects becomes simpler.

High resolution modelling techniques can in the future become more tightly integrated with economic risk assessment. Today's practice seems to be to reduce the geologic risks down to a few economic figures for each trap, and then do the economics for only one or at most two geologic scenarios. The reason for this is that the economic assessment has to decide which type of platform to use, and the calculations take time to perform. Krokstad and Sylta (1997) showed that it is possible to derive more complete probability distributions for the volumes of trapped hydrocarbons in each trap. In the future, one may derive faster schemes for economic assessments and combine these with integrated high resolution basin modelling to derive better economic risk probability distributions for each trap. The advantages will be that one can more realistically assess the economic consequences of most of the possible geologic outcomes from drilling a well in a new trap.

5. Trends and Perspectives

Numerical modelling techniques are becoming more and more important for the study of migration, entrapment and preservation of hydrocarbons. Field work remains important to provide a basis for new geological insights into the processes. Laboratory work remains an under-utilized topic in this field, in particular to investigate and demonstrate hydrocarbon migration cases, for example migration across and along faults. New techniques that can account for a more dynamic geology during simulations will have to be developed to account properly for salt movements and structural inversion.

As computers become more powerful, there is a trend towards modelling with larger geological models. Just as important will, however, be the trends towards improved handling of uncertainties. Monte Carlo simulation is just one approach that can be used to quantify uncertainties and give improved probabilities for estimates of trapped hydrocarbons.

It is anticipated that in the near future oil companies will start to employ hydrocarbon migration simulation tools at a larger scale. The need for improved models and tools may result in a significantly increased effort in hydrocarbon migration research in the next decade.

References:

Berg, R. R. 1975. Capillary pressures in stratigraphic traps. American Association of Petroleum Geologists Bulletin 59, 939-956.

Borge, H. 2000. Fault controlled pressure modelling in sedimentary basins. Doktor Ingeniør Thesis 2000:22. Department of Mathematical Sciences, Norwegian University of Science and Technology.

Borge, H, Sylta, Ø. 1998. 3D Modelling of fault bounded pressure compartments in the North Viking Graben. Energy Exploration & Exploitation 16, 301-323.

Carpentier, B. 2002. New concepts for biodegradation evaluation in oil fields, a combined geological and numerical approach. Presented at the AAPG Annual Conference, March 2002. Abstract only.

Carruthers, D., Ringrose, P. 1998. Secondary oil migration: oil-rock contact volumes, flow behaviour and rates. In: Parnell, J. (ed.). Dating and Duration of Fluid Flow and Fluid-rock Interaction. Geological Society of London, Special Publication 144, 205-220.

Davies, D. J., Mcinally, A., Barclay, F., 2003. Lithology and fluids prediction from amplitude versus offset (AVO) seismic data. Geofluids volume 3, number 4, 219-232.

Dembicki, J.R.H, Andersen, M.J. 1989. Secondary migration of oil: experiments supporting efficient movement of separate, buoyant oil phase along limited conduits. American Association of Petroleum Geologists Bulletin 73, 1018-1021.

di Primio, R.; Dieckmann, V., Mills, N. 1998. PVT and phase behaviour analysis in petroleum exploration. Organic Geochemistry 29, 207-222.

England, W.A., Mann, A.L., Mann, D.M. 1991. Migration from source to trap. In: Merrill, R.K. (ed.). Source and Migration Processes and Evaluation Techniques. Treatise of Petroleum Geology Handbook of Petroleum Geology. American Association of Petroleum Geologists.

Frette, V., Feder, J., Jøssang, T., Meakin, P. 1992. Buoyancy driven fluid migration in porous media. Physics Review Letters 68, 3164-3167.

Grigo, D., Maragna, B., Arienti, M.T., Fiorani, M., Parisi, A., Marrone, M., Sguazzero, P. Uberg, A.S. 1993. Issues in 3D sedimentary basin modelling and application to Haltenbanken, offshore Norway. In: Dore A.G. et al. (eds.). Basin Modelling: Advances and Applications. NPF Special Publication 3, 455-468.

Horstad, I., Larter, S.R. 1997. Petroleum migration, alteration, and remigration within Troll field, Norwegian North Sea. American Association of Petroleum Geologists Bulletin 81, 222-248.

Horstad I., Mills N., Larter S.R. 1992. A quantitative model of biological petroleum degradation within the Brent Group reservoir in the Gullfaks Field, Norwegian North Sea. Organic Geochemistry 19, 107-117.

Hubbert, M. K. 1953. Entrapment of petroleum under hydrodynamic conditions. American Association of Petroleum Geologists Bulletin 37, 1954-2026.

Ingram, G.M. Urai, J.L., Naylor, M.A. 1997. Sealing processes and top seal assessment. In: Møller-Pedersen, P., Koestler, A.G. (eds.). Hydrocarbon Seals. Importance for exploration and production. NPF Special Publication 7, 165-174.

Knipe, R. J. 1997. Juxtaposition and seal diagrams to help analyze fault seals in hydrocarbon reservoirs. American Association Petroleum Geologists. Bulletin 81, 187-195.

Krooss, B. M., Leythaeser, D. 1988. Experimental measurements of the diffusion parameters of light hydrocarbons in water-saturated sedimentary rocks - II. Results and geochemical significance. Organic Geochemistry 12, 91-108.

Kroos, B.M., Hanebeck, D., Leythaeuser, D. 1993. Experimental investigation of the molecular migration of light hydrocarbons in source rocks at elevated temperature. In: Dore A.G. et al. (eds.). Basin Modelling : Advances and Applications. NPF Special Publication 3, 277-291.

Krokstad, W., Sylta, Ø. 1997. Risk assessment using volumetrics from secondary migration modelling: assessing uncertainties in source rock yields and trapped hydrocarbons. In: Dore, A.G., Sinding-Larsen (eds.). Quantification and Prediction of Petroleum Resources, NPF Special Publication 6, 219-235.

Leith, T.L., Kaarstad, I., Connan,J., Pierron, J., Caillet, G. 1993. Recognition of caprock leakage in the Snorre Field, Norwegian North Sea. Marine and Petroleum Geology 10, 29-41.

Leythaeuser, D., Mackenzie, A., Schaefer, R. G., Bjorøy, M. 1984. A novel approach for recognition and quantification of hydrocarbon migration effects in shale sandstone sequences. American Association of Petroleum Geologists Bulletin 68, 196-219.

Leythaeuser, D., Schaefer, R. G., Yukler, A. 1982. Role of diffusion in primary migration of hydrocarbons. American Association of Petroleum Geologists Bulletin 66, 408-429.

Løseth, H., Gading, M., Wensaas, L. 2000. Location of leakage points and timing of leakage from seismic data. Hydrocarbon Seal Quantification Conference. 16-18 October 2000. Extended abstracts, 187-190.

Mackenzie, A. S., Leythaeuser, D., Schaefer, R. G., Bjorøy, M., 1983. Expulsion of petroleum hydrocarbons from shale source rocks. Nature 302, 506-509.

MacKenzie, A.S., Price, I., Leyheuser, D., Muller, P. Radke, M, Shaefer, R.G. 1987. The expulsion of petroleum from Kimmeridge Clay source-rocks in the area of the Brae Oilfield, UK Continental Shelf. In: Brooks,.J., Glennie, K.W. (eds.). Petroleum Geology of North West Europe. Graham and Trotman, 865-877.

Okui, A., Tamura, S. 2001.Integrated geochemical and basin modeling study on biodegradation process in the UK North Sea. Presented at the 20th International Meeting on Organic Geochemistry, August 2001. (Abstract only).

Okui, A., Waples, W., 1993. Relative permeabilities and hydrocarbon expulsion from source rocks. In: Dore A.G. et al. (eds.). Basin Modelling: Advances and Applications. Norwegian Petroleum Society Special Publication 3. Elsevier, Amsterdam, 293-301.

Palmer, S.E., 1991. Effect of biodegradation on water washing on crude oil composition. In: Merrill, R.K. (ed.). Source and Migration Processes and Evaluation Techniques. American Association of Petroleum Geologists Treatise of Petroleum Geology, Handbook of Petroleum Geology.

Pepper, A. S., Corvi, P. J.1995. Simple kinetic models of petroleum formation. Part III: Modelling an open system. Marine and Petroleum Geology 12, 417-452.

Sales, J., 1993. Closure vs. seal capacity – a fundamental control on the distribution of oil and gas; In: Dore A.G. et al. (eds.). Basin Modelling: Advances and Applications. Norwegian Petroleum Society Special Publication 3. Elsevier, Amsterdam, 399-414.

Schenk H.J., di Primio R., Horsfield, B. 1997. The conversion of oil into gas. Part 1: Comparative kinetic investigation of gas generation from crude oils of lacustrine, marine and fluviodeltaic origin by programmed-temperature closed-system pyrolysis. Organic Geochemistry 26, 467-481.

Schwolter, T. T. 1979. Mechanics of secondary hydrocarbon migration and entrapment. American Association of Petroleum Geologists Bulletin 63, 723-760.

Schøn, J.H. 1996. Physical properties of rocks. Fundamentals and Principles of Petrophysics. In: Helbig, K., Treitel, S. (eds.). Handbook of Geophysical Exploration, Seismic Exploration Volume 18. Elsevier. 583p.

Selle, O.M., Jensen, J.I., Sylta, Ø., Andersen, T., Nyland, B., Broks, T.M. 1993. Experimental verification of low-dip, low-rate two-phase (secondary) migration by means of gamma-ray absorption. In: Parnell, J. et al. (eds.). Geofluids'93. Contributions to an International Conference on Fluid Evolution, Migration and Interaction in Rocks, 72-75.

Skjervøy, A., Sylta, Ø., 1993: Modelling of expulsion and secondary migration along the southwestern margin of the Horda Platform; In: Dore A.G. et al. (eds.). Basin Modelling: Advances and Applications. Norwegian Petroleum Society Special Publication 3. Elsevier, Amsterdam, 499-537.

Stainforth, J.G., Reinders, J.E.A., 1990. Primary migration of hydrocarbons by diffusion through organic matter networks, and its effect on oil and gas generation. In: Advances in Organic Geochemistry, 1989. Organic Geochemistry, 16-74.

Sylta, Ø., Pedersen, J. I., Hamborg, M. 1998. On the vertical and lateral distribution of hydrocarbon migration velocities during secondary migration. In: Parnell, J. (ed.). Dating and Duration of Fluid Flow and Fluid-Rock Interaction. Geological Society London, Special Publication 144, 221-232.

Symington, W.A., Green, K.E., Huag, J., Pottorf, R.J., Suma, L.L. 1998. A multidisciplinary approach to modelling secondary migration: a Central North Sea example. In: Duppenbecker, S.J., Iliffe, J.E. (eds.). Basin Modelling: Practice and Progress. Geological Society of London, Special Publication 141, 169-186.

Terzaghi, K., Peck, R.P. 1968. Soil Mechanics in Engineering Practice. Wiley, New York.

Tissot, B.P., Welte, D.H. 1978. Petroleum Formation and Occurrence. A New Approach to Oil and Gas Exploration. Springer Verlag. 538 p.

Walderhaug, O. 1996. Kinetic modelling of quartz cementation and porosity loss in deeply buried sandstone reservoirs. American Association of Petroleum Geologists Bulletin 80, 731-745.

Watts, N. 1987. Theoretical aspects of cap-rock and fault seals for single- and two-phase hydrocarbon columns. Marine and Petroleum Geology 4, 274-307.

Yielding, G., Freeman, B., Needham, D. T. 1997. Quantitative fault seal prediction. American Association of Petroleum Geologists Bulletin 81, 897-917.

CHAPTER 3

3. Experimental verification of low-dip, low-rate two-phase (secondary) migration by means of gamma-ray absorption.

Experimental verification of low-dip, low-rate two-phase (secondary) migration by means of γ-ray absorbtion

O.M. SELLE, J.I. JENSEN, Ø. SYLTA, T. ANDERSEN, B. NYLAND[1], T.M. BROKS[2]

IKU Petroleum Research, N-7034 Trondheim, Norway
[1]Norwegian Petroleum Directorate, P.O.Box 600, N-4001 Stavanger, Norway
[2]Statoil, P.O.Box 300, N-4001 Stavanger, Norway

Abstract: Two 60 cm long water-saturated cores of Bentheimer and Berea sandstones were subjected to low rate (0.1 ml/hour) migration of dodecane. During the experiment the change in water saturation was measured indirectly by means of gamma-ray absorption, which varied with water saturation. Measurements were obtained at 0.15 cm intervals along the core and at height increments of 0.5 and 1 cm for the two cores. Breakthrough of dodecane flow was obtained after several hundred hours. A standard black-oil reservoir simulator was used to compare the observed saturation distribution and flow rates with those obtained using standard capillarity and relative permeability relationships. The experimental results show that the secondary migration process is sufficiently slow to occur at hydrostatic equilibrium. The oil saturation can therefore be determined as a function of capillary pressure and height. These can be computed by iterative procedures when oil flow-rates are known.

The experiments of Dembicki & Anderson (1989) showed that vertical oil migration occurs along preferred pathways and at high saturations once a continuous phase has been formed. Dembicki & Anderson (1989) also suggested that lateral migration favours preferred pathways, and therefore that the secondary migration process may be considered a two- (or three-) phase bulk-flow process.

England et al. (1987) proposed secondary migration at high oil saturations. They list pore space requirements for oil through rocks varying from 24% to 91%, depending on porosity and lithology (England et al., 1987, Table 4). Their data were obtained from the study of oil breakthrough in laboratory cores of typical reservoir rocks. However, definite conclusions as to the underlying processes could not be reached before the oil saturation distribution within the cores was measured during the experiment.

Therefore this paper aims first to measure the oil saturation distribution in homogenous cores under standard conditions and during low migration velocities. Thereafter we use a standard black-oil reservoir simulator to verify the applicability of standard capillarity and relative permeabilities in secondary migration.

ROCK AND FLUID PROPERTIES

The Bentheimer core (Table 1) is a homogeneous sandstone with high quartz content (93%), and only 3% feldspar/carbonate and 4% clay. The Berea sandstone (Table 1) by contrast is stratified and has a low permeability. To avoid any vertical restrictions the Berea sample was orientated with the stratification aligned vertically. Both rock samples used were characterized by mini-permeameter measurements along all 4 sides and both ends. Measurements were done using Statoil's mini-permeameter rig with a spacing of 5 mm in the x- and y-directions. These measurements were used to construct a three-dimensional permeability distribution for the simulation work. Figure 1 shows capillary pressure curves for the two rocks.

Table 1. Rock properties for two sandstone outcrop samples. Porosity is based on brine saturation, and permeability is absolute brine permeability. L = Length of sample, H = Height of sample, W = Width of sample.

Rock type	Dimensions	Porosity	Pore vol.	Permeability
Bentheimer	L = 60.60 cm H = 5.08 cm W = 5.10 cm	22.6 %	345 cm^3	2.26 D
Berea	L = 60.00 cm H = 5.00 cm W = 5.00 cm	18.4 %	274 cm^3	0.066 D

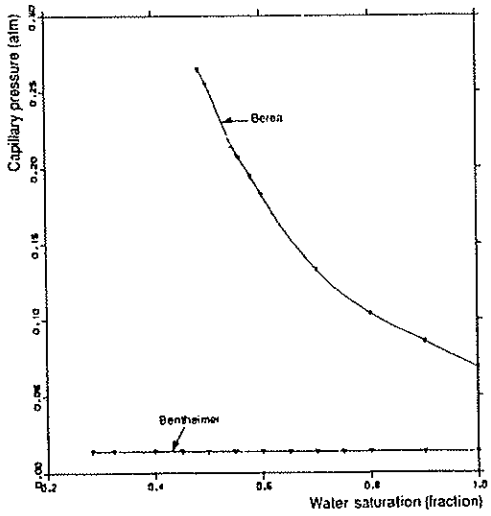

Figure 1. Capillary pressure curves.

EXPERIMENTAL PROCEDURE

The experimental set-up is shown in Figure 2. In order to represent the low-dipping formations typically found in the North Sea, the dip of the rock sample was set to 7.5° in the γ-ray apparatus. The γ-ray source and receiver was moved on a table along the rock sample at height increments of 0.5 cm for the Bentheimer sample and 1 cm for the Berea sample. Oil injection was from an oil column of constant height in the Bentheimer experiment, and from a low-rate syringe pump in the Berea experiment. Injection rates, oil and water production and differential pressures were recorded during the experiment.
Epoxy was used to coat the rock samples. End pieces of teflon were glued onto the Bentheimer sample, while the Berea sample was epoxyed at the ends. The inlet tube was placed in the middle of the inlet side base. The whole of the outlet side was opened into a chamber. The outlet tube was placed in the middle at the top. γ-ray attenuation was used to determine oil migration inside the sample. Fluid properties are listed in Table 2.

The experimental procedures were as follows:

1) Evacuation of sample, injection of CO_2, and evacuation once more.
2) Saturation of sample with dodecane. Vertical flooding.
3) Horizontal permeability measurement.
4) Dodecane calibration of sample by γ-ray measurements.
5) Cleaning of sample with toluene and isopropanol.
6) Evacuation of sample as in 1).
7) Saturation of sample with brine as in 2).
8) Permeability measurement as in 3).
9) Brine calibration as in 4).
10) Migration experiment.

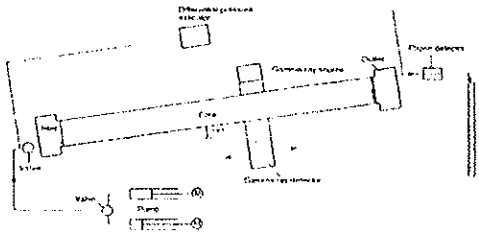

Figure 2. Experimental setup

EXPERIMENTAL RESULTS

Important experimental results are listed in Table 3. The high permeability sample had a much lower entry pressure than the low permeable sample. The entry pressures correspond well with centrifuge-measured capillary pressure from core-plugs. The oil flow rates in the first experiment were controlled by the column height of the injected oil, while the second experiment tried to match the rates using a syringe pump.

The resulting production out of the cores is shown in Figures 3 and 4. Surprisingly, the oil saturations of the samples at breakthrough were almost identical (Table 3). However, the oil distributions were drastically different (Fig. 5). In the high permeability rock, the oil moved immediately to the top and followed the upper surface to the outlet (Fig. 5a). Buoyancy controls the migration, due to the low capillary pressure. It is possible to drain the water down to low saturation with a minor increase in pressure, as seen from the capillary pressure curve. The experiment was terminated when appreciable water production stopped. If the migration pressure is equal to the capillary pressure, the height of the oil column can be calculated (in Darcy units):

$$h = \frac{1.0133 * 10^6 \cdot P_c}{\Delta\rho \cdot g} = 1.6 \text{ cm, which is}$$

in the range observed.

Almost all migration took place in the upper part of the sample, accompanied by a high oil saturation (irreducible water saturation). Virtually no oil migrated in the middle and lower parts of the core, except for the area at the front. For high permeability rocks, it is therefore fair to ignore the negligible capillary pressure effects and consider buoyancy as the main driving force.

In the low permeability Berea rock, the oil saturated the whole core (Fig. 5b), with a low oil saturation in the migration front and an increase in the saturation behind the front. The injection pressure gave a water saturation of 0.80 on the capillary pressure curve. This is in accordance with the saturation measured in the sample. The height of the oil "column" would now be 7.6 m. The oil/water "contact" is therefore well below our sample.

Table 2. Fluid properties

Fluid	$\rho_{20°C}$	$\mu_{20°C}$	$\gamma_{20°C}$	Comments
Dodecane	0.74 g/ml	1.470 cp	33.7 mN/m	γ=brine/dodecane
Brine	1.01 g/ml	1.004 cp		3 wt% NaCl

Table 3 Data from the migration experiments.

Activity	High permeability sandstone	Low permeability sandstone
Pressure at migration startup	0.0295 atm	0.100 bar
Volume oil at breakthrough	36.0 ml	29.0 ml
Oil saturation	10.4 %	10.6 %
Rate of oil migration	0.096 ml/h	0.115 ml/h
Breakthrough time	375 hours	252 hours
Rate of migration after breakthrough	0.12 ml/h	

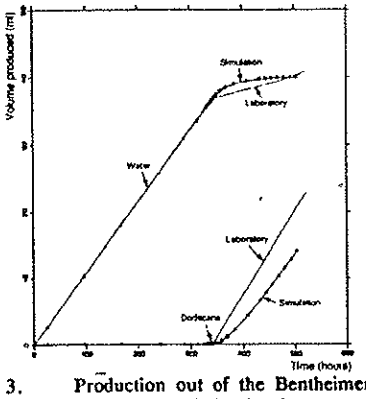

Figure 3. Production out of the Bentheimer core (measured and simulated).

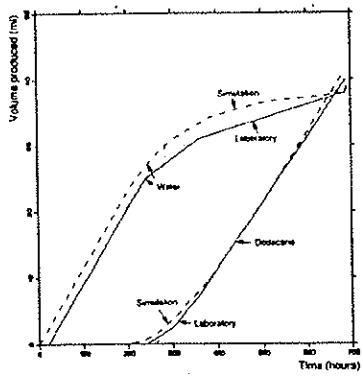

Figure 4. Production out of the Berea core (measured and simulated).

For experimental reasons, migration had to be stopped before water production stopped. The results suggests that the migration in the low permeability sample is strongly influenced by the capillary pressure. The oil saturation during migration corresponds to the saturation derived from the capillary pressure curve, and the height of the oil column is therefore bigger than the height of our sample.

VERIFICATION BY SIMULATION

The main objectives of the computer simulations were to match the production histories and final saturations obtained from the laboratory experiments, and thus verify the active forces in the systems. The simulations of the core flood experiments were performed using a fully implicit black-oil simulator.

A two-dimensional grid with 45 grid blocks in the horizontal (x) and 15 grid blocks in the vertical direction was constructed. 43 of the blocks in the x direction represented the cores, and two of the blocks, one at each end of the grid, represented the dead end volumes.

One of the end blocks was saturated with dodecane and the other with water. Their capillary pressures were both set to zero. Two-phase relative permeabilities were modelled with straight lines. The oil-water capillary pressure curves used in the simulations of experiment 1 and 2 are shown in Figure 1. These and the relative permeability curves were input variables, adjusted to match the results of the experiments.

The two-dimensional grid was tilted 7.5° and initialized with 100% water. Dodecane was injected through the lower part of the lowest end with a constant rate of 0.112 cm^3/hour. The fluids were produced through the upper end of the grid.

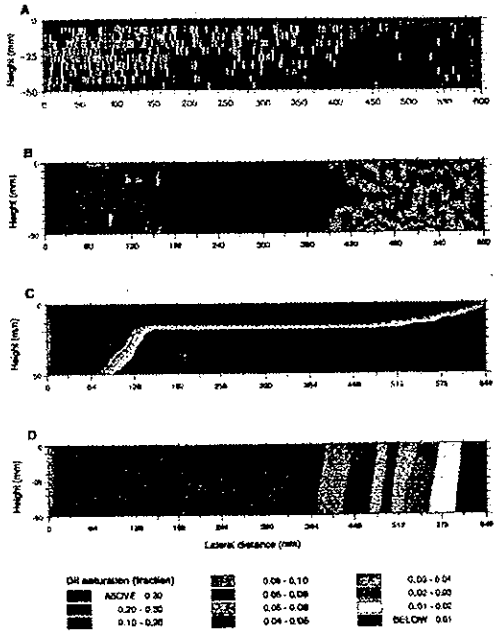

Figure 5a. Measured dodecane saturation distribution at 330 hours. Bentheimer core.

b Measured dodecane saturation distribution at 335 hours. Berea core.

c Modelled dodecane saturation at 330 hours. Bentheimer core.

d Modelled dodecane saturation at 335 hours. Berea core.

SIMULATION OF EXPERIMENT 1: BENTHEIMER

To examine the effect of relative permeability, capillary entry pressure (Pc_e) and capillary pressure (Pc), three different cases were simulated. The volume of injected dodecane and the produced fluids for all of the cases are shown in Figure 3. The stippled lines indicate the experimental values and the solid lines indicate the simulation results.

Reducing the oil relative permeability curve (Krow) from a linear shape to a strongly curved shape with capillary pressure set to zero changed the breakthrough time of the oil from 24 hours to 144 hours.

The simulation of the fluids under the absence of capillary pressure is strongly dominated by vertical segregation. This leads to the conclusion that displacement velocity is controlled by the relative permeabilities, and that the vertical segregation is controlled by gravitational forces.

We increased the entry pressure (Pc_e) from zero to 0.014 atm and linearly increased the absolute capillary pressure to 0.0144 atm at connate water saturation. Oil breakthrough was now modelled to occur at 340 hours.

The production of fluids (Fig. 3) and the final fluid saturations (Fig. 5c) obtained by simulation and experimental measurements correspond well, but are by no means perfect.

The oil saturation profile at the front of the migration process shows that 1.6 cm of the upper part of the core is completely saturated with oil at any time. Gravitational and capillary forces can explain this phenomenon. The net maximum capillary force (Pc) is defined as:

$Pc = Pc_{max} - Pce = 4x10^{-4}$ atm (0.0144 - 0.0140).

The maximum gravity force (F_{max}) is defined as (in Darcy units):

$$F_{max} = \frac{(\rho w - \rho o)\ g \cdot h}{1.0133 * 10^6} = 12.58 * 10^{-4} \cdot h$$

F_{max} = gravity forces (atm)
ρw = water density (g/cm^3)
ρo = oil density (g/cm^3)
g = acceleration constant (cm/s^2)
h = height of oil column from oil-water contact (cm)

The oil rises in the core until it reaches a height h above the oil water interface, at which point capillary - gravitational (hydrostatic) equilibrium is achieved:

$$Pc = 2.517 * 10^{-4} \cdot h$$

When $Pc < F_{max}$ ($h = 5$ cm) the segregation will stop at $h = 1.6$ cm, which satisfies a capillary pressure of 4×10^{-4} atm.

Behind the front, dynamic pressure is higher and a higher capillary pressure results. Since the maximum Pc and maximum oil saturation are achieved, the oil saturation behind the front will equal the front saturation.

SIMULATION OF EXPERIMENTS: BEREA

The permeability of the Berea sandstone is approximately 50 times lower and the maximum capillary pressure is 18 times higher than in the Bentheimer sandstone.

The same cases as in Experiment 1 were simulated. The simulations used laboratory measurements of relative permeabilities and capillary pressure. The capillary entry pressure (Pce) was changed from 0.0763 atm to 0.068 atm to match the reported results from the laboratory experiments.

The simulated results of production and saturation profiles are presented in Figures 4 and 5d and correspond very well with the results from the laboratory experiments. The saturation profile of the migration front was totally changed from that of Experiment 1. The oil now covered the total height of the core. The average oil saturation at the front is 1.3%, increasing behind the front to 20%.

The net maximum capillary pressure (Pc) for the Berea core is 0.2 atm, which is higher than the maximum gravity forces ($F_{max} = 12.6x10^{-4}$ atm).

A capillary - gravity equilibrium is observed when the maximum capillary pressure in the migration front equals the gravity forces:

$$Pc = F_{max}$$

The oil saturation equals 1.3% at this Pc ($Pce + F_{max} = 0.0692$ in Fig. 1), which is in agreement with the observed results. The dynamic oil pressure is higher behind the front and a higher capillary pressure and oil saturation is therefore created. This leads to the conclusion that capillary gravity equilibrium will be achieved in the front, and that saturation will be a result of the lowest of the two forces. It is concluded that the migration velocity is controlled by both relative permeability and capillary entry pressure.

CONCLUSIONS

The direction of oil movement in a dynamic water system is determined from hydrodynamic forces as well as buoyant, gravity and capillary forces. The condition for fluid potential equilibrium is simply that of hydrostatic equilibrium for which the saturation distribution can be determined as a function of capillary pressure and height as:

$$Pc\ (Sw) = \frac{\Delta \rho g h}{1.0133x10^6}$$

The conditions for vertical equilibrium are the existence of vertical permeability, the density difference between the fluids, a capillary transition zone, low fluid viscosities, low injection rates, and independence of reservoir thickness.

In summary, the process of secondary migration is sufficiently slow to enable a flow in hydrostatic equilibrium. Therefore losses during migration may be calculated from an equilibrium profile. This profile can be obtained from capillary pressure curves and relative permeablity curves when the flow rates are known.

REFERENCES

DEMBICKI, JR., H. & ANDERSON, M.J., 1989. Secondary migration of oil: experiments supporting efficient movement of separate, buoyant oil phase along limited conduits. American Association of Petroleum Geologists Bulletin, 73, 1018-1021.

ENGLAND, W.A., MACKENZIE, A.S., MANN, D.M. & QUIGLEY, T.M., 1987. The movement and entrapment of petroleum fluids in the subsurface. Journal of the Geological Society, London, 144, 327-347.

Chapters 4, 5, 6 and 7 are not included due to copyright.

CHAPTER 8

8. Secondary migration in a 2D visual laboratory model.

Z-99 SECONDARY MIGRATION IN A 2D VISUAL LABORATORY MODEL

F. VASSENDEN [1,2], Ø. SYLTA[1], C. ZWACH[3]
[1] SINTEF Petroleum Research, NO-7465 Trondheim, Norway.
[2] Now at Statoil.
[3] Norsk Hydro.

Abstract

Reservoirs and cap-rocks undergo burial during geological time. Hydrocarbons migrate into and fill traps during periods of active expulsion from source rocks. The supply of oil and gas can be abundant until deep burial stops the supply. Capillary leakage of oil and gas from the trap can then potentially decrease the size of the accumulation. A laboratory study of filling into and leakage out of a trap has been undertaken with a visual 2D laboratory model. The model defined a synthetic cap rock having a finite entry pressure overlying a permeable reservoir rock. The trap was formed by imbedding a pyramid-shaped layer of smaller glass beads in a pack of larger glass beads.

During migration of oil into the trap, the oil column in the trap was found to build up to an entry column height, at which leakage through the seal started. A steady state oil filling level was observed at a maximum column height slightly higher than the entry height. When the oil supply to the trap was stopped, the trap emptied to 35% of the entry column height. By repeated filling, no leakage occurred until the oil level reached the original entry level. The emptying of the trap to 35% was also repeated.

The behaviour is explained quantitatively by a theory of capillary snap-off, based on the geometry of the pore space in the glass bead pack. With no adjustable parameters, the theory predicts the oil column after leakage to be 32% of the oil entry column height, in reasonable agreement with the observations. The snap-off phenomenon can be embedded in relative permeability and capillary pressure curves for the seal. With such rock curves, the trap emptying dynamics was quantitatively reproduced by a theory with one adjustable parameter.

The presented theories conceptually explain the filling state of a real trap after a general migration supply history. Quantitative predictions should also be possible if the seal is sufficiently well characterized.

Introduction

Petroleum exploration is often performed with the Gussow fill-spill concept (Gussow, 1954). The burial history of source rocks normally makes heavy hydrocarbons the first to be expelled from the source rock, followed by lighter and lighter hydrocarbons. Hydrocarbons fill traps down to the spill point, and surplus hydrocarbons will spill over to neighbouring traps in the

same geological unit. A consequence of this is that lighter hydrocarbons (gas) should preferentially fill traps near the source, and force oil to be spilled into shallower traps (Gussow, 1954). Therefore, oil traps should typically be discovered further away from the basin axes than gas filled traps.

An alternative approach includes static capillary properties of cap-rocks (Berg, 1981). Berg (1981) defined a static sealing column of a cap-rock from the cap-rock entry pressure (that can be measured) divided by gravity times the density contrast between water and the hydrocarbon phase:

$$h_e = \frac{p_e}{\Delta \rho g} \tag{1}$$

When the static sealing column is greater than the structural closure height, hydrocarbon will spill from one trap to the next in the manner described by Gussow (1954), i.e., laterally within the geological unit. In contrast, if the sealing column is less than the closure height, then this analysis leads to the conclusion that all hydrocarbons that migrate out of the trap will leak up through the cap-rock. The cap rock entry pressure analysis therefore often results in hydrocarbon system interpretations that focus migration within basin centers. The same source can fill several vertically stacked traps, e.g. Jurassic and Tertiary traps. The capillary leakage process described by Berg (1981) implies that the light hydrocarbons would be expected to occur in shallower exploration targets and the heavier oil near the source rock. This is opposite of the sorting obtained in systems controlled by the fill-spill process.

The dynamics of oil flow in the sealing rocks does not play any role in the determination of the sealing properties of the traps in the static assessment. If the seals of traps have dynamic flow properties (see e.g. Sylta, 2002), flow may be directed both laterally through their spill point and vertically through their cap rock seal at the same time, leading to different migration scenarios than the static case.

In this work we aim to investigate these problems by controlled laboratory experiments. The question addressed in this paper is the behaviour of the oil after a capillary controlled breakthrough of oil through a seal has occurred. Possible hypotheses are that the oil would reach a steady state during filling of the trap (maintaining the static fill of sealing column), or that the trap would be emptied completely upon breakthrough. The behaviour after the oil supply stops is also addressed, with possible hypotheses being that the oil level would stay fixed at its maximum level, be somewhat reduced, or reduced to zero. The relevance of these questions for the understanding of the oil distribution in exploration targets is obvious from the above.

In this study, a capillary entry pressure trap was therefore constructed in a 2D visual model in order to discern between these different hypotheses. Quantitative models based on pore geometries were constructed in order to explain the trap drainage dynamics and the residual filling after drainage.

Experimental

2D visual model

The 2D visual model used here was described by Holt and Vassenden (1996). One application of it was discussed by Holt and Vassenden (1997). A sketch of the flow apparatus is shown in Figure 1. The porous medium is kept between two glass plates that fit in a frame of solid

polyoxymethylene strengthened by stainless steel. The inside measures of the frame is 47 by 67 cm.

The model was packed by pouring glass beads in between the glass plates through dedicated filling ports along the top of the model. First, 200-300 μm glass beads were filled through the left filling port. The heap formed looked like a regular pyramid, with the sides tilting at their critical slope (26.8°). This zone constituted the reservoir. Then, 70-110 μm beads were poured onto the pyramid to form a 6.5 cm thick layer of even thickness on top of the reservoir zone, and this constituted the capillary seal. The remaining volume of the model was filled with 200-300 μm beads through both filling ports on top. The bead-pack was compacted by exerting a force on the glass plates while the model was vibrated.

The inlet and outlet sides of the model were each equipped with 16 independent flow ports. Fluids (solvents for cleaning, water for initialization, and oil for the migration experiments) were injected into the flow model by use of two eight channel peristaltic pumps (Gilson Minipuls 3). Oil was injected in a single port, located just below the capillary seal. Several of the ports located in the water zone, both above and below the seal and on both sides of the model, were coupled to a liquid reservoir (separator) near the model. In the migration experiments, the reservoir was filled with the same aqueous equilibrium phase as the 2D model (discussed below). A near-hydrostatic pressure distribution was thus ensured in the water zone during the experiments. The absolute pressure was slightly above atmospheric, in order to avoid the formation of air bubbles. The overpressure was obtained by letting the effluent from the reservoir flow to a beaker located 1.5 m above the model.

The bead pack was illuminated from behind, while photo- and video cameras were placed in the front of the flow model.

The properties of the bead pack are presented in Table 1. The permeabilities and porosities of each porous medium were measured when the 2D model was filled completely with one type of beads. It cannot be guaranteed that precisely the same parameters apply to the different porous media when mixed in one pack.

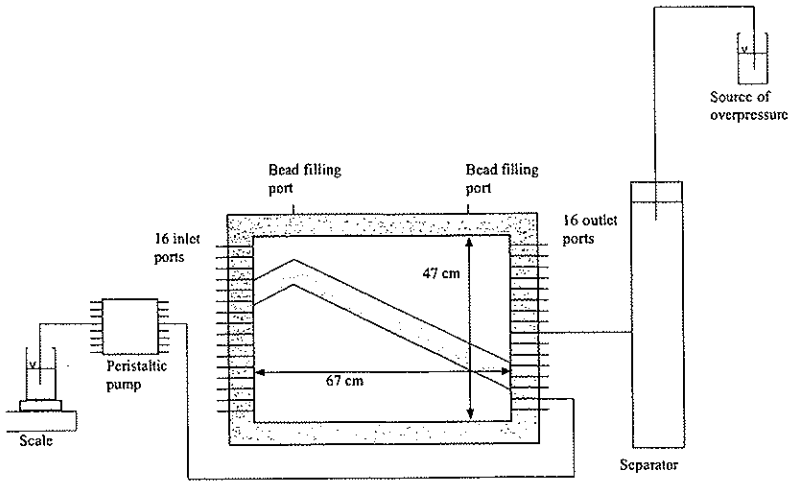

Figure 1 The 2D flow apparatus

Table 1 Porous medium properties.

	Entire inhomogeneous bead pack	Seal material	Reservoir material
Length, cm	67		
Height, cm	47		
Width, cm	1.047±0.026		
Bead size, μm	-	70-110	200-300
Permeability, D	58 [1)]	4 [2)]	72 [3)]
Porosity, fraction	-	0.38 [2)]	0.35±0.01 [4)]

[1)] Effective permeability measured during flow from left to right, with injection and production occurring over the entire height of the model.
[2)] From Holt and Vassenden 1997
[3)] Estimated from pressure drop and rate measured during water injection of homogeneous bead pack
[4)] From model geometry, the mass of glass beads, and a measured glass density of 2.487±0.005 g/ml.

Capillary properties of seal material

The seal material was characterized by a direct measurement of the entry pressure in an air-water porous plate experiment. A layer of 70-110 μm beads formed the porous plate for a pack of 200-300 μm beads packed in a tube. The porous medium was filled with fresh water at ambient conditions, and air was injected at known pressure. The air pressure was increased step-wise until air broke through the layer of 70-110 μm beads. This occurred at an overpressure in the air (relative to water) of 113 mbar. The interfacial tension of the air-water system is tabulated at 72 mN/m.

Fluid system

The requirement that gravity-driven entering of the oil into the seal should be obtained, given the physical dimensions of the model and the entry pressure of the capillary seal, dictated the choice of fluid system to be used in the experiments. The requirement for a useful fluid system is that the interfacial tension and density difference fulfils

$$\frac{\sigma}{\Delta\rho g h_e} = \frac{\sigma_{aw}}{p_e^{aw}} \tag{2}$$

with a practical value of the entry height, h_e. Schechter et al (1991) have presented a three-component system based on iso-octane (iC8), iso-propanol (IPA), and brine (water with 2 wt% $CaCl_2$), which are completely miscible for some compositions, and exhibits two liquid phases for other compositions. The interfacial tension between the two liquid phases can be varied continuously from 38.1 mN/m for the mixture between iC8 and brine to zero at the critical point. The density difference varies along with the interfacial tension. Therefore, by choosing the composition of this ternary system, the ratio between interfacial tension and density difference could be tuned, and a system designed with the desired level of oil filling when oil enters the cap-rock. The two phases were made by mixing components at the mass fractions given in Table 2, and letting the equilibrated phases segregate in a separating funnel. The oil and water phases formed were dyed with Sudan red (40 mg/l) and disulfine blue (10 mg/l), respectively. The interfacial tension was measured with a Krüss ring tensiometer, and the densities were measured with an Anton Paar oscillating tube densiometer. The obtained properties are listed in Table 2.

Table 2 Ternary mixture composition and properties of equilibrium phases at 20°C

Composition	Volume fraction	Mass fraction
IPA (iso-propanol)	0.2758	0.25347
iC8 (iso-octane)	0.3000	0.24289
brine (2 wt% $CaCl_2$)	0.4242	0.50364
σ	2.94	mN/m
ρ_w	958.6	kg/m^3
ρ_o	697.6	kg/m^3
$\Delta\rho$	261	kg/m^3

Injection program

After packing, the 2D model was first saturated with distilled water. Water was displaced by the aqueous equilibrium phase (water phase) before the experiment. Three cycles of oil injection were carried out, with the conditions shown in Table 3. The oil injected was the oleic phase produced by the mixture shown in Table 2.

Table 3 Experimental injection conditions

Experiment	Injection rate, ml/h	Initial condition	Actions during experiment
A	54	Saturated with aqueous equilibrium phase	Un-dyed oil injected. Trap allowed to empty to steady state level during shut-in period. Remaining oil displaced from trap through seal by water phase flooding
B	5.13	Trap and seal exposed to un-dyed oil. Trap empty	Red oil injected. Trap allowed to empty to steady state level during shut-in period.
C	5.13	Trap and seal exposed to red oil. Some red oil in trap.	Red oil injected. Trap allowed to empty to steady state level during shut-in period

It was difficult to obtain sufficiently accurate volumetric data for high-rate injection of un-dyed oil, experiment A. Therefore, volumetric data and pictures presented are from the low-rate experiments B and C. The initial condition and saturation history differed for all three cycles, as shown in Table 3.

Results

Qualitative discussion

Figure 2 shows selected examples from a series of images taken during the first low-rate injection cycle, experiment B. The timing and the characteristics of the different frames are summarized in Table 4. The first four frames of Figure 2 illustrate the growth of an oil zone in the trap. The migrating oil finger has just reached the top of the trap in the first frame, and the accumulation of oil has just started. The second frame shows the trap half-full. Oil had just been detected above the trap at the time of the third frame. This oil had leaked through the

capillary seal at the crest of the trap, as revealed by red oil traces in the seal. These traces are not easily discerned from the colour images, but are clearly seen in the difference images shown in Figure 3 (discussed below). At the time of frame 4, oil injection was stopped. The oil level in the trap increased somewhat between the time of entering (frames 3) and the near-steady state shown in frame 4 (the measured oil level is given in Table 4). This level increased is referred to as over-filling below.

After the oil supply was stopped, the oil column shrunk, as shown by frames 4-6 of Figure 2. Frame 5 was taken shortly after the injection was stopped, and frame 6 at the end of Experiment B. The oil column height is nearly static in frame 6, and very close to the minimum value observed. The static nature of this state was not positively proven over the limited duration of Experiment B. In Experiment C, however, this static state was found to prevail for as long as the experiment lasted and several months after the data collection were stopped.

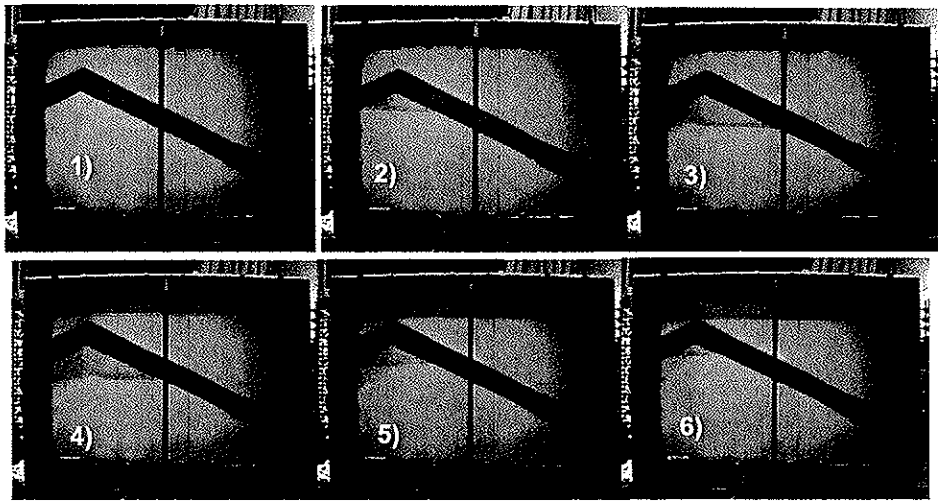

Figure 2 The first slow oil injection, experiment B. Frame numbers are explained in Table 4.

Figure 3 presents difference images, calculated as the difference between the blue channels of each image and the blue channel of the image taken before oil injection. The migrating oil finger below the cap rock is seen in these images. The two first frames show absence of oil above the trap. Frame 3 reveals the first oil detected above the trap, and the oil path through the shale layer. This path is most strongly developed in frame 4, which was taken at the end of oil injection. Flow through the seal occurred in a diffuse region about 11 cm wide. In frames 5 and 6, the oil finger along the seal has shrunk somewhat after oil injection ceased, and the oil column in the trap has become smaller.

Figure 4 shows difference image 6 with contrast enhancement and with lines and arrows highlighting the interesting zones observed. Arrows point at the oil-water contact prevailing at the time of the picture, and at the deepest OWC observed before the injection of oil was stopped. A shade of colouring between the two levels indicate the presence of residual oil in the water-invaded zone. The two vertical lines indicate the outer boundaries of observations of oil in the seal, and mark the occurrence of residual oil in the area of leakage flow.

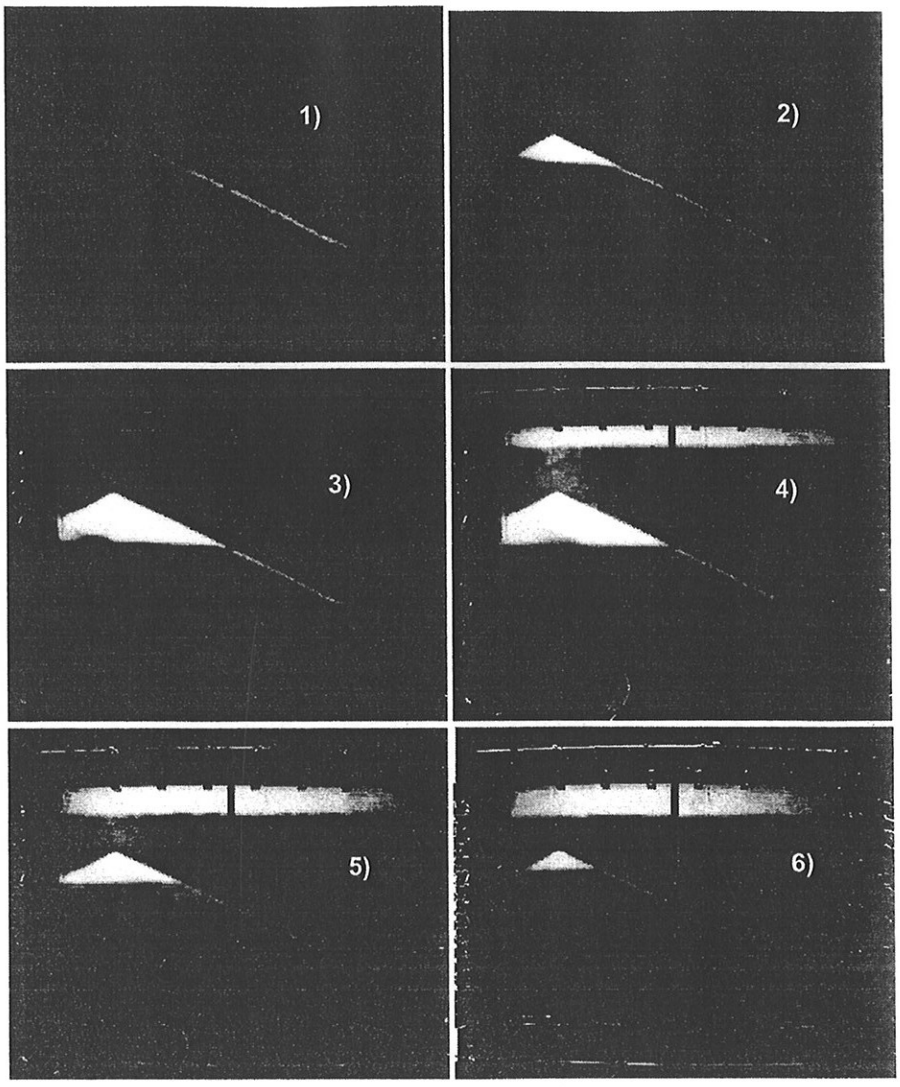

Figure 3 Difference images from the first slow oil injection experiment, experiment B (at the times in Table 4).

Table 4 Timing of images presented and summary of column heights for the images shown in Figure 2.

Frame	Time h	Injected volume ml rock	Oil level in trap cm	Oil level above trap cm	Comment
1	0.8	10	1.2	0.0	oil finger reaches trap
2	4.6	60	5.6	0.0	trap half filled
3	13	175	9.9	0.3	first oil above trap
4	29	376	10.2	3.4	oil injection stopped
5	44	376	6.0	4.9	half empty
6	309	376	3.7	5.8	minimum level

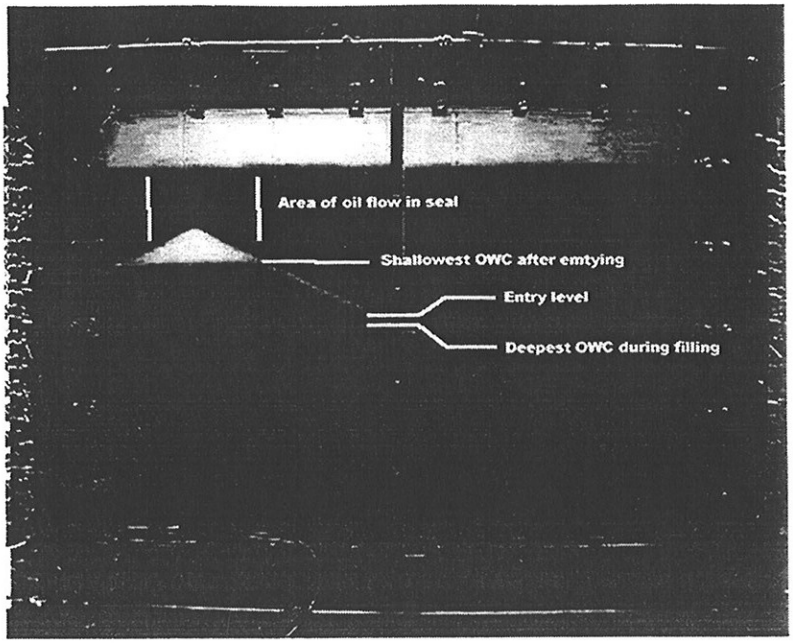

Figure 4 Difference picture for the last time-step shown in Figure 3, highlighting the different zones observed.

Volumetric analysis

The volumetric measurement for the slow oil injection experiments were made on the digital images, using image-processing software (Adobe Photoshop) to read off the thickness of the oil zones below and above the seal. Despite the existence of a 9 mm thick capillary transition zone between oil and water, readouts were reproducible with average measurement noise of 1.3 mm. The volume of oil in the model was estimated from the measured oil zone dimensions, the bead pack thickness, porosity, and the residual water saturation in the oil zone, S_{wi}, which was found to have a value close to zero, in order to ensure a match between the oil volume injected and the volume detected in the model by image analysis.

The development of the oil column height through the low-rate cycles (B and C) is shown in Figure 5. The response in the two cycles was essentially identical. The late data of experiment C was omitted for clarity in Figure 5. The detailed variation of the oil level during filling and emptying of the trap is discussed in the following.

Figure 6 details the oil level variation during filling of the trap. Initially, there is a delay in the filling of the cell, corresponding to the time required for the oil finger to propagate from the injection port to the top of the trap. Thereafter, the trap is found to fill according to the geometry of the trap and the assumption of no leakage (solid line), until leakage through the seal begins. Leakage is proven by the observation of oil above the trap. With oil leakage, the oil column height levels off, and reaches a steady state. Table 5 summarises the observed column heights. The entry column heights are similar for experiment B and C. The steady state filling during injection shows a small difference, with a 0.5 cm over-filling of the trap (steady state filling over the level defined by the entry pressure) for experiment B, and 0.8 cm for experiment C.

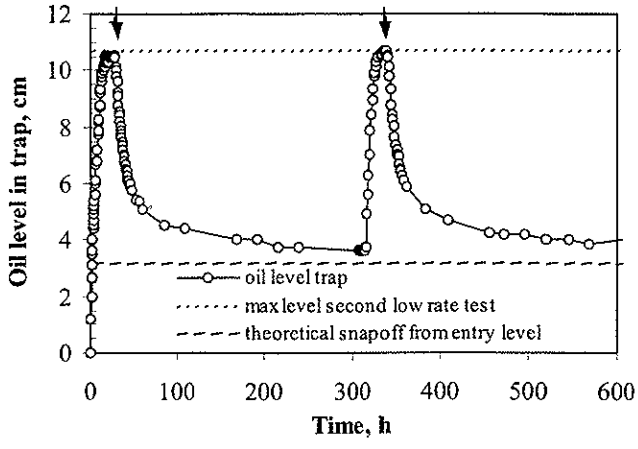

Figure 5 Oil level variations through the low-rate experiments. Arrows indicate the end of oil injections. The snap off level is discussed in the text.

The over-filling in steady-state is believed to be governed by a balance between oil inflow rate and seal transport properties. Exactly at the entry pressure, only one pore (the largest) is filled with oil. If the injection rate is larger than the transport capacity of this pore, additional pores have to be entered, until the capacity matches the injection rate. The additional pores opened could be both smaller pores at the top of the trap and pores located further down on the seal structure. In both cases, the filling level must increase relative to the entering level, in order to supply the additional capillary pressure required to enter new pores. The reason for the difference in over-filling between the two low-rate experiments is not known.

Table 5 Column heights in the three injection cycles.

Experiment	A	B	C
Breakthrough oil column, cm	7	10	9.9
Maximum oil column, cm	11	10.5	10.7
Shut-in period, h	20	290	786
Final oil column, cm	5	3.7	3.7

In experiment A, entry occurred at a much lower column height, and steady state was found at a higher column height than in the low-rate experiments. The early entering is probably due to the viscous pressure drop over the seal due to the too rapid injection. The larger over-filling is a direct consequence of the higher oil injection rate.

A very important observation was made during the filling period of experiment C (not shown in the figure): The leakage of oil through the seal did not start until the oil level was approximately equal to the breakthrough column height in experiment B. This is noteworthy because oil had been leaking out of the trap the entire shut-in period of experiment B, and one could suspect still-open flow paths to resume leakage as soon as injection in experiment C started. The experiment proved otherwise: No (or immeasurable few) flow channels were open to flow at the end of the experiment B shut-in. The same entry pressure had to be overcome in order for oil to enter the seal the second time as the first time.

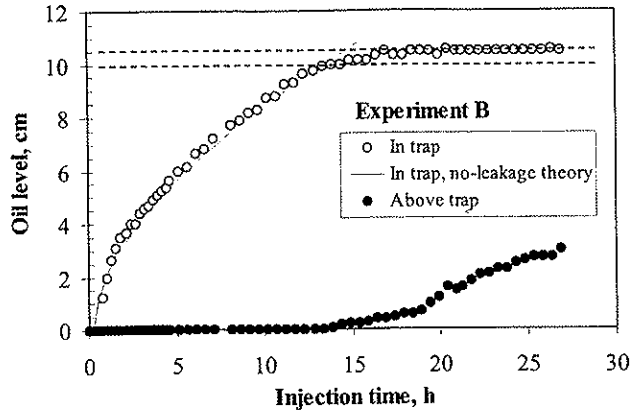

Figure 6 Details of the oil column build-up during the first low-rate injection cycle. The dashed lines show the oil levels at breakthrough and at steady state.

Figure 7 illustrates the long term behavior of the oil column during trap drainage. The figure clearly proves that the low degree of filling observed after a long period of trap emptying in fact is a true static state. A static state at 3.7 cm filling can be inferred for the last cycle. This corresponds to 35 % of the oil column observed when oil first entered the seal.

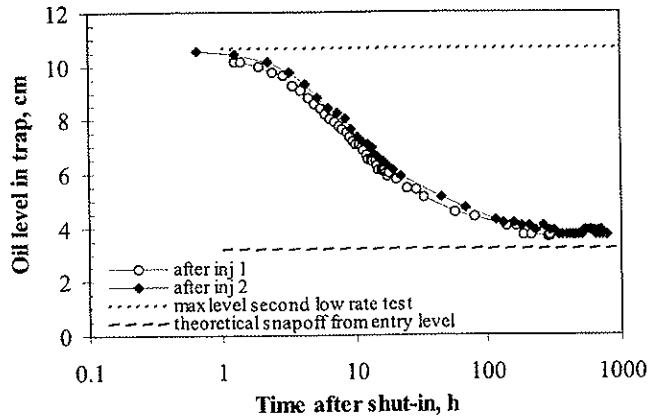

Figure 7 The oil rate variation during shut-in, plotted with a logarithmic time scale.

The most important observations made in the capillary trap filling and emptying experiments are

- entering of oil, and start of leakage through the seal, at well-defined column height.
- steady state at slight over-filling attained during injection
- reduction to 35% of entering column after stop of oil supply.
- the 35% column height is a truly stable state.
- repeated injection cycles experience the same entry column height as the first cycle.

Theoretical interpretation

Snap-off theory

The observed behaviour of the trap filling and draining can be understood on the basis of pore level phenomena. Figure 8 illustrates an oil finger entering a pore in the seal during filling (increasing p_c) and emptying of the trap (decreasing p_c). The model pore has the shape of a triangular prism. The capillary pressure (equivalent to the trap filling level) relates to the interface curvature in two principal directions (r_1 and r_2) through the Young-Laplace equation (see e.g. Adamson, 1990)

$$p_c = \frac{\sigma}{r_1} + \frac{\sigma}{r_2} \tag{3}$$

At entering, the tip of the finger is shaped like a hemisphere, with two equal curvatures. The largest hemisphere fitting into the pore has the radius of the inscribed circle of the pore cross-section, r_i. This defines the entry pressure of the pore (Roof (1970), Ransohoff and Radke (1988), Falls et *al.* (1989)). After entering, oil can flow through the pore, and cause leakage out of the trap. When the trap empties, p_c decreases, and water fill the corners of the flow channel. Also at this lower p_c, oil can flow in the pore. When the curvature radius r equals the inscribed circle radius r_i , a capillary instability is initiated, however. Any fluctuation that accumulates some water will cause the curvature radius to increase, and the resulting increase in capillary pressure will cause the further accumulation of water at that location. This is a so-called snap-off process that causes the oil finger to break into droplets. In a general flow channel with variable cross-sectional dimensions, snap-off will make the oil immobile. Snap-off in the triangular prism occur at a snap-off capillary pressure, $p_s=p_e/2$.

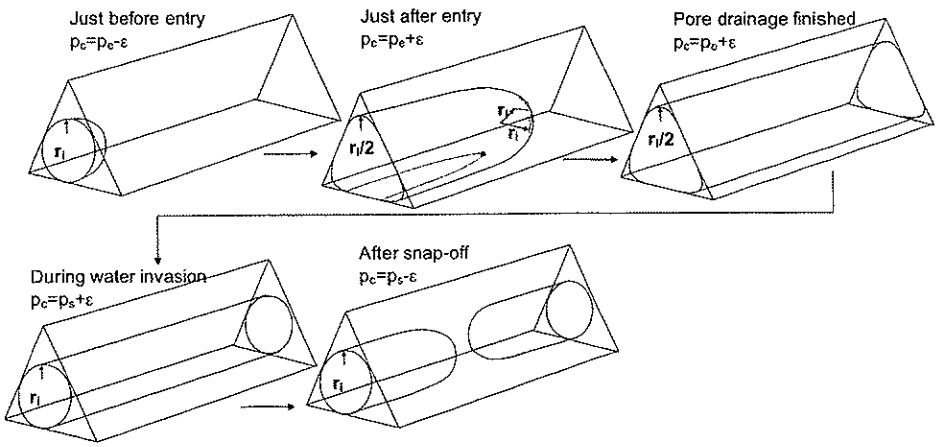

Figure 8 Oil finger in a triangular pore

In the glass bead pack used in the experimental study, the tetrahedral configuration of beads shown in Figure 9 is expected to be abundant. Such clusters of beads contain pore throats formed by three contacting beads. Triangular pore throats will be found frequently also in a random pack of glass beads such as our 2D model. In the random bead back, also larger pores and throats exist, as revealed by the additional porosity found in the random bead pack compared to the tightest pack of spheres (0.35 for the 2D model vs. 0.26 for the tightest packing of equal spheres (Ashcroft and Mermin, 1976)). If the larger pores are too few to be connected, triangular throats may still control transport of fluids in the medium, however.

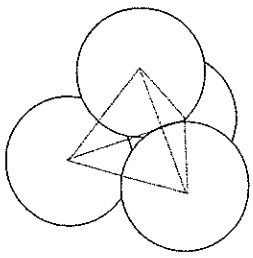

Figure 9 Tetrahedral cluster of spheres in the tightest packing of equal spheres.

Snap-off analysis for a pore throat between three glass beads is more complicated, but the arguments are the same as for the triangular prism. Firstly, the entry pressure is still determined by the largest hemisphere that can be contained between the three beads, and the entry pressure is still described by Equation (3). After entering, the interface in the throat is pressed into the corners between the beads, and the water forms a pendular ring around the contact points between each pair of spheres (Falls *et al.*, 1989). This is illustrated in Figure 10. The pendular ring corresponds to the corner water in the prismatic pore, but the interface shape is more complicated, as it is characterized by two different curvature radii, r_c and r_p. Here, r_c is the radius of the meniscus in the plane of drawing in Figure 10, and r_p is the radius around an axis normal to the plane of bead contact.

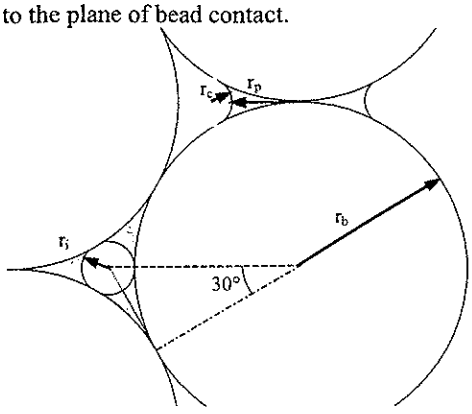

Figure 10 The pendular ring of water at the contact between two spheres and the inscribed circle, with construction aids.

The capillary pressure is defined as the overpressure in the non-wetting phase due to interface curvature. This implies that the radius r_c describes a positive curvature, $1/r_c$. The interface curves towards the phase with the highest pressure, just like a balloon curves towards high-pressure air. In contrast, the radius r_p describes an interface that curves away from the non-wetting phase. This curvature reduces the pressure in the non-wetting phase, and therefore the curvature due to the radius r_p is counted as negative, $-1/r_p$.

The snap-off criterion can be formulated the same way for the bead pack as in the prismatic pore. The criterion is that snap-off occurs when the menisci from the three corners meet, which is when $r_c=r_i$. That occurs at a snap-off capillary pressure of

$$p_s = \sigma\left(\frac{1}{r_i} - \frac{1}{r_p}\right) \qquad (4)$$

Table 6 presents snap-off pressures for several pore geometries. Some of the entry and snap-off pressure values are the same as presented by Falls et al. (1988). The configuration with two beads at the wall is included since it may arise as an experimental complication in the 2D experiments. The square pore throat is found in octahedral clusters in the tightest pack of beads. The triangular prism provides an upper limit for the snap-off/entry pressure ratio, but is also a good approximation of long, straight pores typically formed at contacts with non-spherical grains, and in pores narrowed by diagenesis. Thus it may be that the snap-off/entry pressure ratio of real cap rock approaches 0.5. For a given rock, a microscopic investigation of the pore structure can provide the exact value.

Table 6 Characteristics for three different pore geometries (bead radius r_b is length unit)

	r_i/r_b	r_p/r_b	p_e/σ	p_s/σ	p_s/p_e
Triangular prism *)	*1*		*2*	*1*	*0.5*
Triangular	0.158	0.423	12.9	4.10	0.317
Wall & 2 beads **)	0.25	0.5	8	2	0.25
Square **)	0.414	0.586	4.83	0.707	0.146

*) bead size has no meaning for triangular prism, use units of r_i instead.

Interpretation of experiments in view of snap-off theory

In the 2D model experiment, where the entry oil column height was 10 and 9.9 cm at oil entry (for the two low-rate cycles, see Table 3), triangular pore throats are predicted to have snap off column heights at 3.17 and 3.14 cm, respectively, from the snap-off/entry pressure ratio presented in Table 6. For a theory with no adjustable parameters, this is in reasonable agreement with the observed column height of 3.7 cm after prolonged shut-in. It therefore appears that the snap-off theory provides a reasonable explanation for the static oil column observed long after the oil supply stopped. Several effects may account for the slight deviation, the most important being that the glass beads used have a distribution of sizes. Clearly, the wall pores, square pores and multiply bridged pore throats are not connected through the bead pack, or else the asymptotic filling level after drainage would be lower than predicted for the triangular pore throat.

Dynamics of emptying, a description with relative permeability and capillary pressure curves

While the snap-off theory provides a pore-level explanation for why the oil-water contact stops at a certain level during emptying of a trap, it is interesting to find out if the process can be described by the conventional reservoir engineering tools and concepts, relative permeability and capillary pressure (rock curves). It is particularly important to discuss if relative permeability and capillary pressure data measured with conventional methods for other purposes can be used to predict trap filling and emptying.

A model for the emptying of the trap after the end of injection can be constructed by assuming that oil is flowing through a cross-section A of the capillary seal, which has a thickness L. The thickness of the bead pack is w. The flow zone, having a width A/w in the images of the 2D model, can be seen particularly well in frame 4 of Figure 3, but it is not a sharply defined zone. The precise value does not matter in this model, however. The driving force for oil flow is the decrease in oil flow potential from below to above the capillary seal. Just above the capillary seal, we can assume that oil and water pressures are both equal to the water hydrostatic profile, neglecting the small capillary effects in the coarse-grained porous medium. The oil pressure just below the seal is $\Delta\rho gh$ higher than the hydrostatic water

pressure, where h is the thickness of the oil zone at the highest point of the trap. The driving force for flow is thus $\Delta\rho gh$. The Darcy law gives the flow, q_o, of oil through the shale layer as

$$q_o = \frac{Akk_{ro}(S_w)}{\mu_o}\frac{\Delta\rho gh}{L} \tag{5}$$

The saturation S_w is the water saturation in the oil flow zone in the seal. This saturation has to be consistent with the capillary pressure curve of the seal material:

$$S_w = p_c^{-1}(\Delta\rho gh) \tag{6}$$

If these equations are applied to the steady state oil injection rate, q_{oss}, and the resulting steady state column height, h_{ss}, a value can be found for the product $Ak_{ro}(S_w)$. I.e., the relative permeability for oil in the seal can be determined if the flow area is known, or vice versa. Equations (5) and (6) can be used to calculate the over-filling of the trap during injection. Several approximations are made in this simple derivation, the most prominent being that changes in capillary pressure and saturation through the seal material, and variation with flow are with oil column height is neglected.

Geometrical considerations of the trap pyramidal shape (with the sides of the trap having an angle θ to the horizontal) show how the oil rate flowing out of the trap relates to the rate of change of the oil level:

$$q_o = w\varphi(1-S_{wi})\frac{d}{dt}\left(\frac{h^2}{\tan\theta}\right) \tag{7}$$

Eqs. (5)-(7) define an ordinary differential equation describing how the oil column h varies with time during trap emptying. The detailed behaviour is determined by the shape of the functions $k_{ro}(S_w)$ and $p_c(S_w)$. A parameterization of the rock curves is required for the analytical solution of the differential equation to be possible. During emptying of the trap, the saturation in the seal varies from the steady state saturation found during oil injection, to the saturation where k_{ro} is zero. This saturation interval can be mapped on to the interval 0-1 for a variable x, and the relevant part of the imbibition k_{ro} and p_c functions can be quite generally be assumed to have the shapes:

$$k_{ro} = k_{ro}^{ss}(1-x)^{n_o} \tag{9}$$

$$p_c(x) = (p_{ss} - p_s)(1-x)^{\frac{1}{\lambda}} + p_s \tag{10}$$

where k_{ro}^{ss} and p_{ss} is the steady-state relative permeability and capillary pressure prevailing before the oil injection stopped, and p_s is the snap-off capillary pressure, where $k_{ro}=0$. The shapes of the employed capillary pressure and oil relative permeability curves are compared in Figure 11, on a completely arbitrary saturation axis selected just for the illustration.

In order to compare with the laboratory results, the capillary pressures can be expressed by quantities measured in the experiment as $p_{ss,s}=\Delta\rho gh_{ss,s}$. The steady state oil relative permeability during injection can likewise be calculated from Eq. (5) with the steady state oil injection rate q_{oss}. When Equations (5)-(10) are integrated, and the substitution of laboratory observables is carried out, one obtains for the time variation of the oil column during trap emptying:

$$\frac{h-h_s}{h_{ss}-h_s}=\left[1-t\frac{(1-\lambda n_o)\tan\theta q_{oss}}{2w\varphi(1-S_{wi})h_{ss}(h_{ss}-h_s)}\right]^{\frac{1}{1-\lambda n_o}} \quad (11)$$

This model has one free parameter, namely the product of the rock function exponents, λn_o. All other parameters are fixed by other aspects of the experiment than the emptying dynamics.

Table 7 Model parameters used in the calculation of trap emptying

Experimental observables, drainage dynamics			**Additional observables used to find level of k_{ro}**		
w	1.047	cm	A	11	cm^2
θ	26.8	°	μ	0.63	cP
φ	0.35		L	6.5	cm
q_o	5.14	ml/h	Δρ	261	kg/m^3
h_{ss}	10	cm	g	9.8	m/s^2
h_s	3.7	cm	k	4	D
Capillary pressure and relative permeability curve			λn_o	1.33	

The results of the calculations are shown in Figure 12. This figure compares the measured data from Experiment C, with theoretical curves for the oil level as a function of time. The curve labeled "Model fit" was calculated with Equation (11), with parameters given in Table 7, and the rock curves labeled "imbibition" in Figure 11. A good match was achieved after adjusting the λn_o product. The optimal value of this product was 1.34. In order to illustrate the sensitivity, the figure also shows curves calculated for values 0.5 and 2. These curves lie below and above the best match, respectively.

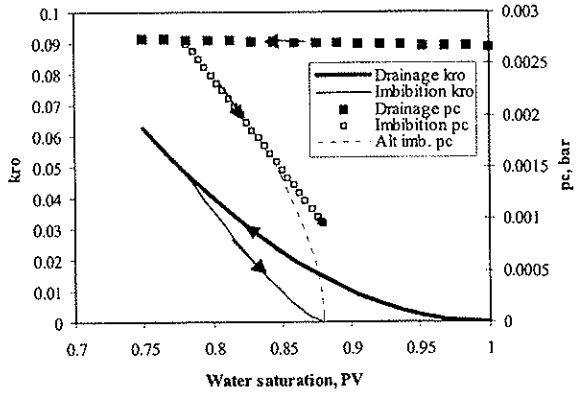

Figure 11 Rock curves used in the model for trap emptying. The drainage curves are only shown for illustration, and are not used in the calculations. The saturation interval spanned by the imbibition curves is completely arbitrary.

In addition to the rock curves giving a good match, Figure 11 also presents an alternative imbibition capillary pressure curve. The alternative capillary pressure curve is almost equal to the best match curve, except at the k_{ro}=0 saturation, where it has a zero value instead of a non-zero value. This alternative curve is what one normally would get from an imbibition capillary pressure measurement in a porous plate experiment, when the capillary pressure is decreased stepwise to zero. The point with p_c=0 would normally be measured by immersion in water, and one would conclude that p_c=0 when the fluids stop flowing. This is wrong when snap-off is active, however. At the snap-off capillary pressure, capillary continuity is lost, and the capillary pressure becomes poorly defined (in-fact, it is the condition k_{ro}=0 that stops the

fluids flowing). Figure 12 shows that the resulting rock curves predicts total trap emptying, in contrast to the observations. Conventionally measured capillary pressure data are therefore not applicable for the prediction of trap emptying.

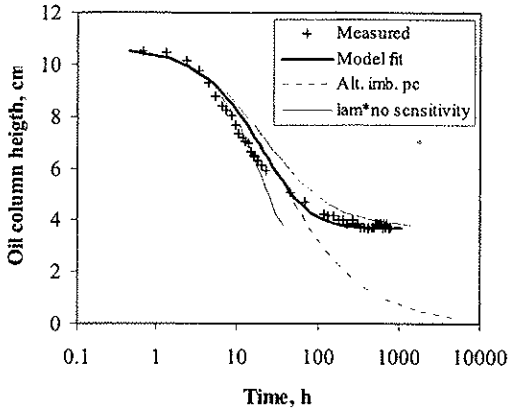

Figure 12 Calculated temporal development of the oil column during emptying compared to measured data from the second cycle of oil injection.

The good match between the measured and theoretical drainage dynamics data shows that a model based on capillary pressure and relative permeability curves for the seal can grasp the essentials of the experiment. The only requirement is that the rock curves reflect the capillary snap-off phenomenon, with the relative permeability to oil being zero at a non-zero capillary pressure.

Conclusions

The filling of and leakage out of a trap was studied with a visual 2D laboratory model. A reservoir and an overlying cap rock with different entry pressures were represented in the model by large and small glass beads. The trap was defined by a pyramid-shaped layer of smaller glass beads imbedded in a pack of larger glass beads.

The model was initially saturated with an aqueous phase, and an oil phase was injected below the cap rock layer. A model fluid system was specially designed for this experiment. The oil column in the trap was found to build up until the capillary pressure at the top of the trap exceeded the entry pressure of the cap rock. As long as oil supply to the trap continued, the column height was constant at a slight over-filling relative to the entry level. When the oil supply ceased, the trap emptied to 35% of the maximal column height. It was shown that this level represented a static state. When oil injection was resumed, the oil column build up to the original entry level before leakage through the seal started. The response in the second oil injection cycle was identical to the first cycle, in all respects.

The ratio between the entry and minimal column heights can be explained by a theory of capillary snap-off, based on the geometry of the pore space in the glass bead pack. With no adjustable parameters, this theory predicted the oil column after leakage to be 31% of the oil entry column height, in excellent agreement with the 35% observed. It was also shown that the dynamics of trap leakage could be explained with the concepts of relative permeability and capillary pressure curves, provided that the capillary pressure had a value larger than zero for the saturation where the oil relative permeability becomes zero. This condition is a way of describing the occurrence of snap-off with relative permeability and capillary pressure curves.

Thus, it has been shown that the 2D model experiment with leakage out of a capillary trap can be explained quantitatively with the snap-off theory. It was found that conventional imbibition capillary pressure experiments will not capture the crucial features that are required to predict the asymptotic filling level.

The experiments and the theory support the Berg (1981) notion of capillary controlled leakage out of hydrocarbon traps. The experiments have revealed the importance of dynamic processes (oil mobility within the seal) in controlling the steady state oil column during steady state oil influx. The experiments have clarified that traps do not empty completely due to capillary leakage, but rather attain a static partial filling at snap-off conditions long after the oil supply has stopped.

Acknowledgements

Norsk Hydro is acknowledged for funding and allowing the publication of this study, and Rolando di-Primio for assistance in the problem formulation. Torleif Holt and Kåre Solbakken are acknowledged for constructing the 2D visual model, during the RUTH research program. Oddmund Frigård and Arild Moen are acknowledged for technical assistance with packing of the model and experimental work.

References

ADAMSON, A.W. 1990: Physical Chemistry of Surfaces, 5th ed., John Wiley & Sons, New York.

ASHCROFT, N.W. and MERMIN, N.D., 1976: "Solid State Physics", Saunders College, Philadelphia.

BERG, R. R. 1981: Calculation of seal capacity from porosity and permeability data. American Association of Petroleum Geologists Bulletin 65, 5, p.900.

FALLS, A.H., MUSTERS, J.J., and RATULOWSKI, J 1989: The Apparent Viscosity of Foams in Homogeneous Bead Packs, SPE Reservoir Engineering (May 1989) 155.

GUSSOW, W. C. 1954: Differential entrapment of oil and gas: A fundamental principle. American Association of Petroleum Geologists Bulletin 38, 5, 816-853.

HOLT, T., and VASSENDEN, F, 1997: "Reduced Gas/Water Segregation by Use of Foam", 9th European Symposium on Improved Oil Recovery, 20-22 October 1997, The Hague

HOLT, T., VASSENDEN, F. 1996: Physical gas/water segregation model in RUTH 1992-1995 Program Summary, Norwegian Petroleum Directorate, Stavanger, 75-84.

LIDE, R. (ed) 1990: Handbook of chemistry and physics, 71st edition, CRC Press, Boston.

RANSOHOFF, T.C. and RADKE, C.J., 1988: Mechanisms of Foam Generation in Glass-Bead Packs, SPE Reservoir Engineering (May 1988) 573.

REID, R.C., PRAUSNITZ, J.M., and POLING, B.E:, 1988: "The properties of gases and liquids." Chemical Engineering Series, McGraw-Hill Book Company, New York.

ROOF, J.G., 1970: "Snap-Off of Oil Droplets in Water-Wet Pores", SPEJ March 1970, p 85, Transactions vol 249 (170)

SCHECHTER, D.S., ZHOU, D., and ORR, F.M. Jr., 1991: "Capillary imbibition and gravity segregation in low IFT systems", presented at the 12th Workwhop and Symposium of the IEA Collaborative Project on Enhance Oil Recovery, Bath, England, October 28-30 1991.

SYLTA, Ø., 2002. Modelling techniques for hydrocarbon migration: Can we do better. Presentation at workshop, EAGE 64'th Conference & Exhibition, Florence 2002. Extended Abstract.

CHAPTER 9

9. On the dynamics of capillary gas trapping: implications for the charging and leakage of gas reservoirs.

On the Dynamics of Capillary Gas trapping: implications for the charging and leakage of gas reservoirs

Øyvind Sylta

SINTEF Petroleum Research, N-7465 Trondheim, Norway (email: oyvind.sylta@iku.sintef.no)

Abstract

Capillary leakage of gas from buried structures can be quantified using Darcy migration concepts together with formulations for cap-rock permeability, relative permeability and entry pressures at low gas saturations. Capillary trapping has a static component defined by the entry pressure of the cap-rock, and a dynamic component defined by Darcy migration velocities and rates of migration into the trap. The importance of the dynamic trapping component increases with burial due to a corresponding reduction in cap rock permeability. The low gas migration velocities through buried cap-rocks make it unlikely that gas escape from these traps will be focused above their tops. Barriers within the cap-rock sequence may increase the gas saturation and increase the lateral width of the leakage zone. This may result in complex leakage routes into shallower structures.

Source rocks that supply gas to deeply buried traps will start to become exhausted as the temperatures increase. This reduces the rates of gas supply into the traps. Dynamic traps which have trapped gas columns that exceed the capacity of the cap-rock entry pressures can then no longer support the same column heights, and they are reduced in size. The reduction in column heights may continue below the capacity defined by cap-rock entry pressures because of hysteresis effects.

The reduction in seal capacity for deeply buried traps can be estimated if the gas fill history of the trap is known. Traps with a low vertical relief can be shielded from the dynamic seal destruction mechanism by the spill process. During periods of reduced or halted gas generation from the source rocks, dynamic traps will continue to leak for million of years. This delayed leakage may be an important source for the filling of shallower traps with gas long after the source rocks have been buried too deeply for generation to take place.

Keywords

Capillary gas leakage, Darcy flow, dynamic leakage, cap-rock, sealing times, gas saturations, migration velocities, permeability.

Introduction

The concept of entry (i.e. displacement) pressures (Berg, 1975) has been used for many years to describe the sealing potential of traps. The use of entry pressures results in a static assessment of cap rock sealing potential (Watts, 1987). In this sense, static means that the oil and/or gas column that can be supported by a cap rock is considered to be constant as long as the properties of the cap rock do not change. Such changes can occur during geologic time as results of burial and associated compaction and diagenesis, but not as a result of the hydrocarbon flow itself. Thus, leakage does not change the sealing potential of a cap-rock. One important consequence of this approach to cap-rock assessment is that a trap will either spill hydrocarbons laterally along a carrier system or leak vertically through the cap rock. Once the entry pressures of the cap-rock have been exceed by a hydrocarbon column, the trap will be unable to support any additional column, and all hydrocarbons subsequently supplied to the trap will leak out of it.

The use of entry pressures and displacement pressures to describe the leakage of hydrocarbons out of traps is taken from the reservoir technology concept of capillary pressures in multiphase systems. According to this concept, which has been shown to apply to reservoir oil and gas systems, there will be a difference in phase pressure between the wetting and non-wetting phase of a multi-phase system that is defined as the capillary pressure between the two phases (Leverett, 1941). The capillary pressure can be measured in the laboratory for different hydrocarbon mixtures and rocks, and is typically related to the effective water or hydrocarbon saturation of the pore space.

During the last 15 years, new insights into modelling approaches of basin scale hydrocarbon migration processes have made it possible to derive filling histories of traps (Sylta, 1993, Burrus, 1991, Johannessen et al. 2002). It is therefore only logical to now consider the influence of hydrocarbon trap filling histories on hydrocarbon leakage in more detail than an entry pressure analysis allows. A natural extension of the analysis is then to incorporate the full capillary pressure description into the leakage description and study the consequences of this improvement. As exploration for gas reserves probes deeper into basins and unconventional deep basin centre gas resources are more frequently sought, an understanding of charging histories and cap-rock leakage mechanisms will prove to be a key tool. Applying this understanding in the exploration for deep gas resources may help avoiding prospects where leakage has caused most of the gas to escape, whereas gas traps with larger columns may be identified.

Process description

Vassenden et al (2003) used a laboratory experiment to study migration into and filling of a synthetic trap, followed by leakage of oil out of the same trap. A glass bead pack was filled into a of 47*67 cm 2D glass container and video cameras were placed in front of the model. The reservoir rocks were represented with glass beads of 200-300 μm, while the cap-rock was represented with bead sizes of 70-110 μm. Vassenden et al (2003) showed results from the experiments as snapshots at 6 time steps (Figure 1). The sequence of snap-shots and plotted injection and production volumes documented that the trap started to leak as soon as

the oil column exceeded the entry pressure of the cap-rock (Slide 3 in Figure 1). Thereafter, the oil column continued to increase in height, but much slower. When the supply was stopped, the column started to shrink, until it stabilized at a column significantly below the column at which it started to leak.

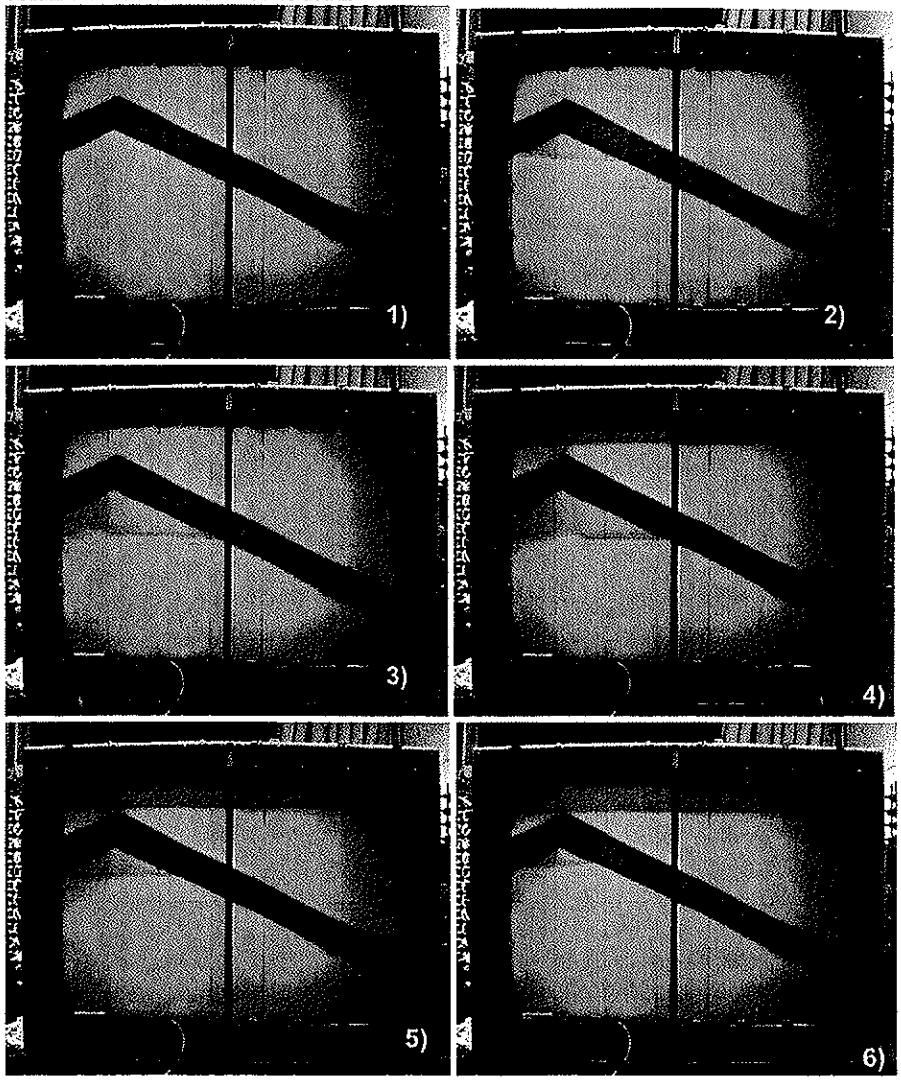

Figure 1 Six frame from showing experiment results after 0.8, 4.6, 13, 29, 44 and 309 hours. Blue is water filled. Dark colour shows the seal. Red areas are oil saturated. From Vassenden et al., 2003.

Vassenden et al. suggested a snap-off theory to describe this reduction of oil column after the supply was stopped. Just as important, however, is the fact that the column was observed to

increase slightly beyond the column defined by the entry pressure of the cap-rock when leakage started. They also observed that the leakage within the cap-rock was not concentrated to a single focused migration pathway. Leakage was observed in a broad zone around the top-point of the trap (Figure 2).

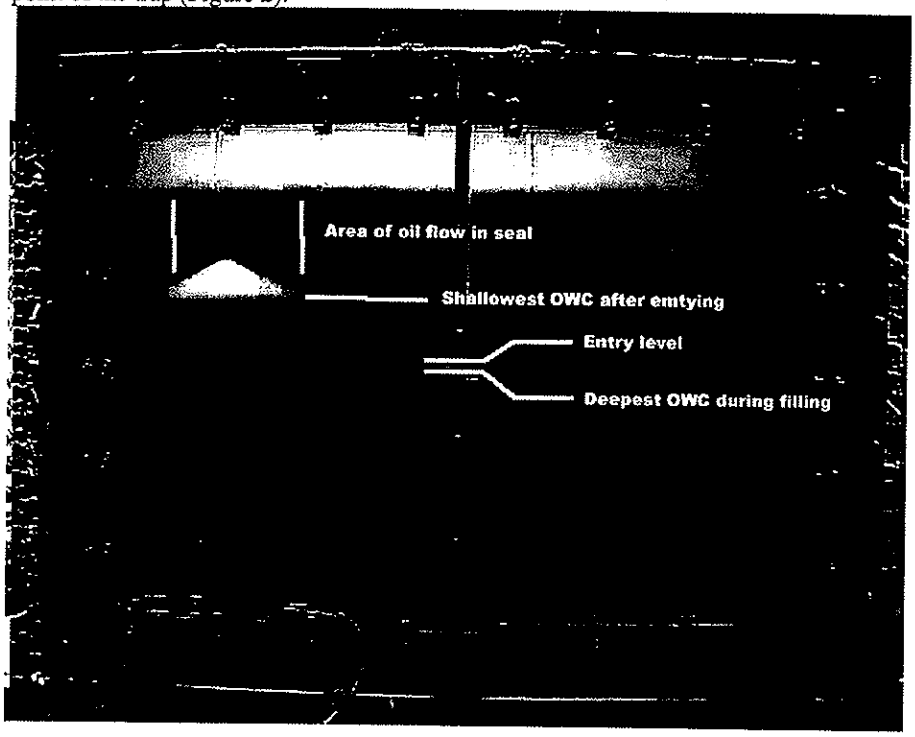

Figure 2 *Difference picture for the last time-step shown in Figure 1, highlighting the different zones. From Vassenden et al., 2003.*

Sylta (2002) analysed the flow properties of cap rocks with the aim to determine which type of modelling technology would be applicable to simulate the leakage process, Darcy flow or percolation techniques. Percolation has been shown to work well in the simulation of secondary migration of single phase systems in carrier systems (Carruthers, 1996), at least for two phase systems with static geometries. Sylta (2002) argued that percolation could not be used for simulating leakage processes through low-permeability mud-rocks because the effective permeability of most cap-rocks is too low. The saturations modelled for hydrocarbon leakage through the mud-rocks are very low, and capillary pressures of the non-wetting phase are not much higher than the entry pressures of the cap-rocks. Therefore, leakage has to be modelled over a fairly large cross-sectional area for most traps. Leakage areas should typically exceed 1 km^2 for most North Sea reservoir if capillary migration in cap rocks is observed above the reservoir.

Sylta (2002) used a classical buoyancy drive to define the capillary pressure at the interface between the seal and the reservoir:

$$Pc = Pe + \Delta\rho gH \quad (1)$$

where Pc is the capillary pressure of the cap-rock, Pe is the entry pressure, H is the height of the oil column and $\Delta\rho$ is the density contrast between the non-wetting and wetting phases (e.g. gas and oil). Variables used in this paper are described in Table 1. Pc can be related to the effective water saturation (Equation 2) via a lithology parameter L and Pe. L represents the sorting of rocks, and controls the shape of the Pc versus effective water saturation, Swt (Equation 3), curve. The functional dependency of relative permeability can be related to the same parameters as Pc (see Equation 2). The relationship between permeability and entry pressure (Equation 2) has been plotted by several authors (Figure 3), and constitute the last part of Equation 2:

$$\begin{aligned} kr &= f(Swt, Pe, L) \\ Pc &= f(Swt, Pe, L) \\ k &= f(Pe) \end{aligned} \quad (2)$$

Shc=(1-Swt) is the effective hydrocarbon saturation. Effective saturations represent those parts of the fluids that are moveable:

$$Swt = \frac{Sw - Swi - Sgi}{1 - Swi - Sgi} \quad (3)$$

The hydrocarbon leakage flow was described for buoyancy driven migration:

$$q = \frac{Q}{A} = \frac{kkr\Delta\rho g}{\mu} \quad (4)$$

Q is the rate of supply into the trap from the source rocks. A is the area through which hydrocarbons leak. It is possible to estimate typical values for: $Q, k, \Delta\rho, \mu$ while g is known. Q can be estimated from hydrocarbon generation and expulsion modelling, while k can be estimated from Figure 3 or from laboratory measurements of permeability and/or entry pressures. The equations above can be solved for the unknowns, assuming a lithology (L) and the results can be plotted as q versus k and H. Figure 5 shows this relationship using the (Standing, 1975) formulations for Pc and kr:

$$S_{wt} = \left(\frac{P_c}{P_e}\right)^{-L} \quad (5)$$

$$k_r = k_r^{\circ}\left(1 - S_{wt}\right)^2 \cdot \left(1 - S_{wt}^{((2+L)/L)}\right) \quad (6)$$

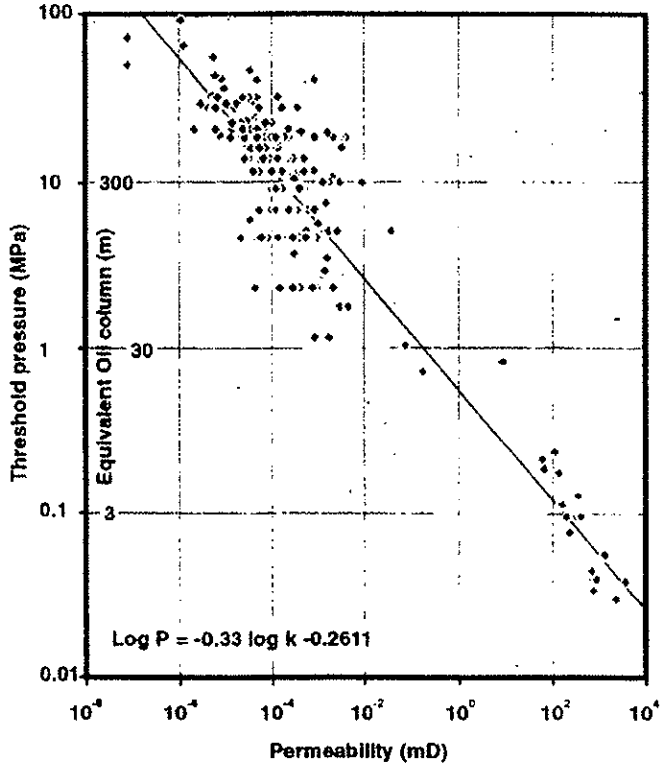

Figure 3. Threshold pressures (MPa Hg) versus permeabilities (mD) for a wide range of undifferentiated lithologies (from Ingram et al, 1997).

Sylta (2002) used Figure 4 to conclude that percolation modelling is not an appropriate process description for modelling leakage through low-permeability mud-rocks because it is not representative for the process when trap filling rates are significant, say greater then 10^6 Rm^3/My of oil and/or gas, and the permeability of the cap-rock is below 3 mD. When these conditions are met, a dynamic hydrocarbon column will be created below the static entry pressure column. The height of the dynamic hydrocarbon column is completely dependent on the filling history and of the flow properties of the seal. These properties can be described and quantified using Equations 1 to 6 above once the geometry of the trap is known.

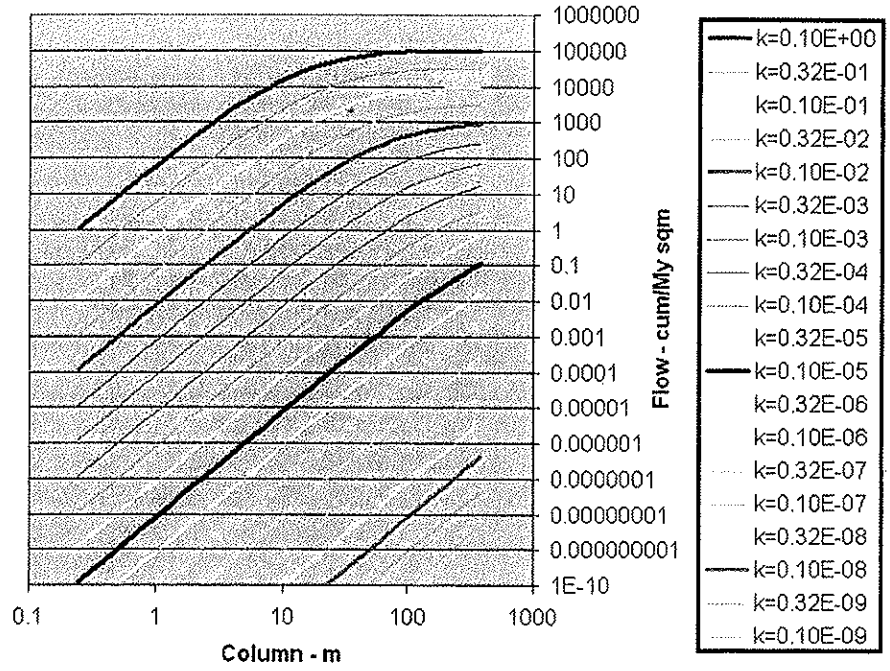

Figure 4. Leakage flow versus dynamic Darcy hydrocarbon column height for different permeabilities. Permeabilities are in mD (from Sylta, 2002).

The analysis of Sylta (2002) assumed a simplified geological model in which the cap-rock was assigned the same properties over the entire trap. This was a required assumption in the analysis, and it will not hold true for many traps. When traps fill below the entry seal point, capillary leakage will typically start at the very top of the trap. Initially, a very small part of the cap-rock will experience leakage, but when a dynamic column builds beyond a few meters in height, then capillary leakage will occur over a larger volume within the cap-rock. The properties of actual cap-rocks may then be expected to vary, and it is not evident that all arguments presented above will apply unmodified to an up-scaled version of the process description. Heterogeneity in the cap-rocks will result in leakage occurring in the most permeable parts of the cap-rock first. It is, however, deduced from the arguments of Sylta (2002) that the flow properties of the most permeable parts of the cap-rocks may not be able to transport all the gas that becomes available for leakage, and the less permeable parts of the cap-rock will be invaded by gas. The analysis presented in this paper makes significant simplifications to the cap-rock properties. The interpretation of the experimental results may need to be modified when the process is up-scaled for heterogeneous cap-rocks. However, the conclusions on dynamic gas columns presented herein need only be modified: the columns may decrease or increase in size, but will not become zero.

Quantifying leakage

In order to assess the leakage properties of a trap, the geometry of the trap must be known. The area of leakage above the trap has to be known to compute the leakage volumes, and therefore a starting point is to describe the area as a function of column height, H:

$$A=f(H) \qquad (7)$$

This relationship can be obtained for any mapped structure, either manually, or by numerical integration in a mapping package. A very simple approach is used here to derive A for a synthetic trap. Figure 5 shows a cone-shaped trap filled with gas down to the static entry pressure column of H and with a dynamic column of height h below. A horizontal slice shows an elliptical shape with the long axis length being 'b*r' where r is the smallest radius in the ellipse. The value of 'r' is related to the column H by r=a*H. For this simple trap, the area of the trap at column H is:

$$A = \pi(aH)(abH) = \pi a^2 bH^2 \qquad (8)$$

The hydrocarbon pore-space volume of the cone down to H is:

$$V = \emptyset_{eff}\frac{1}{3}\pi a^2 bH^3 \qquad (9)$$

where $\emptyset_{eff}$ is the effective pore space fraction available for the gas, N/G Ø (1-Sw).

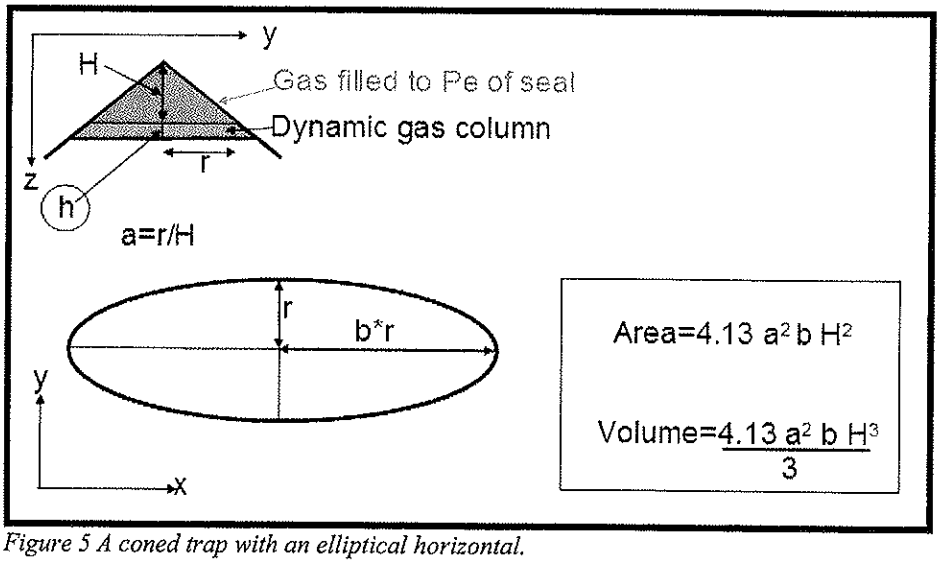

Figure 5 A coned trap with an elliptical horizontal.

The advantage of this formulation is that it is extremely easy to approximate 'a' and 'b' for a trap and generate A(H) and V(H) as graphs from a spreadsheet. Figure 6 shows the area versus column height for a=10 and b=1, 2 and 5. We will use the curve for b=5 in the

following quantification of leakage for this trap. Once the area versus gas column height has been determined, the procedure shown in Figure 7 can be used to iteratively find the correct value for A and h for given values of Q, and k. Q is the maximum filling rate when the trap is filled beyond the entry column seal, and k is the permeability. Q is taken from an assessment of the generation and expulsion history of the source of a trap, while k can be taken from, for example, Figure 3. Here we choose to pick permeability versus entry pressure values from Figure 3 for a trap that can seal a 300m column of oil. This corresponds to a 450m gas column due the difference in interfacial tension and density between oil and gas. The chosen permeabilities are 10^{-5}, 2 10^{-4} and 10^{-2} mD for a low, middle and high permeability cases. Note that these permeabilities are quite high for typical cap rocks. The 3 permeability cases are referred to as the k_l, k_m and k_h cases in the following analysis. These values are only chosen as an illustrative example. The results of the following analysis would not change dramatically if, for instance, the gas column entry pressure seal was reduced for the same permeability due to larger density differences between oil and gas.

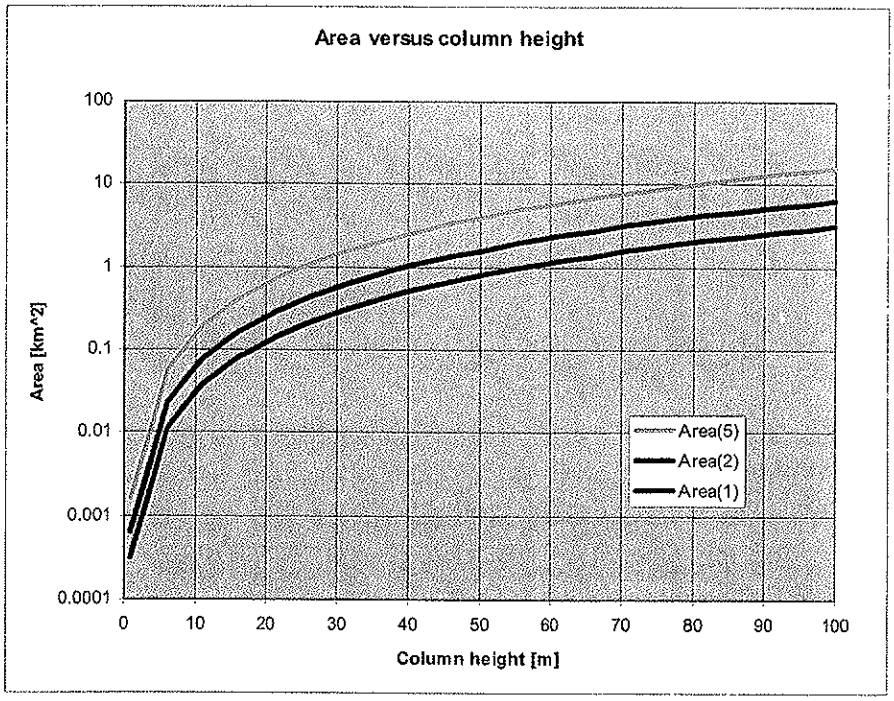

Figure 6 Area versus column heights for elliptic cone with a=10 and b=1, 2 and 5. Uppermost curve is for b=5 (Figure 5 explains 'a' and 'b').

For each of the 3 k-cases, a value of Q is first chosen (Q=1 here), and the procedure in Figure 7 is used to arrive at first an initial value for the dynamic column heights h (red dots in Figure 8). Next, iterative values for h (green points in Figure 8 (left) are found by following the loop

in Figure 7. The final values (purple dots in Figure 8) are determined by repeating the loop until the values of h do not change between each loop. In our case, a total of 3 loops are sufficient to find a stable solution. Figure 8 (left) shows that the three values for h line up on a straight line. The range of the final values is significantly less than the initial estimates of h. The difference between k_h *and,* k_l decreases from 110 m to 65 m for Q=1.

The uppermost data points in Figure 8 (right) show the final estimates of h for Q=10. The gas columns increase approximately 40% when the flow-rate increases 10 times. This means that the process is to a certain degree very robust with respect to the filling history of a trap. When the supply rates increase, the gas column increases. The increased gas column results in higher capillary pressures in the cap-rock. This increases both the relative permeability within the cap-rock and the area of cap-rock that will have capillary pressures that are greater than the entry pressures. As a result the volume of gas that can be transported through the cap-rock increases dramatically and the column height does not increase as fast as the supply rate.

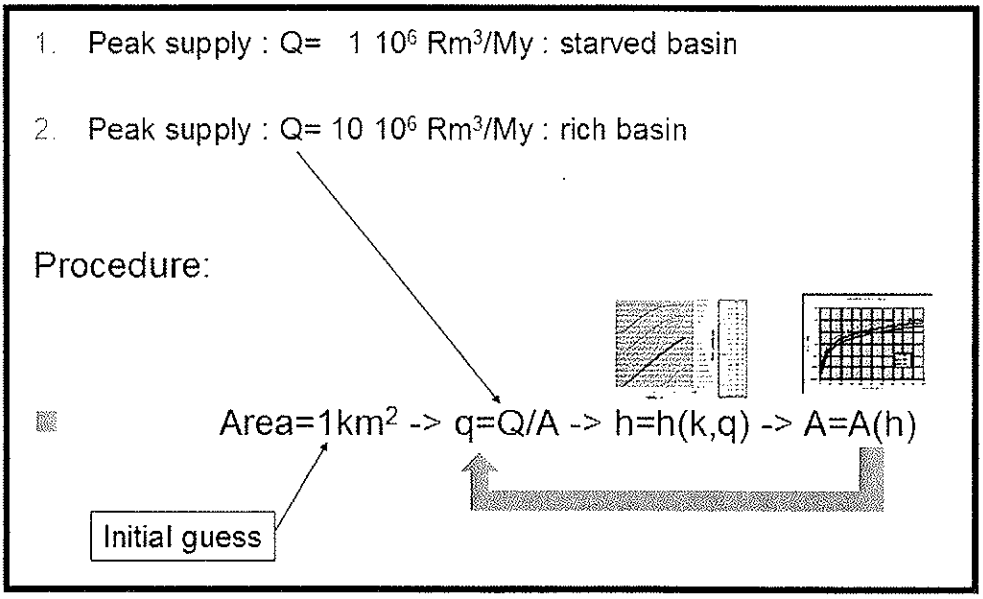

Figure 7 Procedure used to estimate h from Q and k. An initial guess of A is used to calculate q=Q/A (*) and then h is picked from graph. A is calculated from h and this gives a new value of q=Q/A. Iteration continues from (*).

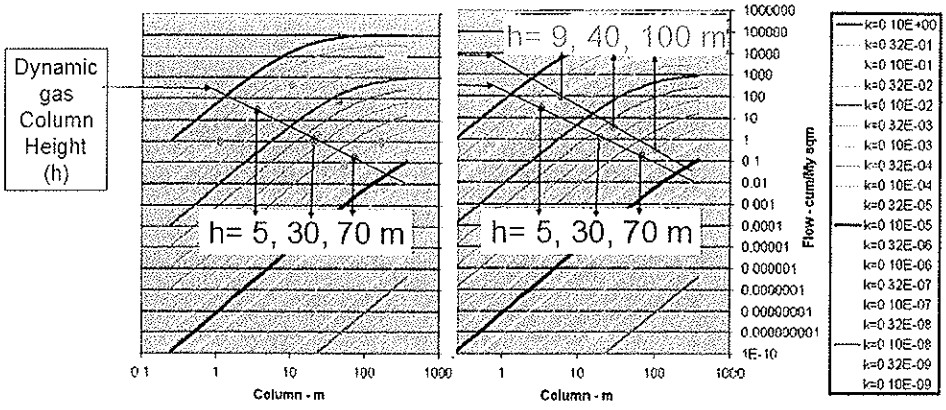

Figure 8 Left: Interpolation of correct column heights from initial values (red dots), via intermediate values (green) to correct column heights (purple) for high, middle and low cap-rock permeability (k_h, k_m, k_l) using Q=1 $10^6 Rm^3/My$. Right: Interpolated values for Q=1 and 10 (green) for same values of k.

Discussion

The analysis presented here shows that cap-rocks that experience a dynamic leakage process will increase column heights. The maximum dynamic gas column heights for buried traps can easily reach 100m in source-rich basins where the peak supply rates of traps can exceed 10^7 Rm^3/My. A steady gas supply rate of 10 10^6 Rm^3/My would fill a 20 m thick trap with the properties used above with a 500 m dynamic gas column with 400 10^6 Rm^3 gas in 40 My. Figure 9 shows the trapped volumes for such a trap versus gas column (using Equation 9). If the supply continued at the same rate beyond the 40 My, the trap would leak continuously with a volume rate corresponding to the supply rate, thus sourcing shallower traps with gas. If the supply from the source rock is stopped, then the leakage would decrease. It would take a minimum of 10 My to decrease the gas column from 500m to 450m because the trapped volume would have to decrease from 400 to 300 10^6 Rm^3 (Figure 9).

The 10 My of continued leakage of gas from the trap will increase if cap-rock hysteresis causes the snap-off pressure to be significantly lower than the entry pressure of the cap-rock. A reduction in snap off to 1/3 of the entry pressure column would result in the gas column being reduced from 500m to 150m. This would mean that a total volume of 350 10^6 Rm^3 could leak from the trap after the supply was stopped, and thus leakage would be maintained for more than 35 My. If the reservoir thickness is greater than 20m, the leakage times could be even longer.

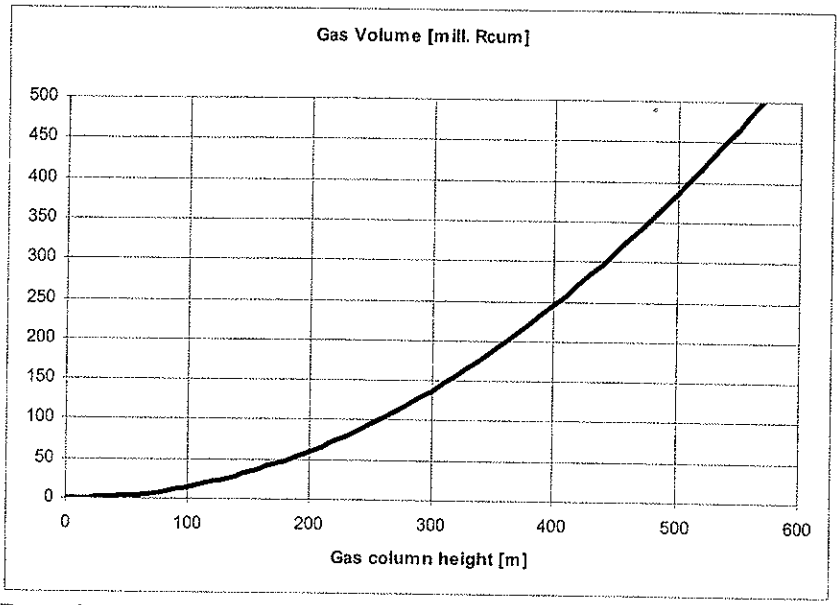

Figure 9 Gas volumes versus column height for a 20 m thick reservoir in an elliptical coned trap with 10% effective porosity (from Equation 9).

Table 2 lists column heights and corresponding trap volumes calculated for our model trap using no limitations in reservoir thickness (the base lies below the gas-water contact). The delay times shown in the rightmost column are calculated by dividing the volumes of gas trapped by the dynamic seal with the maximum supply rates (Q). This gives estimates of how long the trap will be able to leak gas after the supply has been stopped. The leakage can continue for from 2 to more than 100 My. The greater value of Q gives the shorter duration times for leakage because high values of Q result in thicker columns. Thicker dynamic columns lead to higher gas saturations in the cap-rock and therefore higher relative permeabilities and flow-rates. These higher flow-rates will be maintained for some time after the supply has stopped. However, the exact behaviour of the relative permeability and capillary pressures of cap-rocks during hysteresis is not known. We expect the relative permeability to slowly reduce until it reaches zero at the snap-off pressure. Therefore the leakage rates will most likely show exponential decrease rates after the supply has been stopped, thus extending the leakage period beyond those given in the rightmost column of Table 2.

In the case of a heterogeneous cap-rock with entry pressures and permeability changing throughout, the dynamic seal column may not be determined as easily as in our model example. A fully up-scaled process description that can account for these features is not yet available. Most likely, both dynamic seal columns and leakage times may be in the lower ranges of values presented in Table 2 when the process is up-scaled. This is because the gas will typically first fill the low entry pressure pores, and these will also be the ones with the higher permeabilities and the sharpest transition from low relative permeabilities to high

relative permeabilities as the dynamic gas column builds up. It is possible to develop a more extensive process description that accounts for these factors, although it may be unrealistic to expect a simple analytical solution. Numerical modelling will most likely be needed to address the problem, and it is therefore not within the scope of this paper to discuss it in more detail. It is concluded that more work is needed to properly study these effects.

These considerations show that the filling history of traps must be known to compute their leakage history and rates. The maximum value of Q will need to be determined to compute the maximum column of gas that can be supported. The volumes of dynamically trapped gas divided by Q_{max} can be used to assess the leakage duration once gas supply is exhausted or strongly reduced. Figure 10 demonstrates what a dynamic fill and leakage history of a trap might look like. In this example the entry pressure of the cap-rock increases linearly through time. The uppermost curve shows that expulsion peaked some million years ago, possible because the trap has been buried beyond the peak gas generation window. The trap then starts to leak once the volume of gas migrating into the trap exceeds the volume of the entry pressure seal. Static leakage rates are higher than the dynamic leakage rates for the period before gas expulsion peaks (Figure 10, right). The most dramatic differences between these curves are observed after the expulsion rates are reduced, where the dynamic leakage is maintained at high level until the present day.

There are at least three important effects of this difference:

- The dynamic cap-rock leakage maintains a thicker column of gas for some time.
- The dynamic trap can be emptied more than the static trap.
- The dynamic trap maintains leakage into shallower traps after supply is reduced.

Source rocks that supply gas to deeply buried traps will gradually become exhausted as temperatures increase. This reduces the rates of gas supply into the traps. Dynamic traps that have trapped gas columns that exceed the capacity of the cap-rock entry pressures can then no longer support the same column heights, and the trap is reduced in size. Unfortunately, this reduction in column heights will continue below the capacity defined by the entry pressures. Hysteresis effects will cause relative permeability and capillary pressure curves to be different when the gas column decreases, resulting in a lower seal potential for traps with a dynamic seal history. Gas traps that experience dynamic leakage will acts as filters for the leakage process. Gas remains trapped in the deeply buried traps and is slowly reduced during burial. It is likely that a dynamic trap will continue to leak even when diagenesis increases the entry pressure of the cap rock at high temperatures because once the entry pressure has been exceeded and leakage initiated, it will continue. The important step is to get the leakage process started and thereby develop some gas saturation within the pore space of the cap rock.

The mechanism described above may explain why there is a good potential for gas leakage from very deeply buried source rocks even long after they have passed the peak of their gas generation window.

Nature provides an extensive database of drilled traps that can be used to test migration concepts, and case studies are therefore important contributions to validate and test the concept presented here. One challenge with the "natural laboratory" is that rarely is there only

one process that operates in isolation. It is therefore extremely difficult to find a case study where capillary leakage is the only unknown parameter. Usually, the amounts of gas generated, expelled and migrated into the traps are poorly constrained, while cap-rock permeabilities and entry pressures are unknown or have to be inferred from well logs. This can be done as part of an exploration study, but the results are inadequate as scientific proof that the process description works or fails. In order to validate the process description with case study data, several cases with differing geological conditions, must be used.

Traps that have experienced a period of dynamic gas column heights may show signs of early filling that have been deeper than the present day hydrocarbon-water contact. If the pore pressures are sufficiently low to rule out hydraulic leakage as the leakage mechanism, and tectonic events have not induced leakage, then these traps may be candidates for dynamic capillary leakage. Leith et al (1993) recognised cap-rock leakage above the Snorre Field using geochemical techniques, suggesting that migration of hydrocarbons occurred through larger parts of the cap-rock. This would be consistent with expected effects of a dynamic column height, but a more detailed assessment is required before further conclusions can be made.

The reduction in seal capacity for deeply buried traps can be estimated if the gas fill history of the trap is known. The seal capacity reduction is more important for traps with very large structural closures. The effect of the dynamic seal destruction mechanism can be reduced in traps with a lower vertical relief by the spill process. This limits the maximum gas column that can accumulate beneath a trap. Therefore, smaller traps are more likely to be preserved at depth than the large traps. Faults that become more sealing with depth and lead to compartmentalization of traps may increase the probability of dynamic seal creation and destruction because some of the compartments may trap larger columns of gas and lower the spill point.

The low gas migration velocities through deeply buried cap-rocks makes it unlikely that gas escape from these traps will be focused to thin migration stringers above the traps. Gas at low saturations will tend to fill a large fraction of the cap-rock above leaking gas-filled traps. Almost the entire section above the gas trap may become saturated with low-saturation gas. Only if barriers exist within the seal will the saturation increase below the barrier. This increase will be needed to overcome the higher entry pressures of the barrier. Such a barrier may also increase the lateral width of the leakage gas zone if the lateral permeability is sufficient. It does not take much depositional or diagenetic hetereogeneity in the cap-rock to disperse gas laterally throughout a larger portion of the section above a deep gas trap. Lenses of silt and/or sand just below tighter portions of the seal may easily act as conduits for localized lateral migration of gas. This may result in very complex filling routes into many small structures above just one deep gas structure.

The methods, procedures and analysis performed in this paper all assume that migration of gas do in fact occur at low saturations and at low permeabilities. Low gas saturations in cap-rocks are frequently reported from exploration wells. The low relative permeabilities that are assumed here have, however, not been measured and reported for real cap-rocks yet. They are observed for low-permeability sands and silts, and it does not seem likely that the flow regime should completely change from sands/silts to clays and cap-rocks. The assumption made here is therefore the most reasonable assumption one can make about flow in cap-rocks at the

present time. More research is needed on this topic in order to refine the models and determine properties that can lead to more accurate determination of the capillary sealing potential of traps.

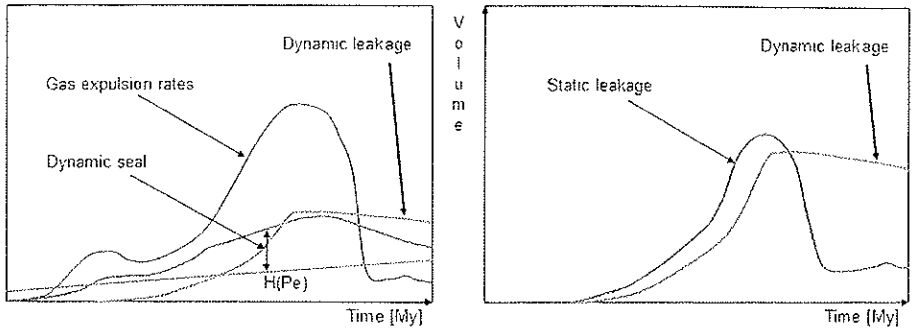

Figure 10 Fill and leakage history of a trap. Left: Straight red line shows static column seal capacity (m) through time. Red curve is total sealed column that could result with the shown filling rates. Green shows the resulting dynamic leakage volumes. Right: Resulting dynamic (red) and static (green) leakage volumes versus geologic time (see text for discussion).

Conclusions

This paper discusses the capillary leakage processes that operate in many deep traps when their maximum vertical closure is greater than the capillary entry pressure of the cap-rock. It is concluded that gas leakage is typically a dynamic Darcy flow process and that gas filling rate histories will determine the actual vertical column heights that gas traps can build. Dynamic gas columns can exceed the entry pressure column heights by more than 100m in many cases, but may also be quite small when the gas supply rate from the source rocks are low.

Column heights and rate of leakage can be quantified from estimates of permeability, entry pressure, lithology and the gas filling history. Most traps that undergo capillary leakage through a cap-rock will experience dynamic capillary leakage, and so the gas filling history of the accumulation has to be determined to quantify capillary leakage. Shallow traps can be fed for a long time by deeper gas traps that continue to leak after the source rocks have stopped generating substantial amounts of gas.

Tables

Table 1. *Description of variables used in this paper.*

Q =	Flow [m^3/s]
q =	flow-rate [m^3/m^2 s]
H =	total height of gas column defined by entry pressure [m]
h =	height of gas column below H [m]
k =	absolute permeability [Darcy or m^2]
k_r =	relative permeability (0-1)
k_r^o =	relative permeability at maximum hydrocarbon saturation ($S_w = 1-S_{oi}$)
$\Delta\rho$ =	density contrast between hydrocarbon phase and water [kg/m^3]
S_g =	gas saturation (average from h = O to h = H)
S_{gi} =	minimum gas saturation for flow to occur
S_w =	water saturation (between S_{wi} and 1 - S_{gi})
S_{wi} =	irreducible water saturation
μ =	viscosity of hydrocarbon phase [Pa s]
S_w^* =	effective water saturation (0 - 1) in Corey equation
$\emptyset$ =	porosity of carrier bed, isotropic medium
P_e =	entry pressure [Pa]
P_c =	capillary pressure [Pa]
L =	Lamda describes the sorting of rocks in kr and Pc curves.

Table 2 Calculated dynamic cap-rock sealing for 3 permeability and 2 filling cases.

Q [mill.Rm³/My]	Permeability [mD]	h [m]	Area [m²]	q [m³/Mym²]	Vdynamic [mill.Rm³]	Vdynamic/Q [My]
1	0.01	5	0.04	25	7	7
	0.0002	30	1.5	1	44	44
	0.00001	70	7.9	0.12	106	106
10	0.01	9	0.1	100	14	1.4
	0.0002	40	2.6	3.8	59	5.9
	0.00001	100	36	0.28	157	15.7

References

Berg, R. R. 1975. Capillary pressures in stratigraphic traps. American Association of Petroleum Geologists Bulletin **59**, 6, 939-956.

Burrus, J., Kuhfuss, A., Doligez, B., Ungerer, P. 1991. Are numerical models useful in reconstructing the migration of hydrocarbons? A discussion based on the Northern Viking Graben. *In:* England, W.A., Fleet, A.J. (eds.), *Petroleum Migration.* Geological Society Special Publication **59**, 89-109.

Carruthers, D., Ringrose, P. 1998. Secondary oil migration: oil-rock contact volumes, flow behaviour and rates. *In:* Parnell J. (ed.) *Dating and Duration of Fluid Flow and Fluid-Rock interaction.* Geological Society, London. Special Publications *144*, 205-220.

Frette, V., Feder, J., Jøssang, T., Meakin, P. 1992. Buoyancy driven fluid migration in porous media. Physics Review Letters **68**, 3164-3167.

Grigo, D., Maragna, B. Arienti, M.T.,Fiorani, M., Parisi, A., Marrone,M., Sguazzero, P., Uberg, A.S. 1993. Issues in 3D sedimentary basin modeling and application to Haltenbanken, offshore Norway. *In:* Dore et al. (eds.) *Basin Modelling: Advances and Applications.* NPF Special Publication **3**, 455-468, Elsevier, Amsterdam.

Hermanrud, C. 1993. Basin Modelling techniques – an overview. In Dore *et al.* (eds): *Basin Modelling: Advances and Applications.* NPF, Special Publications **3**, 1-34.

Ingram, G.M. Urai, J.L., Naylor, M.A. 1997. Sealing processes and top seal assessment. *In:* Møller-Pedersen, P., Koestler, A.G. (eds.). *Hydrocarbon Seals. Importance for exploration and production.* NPF Special Publication **7**, 165-174.

Johannesen, J., Hay, J., Milne,J.K., Jebsen,C.,Gunnesdal,S.C., Vayssaire,A. 2002. 3D oil migration modelling of the Jurassic petroleum system of the Statfjord area, Norwegian North Sea. Petroleum Geoscience, **8**, 37-50.

Leith, T.L., Kaarstad, I., Connan,J., Pierron, J., Caillet, G. 1993. Recognition of caprock leakage in the Snorre Field, Norwegian North Sea. Marine and Petroleum Geology 10, 29-41.

Leverett, M. C. 1941. Capillary behaviour in porous solids. Trans. AIME 142, 159-172.

Sylta, Ø. 1993. New techniques and their application in the analysis of secondary migration. *In:* Dore et al. (eds): *Basin Modelling: Advances and Applications*. NPF, Special Publications **3**, 385-398.

Sylta, Ø., Pedersen, J. I., Hamborg, M. 1998. On the vertical and lateral distribution of hydrocarbon migration velocities during secondary migration. *In:* Parnell, J. (ed.). *Dating and Duration of Fluid Flow and Fluid-Rock Interaction*. Geological Society London, Special Publication **144**, 221-232.

Sylta Ø. 2002. On the use of modelling techniques for hydrocarbon migration in carriers and seals. Presentation at EAGE workshop on basin modelling techniques at the annual meeting in Firenze, 2002. Extended abstract.

Standing, M.B. 1975. *Notes on relative permeability relationship*. Division of Petroleum Engineering and Applied Geophysics. The Norwegian Technical University, Trondheim.

Ungerer, P., Doligez, B., Chenet, P.Y., Burrus, J., Bessis, F., Lafargue, F., Giroir, G., Heum, O., Eggen, S. 1987. A 2-D model of basin scale petroleum migration by two-phase fluid flow. Application to some case studies. *In:* B. Doligez (ed.) *Migration of hydrocarbons in sedimentary basins*. Technip, Paris, 415-456.

Vassenden, Sylta, Ø., Zwach, C. 2003. Secondary migration in a 2D visual laboratory model. Poster presented at the cap and fault seal conference in Montpellier, September 2003. Abstract only.

Watts, N. 1987. Theoretical aspects of cap-rock and fault seals for single- and two-phase hydrocarbon columns. Marine and Petroleum Geology **4**, 274-307.

CHAPTER 10

10. On the use of modelling techniques for hydrocarbon migration in carriers and seals.

On the use of modelling techniques for hydrocarbon migration in carriers and seals.

Øyvind Sylta

SINTEF Petroleumsforskning as (email: oyvind.sylta@iku.sintef.no)

Abstract

Hydrocarbon migration at basin scale and geologic time-scales may be modelled with a number of techniques. Finite difference and control volume methods with a (Darcy) fluid flow description suffer from computing resource limitations, whereas percolation methods assume that Darcy flow is not applicable for the migration process. Ray-tracing and ortho-contouring techniques are being used in the study of hydrocarbon migration in carrier systems. This paper reviews the different techniques being used today and discusses their applicability to important processes relevant to hydrocarbon migration: secondary migration, and hydrocarbon capillary leakage from traps.

The percolation modelling methodology does not give a proper process description for capillary leakage out of traps because leakage rates are too large to be accommodated within a thin migration backbone in low-permeability mud-rocks. Darcy multi-phase flow modelling may suffer from numerical dispersion in mud-rocks, but does describe the process properly.

Percolation and ray-tracing methods provide acceptable descriptions of the secondary migration process, while the existing implementations of Darcy fluid flow will suffer from a lack of resolution, both laterally and vertically. Darcy flow modelling approaches will therefore tend to overestimate migration losses. Migration stringers of less than 1 m heights must be represented by the model, either by refining the geometry of the uppermost parts of the carriers or by using saturation dependent capillary pressure and relative permeability functions within the simulators.

Possible improvements to the methods include tests that the user can make using existing techniques and numerical improvements that vendors of hydrocarbon migration software may provide.

Introduction

Fluid flow at basin scales has been simulated in computer models since the 1980's (Welte and Yukler, 1980). During the 1990s, many oil companies have introduced multi-dimensional modelling in their hydrocarbon exploration decision process (Burley, 2000, Grigo et al., 2003). The modelling of 2D cross-sections (Ungerer et al, 1987) has probably been the most widespread technique used and reported in journals, whereas examples of "full" 3D simulation case studies (Grigo et al., 1993, Johannesen et al., 2002) are still few. Sufficient

experience has, however, been gained to start an in-depth discussion on which methods are better for different geological settings.

This paper discusses the validity of published migration modelling methods. The methods discussed are listed in Table 1. Each method can be applied with different combinations of properties, and the subdivision in Table 1 may be somewhat subjective. The Darcy flow finite difference (FD) and control volume (CV) simulation techniques can be used for two-component as well as multi-component solutions, and in 2D or 3D simulations. The Darcy methods are not differentiated because the properties described in the table would all be very similar. The term "slow" in Table 1 defines a process that needs more than e.g. 2 hours to complete on a modern computer, whereas "very fast" would only take minutes to complete for a normal simulation run. A normal simulation run is a geologic case that has been defined for a real basin scale flow simulation, with properties that are not tuned to sacrifice accuracy or resolution for speed. Oil companies may therefore use the results from such a simulation run to address exploration problems and risks.

Table 1 Methods used to simulate hydrocarbon migration (*)

Method	***Computing speed***	***Maximum dimension***	***Max model size (nodes)***	***Note (**)***
Darcy flow FD/CV	Slow	3	50.000	So=constant in cell
Percolation, single phase	Very fast	3	20.000.0000	So=constant
Percolation, multiple phases	Fast ?	3	20.000.000 ?	So=constant
Ray-tracing, single carrier	Very fast	2	1.500.000	So=f(q,k,..)
Ray-tracing multiple carrier	Fast ?	3	2.000.000	So=f(q,k,..)
Ortho-contouring	Very fast	2	5.000.000	Not relevant

** : All figures are estimates made by the author.*
Figures may differ for alternative numerical schemes implemented by software vendors.
***: So = Hydrocarbon saturation within a computing node (cell).*
q=hydrocarbon migration flow-rate.
?=Undocumented (unpublished) and/or uncertain values.

The computing speed can be an important parameter to consider when the choice of method is made. In many exploration settings, results of analyses are required within a few days or even hours to be of any use. Often a whole range of geological scenarios have to be modelled, and

many simulation runs will be required to address all the relevant risk factors. If each simulation run takes 2 days to complete, then one has to plan accordingly.

The maximum model size in Table 1 indicates the number of cells (nodes) that each method can deal with at reasonable run-times and on today's workstations/PCs. This is not an absolute value for each method. Computer memory advances and increases in disk access speed and capacity will work to push the limits. There are, however, limitations to the growth in model size for many methods, because the computing times may increase exponentially, and not linearly when models increase in size. Today's adaptation of parallel computing for fluid flow modelling can lead to future step changes in speed and model sizes for methods that are limited in functionality today. These changes are not discussed in this paper.

If the Darcy CF/CV simulation methods had been sufficiently fast to allow for high-resolution modelling, the other methods (Figure 1) would have been redundant. The Darcy techniques (Ungerer et al., 1987, Hermanrud, 1993) use the Darcy permeability concept as the basis for formulating a set of partial differential equations for fluid flow. The multiphase description is handled by the phase relative permeabilities, typically for two liquid phases (oil and water) and one gas phase. The hydrocarbon system can be either modelled as a multi-component system, or as a type "black-oil" system with solution of gas in the liquid phase using type-curves for the PVT handling of the oil and gas. The multi-component option increases the computing times and required memory of the computer, because a "flash" calculation is required for every grid-node and every time step modelled. The complexity of the system may otherwise not be that much affected by the addition of the multi-component option.

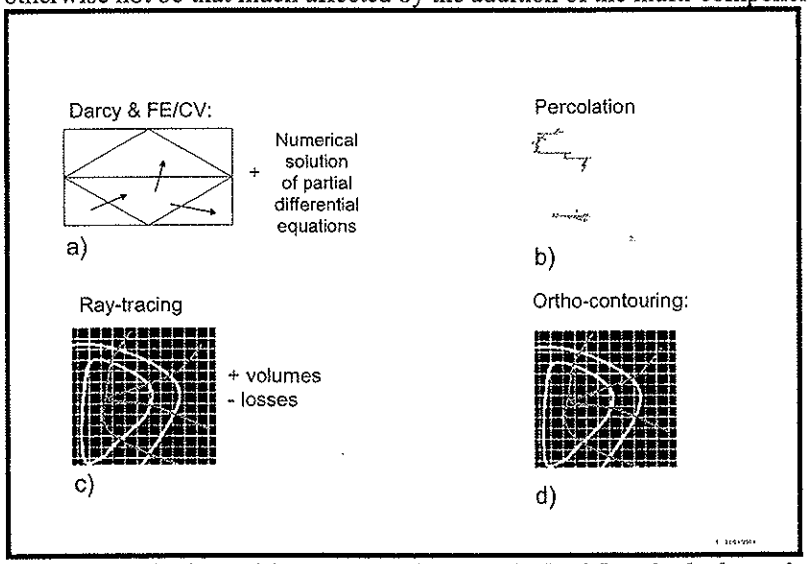

Figure 1 Methods used for assessing basin scale fluid flow for hydrocarbon migration
A: Darcy grid-node based system. HC transfer from node to node by matrix inversions
B: Percolation finds the most favourable pathways and all hydrocarbons migrate here
C: Ray-tracing traces HC along steepest dip in carrier. Losses are calculated.
D: Ortho-contouring shows lines orthogonal to contour lines of a map.

The Darcy CF/CV method typically uses global matrix inversion methods to compute the transport of hydrocarbons from one time step to the next. The method is therefore extremely compute intensive, and quite coarse models are used to produce results in realistic time frames. The method can be significantly speeded up by applying fast matrix solvers, and a parallel approach may be extremely beneficial to this method. It remains, however, to see how successful this approach can be.

Today the maximum model size of the Darcy flow FD/CV methods typically allow for modelling e.g. 20 layers and with 50*50 cells in each stratigraphic unit. The average vertical and lateral resolutions would therefore be e.g. 200 m and 1 km, respectively.

One reason why the existing "full" Darcy flow solutions are slow is because they assume a constant saturation of the hydrocarbon phase(s) within each computing node (cell), and solve the fluid flow differential equations using explicit/implicit schemes after numerical differentiation. The percolation (Frette et al., 1992, Carruthers and Ringrose, 1998) and ray-tracing (Sylta, 1993) methods make important simplifications of these fluid flow equations and the calculation are therefore speeded up. In the percolation method, flow is modelled at an "entry pressure" (threshold pressure) and the hydrocarbon saturation (So in Table 1) is assumed to be constant. Hydrocarbon migration from one cell to the next is computed by looking for the neighbour cell with the lowest resistance (threshold pressure) to flow. All flow is then modelled to pass into this neighbour cell. When this process proceeds, a migration backbone results, and all subsequent migration is modelled to occur along the backbone. Buoyancy is treated as the driving forces, while an overpressure gradient field may be used as input to the simulations (Carruthers and Ringrose, 1998). When a migration backbone reaches a seal, a hydrocarbon column builds up. The percolation finds the next node with the lower entry pressure somewhere down along the migration backbone and continues incorporating new nodes until it finds a "new" pathway (see Figure 2). By concentrating the computing resources on the hydrocarbon migration backbone, the percolation method becomes extremely efficient. The existing implementations of the percolation method have exhibited some limitations with respect to how they treat the geologic system. The dynamics of geological time (subsidence etc.) have not been fully incorporated, and fault geometries and properties are not represented with sufficient degree of accuracy. These shortcomings may be overcome in future versions of the methodology.

Ray-tracing (Figure 1 and Table 1) assumes that hydrocarbon flow-rates, and therefore hydrocarbon saturations change very slowly compared to the time-step durations and a steady state model can therefore be applied to the migration process (Sylta, 1987, 1993). Overpressures are considered to be compartmentalized due to high permeabilities of carrier systems. Lateral compartment boundaries are typically faults and reservoir pinch-outs. Therefore only buoyancy driven migration is treated and flow is modelled to occur up the steepest slope in a thin zone just below the seals of carriers. The thickness of the migration pathway is calculated from the flow-rates, carrier bed dips and permeabilities (Sylta et al., 1998). Multi-component systems can be treated (Sylta, 1989) but most applications have used simpler descriptions of the hydrocarbon system (Schroeder and Sylta, 1993, Skjervøy et al, 2000). Ray-tracing methods have not yet been applied to migration within mud-rocks.

Ortho-contouring is a method by which mapping packages are used to study secondary migration pathways. Contours are constructed at angles of 90° to the strike of a map. The map is often represented as a regular grid in the computer. Triangular and other geometry representation can be used. Ortho-contours will show the direction of oil and/or gas migration pathways when there is little influence of hydrodynamics and carrier entry pressure variations. This method does not compute flow as such, but it allows geologists to assess flow directions and forms the basis of a significant portion of the prospect analyses that are performed in exploration departments of oil companies. The method is attractive to geologists because it can be performed both manually and computerized methods. In the following we will not discuss this method of analysis in further detail for the simple reason that it does not allow for the numeric "transportation" of volumes or mass.

During migration, dispersion of the hydrocarbon phases is not considered by the non-Darcy methods. Both ray-tracing and percolation therefore focus the hydrocarbons away from the source rocks. In contrast, the Darcy techniques may spread the hydrocarbons when the permeability of the rock is sufficiently low and the amounts of hydrocarbons migrating through the area is high.

There are significant differences between the four methods with respect to the actual conceptual description of the geological system that they consider. The resulting simulators show very different characteristics, advantages and problems. It would be extremely convenient if we could just mix and match these methods at our own convenience, i.e. use the methods that are faster when we want to and use the most complex method when all aspects of the system need to be investigated. Before such a strategy can be adopted by building hybrid simulators, we need to investigate whether all methods represent adequate descriptions of the geological processes that are simulated. This paper discusses secondary migration and leakage migration, not primary migration.

Capillary leakage from traps

Only the percolation and Darcy flow methods have so far been proposed for simulating the process of hydrocarbon leakage out of traps. With Darcy flow, high rates of migration into a trap may cause the hydrocarbon column to increase so that hydrocarbon capillary pressures significantly exceed the entry pressures of the cap-rock, resulting in higher hydrocarbon saturations and higher relative permeabilities, while the percolation method will not exceed the entry pressures of the cap rock (Figure 2, left). Figure 2 (right) shows modelled percolation flow pathways for a real case. Note the focused migration pathways modelled in the cap-rocks by the percolation method. One result of the differences in migration patterns with the two methods is that calculated hydrocarbon migration losses may be very different. The Darcy method will distribute hydrocarbons at low-saturation within a relatively broad migration "chimney" above the trap, while the percolation will only saturate a very thin migration backbone. The percolation method may, however, fill larger areas when barriers to flow are present within the seal, i.e. zones of lower threshold pressures. The migration losses

may then be modelled to be substantial. The above discussion suggests that it may be unrealistic to assume that both methods of modelling hydrocarbon migration within cap-rocks are correct.

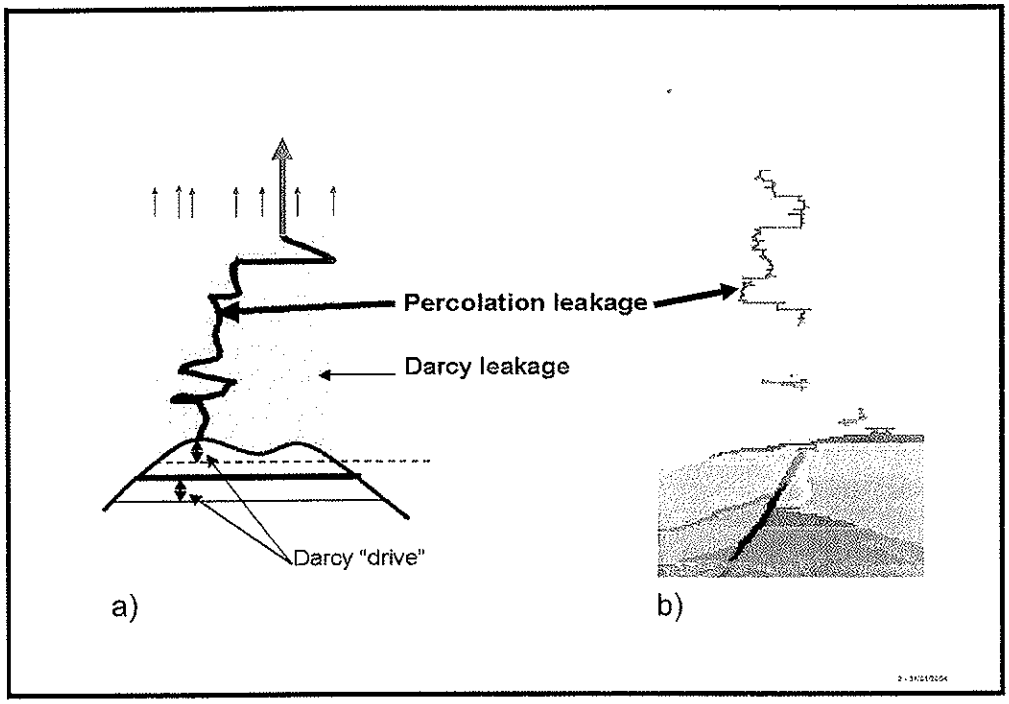

Figure 2 Percolation versus Darcy leakage.

- *Left: Thick lines for percolation leakage. Thin lines for Darcy leakage model. Hydrocarbons migrate through the entire shaded grey area in the Darcy leakage.*
- *Right: Modelled hydrocarbon migration pathways colour coded for hydrocarbon phase (green=liquid, red=vapour) for a percolation model (El-Chamri et al., 2002, Figure 14).*

Assuming constant flow properties for cap-rocks, some simple calculations may help determine which method should be preferred for cap-rock migration simulations. Figure 3 suggests that a simple relationship may be used for entry pressures versus permeabilities for even fine-grained mud-rocks. The figure is based on data of Ibrahim et al. (1970), and the equivalent oil column seal is computed by converting the threshold pressures from mercury MPa to oil column heights using:

$$h_{HC} = \frac{Pe_{Hg}}{\Delta\rho g}\left(\frac{\gamma_{HC}\cos\theta_{HC}}{\gamma_{Hg}\cos\theta_{Hg}}\right) \qquad (1)$$

where the (.) part of the equation corrects for phase properties. The parameters in Equation (1) are described in Table 2.

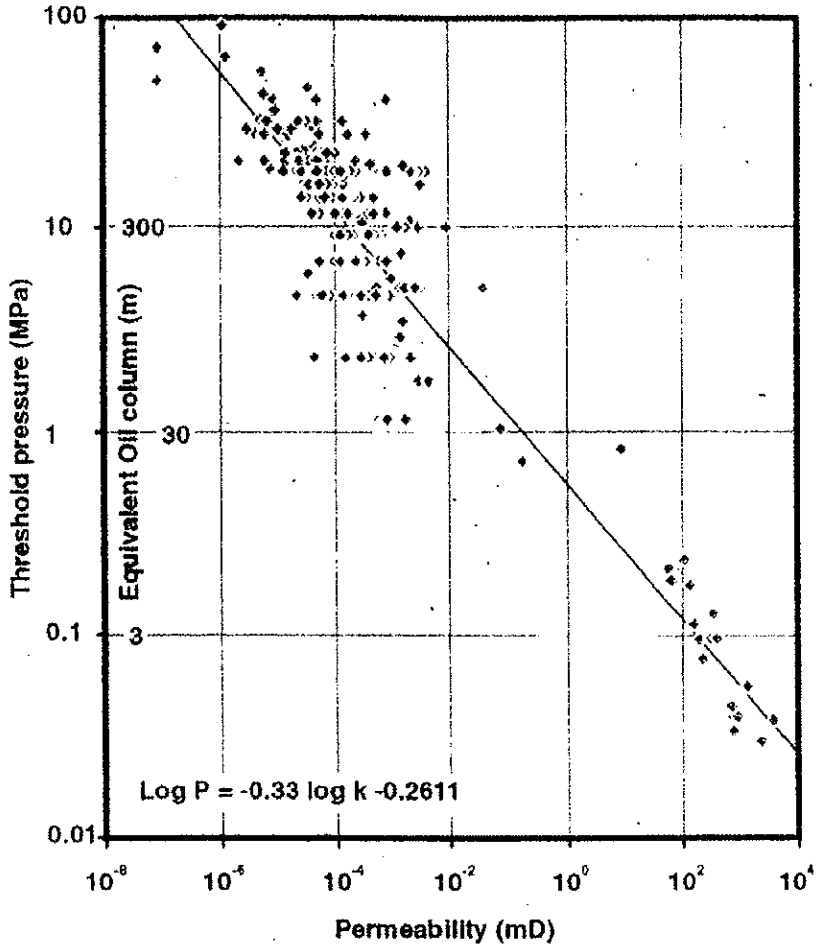

Figure 3. Threshold pressures (MPa Hg) versus permeabilities (mD) for a wide range of undifferentiated lithologies (from Ingram et al, 1997).

The capillary pressure at the top-point of a trap can be calculated from the density contrast between water and the hydrocarbon phase, the height of the "Darcy drive" and the entry pressure of the cap-rock (see Figure 2, left and Figure 4). The capillary pressure (Pc) at the top-point of the trap equals the entry pressure (Pe) of the cap-rock when oil fills down to (a) in Figure 4. Subsequent in-filling of oil into the trap leads to initiation of leakage. If the supply is greater than the leakage, oil may fill down to (b) in Figure 4. The capillary pressure at the top-point will then increase to:

$$Pc = Pe + \Delta\rho gh \qquad (2)$$

It is here convenient to define the second term in Equation (2) as a "Darcy drive" for the flow. This Darcy drive, resulting from the buoyancy drive of the excess oil column below the column defined by the entry pressure of the cap-rock seal, causes the cap-rock oil saturation to increase. The saturation increase is demonstrated in the Pc(Swt) curve (Figure 4, right), where Swt moves from point (a) to (b). A further increase in the oil column height would move Swt from (b) to (c). Swt is the effective water saturation, while Shc=(1-Swt) is the effective hydrocarbon (oil) saturation. Effective saturations represent those parts of the fluids that are moveable:

$$Swt = \frac{Sw - Swi - Soi}{1 - Swi - Soi} \qquad (3)$$

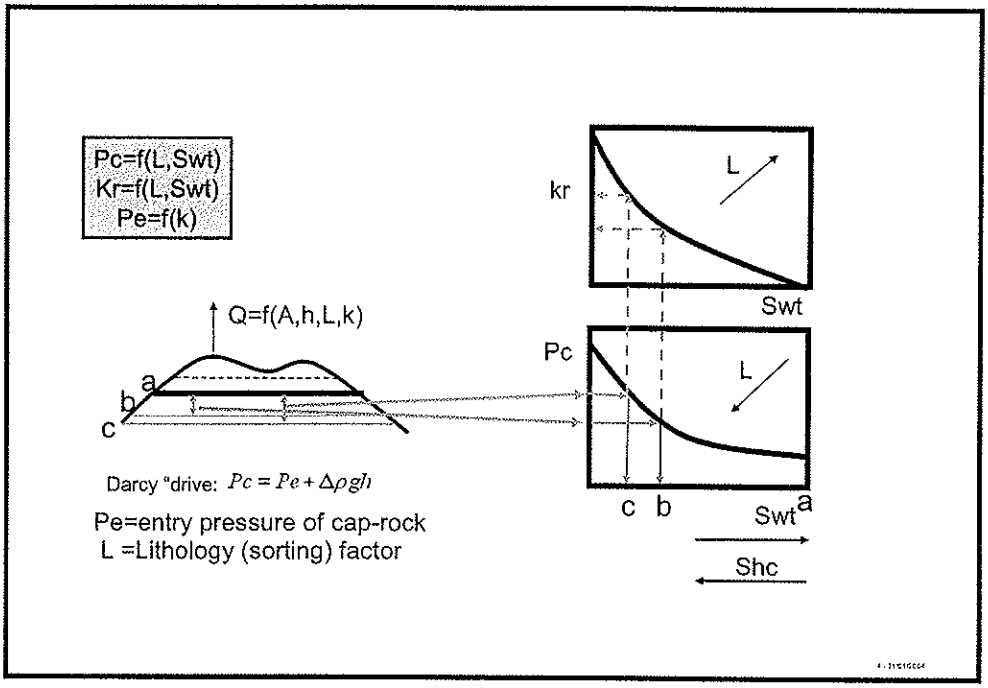

Figure 4 Hydrocarbon saturations in cap-rock above trap are calculated from height of oil and gas columns

The oil relative permeability (kr in Figure 4) increases when Shc increases. The kr starts off at (a) in kr(Swt) for Pc=Pe and increases to (b) and (c) as the oil column increases. The result is that the total permeability of the cap-rock (k*kr) increases when the oil column increases. The hydrocarbon leakage flow can be described for buoyancy driven migration:

$$q = \frac{Q}{A} = \frac{kkr\Delta\rho g}{\mu} \qquad (4)$$

For steady state conditions, when rates of supply are the same as leakage, Q is the rate of supply into the trap from the source rocks, e.g. 10^6 m^3/My, while A is the area through which hydrocarbons leak. Equation (4) represents a simplified description of the flow in that a constant value for kr is assumed in the following, while actual traps will show varying oil columns and therefore variable kr over the area A. For the following analysis we estimate typical values for: $Q, A, k, \Delta\rho, \mu$ and g (known). Typical values of q (Q and A) can be estimated from hydrocarbon generation and expulsion modelling, while k can be estimated from e.g. laboratory measurements of shale permeabilities (Kroos et al, 199?). The only unknown in Equation (4) is therefore kr. There is, however, a relationship between kr and (q,k) through the Pc and kr curves in Figure 4 and k versus Pe in Figure 3:

$$\begin{aligned} kr &= f(Swt, Pe, L) \\ Pc &= f(Swt, Pe, L) \\ k &= f(Pe) \end{aligned} \qquad (5)$$

where L is a lithology dependent parameter that describes the shape of the kr and Pc curves (see later). For an assumed lithology, with a known value for L, there are now 3 unknowns (Swt, h and kr), and 3 Equations (2, 4 and 5). These equations can therefore be solved for the unknowns, and the results can be plotted as q versus k and h.

There are many possible alternatives to describe the Pc and kr curves. We use the approach of Sylta et al. (1998) and use (Standing, 1975):

$$S_{wt} = \left(\frac{P_c}{P_e}\right)^{-L} \qquad (6)$$

L is a geologic rock property parameter (low values for poorly sorted rocks, high values for well-sorted rocks) that describes the shape of the capillary pressure (Figure 4) and relative permeability curves. The relative permeability is defined as (see Table 2 for parameters):

$$k_r = k_r^o \left(1 - S_{wt}\right)^2 \cdot \left(1 - S_{wt}^{((2+L)/L)}\right) \qquad (7)$$

The advantages of these equations are that they are simple to code, can be calibrated to laboratory measurements, and can account for different geological systems by changing the L parameter. A possible problem with using these equations is that laboratory experiments can validate the use of the equations for reservoir rocks, but measurements of cap-rock relative permeability are not at all trivial (see Discussion later).

Figure 5 has been derived by combining Equations 2, 4, 5, 6 and 7, and setting the value of L to 2. The Figure thus shows curves of steady state hydrocarbon leakage rates (y-axis) versus "Darcy column height" (x-axis) for cap-rock permeabilities ranging from 0.1 mD to 10^{-10} mD, assuming buoyancy as the driving mechanism. Figure 5 can be used to assess under which

conditions percolation methods can be used to simulate vertical hydrocarbon leakage out of a trap. One approach to this assessment is to consider a typical geological scenario where for instance 10 10^6 m^3 oil leaks out of a trap over 10 My, giving a leakage rate – q - of 10^6 m^3/My. The percolation process description results in a focused migration. For percolation to describe properly the leakage process, it must be able to leak these amounts of oil out of the trap through a narrow migration backbone. A typical percolation leakage pathway out of a trap can therefore not be modelled to be wider than, say, 200m*200m=40.000 m^2. The value of A in Equation (4) must be small, and a value of 200m*200m is certainly an upper limit. Percolation may therefore only be considered to constitute a proper process description when:

$$q > \frac{10.000.000/10}{200*200} = 25\frac{m^3}{m^2 My} \qquad (8)$$

The y=25 value in Figure 5 is taken as the lower limit for using the percolation process description. Geological conditions that have cap-rocks with permeability curves that result in values above the Percolation flow-rate threshold can be modelled with percolation, while those that fall below the line should be modelled with Darcy flow techniques. The thick (red) horizontal line in Figure 5 separates the ranges where flow-rates will be modelled sufficiently high within percolation-sized flow-paths for percolation to be applied in the modelling of hydrocarbon leakage. For combinations of permeability and column heights that plot below the line, Darcy flow modelling has to be used because the area required to leak sufficient amounts of hydrocarbons is too large for the percolation process to be applicable. Another condition that is required for percolation modelling is that the Darcy column seal should not be too large. An upper limit of 10 m is suggested.

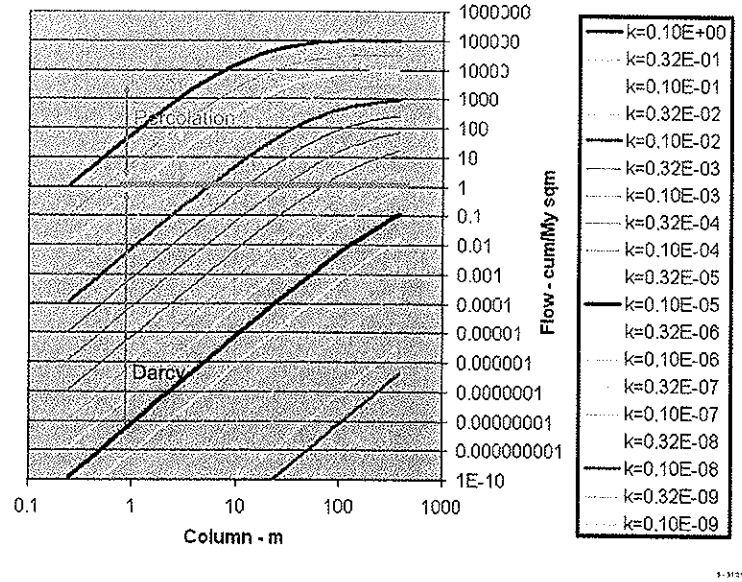

Figure 5. Flow versus Darcy hydrocarbon column height (defined in Figure 4) for different permeabilities. Permeabilities are in mD.

Figure 5 shows that for cap-rock permeability less than 10^{-2} mD, the method of percolation modelling does not provide a valid description of the cap rock leakage process because insufficient quantities of oil and gas can be transported through the percolation pathway at these low permeabilities and relative permeabilities. This corresponds to a cap-rock equivalent oil column seal of approximately 100m in Figure 3. For traps that seal thicker oil columns than 100m, percolation modelling should not be used as a general methodology for the simulation of oil and/or gas migration in mud-rocks.

The percolation method can thus not be used as a general process description of migration in mud-rocks, but it can be used in special cases. When the filling rates are very low, percolation modelling may be considered. This may be the case in some very old basins with very low geothermal gradients, slow burial of the source rocks through the oil and gas window and therefore low rates of hydrocarbon filling into traps. Another case where percolation may be considered is in the assessment of (shallow?) multi-pay systems in deltas. Here the permeability of the cap-rock may be significant, and the hydrocarbon column within each pay zone can be quite thin. The system is still economic due to the many pay zones in combination with the high permeabilities of the reservoirs. Before using tools based upon the percolation method, one should, however, assess whether the geological system satisfies the conditions in Figure 5. This is a simple exercise:

1. Compute "typical" filling rates for the basin (q) from generation modelling.
2. Assess typical mud-rock permeability of the cap-rocks.
3. Use Figure 5 to assess whether permeability is consistent with percolation limit.

One of the most important problems that may arise when the percolation process description is used in case studies is the bypassing of smaller sand lenses. The narrow migration backbone through the cap-rock sequence can easily miss sand units that are laterally discontinuous (Figure 6a). If the sand lenses are not present directly above the top-point of low-relief structures, oil migration may bypass the sand. If the sand is completely isolated, this may not be a major problem, but the local sand can easily be in some contact with another sand unit that lies further away from the leaking trap. Hydrocarbons can leak further into shallow reservoir units that lie off to the basin flanks (Figure 6a). This may result in missed opportunities in an entire reservoir sequence at the basin flank. In the case outlined in Figure 6a, the actual amounts of oil leaking into the sand lenses may easily be up to 10% of the total leakage rates. In systems where filling rates are high, this may represent substantial volumes of oil and/or gas.

When vertical hydrocarbon migration is modelled to occur through thick mud-sequences, such as more than 1000 m thick shales, significant cap-rock losses may be incurred. If the initial hydrocarbon saturation for flow (Swi) is taken to be 10%, shale porosity is 5% and the cross-sectional area over which leakage occurs is 1 km^2, then migration losses through a 1 km thick mud-rock would amount to 5 10^6 m^3 over just one trap. The results of a percolation

modelling would not be able to account for these losses, and too much oil and gas would be transported into shallower reservoirs.

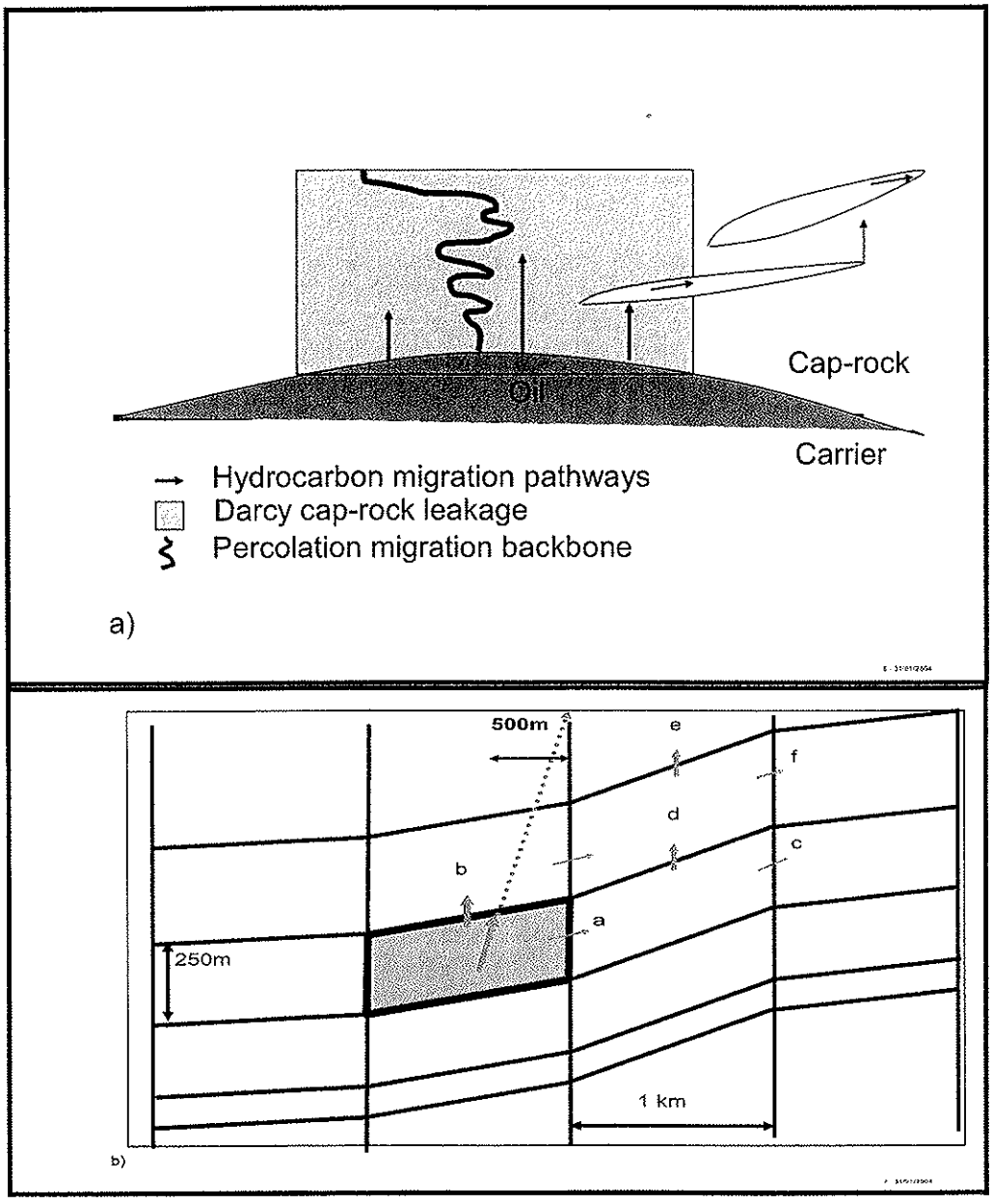

Figure 6. Darcy leakage sources sand lenses and units above low-relief trap. Percolation backbone misses the sand.

Even though Darcy flow modelling is the most appropriate process description to use for modelling hydrocarbon leakage through mud-rock sequences, the Darcy flow processes will also exhibit problems when used. Numerical dispersion may cause too wide vertical migration (Figure 7). The Darcy flow modelling is very compute intensive, and large cells are often used in the simulations in order to speed up the simulation runs. Lateral grid sizes may be set to 1km*1km in the simulations. If there is a lateral component to the vertical leakage, say 10%, as shown in Figure 6b, many numerical schemes will move a small fraction, say 2%, of the oil volumes in a node laterally into the next cell (a in Figure 6b), while most (98% here) would be modelled to migrate vertically into the next shallower node (b). From (a), oil would be modelled into (c), (d), (e) and (f) in the Figure. Node (f), is in this case located 2 km to the east of the starting node, and 300 m shallower. Only 1.2°/oo of the oil flowing out of the first cell reaches (f), but if the total volume is 10^6 m^3 per time step for a period of 4000 time steps, then the total volume reaching (f) would be 5 10^6 m3. Without the numerical dispersion, oil would migrate a lateral distance of 1 km only after moving 10 km vertically. The trap may therefore be modelled as a source for shallower traps that are located laterally too far from it.

The low resolution of many Darcy flow models may result in too high oil saturations being modelled in the cap-rocks. The use of constant oil saturations within each computing node results in too large average saturations being modelled when the vertical migration pathway has to overcome tight zones. Losses may then be modelled too large when model resolution is low. This problem is probably only a secondary effect in most cases, because the vertical thickness of the mud-rock sequence will tend to be modelled with thicknesses that do not significantly exceed 100m, and the total volumetric inaccuracy is therefore minimized for vertical migration.

Secondary migration

Secondary migration of oil and gas occurs along thin stringers in permeable carriers (Selle et al., 1993), and both percolation (Carruthers and Ringrose, 1998) and ray tracing (Sylta, 1993) can be used to simulate this process. Darcy FD/CV techniques can also be applied, but problems with numerical resolution do exist, and are discussed below. Due to the large cell sizes used in these simulation types, the average hydrocarbon saturation is likely to be modelled to be too large. The problem of resolution can best be discussed using data from published hydrocarbon migration studies. Very few well documented 3D studies are available. From the point of view of hydrocarbon migration, the work of Johannessen et al. (2002) is perhaps the best documented example. They simulated hydrocarbon migration in the North Sea Tampen Spur area over geologic time scales using a 3D Darcy flow approach and achieved a good calibration to the fields in the area. Their vertical subdivisions of the geological features are shown in Figure 7. The lateral resolution was set to 1km*1km, which is sufficiently accurate to resolve the volumes of all major structures in the area (see discussion later).

Migration was modelled from Jurassic source rocks into mostly middle Jurassic carriers and reservoir units. The model was calibrated to many fields in the area, including the Brent, Murchison, Statfjord and Snorre Fields. Figure 8 shows resulting hydrocarbon saturations in a carrier.

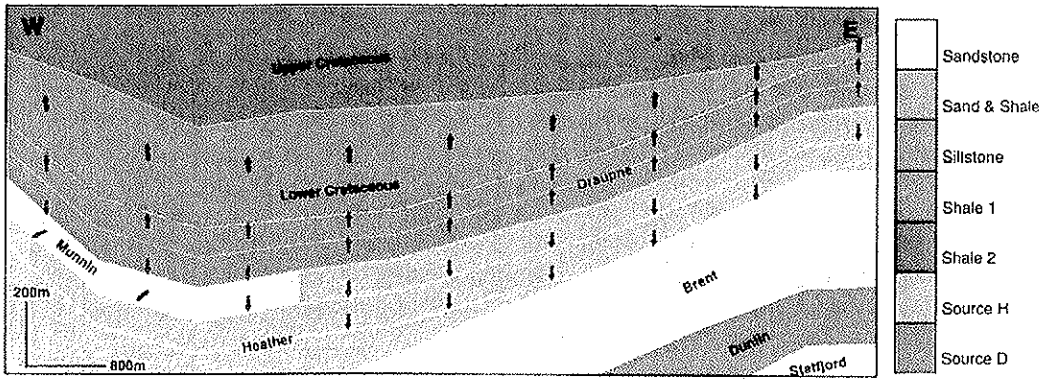

*Figure 7. Cross-section showing subdivision of the Jurassic/Cretaceous sequence used in a modelling of hydrocarbon migration in the Tampen Spur area. Lateral grid cell sizes are 1km*1km. Modified from Johannesen et al (2002).*

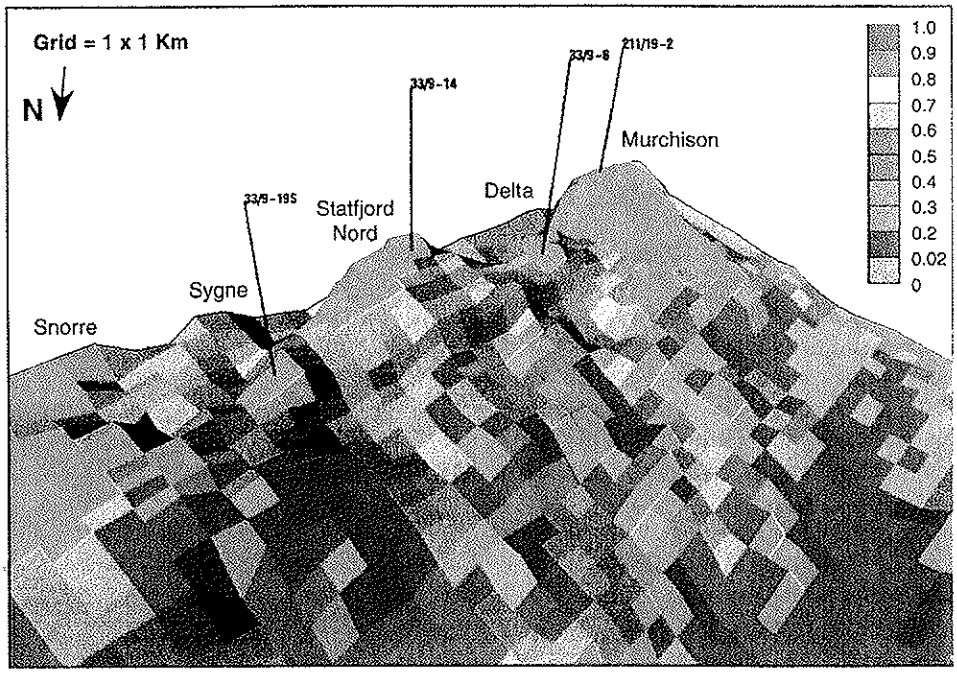

Figure 8. Modelled oil saturation in traps and carrier in the Brent sequence, Tampen Spur area using the grid cell sizes in Figure 7. Modified from Johannesen et al (2002).

Hydrocarbon saturations are modelled to increase in areas of focused flow and within the structural highs, where trapping causes hydrocarbon columns to increase until further up-dip spill is achieved. The average saturations within the Brent carrier were modelled to vary significantly, also outside of trapping structures. Average hydrocarbon saturations over a 100 m thick interval were modelled to exceed 40% in some spill areas (see Figure 8). This is prominent in the fill-spill system from Murchison through Delta and into the Statfjord Nord structure (Figure 7). The resulting modelled losses within a 100 m thick node with an area of $10^6 m^2$ can be found from:

$$Vcell = AH\phi\eta So = 10^6\ m^2 * 100\ m * 0.28 * 0.9 * 0.40 = 10\ 10^6\ m^2 \quad (9)$$

where ϕ is the porosity, η is the net/gross of the carrier, and So is the average hydrocarbon saturation modelled within the cell. In many spill-path cells the modelled hydrocarbon migration losses would therefore be greater than $10\ 10^6\ Sm^3/km^2$. Over a modelled distance of 10 km, spill-path losses may exceed the volumes found in a giant oil field.

Sylta (2002) argued that typical hydrocarbon secondary migration column thicknesses would be less than 1m and with hydrocarbon saturation in the range 10 to 20%. The first problem with the reported results in this particular case is that the width of the spill paths is quite likely less than 1 km. The lateral focusing of hydrocarbon migration along foot-wall ridges could make the migration stringer less than 100m wide. This would have been resolved by the model if the lateral resolution was greater. The second problem is the vertical resolution of the model, which is around 100m (see Figure 7). Sylta (2002) calculated vertical thicknesses of hydrocarbon migration stringers to be less than a few meters in good carrier rocks. The numerical solution of the fluid flow model requires the 40% oil saturation to achieve sufficient relative permeability and capillary pressure to transport the modelled flow-rates within the carrier rock. The 40% oil saturation may be correct, but it does not represent the average oil saturation within the entire carrier thickness. The 40% should be modelled to be the average oil saturation within only the 1m thick oil stringer. The modelling approach used assumes constant hydrocarbon saturations within the entire cross-sectional area of the grid-node, and therefore the average oil saturation is applied to the wrong thickness. There is insufficient information in the paper to calculate accurately how much the loss is overestimated, but a conservative estimate based upon Sylta (2002) suggests that the losses should be reduced to less than 20% due to lateral resolution problems, and down to less than 5% in the vertical direction. Over the 10 km distance, migration losses would be reduced with 99% (0.2*0.05=0.01) from $100\ 10^6\ m^3$ to $1\ 10^6\ m^3$.

It is important to note that these findings are representative of the Darcy type of modelling, and not a result of the misapplication of the technology by the authors of this particular reported case study. The reason for the chosen grid-node sizes is typically that the run-time of

each simulation has to be constrained to a few days or weeks. A doubling of the vertical resolution can typically lead to much more than a doubling of the run-time, making the time-frame for finishing a typical case-study too long. In order to improve on the situation, one first needs to become aware of the problem when it occurs. This can be done by computing the actual losses within the grid-node cells. If the integrated oil saturation over the height of the carrier is computed only for those areas where there is a dynamic flow situation (outside the traps), then one can easily view where there is a danger of overestimating the losses. In these areas, one may introduce a finer vertical resolution of the top of the carrier. This would allow for more correct estimates of saturation distributions without changing the actual methods used in the simulator. One advantage of this approach is that it can be employed by the modeller without making any changes to the simulation code. The process could also be automated by including the concept into the simulation code. A dynamic re-gridding approach could thus help solve this problem, reducing the need for using excessive computing resources in the simulation runs.

Sylta (2002) suggested changing the hydrocarbon saturation description inside the computing nodes. By applying depth-dependent hydrocarbon saturations within each computing node, it is possible to solve analytically for the heights and saturations of migrating oil stringers and convert these to an effective permeability description that can then be used in the Darcy flow simulations. Sylta (2002) gave equations for this solution.

Trap size resolution may be a problem for low-resolution models. The effect of trap resolution on predicted hydrocarbon volumes in 3D basin models can be investigated numerically. Krokstad and Sylta (1996) used a ray-tracing technique to model secondary migration in the eastern part of the Northern North Sea (Figure 9). The modelling was performed using regular grids with node sizes of 750m*750m. Hydrocarbons were modelled to be generated and expelled from Jurassic source rocks into the Brent carrier and reservoir system. Oil and gas were modelled to be trapped in a number of Middle Jurassic closures, some of which had been drilled. The drilled traps were used in the calibration of the model. Here we use the same geologic model and parameter definition to investigate the sensitivity of grid resolution on trapped hydrocarbon volumes. An automatic re-sampling scheme was developed for this investigation (Figure 10). During the loading of each input grid, (depths, thicknesses, oil and gas expulsion etc.), a linear interpolation between the nodes of the original 750m*750m grid was performed to create a modified input grid "on-the-fly". A user controlled parameter (refine) was used to control the resolution of the loaded model. The loaded grid would have 500m*500m node sizes when a refine value of 0.67 was used, while the size would increase to 1500m*1500m for refine=2. A single value of refine would be used for an entire simulation run. Each run would simulate the secondary migration of oil and gas from Late Jurassic time until the present day (Krokstad and Sylta, 1996). The pressure, temperature, oil and gas expulsion histories were kept constant between the runs, but changed with geologic time within each run.

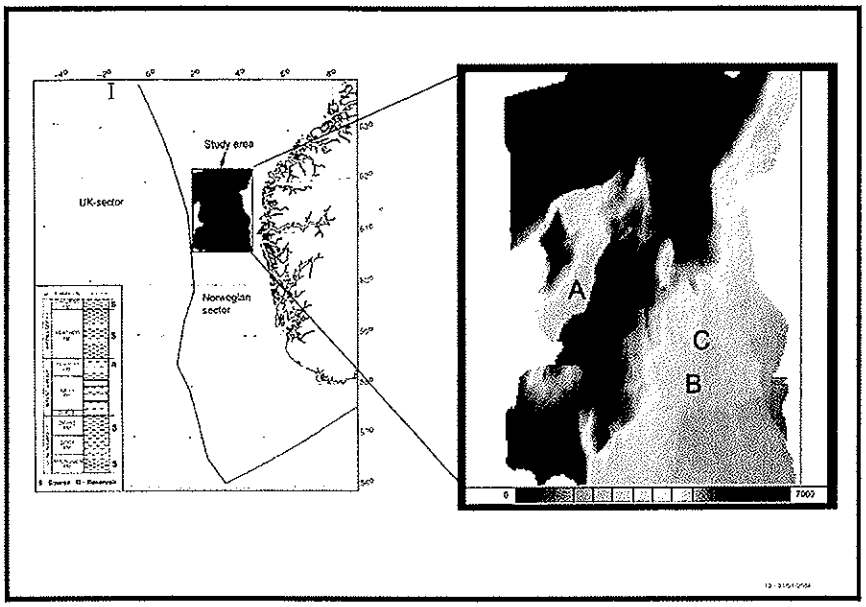

Figure 9. Top Middle Jurassic carrier depth map used in modelling node size sensitivity on trapped volumes of oil and gas. (Modified from Krokstad and Sylta, 1996). A,B,C: Locations of traps A and B in Figure 11 and trap C in Figure 12.

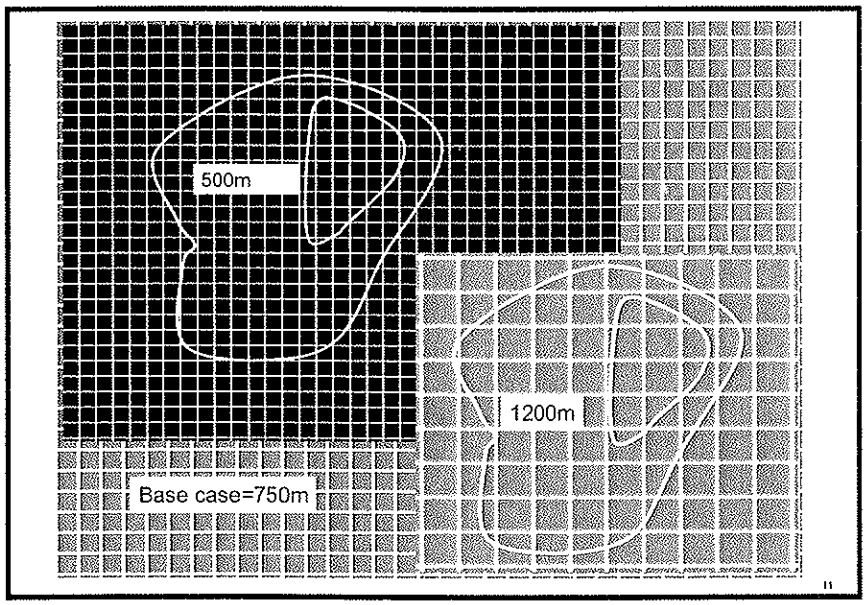

*Figure 10. Resampling of grid nodes. Higher resolution grids (upper left) and lower resolution grids (lower right) are constructed by linear interpolation of value in each node from the 750m*750m input grid.*

A series of simulations were run with refine varying systematically from 0.67 to 3.5. More than 100 runs were used, and the modelled node sizes ranged from 500m to 2600m. The amounts of trapped oil and gas at 0 Ma were extracted for a series of traps. Figure 11 shows modelled trap volumes for two traps in the study area using the ray-tracing technique, and systematically varying the grid resolution. These two traps are fairly representative of the findings for most of the traps. For these two traps, the accuracy of the modelled volumes is within +-10% when grid node sizes are around 750m*750m, increasing somewhat towards +-20% at 1km*1km grid node sizes, and becoming unacceptable large (+-30%) around 1.5km*1.5km grid sizes. This suggests that 1*1km grid size resolution may be acceptable for Darcy flow modelling, but increasing the grid node sizes beyond 1.5km^2 should be avoided (see vertical line at refine=1.2 in Figure 11).

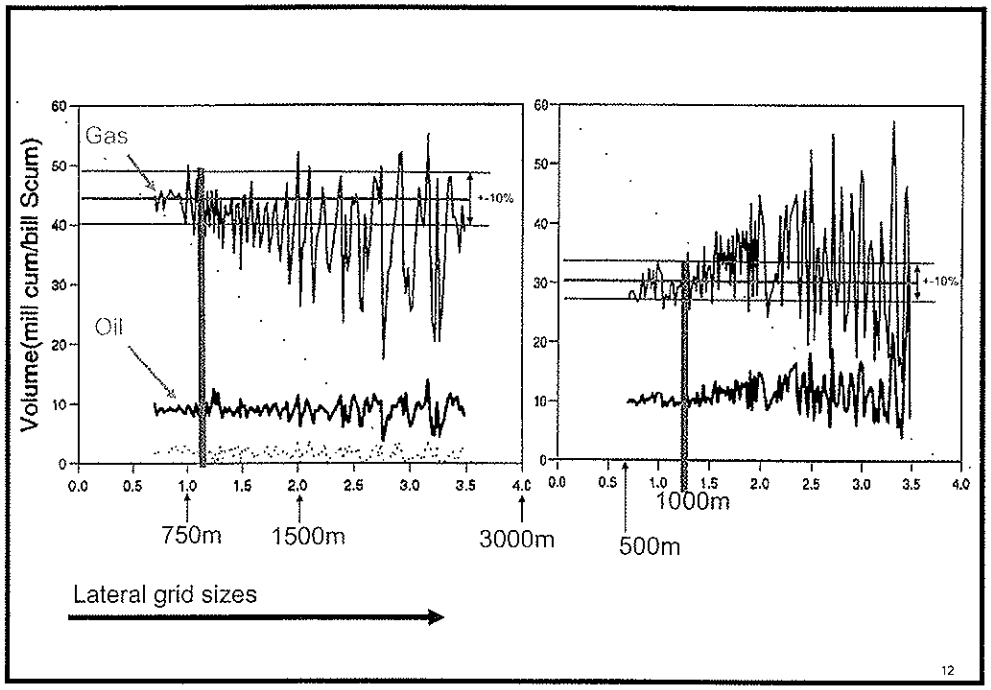

*Figure 11 Trapped oil (bold curve below) and gas in traps A (left) and B (right) modelled with varying lateral resolution. An x-axis value of 1 corresponds to 750m*750m grid sizes resolution. X=0.67 is 500m*500m, and x=2 is 1500m*1500m grid size. Locations are shown in Figure 9.*

There is some drift in the modelled volumes of trapped oil and gas in Figure 11. Trap A shows a decrease in the trapped gas when refine increases, while trap B increases. The drift is most notable for values of refine > 1.2. The gas volumes seem to be more sensitive than the oil volumes, but this is mostly a plotting effect because there is more gas (in billion cum) than

oil (in million cum) trapped in these pools. Not all traps show the same type of dependency. Small traps typically are much more sensitive to model resolution. Figure 12 shows the results for a smaller trap with trapped oil around 6 10^6 m^3 for refine=0.7. Already at refine=0.95 there is a major peak in the modelled volume of trapped oil in this trap. The peak value is 300% (around 18 10^6 m^3) of the high-resolution value. The figure suggests that for smaller traps, the accurate calculations of trap phases and volumetric require high-resolution models with node-sizes that do not significantly exceed 500m*500m.

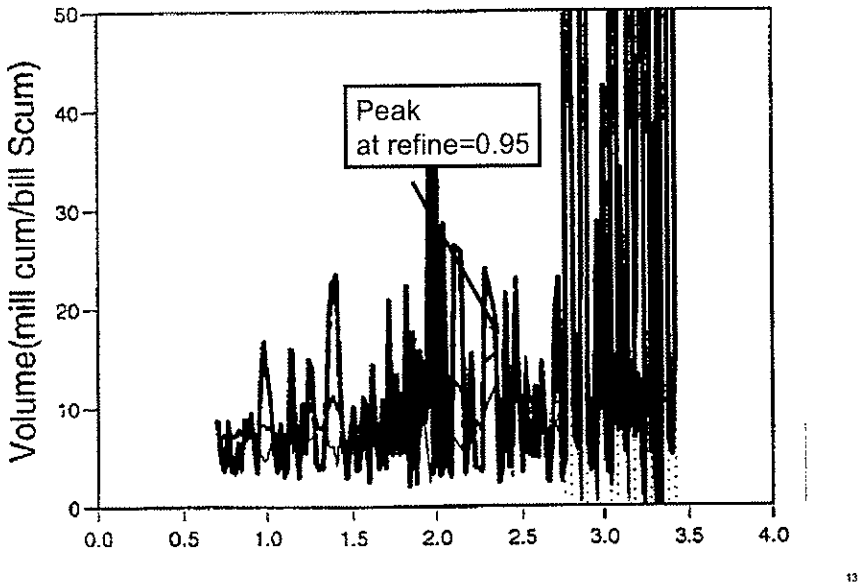

Figure 12 Trapped oil (bold curve) and gas in trap C modelled with varying lateral resolution (X-axis explained in Figure 11). Location are shown in Figure 9.

How to do better?

Over the last 15 years the author has seen many case studies where migration modelling has changed the risk assessment of prospects and license applications. Very few of these have been published. In one of the first applications, an unidentified prospect was filled with hydrocarbons by the simulator. The interpreter had not seen the closure because there were too many other possibilities. More typically, geologic risk factors are identified by hydrocarbon migration modelling, and the risked volumetric of prospects may have to be decreased as a result. Focusing on what we can do better should perhaps then deal with those elements in hydrocarbon migration modelling that can help in describing the geologic risk factors better. A short-list of suggested improvements in the methodologies may contain:

- Variable saturations inside computing cells for coarse models.
- Use probabilistic percolation modelling to simulate "Darcy leakage".
- Parallel processing techniques for Darcy flow modelling.
- Assess flow-regime in mud-rocks before applying percolation on leakage modelling.
- Use very low entry pressures and high relative permeabilities to reduce losses in carrier rocks when using Darcy flow modelling.
- Consider modelling Darcy flow carriers with uppermost carrier nodes less than 1 m thick.
- Experimental work to validate the use of the L parameters for different lithologies.

Conclusions

This paper has shown that all types of hydrocarbon migration modelling have serious problems associated with them. Darcy FD/CV methods have shortcomings in modelling migration in carrier systems, while percolation methods may be wrong to use in modelling hydrocarbon leakage out of traps. Ortho-contouring and ray tracing are techniques that so far have only been demonstrated to work for simple carrier systems.

One reason for the shortcomings of the methods is the order of magnitude in difference in flow properties for carriers and shales. Researchers and oil companies are today therefore not able to assess all geologic risks with just one tool (or method), but need to be active in pursuing different approaches. In spite of shortcomings of existing technologies, they can be used to give first order estimates of the hydrocarbon migration system. This is far better than having no estimate at all. However, basin modellers should **be open to new approaches** in hydrocarbon migration modelling in the future.

References

Burley S.D, 2000. 4D basin modelling as an exploration tool. Geofluids III Conference, June 2000, Barcelona, Spain. Abstract only.

Carruthers, D., RINGROSE, P., Secondary oil migration: oil-rock contact volumes, flow behaviour and rates. In Parnell J. (ed) 1998. *Dating and Duration of Fluid Flow and Fluid-Rock interaction. Geological Society, London. Special Publications 144.* p205-220.

El-Ghamri, M.A., Warburton, I.C., Burley, S.D., 2002. Hydrocarbon generation and charging in the October field, Gulf of Suez, Egypt. Journal of Petroleum Geology, Vol. 25(4), October 2002, p433-464.

Frette, V., Feder, J., Jøssang, T., Meakin, P. 1992. Buoyancy driven fluid migration in porous media. Physics Review Letters 68, 3164-3167.

Grigo, D., Maragna, B. Arienti, M.T.,Fiorani, M., Parisi, A., Marrone,M., Sguazzero, P., Uberg, A.S. 1993. Issues in 3D sedimentary basin modeling and application to Haltenbanken, offshore Norway. In Dore et al (Eds) Basin Modelling: Advances and Applications. NPF Special Publication 3, pp455-468, Elsevier, Amsterdam.

Grigo, D. Cavecchi, C., Bozzoni, P., 2003. 1991-2001 Ten years basin modelling activity at ENI-Agip - Exploration result summary. Abstract only.

Hermanrud, C. 1993. Basin Modelling techniques – an overview. In Dore *et al.* (eds): *Basin Modelling: Advances and Applications*. NPF, Special Publications 3. Elsevier, Amsterdam, p1-34.

Johannesen, J., Hay, J., Milne,J.K., Jebsen,C.,Gunnesdal,S.C., Vayssaire,A.,2002. 3D oil migration modelling of the Jurassic petroleum system of the Statfjord area, Norwegian North Sea. Petroleum Geoscience, Vol 8., p37-50.

Krokstad, W., Sylta, Ø., 1996. Risk assessment using volumetrics from secondary migration modelling: assessing uncertainties in source rock yields and trapped hydrocarbons. In: Dore, A.G., Sinding-Larsen (eds.). Quantification and Prediction of Petroleum Resources, NPF Special Publication 6, pp 219-235.

Selle O.M., Jensen, J.I., Sylta Ø., Andersen, T., Nyland B., Broks T.M. 1993. Experimental verification of low-dip, low-rate two-phase (secondary) migration by means of gamma-ray absorption. In Parnell J. *et al.* (eds): *Geofluids'93. Contributions to an International Conference on fluid evolution, migration and interaction in rocks*. p72-75.

Schroeder, F.W., Sylta, Ø., 1993. Modelling the hydrocarbon system of the North Viking Graben: a case study. In Dore *et al.* (eds): *Basin Modelling: Advances and Applications*. NPF, Special Publications 3. Elsevier, Amsterdam, p469-484.

Skjervøy, A., Sylta, Ø., Weissenburger, S., 2000. From basin modelling to basin management: reuse of basin-scale simulations. In: Ofstad et al (Eds). Improving the Exploration Process by Learning from the Past. NPF Special Publication 9, p141-157. Elsevier, Amsterdam.

Sylta, Ø. 1987: SEMI - A program for the modelling of buoyance driven, SEcondary MIgration of oil and gas by means of a ray-tracing technique. IKU Report 25.2403.00/01/87, 51p.. Open.

Sylta, Ø. 1989: Modelling of secondary migration and entrapment of a multicomponent hydrocarbon mixture using equation-of-state modelling techniques. Petroleum Migration Meeting, Burlington House, London, September, 15p..

Sylta, Ø., 1993. New techniques and their application in the analysis of secondary migration. In Dore *et al.* (eds): *Basin Modelling: Advances and Applications*. NPF, Special Publications 3. Elsevier, Amsterdam, p385-398.

Sylta, Ø., Pedersen, J. I., Hamborg, M. 1998. On the vertical and lateral distribution of hydrocarbon migration velocities during secondary migration. In: Parnell, J. (ed.). Dating and Duration of Fluid Flow and Fluid-Rock Interaction. Geological Society London, Special Publication 144, 221-232.

Sylta, Ø., 2002. Quantifying secondary migration efficiencies. Gefluids 2, pp 285-298.

Standing, M.B., 1975. Notes on relative permeability relationship. Division of Petroleum Engineering and Applied Geophysics. The Norwegian Technical University, Trondheim.

Ungerer, P., Doligez, B., Chenet, P.Y., Burrus, J., Bessis, F., Lafargue, F., Giroir, G., Heum, O., Eggen, S., 1987. A 2-D model of basin scale petroleum migration by two-phase fluid flow. Application to some case studies. In: B. Doligez (editor), Migration of hydrocarbons in sedimentary basins Technip, Paris, pp 415-456.

Welte, D. H., Yükler, A. 1980: Evolution of sedimentary basins from the standpoint of petroleum origin and accumulation - an approach for a quantitative basin study. Organic Geochemistry 2, 1-8

Table 2. Description of variables used in this paper.

$Q =$	Flow [m^3/s]
$q =$	flow-rate [m^3/m^2 s]
$w =$	width of flow-path [m]
$H =$	total height of flow path [m]
$h =$	height above base of flow-path ("oil-water contact") [m]
$k =$	absolute permeability [Darcy or m^2]
$k_r =$	relative permeability (0-1)
$k_r^o =$	relative permeability at maximum oil saturation ($S_w = 1\text{-}S_{oi}$)
$\Delta\rho =$	density contrast between hydrocarbon phase and water [kg/m^3]
$S_o =$	oil saturation (average from h = O to h = H)
$S_{oi} =$	minimum oil saturation for flow to occur
$S_w =$	water saturation (between S_{wi} and 1 - S_{oi})
$S_{wi} =$	irreducible water saturation
$\alpha =$	dip of carrier
$\mu =$	viscosity of hydrocarbon phase [Pa s]
$S_w^* =$	effective water saturation (0 - 1) in Corey equation
$\emptyset =$	porosity of carrier bed, isotropic medium
$P_e =$	entry pressure [Pa]
$P_c =$	capillary pressure [Pa]
$v =$	average velocity of the hydrocarbons migrating [m/s]

CHAPTER 11

11. 3D Modelling of fault bounded pressure compartments in the North Viking Graben.

3D Modelling of Fault Bounded Pressure Compartments in the North Viking Graben

Hans Borge and Øyvind Sylta
IKU Petroleum Research
N-7034 TRONDHEIM, NORWAY

ABSTRACT

The work presented in this paper involves modelling of the overpressure distribution in Jurassic reservoir and carrier rocks in the North Viking Graben. The main concept used in this study is that faults may form low-permeability barriers to fluid flow in compacting basins, and may thus influence overpressure distribution. The mapped faults in the study area are linked together so that they divide the area into 225 compartments. A model based on Darcy's law and information about offset and burial depth describes the flow conditions across the faults and between the compartments. This model describes a regional fault permeability architecture. A commercial reservoir simulator is used to calculate the fluid flow and the pressure development in all the compartments. The model was calibrated to pressures measured in 16 released exploration wells. The best match to these wells was obtained with a mean deviation of 9.5 bars and a standard deviation of 18.5 bars between the observed and predicted overpressures for the Brent Group. The results from this pressure modelling can be used to simulate secondary migration of oil and gas.

INTRODUCTION

The main idea behind the model developed to calculate a realistic present day pressure map is that faults form barriers to fluid flow. The Middle Jurassic Brent Group in the North Viking Graben is divided into pressure compartments bounded by the mapped faults. Faults can cause big lateral pressure differences in a reservoir (Mann & Mackenzie, 1990), and thus constitute a lateral seal for the pressure compartments. Distinct pressure-depth gradients in the pre-Cretaceous sandstones in the UK Central Graben suggest compartmentalisation and hydraulic separation of the sandstone into pressure cells (Darby, Haszeldine and Couples, 1996). Over- and underlying sealing layers may thus cause vertical boundaries for the pressure compartments. Figure 1 illustrates the concept of pressure compartments. In this study, no geometrical reconstruction of faults is carried out other than linking the mapped faults together in order to form the pressure compartments. According to this model all changes in overpressure occur across the faults. What appear to be fluid compartments in a subsurface basin can result from dynamic movement in which almost all of the changes in fluid potential occur associated with zones of low permeability (Bredehoeft, Belitz and Sharp-Hansen,1992). It is assumed that fluids inside a pressure cell are in free hydraulic communication. The pressure is treated as transient and the compartments as dynamic over time.

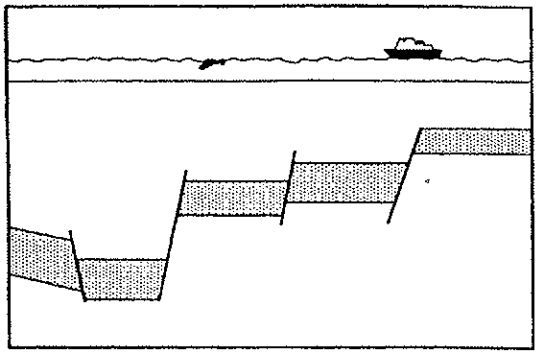

Figure 1. Schematic outline of pressure cells

The connectivities between the neighbouring compartments are calculated based upon data provided by seismic such as thickness of reservoir, depth to fault, length of fault and size of fault offset/overlap. A transmissibility model for the faults is inferred. The ability for water to flow between connected cells is described only by the transmissibility. This is a quite useful approach because most commercial reservoir and basin simulators have an arbitrary connection device, which means that it is possible to connect any two grid blocks. The data provided by seismic are treated as variables, while the rest of the parameters in the transmissibility model have the same values all over the study area. In this way a regional model for fault based permeability architecture is introduced. If the parameters were allowed to vary freely from fault to fault, the calibration would probably become too large. The main task is to model fault- or fault zone- permeability when evaluating sealing or preferential paths for fluid flow migration. Previous work on this topic is very scarce in the literature and exists only at the qualitative level (Antonellini & Aydin, 1994).

The pressure compartments were coded into the SimBest II reservoir simulator from SSI and connected according to the inferred model. Other simulators, e.g. Eclipse, may also be used. "Wells" at the boundary of the study area control the development of overpressure. Overpressure development in a sedimentary basin is directly related to the rate of fluid escape from the sediments (Yu & Lerche, 1996). However, the mechanism or mechanisms generating the overpressure is highly debated (Osborne & Swarbrick, 1997, Walderhaug, 1996 and Kooi, 1997). The modelling presented in this paper does not concentrate on the generation of overpressure, but the lateral dissipation which is assumed to be governed by the partly sealing faults.

It is assumed that the fluid flow modelled in this study reflects the contribution to the overpressure from undercompaction of sediments during burial subsidence. Other factors such as fluid thermal expansion, dewatering of clays and hydrocarbon generation are considered less important (Yu & Lerche, 1996), and are not included in the simulations.

The study area, located between 2° and 4° E and 61° and 62° N (Figure 2), which is about 40 km west of the Sognefjord, represents an area of about 20000 km^2. It includes quadrants 34 and 35 and the northern parts of quadrants 30 and 31 on the Norwegian

continental shelf. This area contains several oil and gas fields, e.g. Visund, Huldra, Agat, Veslefrikk and the northern parts of the Troll field.

The resulting pressure maps can be used as input to secondary migration simulations (Sylta, 1996). Hydrodynamic pressure (potential) differences across faults may increase or decrease the oil and gas leakage across the faults. It is therefore of crucial importance to the success of hydrocarbon secondary migration studies that the results from the pressure modelling are used. Otherwise, the fault leakage model becomes too unconstrained and the predictive capability of the model may be non-existent.

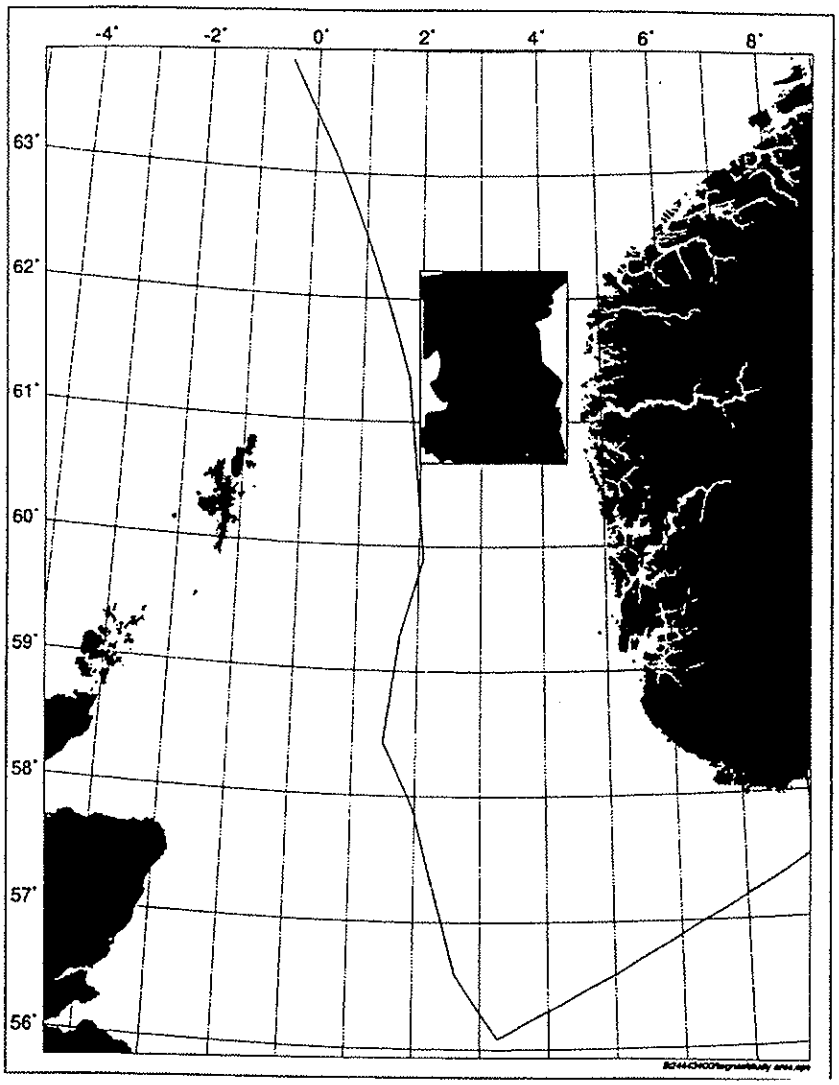

Figure 2. The study area

Pressure cells

The compartmentalisation of the study area was carried out by using the mapped faults shown in Figure 3. In order to create pressure compartments, some of the faults were tied together by extending them beyond the seismically resolved tip to the nearest fault. The results of this process can be seen by comparing Figure 11 with Figure 3. Based upon this assumption, the study area is divided into compartments bounded by the blocky lines shown in Figure 4. This could be a realistic way to consider the compartmentalisation because even faults which are too small to be seen on seismic can contribute to the compartmentalisation of a block (Gauthier & Lake, 1993). Extending the faults beyond the seismic resolution increases the connectivity of the fault pattern (Pickering *et al.*, 1997). The fault compartment interpretation involves making closed compartments by connecting fault traces in a geologically reasonable manner. We did not remove any fault segments. Faults that are not part of closed polygons automatically lie inside the compartments and therefore are not used in the pressure modelling.

It has long been known that fault systems have a degree of self-similarity across a wide range of scales (Yielding, Walsh & Watterson, 1992; Wen & Sinding-Larsen, 1994; Gauthier & Lake, 1993). Considerable progress has been made in recent years in methods of predicting sub-seismic fault populations. Prediction of realistic spatial distributions of sub-seismic faults is much less certain (Heath, Walsh & Watterson, 1994). However, extensional fractures are non-fractal and frequently terminate against fractures of the same family (Loosveld & Franssen, 1992). These factors may justify the subjective fault connections made in this study rather than developing a model or algorithm connecting faults based upon fractal or self-similar criteria.

FAULT PERMEABILITY CHARACTERISATION

A cataclastic fault may result in either a permeability increase or decrease (Knipe 1992, Loosveld & Franssen, 1992), but the latter is more common (Loosveld & Franssen, 1992). Granulation and cataclasis, associated with faulting in porous sandstone, cause the porosity to drop approximately one order of magnitude in a deformation band and almost to zero adjacent to a slip plane; permeability drops one to four orders of magnitude normal to a deformation band and more than seven orders of magnitude perpendicular to a slip plane (Antonellini & Aydin, 1995). In addition to this, the high overpressures in the deep and intermediate parts of the basin indicate that the faults act as seals. During periods of active movement, the faults may have gone through short transient periods when the faults acted as fluid migration pathways (Knipe, 1992). Possible non-sealing periods like this are unlikely to affect the lateral fluid flow on a geologic time scale. The pressure build-up in this area took place after the faults were active, so that it is natural to assume that all the faults to a certain extent are sealing.

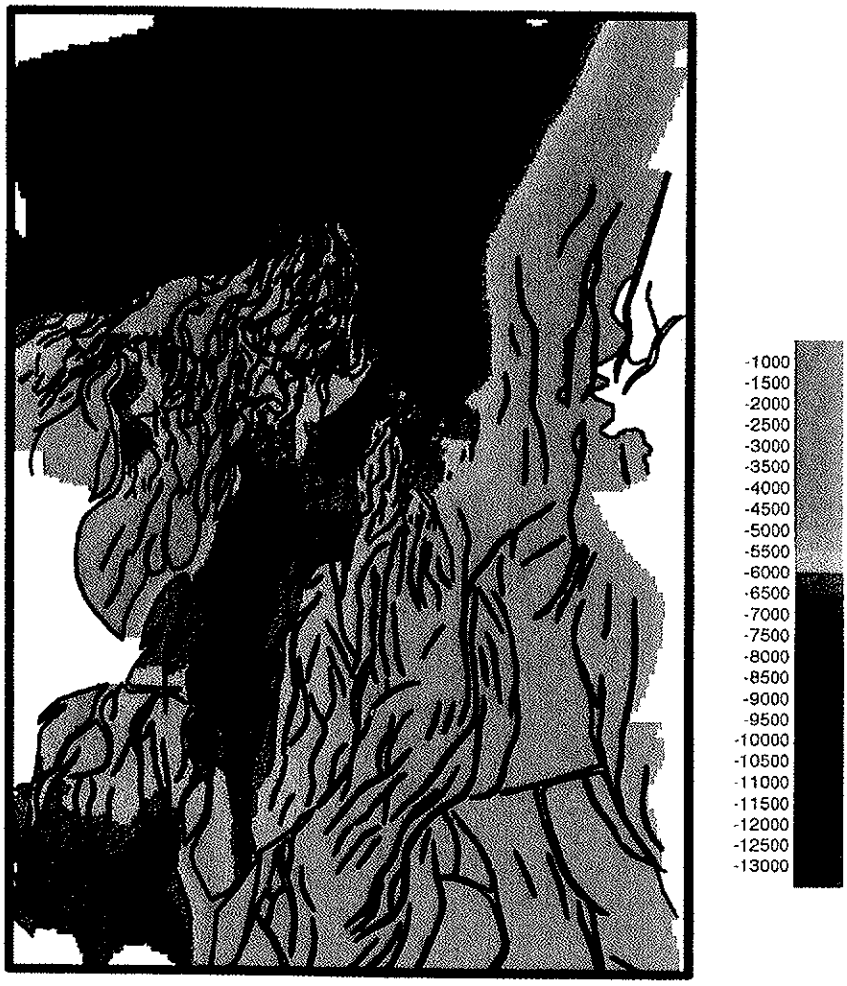

Figure 3. Present day depth (m) map of Top Brent Group with interpreted faults mapped from seismic data

Figure 4. The study area divided into pressure compartments. Pixels between the compartments without fill are defined as inside of faults and are not part of any pressure compartments. Each compartment is shown in one greyscale value. The actual value is arbitrary, and does not indicate pressure or overpressure.

In order to deduce a model for fluid flow, a fault is considered as a low permeable block located between two reservoirs as illustrated in Figure 5. The transmissibility, which is the ability of water to flow through a porous block, is given in Equation 1.

Faults are considered to be low-permeable blocks with a specific thickness. Therefore we do not have to determine whether the faults are surrounded by damage zones or deformed zones in the model. Irrespective of the structures forming the faults, the impact on fluid flow can be accounted for by this block.

$$T = \frac{\Delta l\, H\, K}{b} \tag{1}$$

Equation 1 forms the basis for a "Fault Transmissibility Model". It is assumed that one of the most important properties of faults is whether they have an offset or an overlap. The model introduced by Equation 2 and illustrated in Figure 7 accounts for fault throw effects. It is desirable that the transmissibility should be more or less proportional to the contact area when overlaps are modelled, because sand-sand contacts usually are "non-sealing" (Nybakken, 1991). Thus, in the case of decreasing overlap, the transmissibility decreases linearly to $p\%$ of the original transmissibility given in Equation 1. Faults in the Brent province (located only few km west of the study area) with throws greater than the reservoir thickness have a better than 90% probability of sealing (Knott, 1993). This observation suggests a relatively low value of the parameter p and justifies large differences in transmissibility between overlapping faults and faults with an offset. It is further assumed that the transmissibility function follows an exponential curve in the case of increasing offset. Even if the fault throw is small ($\theta \approx -H$) , the permeability is considerably decreased by the fault block. The argument is that cataclasis and shale smearing will reduce the permeability even at small fault throws. If there is no throw, which means that the reservoirs overlap completely, the model will simplify to Equation 1.

$$\begin{aligned} T(\theta) &= \frac{\Delta l\, K}{b}\,[(p-1)\theta + p\,H\,] \qquad \theta < 0 \\ (\theta) &= \Delta l\, pH\, e^{-B\theta}\ \frac{K}{\sqrt{b^2+\theta^2}} \qquad \theta > 0 \end{aligned} \tag{2}$$

Numerical simulations of K_{eff} / K (the ratio between effective horizontal permeability and the permeability in a shale-free sandstone matrix) vs. fault density have shown that the effective permeability decreases linearly (or very close to linearly for the 3D models) with increasing fault density (Heath, Walsh and Watterson, 1994). This observation may support the linear part of the transmissibility curve in Figure 7. If the overlap variable $\theta \in (-H,0)$s comparable to or proportional to the fault density, the statement above supports the assumptions that $T(\theta)$ / T decreases linearly with increasing offset, where T and $T(\theta)$ are taken from Equation 1 and 2 respectively. In addition, fault seal data from the northern North Sea show that increasing the maximum fault throw compared to the reservoir interval thickness increases the fault seal probability (Knott, 1993). The regional fault seal model given in Equation 2 is a

simplification intended to describe the regional lateral fluid flow behaviour. The model is not designed for investigating individual faults in detail for prospect analysis.

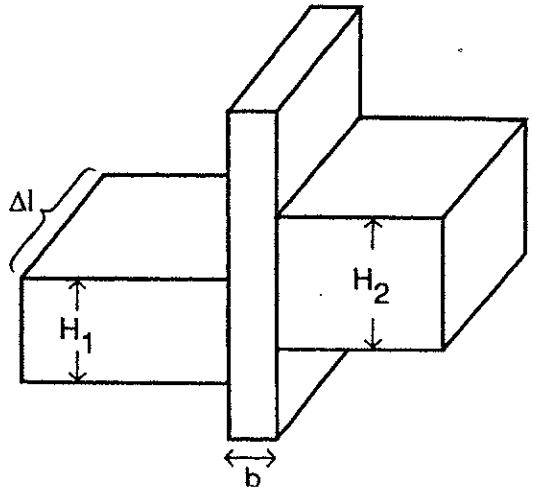

Figure 5. Schematic outline of a fault

Table 1

Nomenclature

K :	Permeability inside the fault block
b :	Width of fault block
Δl :	Length of fault block
T :	Transmissibility
H :	Thickness of reservoir, $H = \min\{H_1, H_2\}$
ϕ :	Porosity
D :	Water-depth
z :	Depth to fault
δ_{sh}:	Rate of change in permeability (log) versus porosity (log) in log (permeability) - log (porosity) relationship for shallow depths, i.e. $\phi > \phi_b$.
δ_{dc}:	Rate of change in permeability (log) versus porosity (log) in log (permeability) - log (porosity) relationship for deep parts, i.e. $\phi > \phi_b$.
K_b:	Permeability where K - ϕ curve changes between deep and shallow relationships.
ϕ_b:	Porosity where K - ϕ curve changes between deep and shallow relationships.
c :	Rate of change in porosity versus depth
ϕ_0:	Porosity at seabed
u :	Offset/overlap (see Figure 6)
p :	Percent remaining fault-transmissibility when both the overlap and the offset is zero.
B :	Parameter controlling the exponential decrease of the transmissibility function.

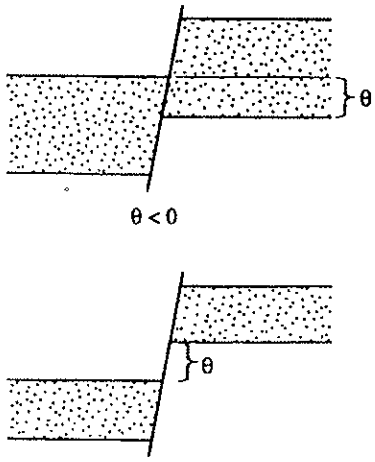

Figure 6. Fault with overlap (θ > 0, above) and fault with offset (θ > 0, below).

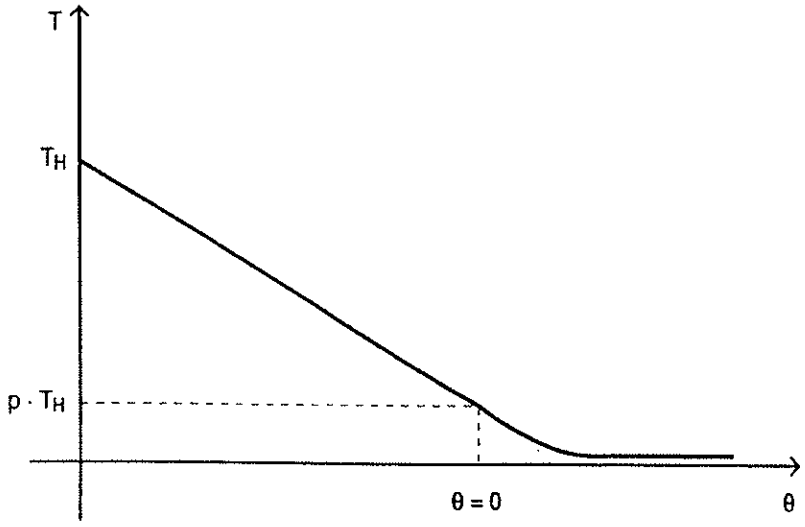

Figure 7. Transmissibility function - the "Fault model"

The permeability of clastic rocks is often treated as dependent on porosity, which again is considered to be a function of depth (Sclater & Christie, 1980). In order to include these properties and complete the fault transmissibility model, the relationships between permeability and porosity presented in Equation 3 and illustrated in Figure 8 are used. Note that by using this permeability model it is possible to differentiate the relationship between permeability and porosity in the deep and shallow areas in the basin. This introduces a great flexibility to the calibration work and is supported by Loosveld & Franssen, 1992.

$$K = K_b \left(\frac{\phi}{\phi_b}\right)^{\delta_{de}} \qquad \phi<\phi_b$$
$$K = K_b \left(\frac{\phi}{\phi_b}\right)^{\delta_{sh}} \qquad \phi>\phi_b \tag{3}$$

The porosity is given by Equation 4 which is the most usual porosity function used in numerical basin models (Wangen, 1992). This porosity model is deduced for isostatic burial history models and it provide a useful premeability-depth relationship for the fault blocks.

$$\phi>\phi_0 e^{-c(WD-z)} \tag{4}$$

The variables and parameters in Equations 1, 2, 3 and 4 are explained in Table 1. The parameters b, p, B, ϕ_b, X_b, δ_{de}, δ_{sh}, ϕ_0 and c have to be determined during the calibration of the model although reasonable starting values can be obtained for b, ϕ_b, ϕ_0 and c by geological reasoning. All the parameters are given the same value over the entire study area. Properties like width of fault, thickness of reservoir, water depth, depth to fault and offset/overlap differentiate the transmissibility values between the faults. Transmissibilities between neighbouring compartments are calculated by using Equations 2, 3 and 4 on a fault segment to fault segment (grid node) basis and adding the contributions along the blocky lines in Figure 4. The grid resolution is 500m.

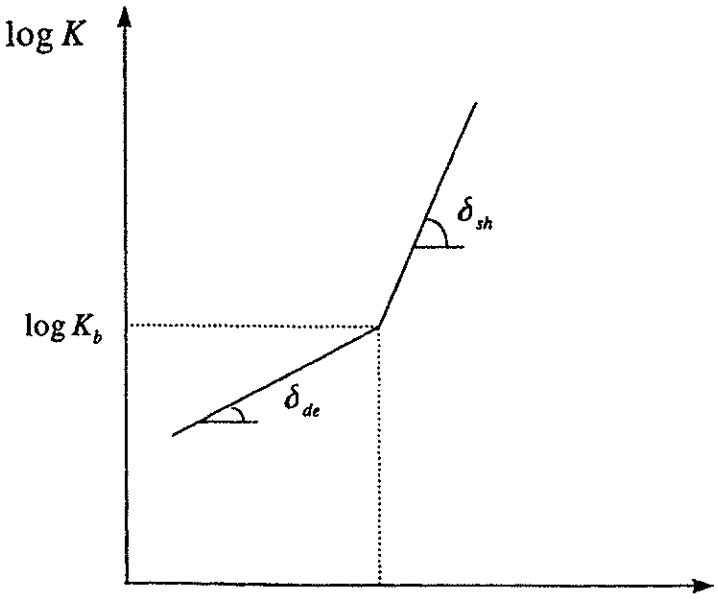

Figure 8. Permeability vs. Porosity

A simplification used in this study is to keep the geometry, and thus the sealing properties, constant through time. However, this simplification is not as limiting as it might seem. There are three main categories of seals: collapse seals, cement seals and juxtaposition seals (Knipe, 1992). The collapse and juxtaposition seals are more or less constant throughout the time we are modelling the pressure, since the faults have not been active since early Cretaceous. The cement seals are more difficult to handle in this model. The idea is that the model during the calibration process will provide a mean value of the sealing effect through time, which is sufficient to describe the sealing effects for the purpose of basin-scale pressure modelling. In addition, the faults in the study area are extensional fractures developed in the Jurassic and they have not been active since early Cretaceous.

THE SIMULATIONS

All the pressure compartments are represented in the SimBest II simulator from SSI by the present day depth to the top Brent Group and the thicknesses of the Brent Group, Dunlin Group and Statfjord Formation. In addition, thick sequences of shale/seal were added both above and below these reservoir units. The reservoirs in all the neighbouring compartments were then set up with the fault transmissibility model, by use of an arbitrary cell connection device available in the simulator. This situation is illustrated in Figure 9. In this way a pseudo 3D model for fluid flow is achieved. A similar pseudo 3D model including more geological units can be found in Bredehoeft *et al.*, (1992).

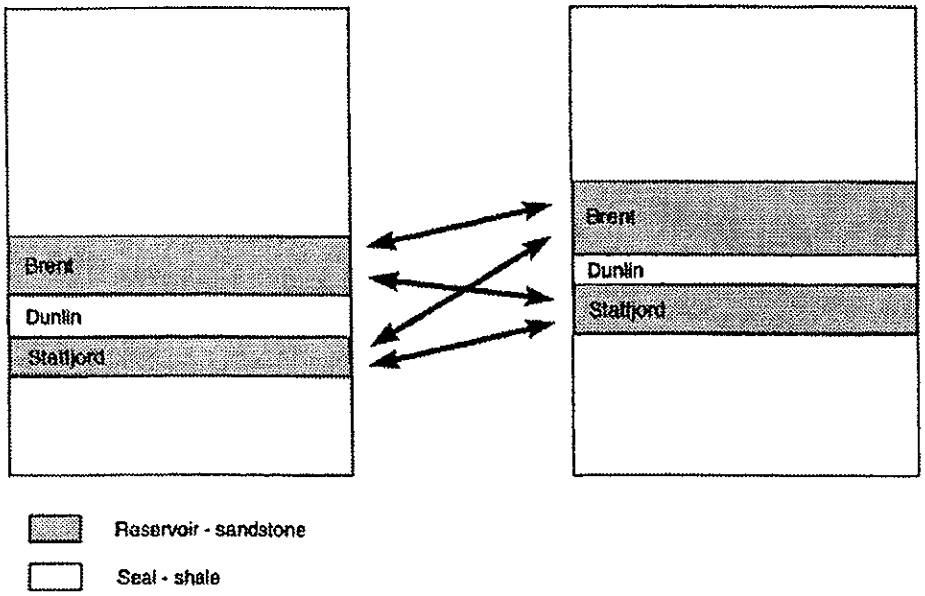

Figure 9. Possible connections specified between two neighbouring pressure cells. The arrows show flow connections using fault model.

In order to make use of a 3D reservoir simulator technology, which already exists, we transform the problem from one in which the potential difference between the basin and the flank is caused by an increase in the overpressures in the basin (e.g. Ungerer *et al.*, 1990), to one in which the potential difference is caused by a lowering of pressures at the flank. Instead of building up an overpressure, this system is initiated with a large overpressure of about 400 BAR over the entire study area. Two pressure compartments on the flank, one in the Visund area and one in the 34/4 block (see Figure 11) are defined as boundary compartments. In each boundary compartment, a "production well" has been defined in order to create differences in the overpressure. These differences are modelled to be the driving forces in the system and the overpressure histories in the boundary compartments are forced to follow the curves outlined in Figure 10, upper part. The pressure curve for the flank in Figure 10 upper part represents hydrostatic pressure. In order to find the real modelled overpressure this curve must be subtracted from the other curves as illustrated in the lower part of Figure 10.

The present day overpressure in the boundary cells is known from wells located within them. The boundary cell pressure histories (the curves in Figure 10), are of course not known. These curves were constructed in order to give an acceptable match to the present day overpressure in the calibration wells presented in Table 2. The large and rapid drop in overpressure on the flank and in the Visund area in Figure 10 represents a large increase in the difference in overpressure between the deep and shallow parts of the basin caused by a rapid pressure release on the eastern flank. The best matched overpressure presented in Tables 2 and 3 occurred only about 1.3 Myr after this marked drop. Thus this drop may well correspond to a large pressure release caused by an rapid uplift of the flank due to the disappearance of the last ice-age. Without introducing this pressure drop it was not possible to match the model. Groundwater is drained laterally through the Brent and Statfjord layers due to the differences in overpressure shown in Figure 10. By changing the parameters in the transmissibility model the flow rate is adjusted until the modelled overpressures match the observed overpressures in the released exploration wells in the study area.

In order to achieve the best match it was necessary to increase the vertical permeability in the seal shown in Figure 9. The drained water in the Brent Group and Statfjord Formation is thus partly replaced by vertical flow from the thick overlying and underlying sequences. The model thus incorporates vertical fluid flow into the sands expelled from over- and underlying shales. These observations show that both vertical and lateral fluid flow affect the present day overpressure distribution in the basin.

The SimBest II reservoir simulator uses a finite difference formulation of the conservation of mass and Darcy law to describe the water flow. This results in a system of coupled algebraic equations. The simulator treats the pressures fully implicit by using the proprietary SSI matrix solver ESPIDO which SSI claims is a fast, robust and powerful method.

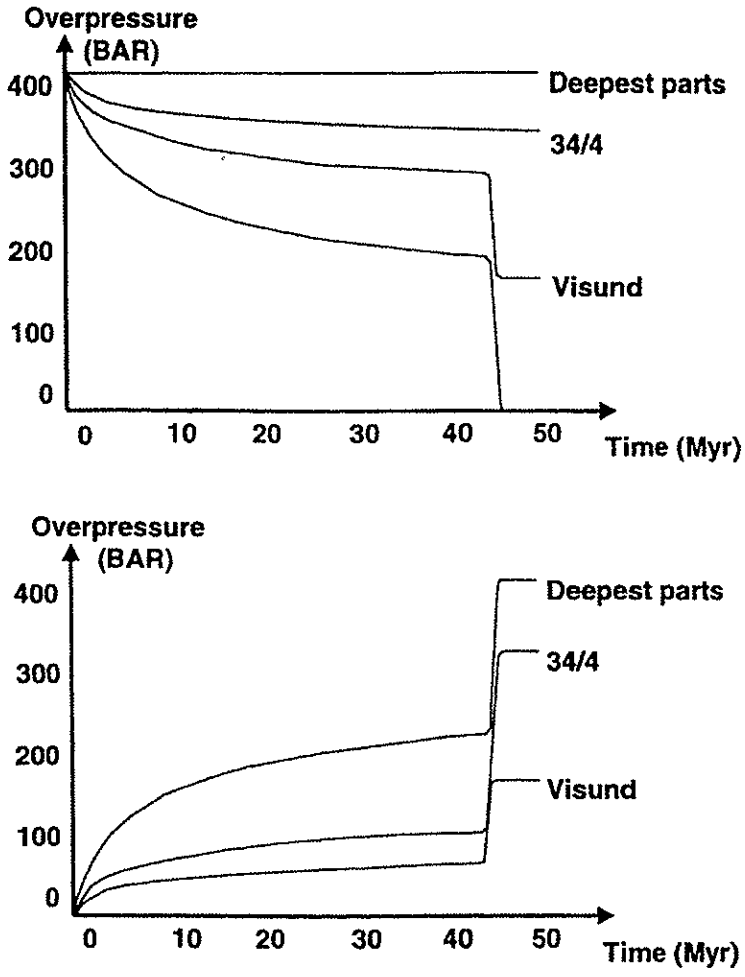

Figure 10. Modelled overpressure histories (upper part) and the actual modelled overpressures (lower part) in the boundary cells. The dynamic basin overpressure histories (lower) are transformed into astatic basin formulation (upper) in order to makeuse of existing pressure simulators. See Figure12 for location of these cells.

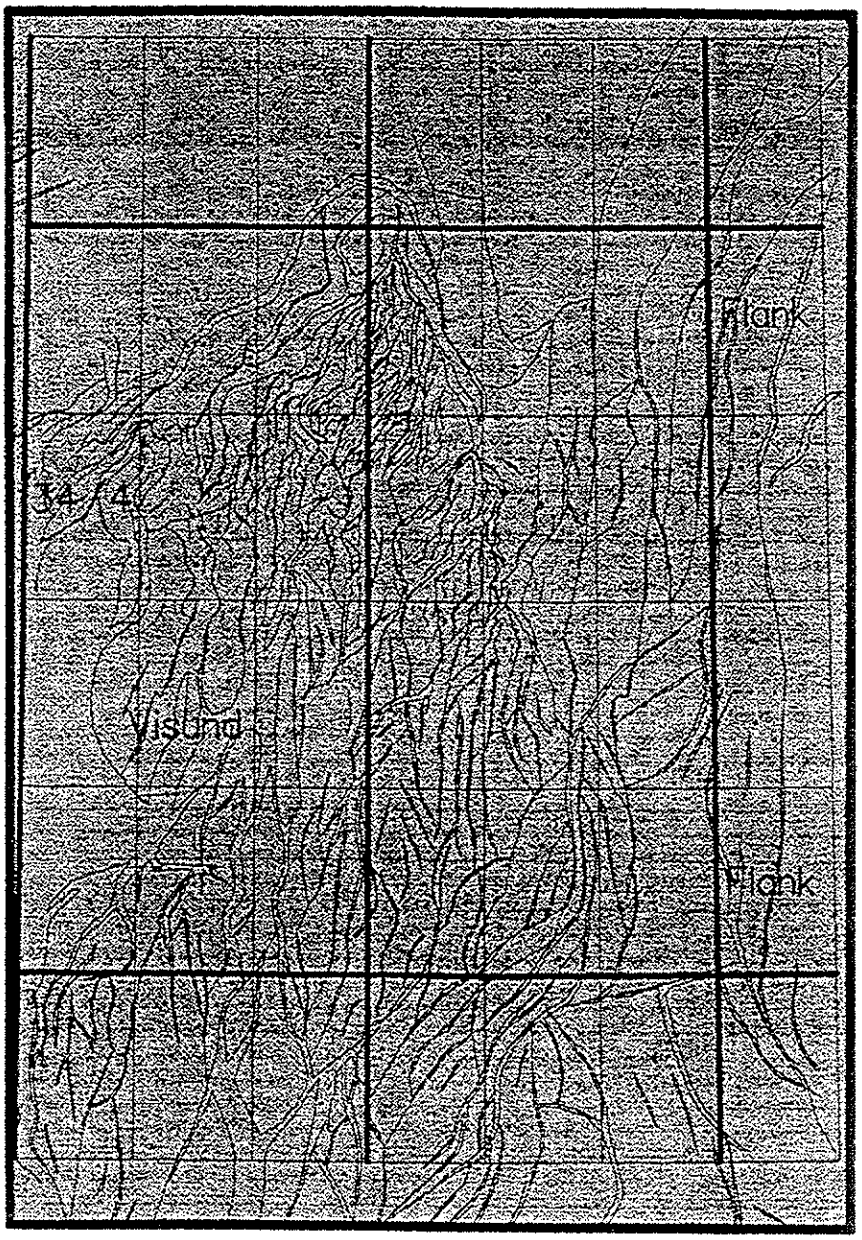

Figure 11. The locations of the boundary cells and mapped faults linked together

DATA INPUT

The pressure modelling, as performed in this study, requires three types of data: A present-day depth-converted map of the top of the reservoir, the present-day thickness of the reservoir and the mapped outline of pressure compartments. The Top Brent

Group depth map, including outlined pressure compartments of the study area, is shown in Figure 4. Further details about the area can be found in Sylta, 1993.

A two-way time (TWT) map (grid) was provided. This TWT grid was depth-converted using a simple time-depth lookup curve. Three isopachs from the seismic mapping were constructed. These were the Brent Group, the Dunlin Group and the Statfjord Formation. The TWT isopachs were converted to depth using a constant interval velocity of 3500 m, which is considered to be of sufficient accuracy for the work performed in this study.

The data discussed above are the only basic input data required for the modelling. Other input data are assumed by the modellers, e.g. shale permeabilities etc. The simplicity of the required input data is one of the strengths of the pressure modelling performed in this study: it is desirable to only require data that geologists are able to provide.

The pressure data used for calibration in the study were taken from the Well Data Summary Sheets published by the Norwegian Petroleum Directorate (NPD). Based on geological tops and pressure measurements from RFT-tests, the groups and formations were identified and an upper and lower limit for the overpressures calculated.

RESULTS

During a comprehensive calibration process the parameters given in Table 2 appeared to give the best match. The overpressure in the study area is plotted in Figure 13 while the deviations in overpressure are given in Table 3. The intervals of measured overpressure in Table 3 are calculated as an upper and lower deviation from hydrostatic pressure measured by RFT tests.

The results incorporate all the known main trends of the overpressure in the study area today. The models predict nearly hydrostatic conditions on the eastern flank and very high overpressure in the North Viking Graben which is located in the lower left corner of the study area. Moving eastwards from the North Viking Graben area the overpressure gradually decreases towards hydrostatic. Moving eastwards from the Visund field, located in the middle of block 34/8, it is necessary to cross a basin with high overpressure before arriving at the flank. With some exceptions, the overpressure increases with increasing depth. This is in good accordance with the observations made in the UK Central Graben by Darby, Haszeldine & Couples (1996).

The average fault transmissibilities between the connected pressure compartments are plotted in Figure 14. Note the consistency between the transmissibility values in Figure 14 and the modelled present day overpressure in Figure 13. Low transmissibility between two neighbour cells tends to give a large difference in overpressure while high transmissibility values may allow the overpressure to stay more or less equal across the faults. Red colours on the eastern flank in Figure 14 indicates high connectivity between the pressure compartments. Figure 14 indicate lower transmissibilities along a diagonal from the lower left corner to the upper right corner. In Figure 13 the corresponding areas are clearly overpressured. The faults near the Visund field (see Figure 11 for the location) have relatively high transmissibility values. According to the model, formation water is allowed to drain laterally in this area resulting in an intermediate overpressure as indicated by Figure 13. Conclusively,

the correspondence between the connectivity and the pressure compartments suggested by the model presented corresponds well to the resulting overpressure.

Table 2.

Best match parameter values.

b	p	B	ϕ_b	K_b	δ_{de}	δ_{sh}	ϕ_c	c
20	0.05	0.0069	0.1	$1.55 \cdot 10^{-5}$	1	10	0.45	0.0004

Table 3.

Deviation table, Brent Group (nearest sand/reservoir are used in the wells where the Brent Group is absent). See Figure 12 for location of the wells.

Well	Measured overpressure (BAR)	Modelled overpressure (BAR)	Deviation (BAR)
30/02-02	294.1-302.5	310.7	8.2
30/03-02	41.6-50.6	113.9	63.3
31/02-01	5.8-6.5	7.2	0.7
31/02-05	5.4-5.5	7.1	1.6
31/02-08	8.6-10.3	12.8	2.5
31/03-03	8.6-9.5	6.5	-2.1
34/02-03	255.3-255.9	262.3	6.4
34/02-04	201.5-247.9	216.8	0.0
34/10-23	385.4-390.2	401.9	11.7
35/03-04	48.1-64.5	57.0	0.0
35/03-05	10.4-15.6	28.3	12.7
35/08-01	200.0-206.9	215.2	8.3
35/08-02	170.7-184.1	179.5	0.0
35/08-03	184.2-192.5	185.6	0.0
35/11-01	6.8-7.2	10.1	2.9
35/11-02	145.3-158.5	113.9	-31.4

Standard deviation = 18.5
Mean deviation =9.5

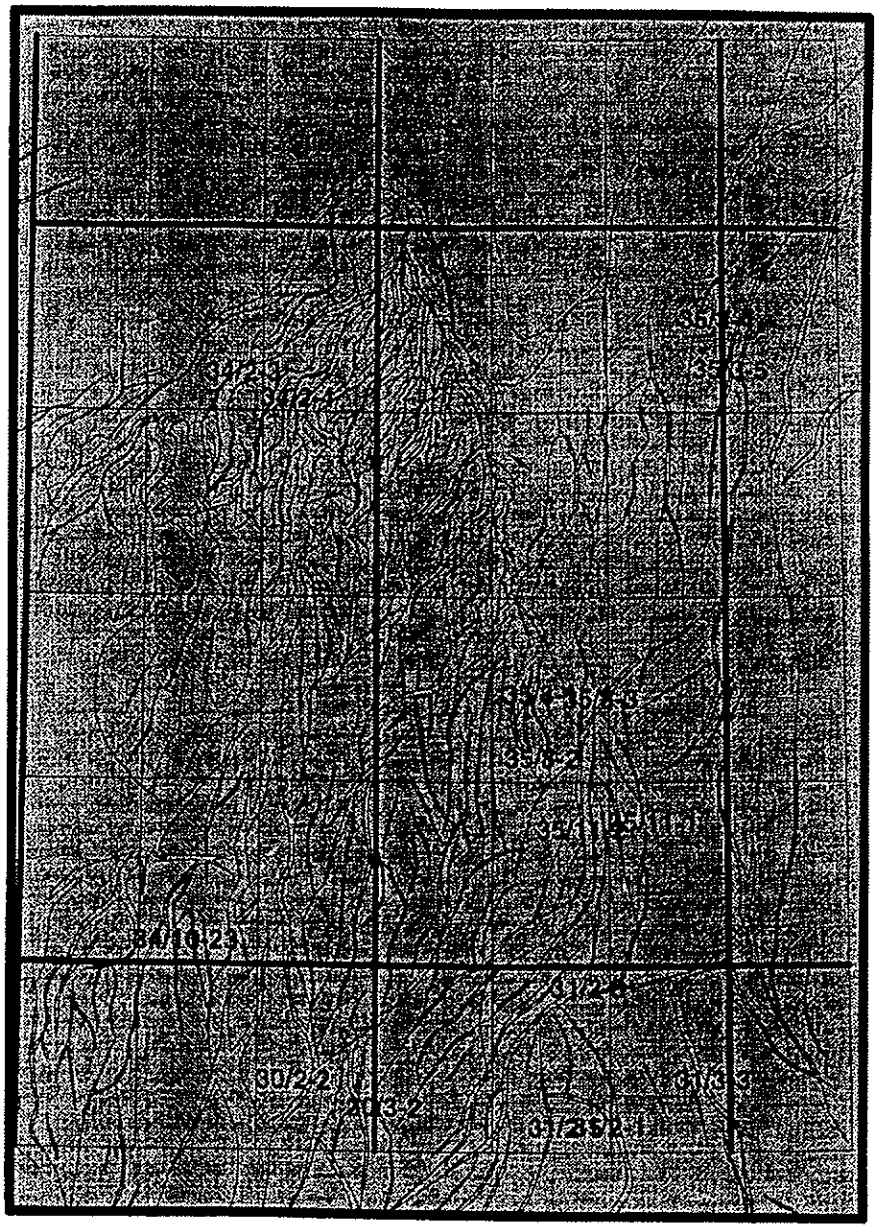

Figure 12. The location of the calibration wells

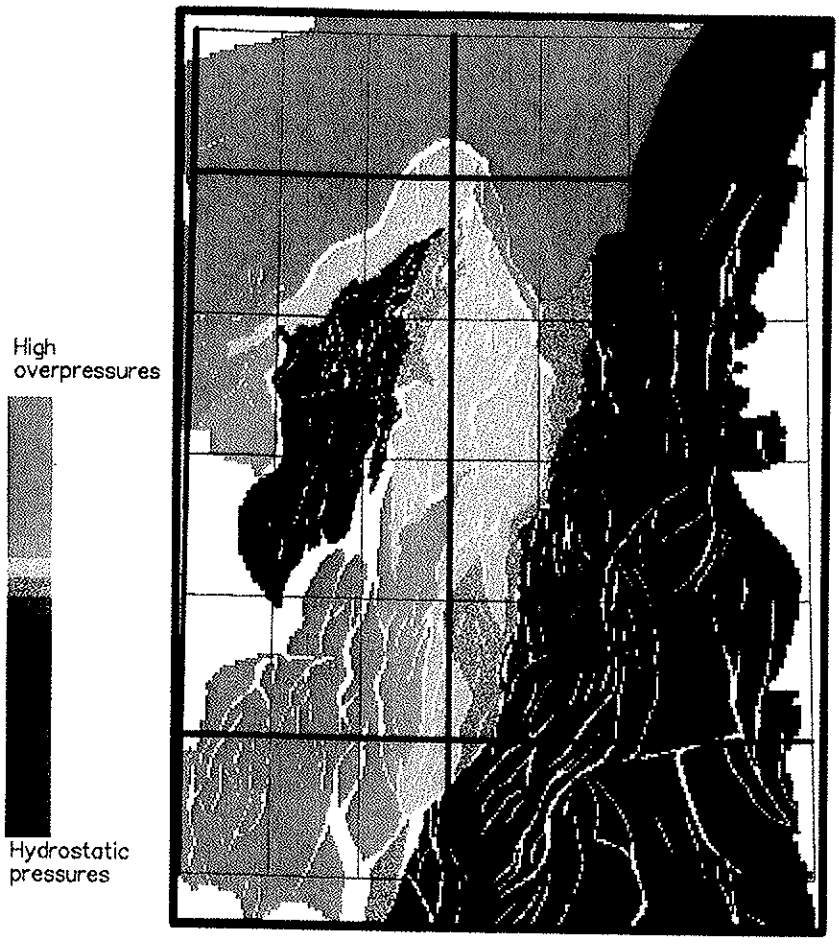

Figure 13. Present-day overpressures in the Brent Group.

SENSITIVITY

In order to understand the importance of each individual parameter in Table 2, a sensitivity analysis was carried out. This was done by varying one parameter while the others parameters remained fixed and then studying the standard and mean deviation of the modelled overpressures. The most obvious effect was that an increase in the transmissibilities resulted in a generally lower basin-wide overpressure and vice versa. This was the case for all the parameters. None of the changes reduced the mean or standard deviation significantly. This means that the deviation function is very close to a local minimum.

Varying parameter B did not cause any changes in the overpressure and this parameter influenced the result only when ρ had an unrealistically high value. Since B describes the shape of the exponential curve in Figure 7, it is assumed that there is almost complete sealing, and therefore very little water flow, across faults with some

offset. All the parameters in Table 2 with the exception of B are plotted in the sensitivity diagram in Figure 15. The curves in Figure 15 show the percentage increase or decrease in mean and standard deviation caused by the specified changes of the parameter on the x-axis.

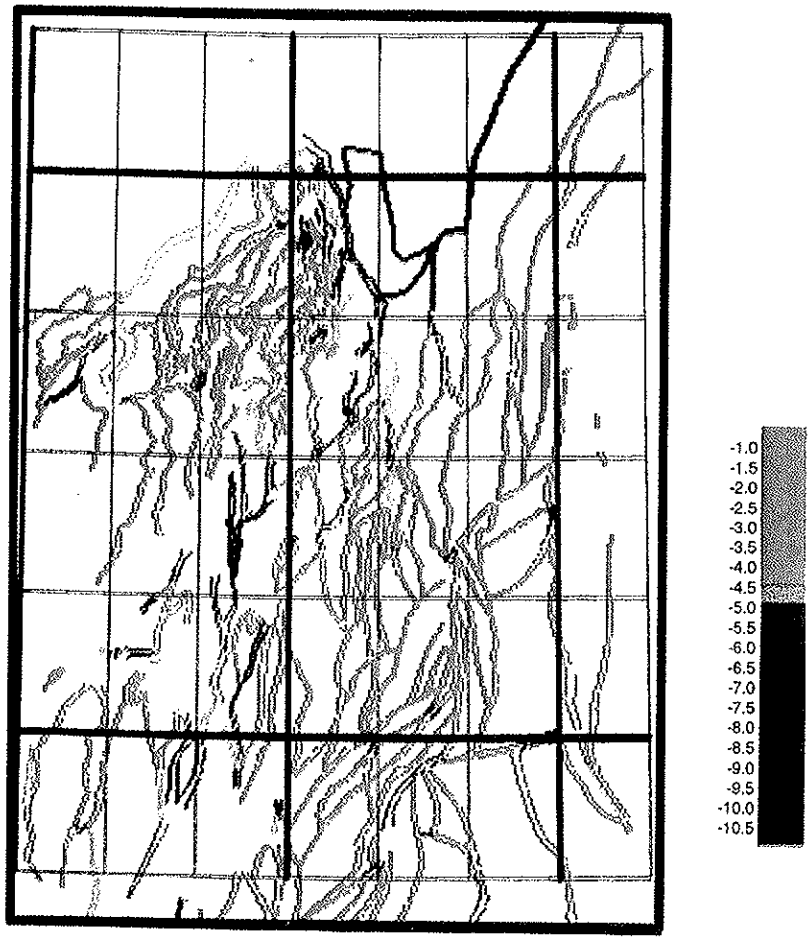

Figure 14. Average cross-fault transmissibilities [m_3], $\log_{10}$ scale.

All the parameters meet the expectations e.g. increasing the transmissibilities results in higher overpressures. The system seems to remain stable as long as the width of the fault blocks (b) lies within the range of 20 - 25m. Extending the values beyond this range caused a large increase in the deviations. As long as the values of p are between 0 and 0.1 hardly any change to the mean and standard deviation is seen. Based upon this observation, faults with offset are interpreted to be more or less completely sealing since the p parameter represents the percentage remaining transmissibility at no overlap (Table 1). The model is very sensitive to changes in K_b and ϕ_b (the co-ordinates for the breaking point between the shallow and deep parts of the permeability-porosity-curve). Only small variations cause a dramatic increase in

the deviations. The modelled overpressures are very sensitive to changes in c and ϕ_0 as well (the parameters that changes the porosity), while the δ_{sh} and δ_{de} mainly influence the pressures in the shallow and deep parts, correspondingly.

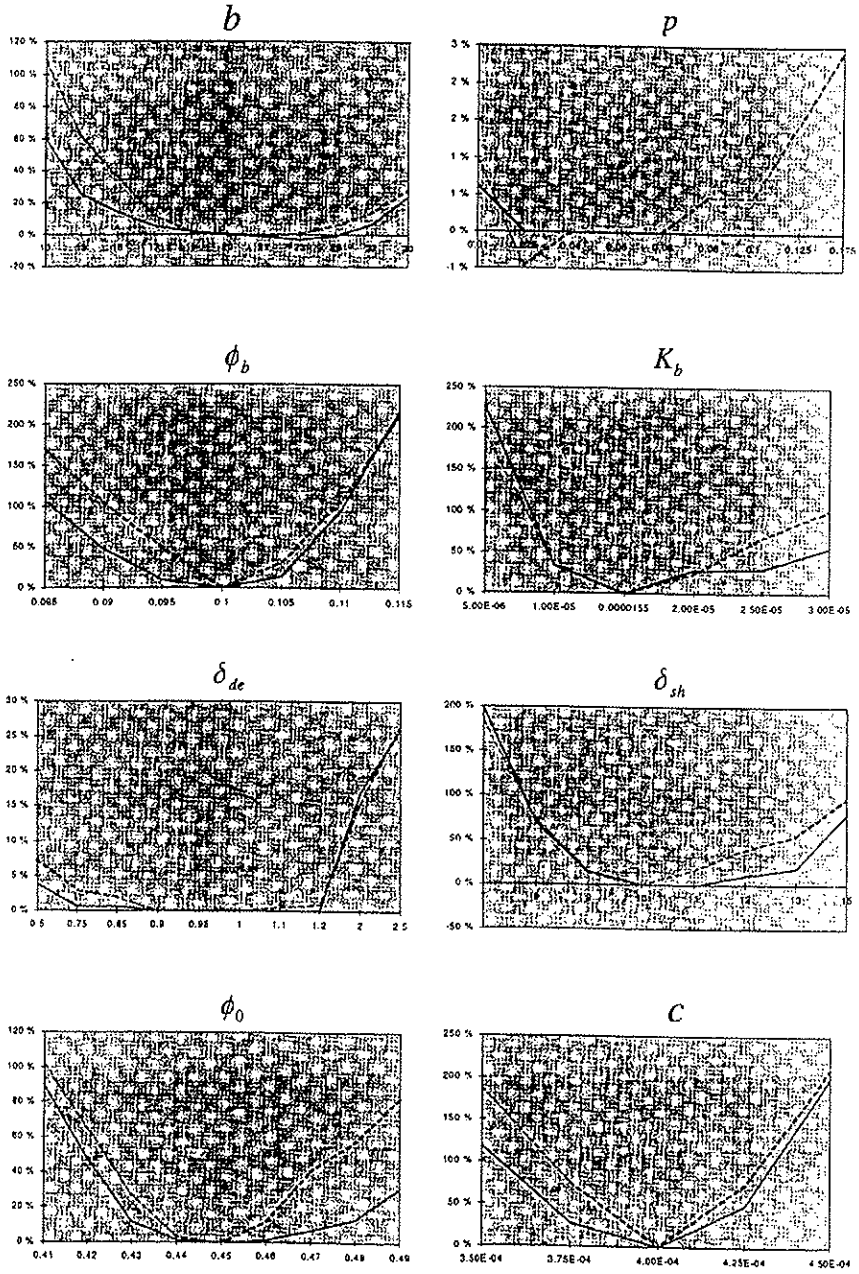

Figure 15. The percentage variation of mean (continuous lines) and standard (dotted lines) deviation (y-axis) vs. variation of parameters (x-axis)

DISCUSSION AND CONCLUSIONS

The deviations in Table 3 are with the exception of wells 30/03-02 and 35/11-02, very acceptable. Well 30/03-02 is located at the edge of the study area and this large deviation may be due to a boundary effect. If the study area were extended southwards a probable drainage path from the southern parts of block 30/03 to the hydrostatic flank would have been included. A drainage to the eastern flank would have reduced the modelled pressures in well 30/03-02. In addition to this, the sensitivity analysis suggests that there is too good communication between well 35/11-02 (which is underestimated) and well 30/03-02. The modelled overpressure in the two cells containing these wells follow each other during both the calibration of the model and the sensitivity study. The pressure cells between blocks 30/03 and 35/11 are long, narrow and oriented in a north-east direction. This means that there are relatively few seals between these two areas. Some of the explanation of the two large deviations in Table 3 may be that the process of defining pressure compartments and/or the fault permeability model is inadequate to describe the fluid flow in this area.

It is important to point out that the best match parameter values presented in Table 2 applied to the model are not an attempt to describe the true transmissibilities across the faults in the study area. It is of course impossible to measure the transmissibilities across large faults in order to verify a transmissibility model for a basin. The main idea behind the approach represented in Equation 2 is that this model describes the distribution of transmissibilities among the faults i.e. the permeability architecture, and thereby reveal a lateral basin-wide pattern of fluid flow.

In one- and two-dimensional models for predicting overpressure, vertical fluid flow compaction plays a key role in creating overpressures (Wangen 1992, Yu & Lerche, 1996). The pseudo three dimensional approach developed in this study does not have the same need for vertical fluid flow in order to create overpressure because the differences in overpressure are introduced by putting "production wells" in some boundary compartments. Nevertheless, in order to achieve the best match it is necessary to increase the vertical permeability so that the vertical fluid flow becomes significant compared to the lateral fluid flow. Based upon this observation, it is necessary to draw the following two conclusions: (1) Smaller scale fractures and faults in sealing layers may cause increasing permeabilities in some areas. This could be a possible explanation why it was necessary to model some communication through the Dunlin Group in Figure 9; (2) It is therefore of crucial importance to find a realistic ratio between lateral and vertical fluid flow when modelling pressure development in three dimensions.

Based upon the results and the relative low deviations all over the study area, we suggest that the lateral overpressure distribution in the pressure compartments is, to a large extent, controlled by the faults and the lateral fluid flow. To describe the regional lateral fluid flow it is not sufficient to characterise the faults as sealing or non-sealing. The results imply that fault transmissibilities can be computed in spite of very large fault seal differences at a local scale. The fact that it is possible to calibrate the model very closely to the measured pressures suggests that the model is a good approximation. Future drillings can reveal the model's ability to predict overpressures.

ACKNOWLEDGEMENTS

PGS provided the mapped data, interpreted the faults and made the initial version of the fault compartment interpretation.

REFERENCES

Antonellini, M., Aydin, A., 1994: *Effect of Faulting on Fluid Flow in Porous Sandstones: Petrophysical Properties.* AAPG Bulletin vol. 78, No. 3, March 1994.

Antonellini, M., Aydin,, A., 1995: *Effect of Faulting on Fluid Flow in Porous Sandstones: Geometry and Spatial Distribution.* AAPG Bulletin vol. 79, No. 5, May 1995.

Bredehoeft, J.D., Belitz, K., Sharp-Hansen, S., 1992: *The Hydrodynamics of the Big Horn Basin: A Study of the Role of Faults.* AAPG Bulletin vol. 76, No. 4, April 1992.

Darby, D., Hazeldine, R.S., Couples, G.D., 1996: *Pressure Cells and Pressure Seals in the UK Central Graben. Marine and Petroleum Geology,* Vol. 13, No. 8, 865-878.

Gauthier, B.D.M., Lake, S.D. 1993: *Probabilistic Modelling of Faults Below the Limit of Seismic Resolution in Pelican Field, North Sea, Offshore United Kingdom.* AAPG Bulletin vol. 77, no. 5, May 1993.

Heath, A.E., Walsh, J.J., Watterson, J., 1994: *Estimation of the Effects of Sub-seismic Sealing Faults on Effective Permeabilities in Sandstone Reservoirs.* North Sea Oil and Gas Reservoirs -III, Norwegian Institute of Technology.

Knipe, R.J., 1992: *Faulting Processes and Fault Seal. Structural and Tectonic Modelling and its Application to Petroleum Geology.* NPF Special Publication 1.

Knott, S.D, 1993: *Fault Seal Analysis in the North Sea.* AAPG Bulletin vol. 77, no. 5, May 1993.

Kooi H: *Insufficiency of compaction disequilibrium as the sole cause of high pore fluid pressures in pre-Cenozoic sediments.* Basin Research Vol. 9, No. 3, September 1997.

Loosveld, J.R.H., Fransen, R.C.M.W., 1992: Extensional vs. Shear Fractures: Implications for Reservoir Characterisation. SPE 25017.

Mann, D.M., Mackenzie, A.S. 1990: *Predictions of pore fluid pressures in sedimentary basins.* Marine and Petroleum Geology vol. 7, February 1990.

Nybakken, S. 1991: *Sealing fault traps - an exploration concept in a mature petroleum province: Tampen Spur, northern North Sea.* First Break vol.9, no. 5, May 1991.

Osborne M J, Swarbrick R E: *Mechanisms for generating overpressure in sedimentary basins: A reevaluation.* AAPG Bulletin, Vol. 81, No. 6, June 1997.

Pickering, G., Peacock, D.C.P., Sanderson, D.J., Bull, J.M., 1997: *Modelling tip zones to predict the throw and length characteristics of faults.* AAPG Bulletin vol. 81, no. 1, January 1997.

Sclater, J.G., Christie, P.A.F., 1980: *Continental stretching: an explanation of the post-Mid-Cretaceous subsidence of the Central North Sea basin.* J. Geophys. Res., 85, 3711-3739.

Sylta, Ø., 1993: *New techniques and their applications in the analysis of secondary migration. Basin Modelling: Advances and Applications.* NPF Special Publication no. 3.

Sylta, Ø., 1996: *Pressure compartments and fault sealing of hydrocarbons: A modelling*

approach. Abstracts: Hydrocarbon seals - Importance for exploration and production. NPF, January 1996.

Ungerer, P., Burrus, J., Dolgiez, B., Chénet, P.Y., Bessis, F., 1990: *Basin evaluation by integrated two-dimensional modelling of heat transfer, fluid flow, hydrocarbon generation and migration.* AAPG Bulletin vol. 74, No. 3, p 309-335.

Walderhaug O, 1996: *Kinetic modelling of quartz cementation and porosity loss in deeply buried sandstone reservoirs.* AAPG Bulletin, Vol. 80, No. 5, May 1996.

Walsh, J.J., Watterson, J., Yielding, G., 1994: *Determination and Interpretation of Fault Size Populations: Procedures and Problems. North Sea Oil and Gas Reservoirs III*, Norwegian Institute of Technology.

Wangen, M., 1992: *Pressure and Temperature Evolution in Sedimentary Basins.* Geophys. J. int., 110, 601-613.

Wen, R., Sinding-Larsen, R., 1994: *Probability Kriging of Sub-seismic Fault Throws with Multifractal Distributions.* Geostatistics for the Next Century, 488-497.

Yielding, G., Walsh, J.J., Watterson, J., 1992: *The Prediction of Small-scale Faulting.* First Break vol. 10, No. 12, December 1992.

Yu, Z., Lerche, I., 1996: *Modelling abnormal pressure development in sandstone/shale basins.* Marine and Petroleum Geology, Vol. 13, No. 2, p 179-193.

CHAPTER 12

12. Evaluation of late caprock failure and hydrocarbon trapping using a linked pressure and stress simulator.

Evaluation of late caprock failure and hydrocarbon trapping using a linked pressure and stress simulator

Lothe, A.E.[1,2], Borge, H.[1] & Sylta, Ø.[1]

[1]Sintef Petroleum Research, N-7465 Trondheim, Norway,
[2]Geological Institute, University of Bergen, Allégaten 41, N-5007 Bergen, Norway

Abstract

Hydraulic fracturing and leakage can be controlling factors for hydrocarbon leakage in overpressured sedimentary basins over geological time. Knowledge of the lateral flow properties of major faults is needed to simulate how pressure generation and dissipation can influence the sealing potential of caprocks. The hydraulic fracture processes within the caprock need to be evaluated to quantify timing and the amount of hydraulic leakage.

In order to address these issues we use a simulator, which calculates pressure generation resulting from mechanisms such as shale compaction and drainage, and mechanical and chemical compaction in sandstones. Pressure dissipation and lateral flow are simulated between different pressure and stress compartments defined by major fault patterns at the top reservoir level. An empirical model for the minimum horizontal stress is applied to the Griffith-Coulomb failure criterion and the sliding criterion to estimate hydraulic fracturing.

When varying the coefficient of internal friction and frictional sliding there are no or minor changes in the amount and timing of hydraulic fracturing and leakage in the modelled pressure compartments. When varying fault permeability, low fault permeabilities give early leakage, while high permeabilities result in late or no hydraulic fracturing and leakage. Our simulations also suggest that leakage in one pressure compartment influences the neighbouring compartments and large compartments control the leakage pattern in surrounding areas. The amount of cumulative leakage depends on the timing and size of the compartment. Uncertainties of timing and leakage for different compartments can be estimated by using the pressure measured in the wells today as calibration. The uncertainty in the estimates can be used as guidelines for possible hydrocarbon leakage risks.

Keywords: hydraulic fracturing, hydraulic leakage, overpressure, basin modelling

Introduction

Knowledge of the timing and distribution of hydraulic fractures is essential for evaluating hydrocarbon potential in many overpressured sedimentary basins (Grauls 1998, Hermanrud & Bolås 2002). Overpressure can be generated by several mechanisms including rapid sedimentation and compaction disequilibrium of sediments, hydrocarbon diagenesis, sediment diagenesis (Swarbrick & Osborne 1998), aquathermal pressuring (Chapman 1980, Miller & Luk 1993) and lateral compression (Bour et al. 1995). Field data indicate that overpressuring of sedimentary units can cause episodic fluid expulsion into overlying layers during basin subsidence (Hunt 1990). The understanding of hydraulic fracturing and leakage has been limited by lack of good field exposures and also lack of cores from fractured caprocks (Cosgrove 1998). One way to achieve new knowledge of which parameters that influence hydraulic failure of caprocks leading to leakage, is to use basin simulators that couple pressure (Borge & Sylta 1998, Borge 2000) and time-related stress (Lothe et al. in press).

The relation between hydraulic fracturing and leakage in sedimentary basins is not well known. It is recognized that large volumes of fluid can become trapped during significant overpressure build up in pressure compartments (Darby et al. 1996). A rapid fluid pressure release should be expected when the caprock fails (Cosgrove 1998). Capillary leakage of hydrocarbons is not taken into account in this work, because only the water phase flow is modelled. The failure mode will depend on the burial depth, stress regime and pressure. The simplest scenario assumes leakage along one fault (Verbeek & Grout 1993). Overpressures in this case will be highest at the top of the pressure compartment resulting in fault nucleation and growth from the reservoir into and through the caprock. Alternatively, fracture swarms may develop as shear failures in the deeper parts of the caprock and tensile failures in the shallower parts (Cosgrove 1998). This is illustrated in Figure 1, where high overpressures have build up in the deepest part of the reservoir. Low transmissibilities across non-juxtapost reservoir faults decrease the lateral fluid flow and hydraulic failure and leakage will occur. Reactivation of pre-existing faults is a third possibility (Wiprut & Zoback 2002). However, mechanisms involving slip along pre-existing fault zones facilitated by overpressure build-up or tectonism are not considered. We will analyse possible overpressure initiated failure at the highest point of the compartments along faults with shear failures at deep burial depths and mixed or tensile failures at shallower depths (Figure 1).

Lateral fluid flow between pressure compartments is an important and sometimes controlling factor on pressure build-up in an overpressured basin. Lateral fluid flow in faulted reservoir systems is predominately controlled by the permeability of the major bounding faults. Different attempts have been made to measure fault permeabilities in the laboratory (Morrow et al. 1984, Zhang et al. 2001, Sperrevik et al. 2002). Sperrevik et al. (2002) observed a relationship between the fault permeability and the mineralogy of the faulted rock, the effective stress conditions, and the history to the reservoir prior to, during and after deformation. They measured very low permeabilites ($<10^{-7}$ mD) in faults with clay smears at depth (>3.5 km). The fault rock permeability with a phyllosilicate-framework lies in the order of $<10^{-4}$ mD at >3.5 km depth. Revil & Cathles (1999) present examples of measurements in shaly sands, and demonstrated a rapid decrease in permeability with increasing clay content. Zhang et al. (2001) claimed that large permeability anisotropy due to anisotropic alignment of clay shape fabrics is important in focusing flow along faults in clay-rich rocks. In the present work we do not discuss the mechanisms of how lateral flow across a major fault could occur, but rather consider how changes in the fault permeability may influence hydraulic fracturing and leakage.

Hydrocarbon leakage is expected to be sensitive to hydraulic fracturing and water fluid leakage in an overpressured area. Hydrocarbon fill history is also time-dependent and relies on the charge, trapping, hydraulic fracturing and leakage histories. In this study we are concerned with the aim of predicting and quantifying the uncertainties regarding the timing and amount of leakage from overpressured areas. The results may be used in basin modelling estimates for undrilled prospects.

The simulations in this study are carried out on a data set from the Halten Terrace, offshore Mid-Norway (Figure 2). The pressure distributions in this area is described in e.g. Teige et al. (1999), Skar et al. (1999) and Berg et al. (2000), and pressure simulations have been carried out by Borge (2000, 2002) and Lothe et al. (in press). The geology in the area has been extensively described; see Koch & Heum (1995) and Blystad et al. (1995) for further information. The study area is selected because of two main reasons: 1) None of eight wells penetrating Jurassic reservoir rocks at Haltenbanken prior to 1996 found hydrocarbon, and cap rock leakage seemed to be the main explanation for these results. Later drilling have however results in hydrocarbon discoveries (Hermanrud & Bolås 2002). 2) A pressure compartmentalisation is described in the area (e.g. Berg et al. 2000). The main focus of this paper, however, will be on the method and not on the specific study area.

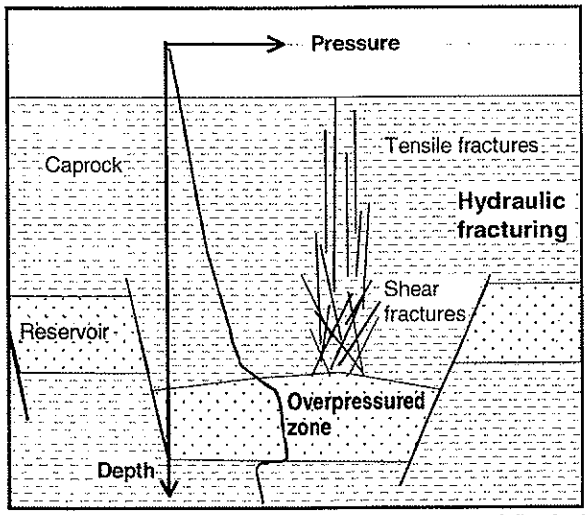

Figure 1 *Sketch showing hydraulic fracturing and leakage of fluids from overpressured reservoir units.*

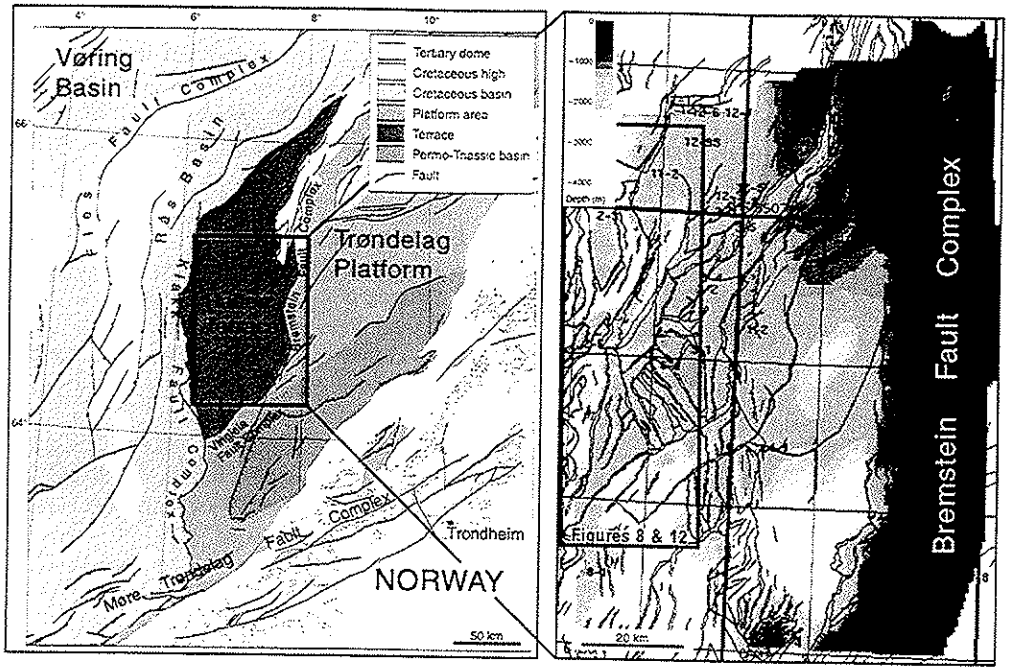

Figure 2 *Left map shows the Mid-Norwegian region, where study area is marked. Modified from Blystad et al. (1995). Right map shows present-day depth map of the top reservoir (top Garn Formation). Calibration wells and major faults at top reservoir are marked. Frame shows area presented in Figures 8 and 12.*

Methods and data

In the present study the fault traces mapped at the top reservoir level delineate the lateral extent of the pressure and stress compartments that are utilized in a pressure and stress simulator ("Pressim", Borge 2000, Lothe et al. in press). The lateral Darcy flow of formation water across low-permeable faults is calculated using an explicit forward Euler solution technique (Borge 2002). Effective top seals stop flows out of compartments. Depth-converted maps of the overlying sediments are used to construct the burial history that is adjusted for decompaction. The development of pressure and stresses are reported for a series of time steps. Time steps are correlated to the depositional ages of the stratigraphic horizons that are used to build the model. Porosity-depth relation in the shales is used to model mechanical compaction and a kinetic model for quartz cementation (Walderhaug 1996) is used to model chemical compaction of the sands. Hydrocarbon migration is not taken into account in this work that present one-phase simulation.

The geo-mechanical properties for the caprock are allowed to vary through time with changing burial depths (Lothe et al. in press). Isotropic horizontal stresses are assumed and the minimum horizontal stress is estimated using an empirical formula (Grauls 1996). The vertical stress varies versus time depending on sedimentary loading. No strain is included and a passive sedimentary margin is assumed. Fault permeability is modelled as depth dependent. The fault transmissibility depends on the burial depth, the length, width and the dip-slip displacement of the faults, thickness of the reservoir layers and the permeability inside the fault block (Borge & Sylta 1998). Juxtaposition faults (faults where the reservoir is self-juxtaposed) have high transmissibilites, while faults with no overlap have lower

transmissibilites. The Griffith-Coulomb failure criterion and the frictional sliding criterion are used to simulate hydraulic fracturing from the overpressured compartments (Figure 3).

The data used are a present-day depth-converted map of the top reservoir unit (top Garn Formation), the present-day thickness of the reservoir, and a fault map at top reservoir level (Figure 2 & Table 1). Drill stem tests and formation tests are used for the pressure measurement in the different wells. The pressure data from 43 wells in the area are available at the top reservoir level, and are used to calibrate the model (Table 1). The mean deviation ($\text{mean deviation}=\frac{1}{n}\sum_{i=1}^{n}\left|P_{i,\,measured}-P_{i,\,modelled}\right|$) is calculated between modelled and measured overpressure in the pressure compartments containing pressure observations from wells. An arbitrary paleo-water depth of 200 m is used in the study area. Poisson's ratio and Young's modulus are varied with depth, based on calibration with laboratory measurement of North Sea Shale (Horsrud et al. (1998), see Lothe et al. in press). The input parameter used in the base case is listed in Appendix. The fault permeability used in the base case is empirical (see discussion), but will be varied in the sensitivity runs. The simulations covers the flow and stress development for the last 90 Ma.

Table 1 *Input data used in the simulations*

Input data	**Pressim - water flow simulations**
Depth-converted seismic horizons	Seven time-steps; 90 Ma, 80 Ma, 65 Ma, 20 Ma, 5 Ma, 2 Ma and Present
Isopach map reservoir	Garn Formation (185 Ma - 160 Ma)
Fault maps	Fault map at top Garn Formation level
Pressure data	Pressure measurements in Garn Formation from 43 wells used to calibrate the simulations. The wells are 6407/8-2, 6407/7-3, -5, 6407/9-1, -2, -3, -4, -5, -6, 6407/4-1, 6407/9-7, 6406/8-1, 6407/2-1, 6407/6-4, 6406/3-1, 6407/2-3, 6406/6-1, 6406/2-6, 6506/12-1, -3, -5, -8, 6407/1-1, -2, -3, 6406/3-2, -4, 6406/2-3, 6507/11-4, 6507/12-1,2, -3, 6407/2-2, 6507/11-2 (see also Lothe et al. in press).

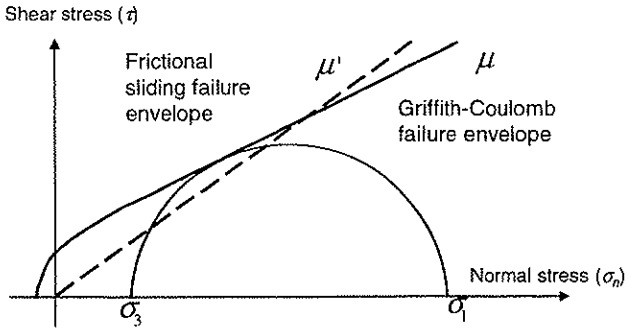

Figure 3 *Failure criteria used in the simulations.*

Results

The aim of the simulations was to determine which input parameters will have a major impact on the timing and extent of hydraulic leakage in an overpressured sedimentary basin. A base case was run to use as a reference for simulation methods. The base case illustrates the variations in the modelled pressure and hydraulic leakage. Different simulations were carried out by varying the coefficient of internal friction (μ) and the coefficient of frictional sliding (μ'; see also Lothe et al., in press). The time-dependent sensitivity of late hydraulic fracturing

and amounts of leakage were studied by varying the permeability and thereby the transmissibility of major faults that control the lateral extent of the pressure compartments.

The pressure build-up over the last 90 Ma was simulated for the base case. Figure 4 illustrates the overpressure distribution in the area from 5 Ma to present day. Hydrostatic pressures prevail in nearly the whole basin at 5 Ma. Between 5 Ma and 2 Ma a rapid pressure increase occurs in the western part of the area. This trend continues until today, with an increase in overpressure in the most deeply buried units and a spreading of the overpressured part of the simulated area (Figures 4 & 5). The high overpressures lead to hydraulic fracturing and leakage through the caprock above the reservoir between 2 and 1.5 Ma (Figure 5). The modelling shows that the failure strength is exceeded only in the compartments with the high overpressures (Figures 4 & 5). One of the compartments where hydraulic fracturing occurs is compartment K (Figures 6 & 7, located in Fig. 8a). In the simulation this compartment reaches its limits for hydraulic fracturing at 1.9 Ma, which is marked with a peak in the leakage rate (Figure 7). When we study the changes in effective stress through time in this compartment, we observe a rapid decrease when the pressure increases (Figure 7). The first rapid increase in overpressure starts around 5 Ma. At around 3.2 Ma the overpressure decreases, before a new peak builds up around 1.9 Ma.

From the evaluation of the overpressure curves one would perhaps expect hydraulic leakage to occur around 3 Ma in compartment K. However, the model suggests that this does not happen until 1.9 Ma (Figure 7). The reason is that the neighbouring compartments to K, WK and EK start to leak around 3.2 Ma (Figure 8). This leads to a loss in accumulated overpressure in K around 3 Ma and illustrates that leakage from one compartment may have a critical effect on leakage from neighbouring compartments. The same effect is observed in the south, where early leakage in compartment P controls the timing of later leakage in compartment WP.

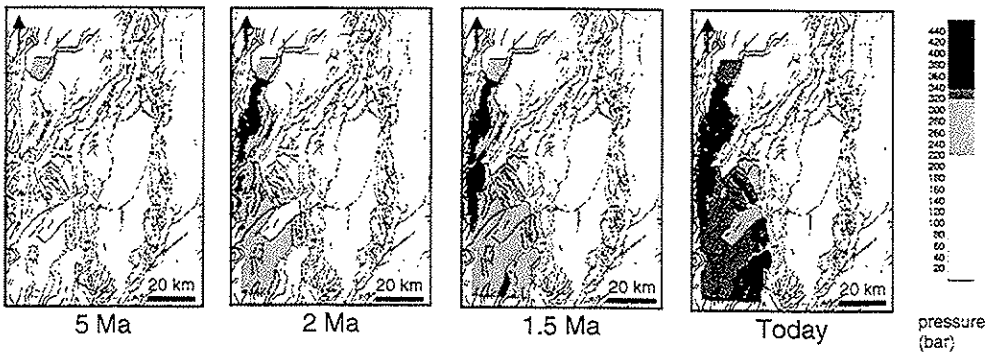

Figure 4 *The development of simulated overpressure using the base case during the last 5 Ma in the western part of the study area. Grey scale shows overpressures in bars.*

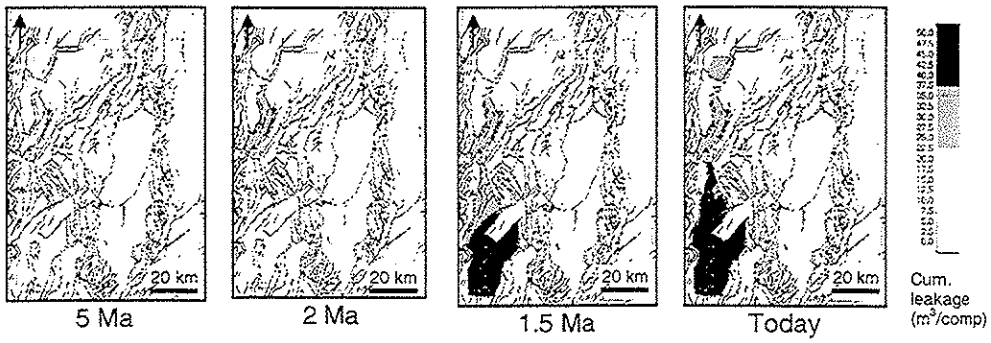

Figure 5 *Development of hydraulic fracturing and leakage during the last 5 Ma in western part of study area for the base case. Grey scale indicates cumulative leakage in m^3/compartment.*

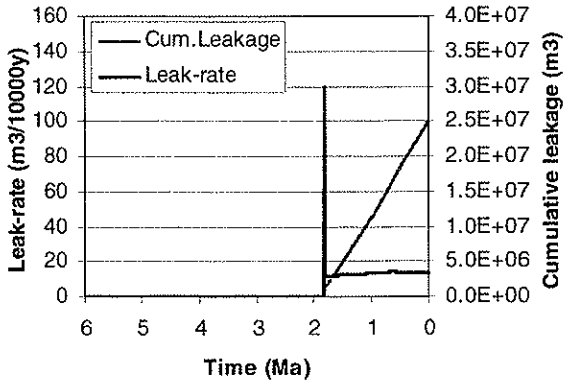

Figure 6 *Modelled cumulative leakage (m^3) and leakage rate (m^3/10000y) for compartment K during the last 6 Ma. Note that leakage occurs in one major pulse.*

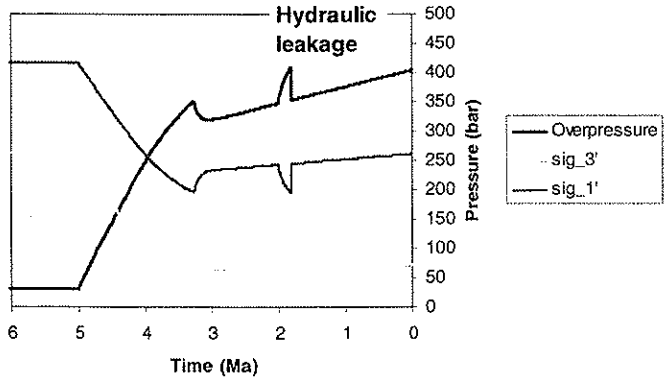

Figure 7 *Modelled overpressure (bar), effective minimum horizontal stress (bar) and effective vertical stress (bar) for compartment K. Note rapid pressure build-up around 5 Ma. Hydraulic leakage is modelled to occur around 1.9 Ma (see Fig. 6).*

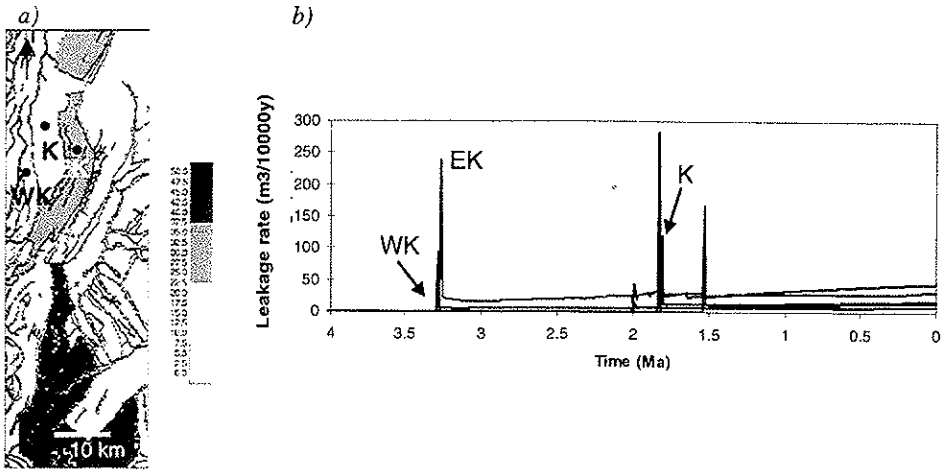

Figure 8 *a) Leakage volumes in different pressure compartments. Grey scale shows cumulative leakage to present day (m^3). b) Timing of leakage from the different compartments in the study area. The earliest leakage event from compartments WK, EK and K is marked.*

The significance of coefficient of internal friction and frictional sliding

Pressure generation processes started to become effective during the last 5 Ma in the basin. This is mainly due to rapid late burial and the associated quartz cementation in the reservoir unit (Dalland et al. 1988, Teige et al. 1999). In the simulator, two failure criteria were used, first the Griffith-Coulomb and secondly the frictional sliding criterion (Figure 3). To test which parameters control the amount and timing of hydraulic fracturing and leakage, the coefficients of internal friction (μ) and frictional sliding (μ') were varied (Figure 9). In the base case μ= 0.6, and μ'=0.7 (Figure 6). Figure 10 shows results from such simulations where the coefficients are varied, from μ=0.3 and μ'=0.7, to μ=0.6 and μ'=1.0. These simulations gave minor changes in the leak-rate, cumulative leakage ($2.2\text{-}2.5 \cdot 10^7$ m^7) and the timing (<150 Ka) for the failure (see also Lothe et al. in press). The largest changes were found in the peak leakage rates at failure for very high values for μ' (1.0), which result in lower peak leakage rates (Figure 10b).

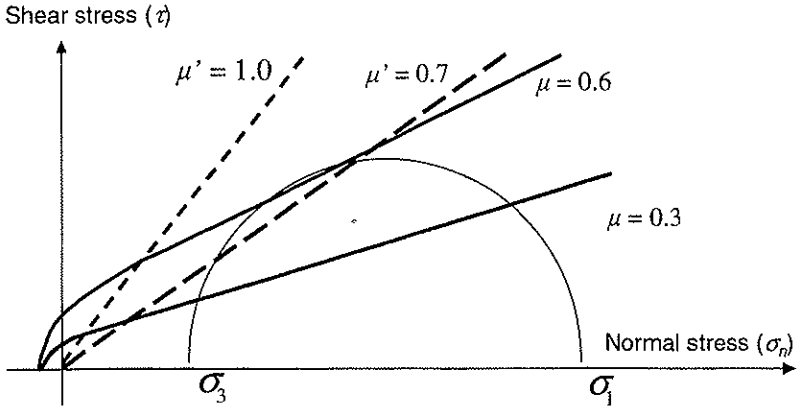

Figure 9 *The coefficients of internal friction and frictional sliding used in two different simulations (μ=0.3 and μ'=0.7, and as μ=0.6 and μ'=1.0).*

a) *b)*

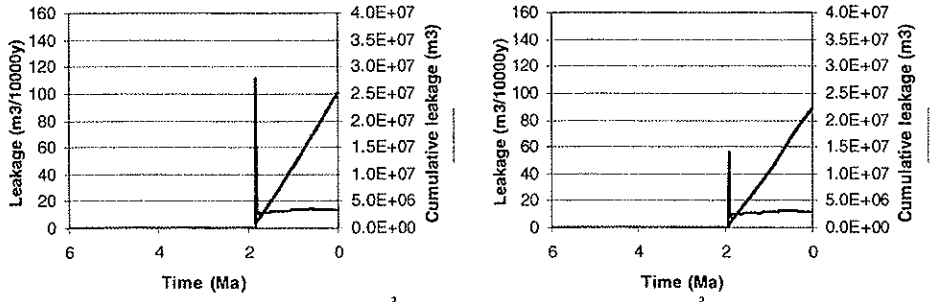

Figure 10 *Cumulative leakage (m^3) and leakage rate (peak)(m^3/10000y) in compartment K in runs with a) μ=0.3 and μ'=0.7 and b) μ=0.6 and μ'=1.0.*

Significance of the permeability across major faults

Sensitivities of the timing of failure and amount of leakage to fault permeability was also tested (Figure 11). The fault permeability curve used is discussed in Borge & Sylta (1998), where kinks in curves are supported by Loosveld & Franssen (1992). The fault permeability curves are based on empirical data (see discussion) and also on the calibration between simulated pressures and measured pressures in the basin. The permeability values were applied in a low, base and high case for all the master faults that define pressure compartments (Figure 12). Using low fault permeabilities resulted in a pressure build-up that takes place at an earlier stage. More compartments therefore suffer from hydraulic fracturing and leakage compared to runs using higher permeabilities (base and high case) (Figure 12). Using high permeabilites resulted in some compartments that did not fail at all. The timing of failure in compartments WK, EK and K, in the northern part of the study area, differed with only a few hundred thousand years when the low and the base case were compared (Figure 12b & d). Comparing the base case and the high case however, a marked delay in the timing of the hydraulic fracturing for compartments WK and EK, from 3.3 Ma to 1.8 Ma is observed, and there is no leakage from compartment K (Figures 12d & f). In the southern area

compartment P fails approximately 1 Ma earlier in the low case compared to the high case. For the neighbouring compartment WP, no leakage is observed in the high case.

For the same three cases, the cumulative leakages for the respective compartments have been calculated (Figure 13). The results for the base case show that the highest cumulative leakage took place from compartment EK in the northern area and compartment P in the southern area. Because the amounts of leaked fluid from the two compartments were much larger than from the neighbouring compartments, the two would control the amount and also the timing for the leakage in the neighbouring cells. Compartment K is as an example of this effect (Figures 7 & 8). There is a progressive reduction in the total amount of cumulative leakage due to the time-dependency when comparing the leakage from compartment EK in the low, base and high cases (Figure 13). This is also observed for other compartments, except for compartment P, which displays an increase in cumulative leakage in the high case compared to that of the base case. This is because the neighbouring compartment to the south (compartment S) does not fail in the high case (Figures 12e & 13c). Accordingly, higher fluid pressures are developed in compartment P and the cumulative leakage is much higher relative to those in the low and base cases. This effect overrules the effect of timing on the cumulative leakage in this example.

A strong dependence on fault permeability for both the timing of hydraulic failure and hydraulic leakages rates noted from the previous descriptions. To quantify the uncertainty in the simulations, fault permeabilities have been systematically varied to investigate their effect on the timing and amount of leakage in selected overpressured compartments. As shown in Figure 11, the permeability across the faults varies according to depth of burial. To be able to compare the different cases, the permeability typical for a burial depth of 4 km was used. Figure 14 shows how the timing of leakage varies versus fault permeability for results for compartment K analysed in isolation. Figure 15 shows the same sensitivity for other overpressured compartments in the study area. The data points on the curves show at which time a particular compartment fails in different permeability runs when the permeabilities of the fault zones are varied.

The simulations show a strong dependency of the permeability across the major faults on the timing of hydraulic fracturing in overpressured areas. An early and significant build-up of overpressure was displayed in the simulation runs where a low permeability was applied. However, deviations between the simulated pressures and pressures measured in wells are large (Figure 15). This is because the early hydraulic fracturing gives too high leakage rates and too low simulated pressures for the present situation. When high fault permeabilities are used few compartments, and in the extreme case no compartments, will fail. A marked jump in the timing (from 5 Ma back to greater than 20 Ma) of the hydraulic failure in the different compartments for varying permeability models is observable in Figure 15. It changes from a very early failure using low permeability input, to late failure using higher permeabilities. Studying the changes during the last 5 Ma in more detail, we observe less change in timing of leakage from around 4 to 3.5 Ma and from 1.9 Ma to 1.7 Ma (Figure 16). This is typical for all of the studied compartments, except for compartment P, which fails in all cases.

When cumulative leakage versus permeability is studied, two compartments with higher leakage rates are observed; compartment EK in north and compartment P in south (Figure 17). These two compartments show high cumulative leakage in the runs when they go to failure using low permeability faults, but a rapid decrease in leakage approaching no failure with high permeability faults. The deviations between simulated pressures and those measured in

the calibration wells for the varying permeability runs increase when the permeability is either very low and an early leakage occurs or permeabilites are very high and no failure occurs (Figure 17).

In the northern area, the first leakage is observed for compartments EK and WK followed by compartment K for all simulated fault permeabilities (Figure 18a). Cumulative leakage versus permeability curves are used to distinguish between compartments EK and WK (Figure 18c). Leakage is markedly higher for compartment EK at low fault permeabilities, because a larger fluid pressure has built up in this compartment due to its deep burial and to the relative size of the compartment. This compartment controls the leakage in the smaller, neighbouring compartments. There is also a relative decrease in the leakage from compartment EK in the runs where compartment K has a larger leakage at a permeability of $1 \cdot 10^8$ mD (Figure 18c). Studying the cumulative leakage in the three different compartments and the uncertainty in the runs, we see that compartment WK will most likely go to failure, but at low leakage rates (Figures 18a & c). Compartment K will have a low leakage rate if the compartment goes to failure using low permeabilities ($<1 \cdot 10^7$ mD). Using high permeabilities, the compartment will not fail (Figure 18c).

In the southern area, the timing of leakage does not show such a clear trend for varying permeability runs as in the north. Compartment WP is an exception, in that it has the same plateaus in the timing of failure as the northern compartments (between 1.8-2 Ma, and between approx. 4.5 -3.6 Ma) (Figures 18a & b). For compartments P and S, the timing is more linearly linked to the permeability (Figure 18b). This is because S is the largest compartment in this area, with high hydraulic leakage rates at low fault permeabilites (Figure 18d). Therefore it influences the leakage from compartment P, where an increase in the cumulative leakage is observed for lower permeability runs when compartment S is still intact (Figures 18b & d). The amounts of hydraulic leakage vary significantly for the low, base and high cases, especially for the two largest compartments in the northern and southern areas, compartment EK and compartment P, respectively (Figures 18c & d).

When plotting the timing of hydraulic fracturing versus cumulative leakage for all the compartments, a linear trend in each compartment between 5 Ma and Present emerges (Figure 19a). When failure occurs before 5 Ma, extreme values for cumulative leakage are observed. A similar situation is seen for runs with large mean deviations (>15 bar; Figure 15). A linear trend between timing and amount is observed for the small compartments during the last 5Ma (Figure 19b). The two larger compartments (P and EK) are characterized by a more complex relationship between timing and cumulative leakage.

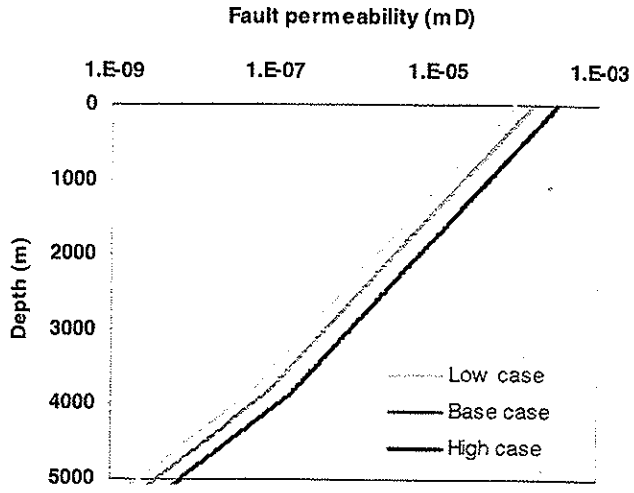

Figure 11 *Depth dependent fault permeabilities used for three different cases; low, base and high case used as modelling input for all faults in the study area.*

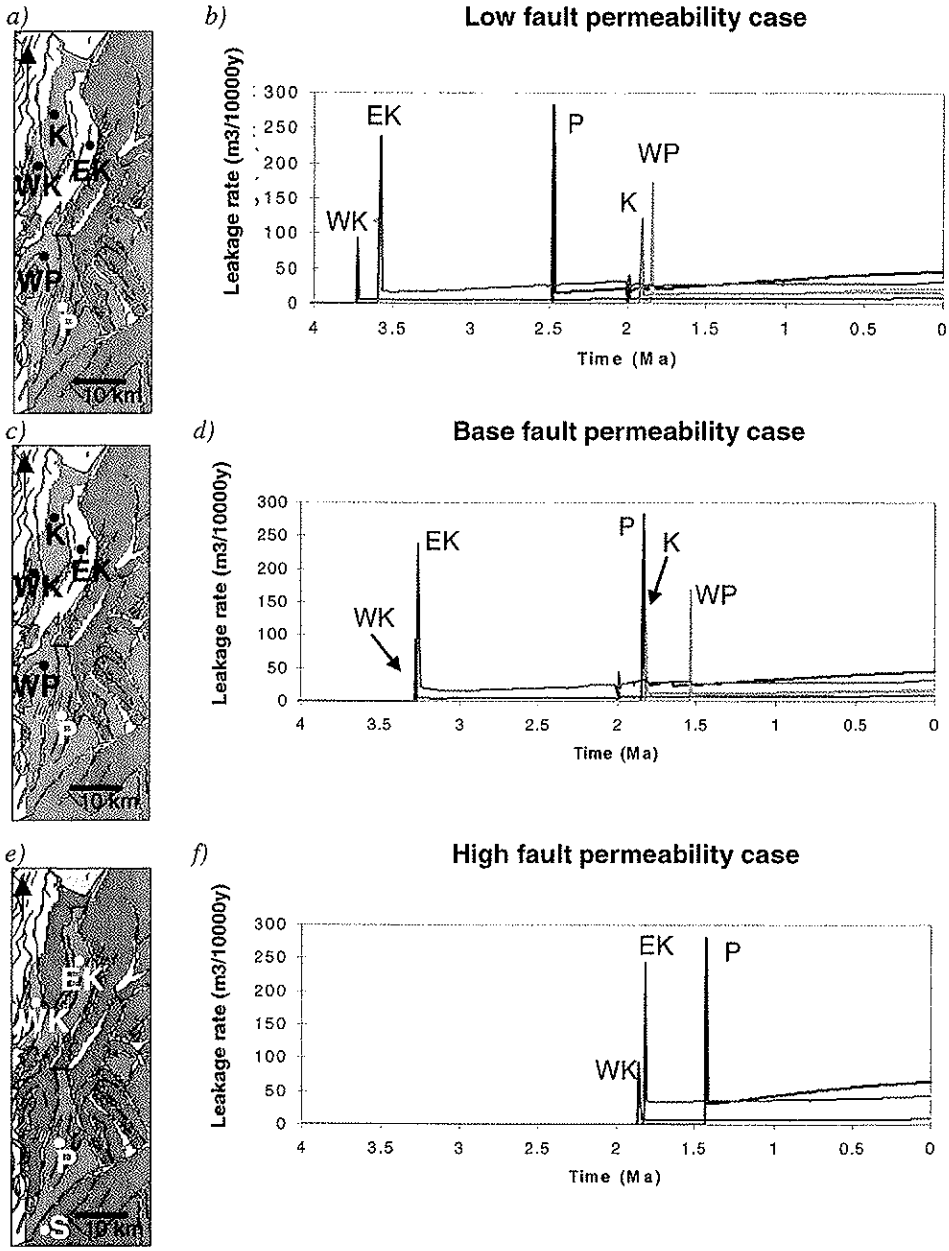

Figure 12 *Fault permeabilities varied in the low, base and high cases. Maps a, c, and e) present cumulative leakage in the different compartments. (Colour scale as in Figure 8; m^3). Graphs b, d and f) show the variation leakage throughout the last 4 Ma. Note that enhanced permeability causes delay in the timing of the hydraulic fracturing.*

a) Low fault permeability case

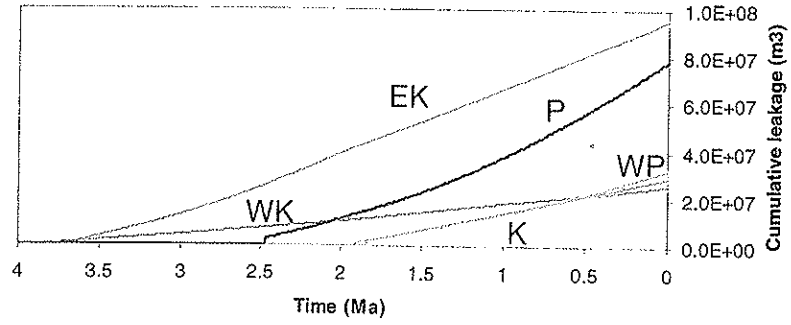

b) Base fault permeability case

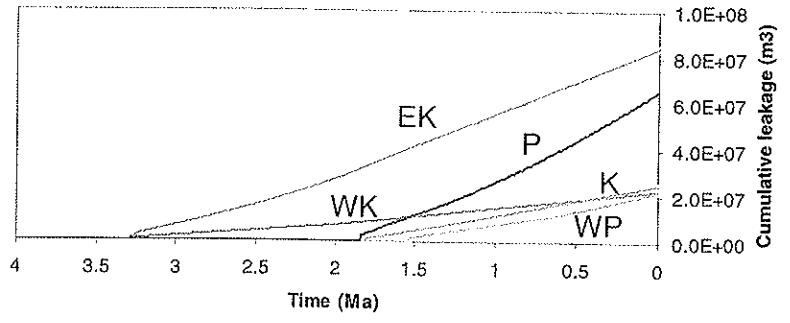

c) High fault permeability case

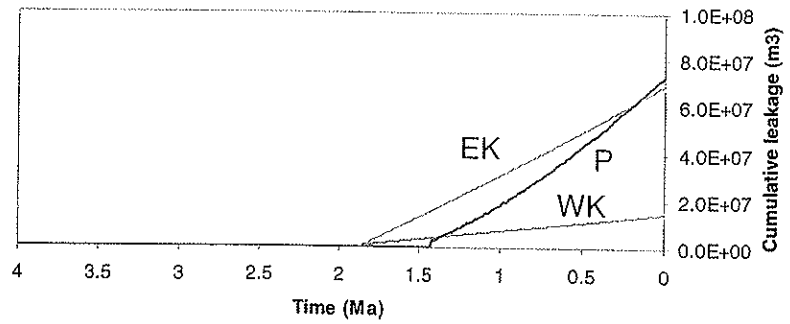

Figure 13 *The cumulative leakage with time in the three fault permeability cases for different compartments.*

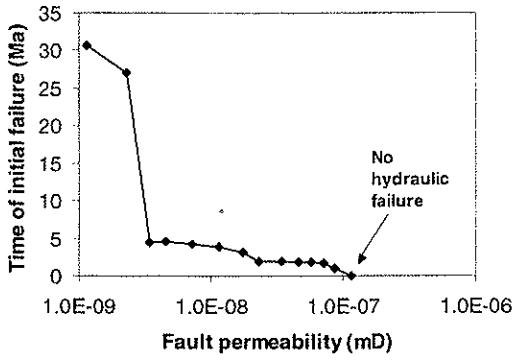

Figure 14 *Time of hydraulic failure for compartment K versus fault permeability at 4 km depth. The data points show results from different runs. The highest fault permeability gives no pressure build-up and, hence, no hydraulic fracturing in the compartment.*

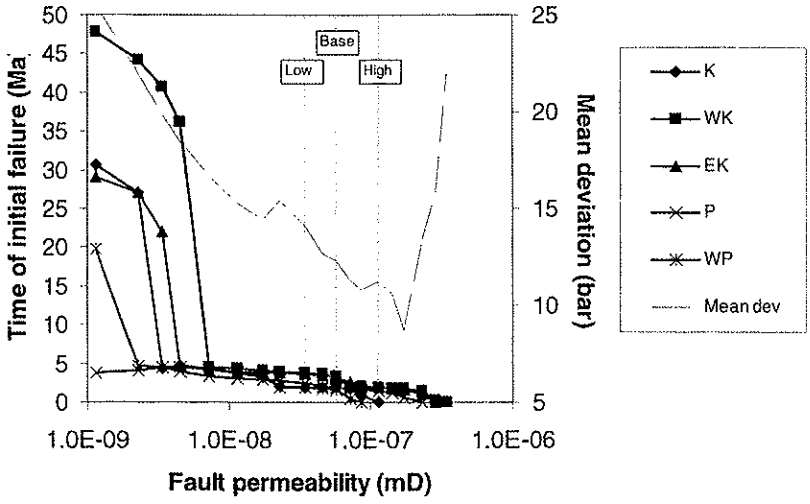

Figure 15 *Timing of failure in different compartments depending on the fault permeability at 4 km depth. The right y-axis shows the mean deviations between measured and simulated pressures in the whole basin in the different runs. The fault permeabilities used in the low, base and high cases are marked.*

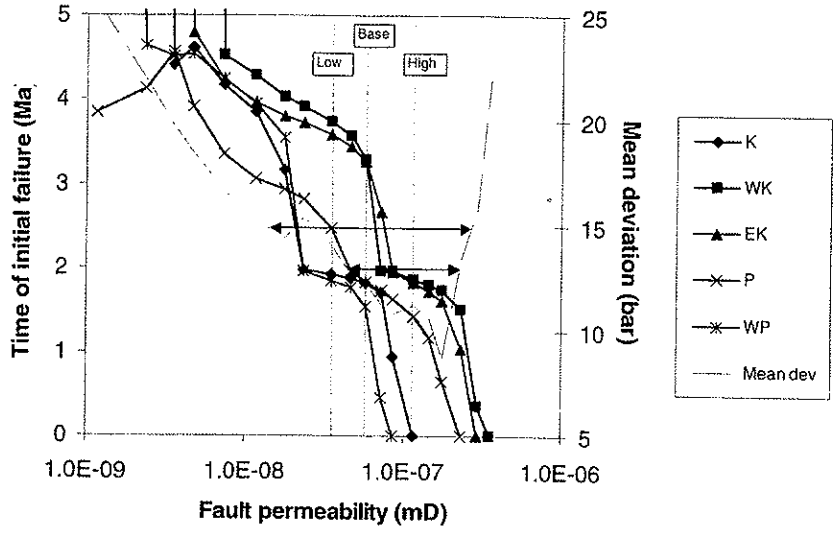

Figure 16 *Illustration of the fault permeability at 4 km depth versus timing of hydraulic leakage in the different compartments for the last 5 Ma. The right y-axis shows the mean deviations in the different runs. The fault permeabilities used in the low, base and high cases are marked.*

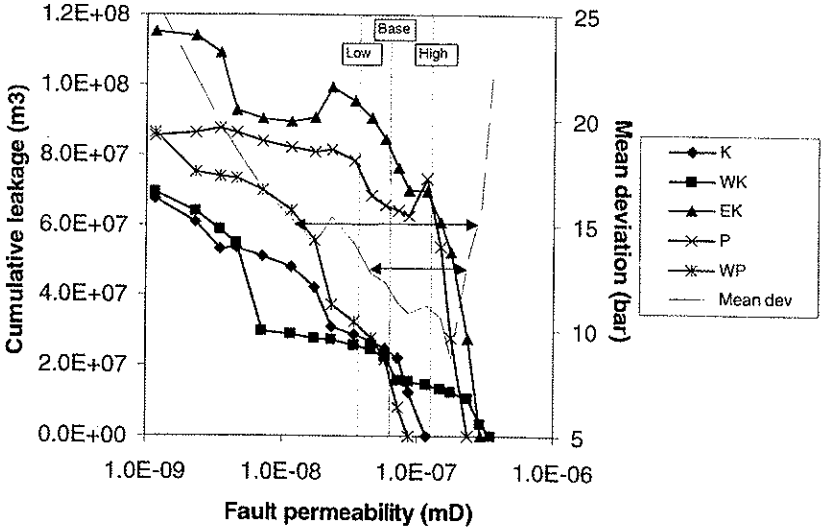

Figure 17 *Cumulative leakage (m^3) versus permeability (mD) for the simulated fault at 4 km burial depth. Note the high cumulative leakage simulated for compartments EK and P. The right y-axis shows the mean deviations in the different runs. The fault permeabilities used in the low, base and high cases are marked. Note that the base and high case give mean deviation <13 bar.*

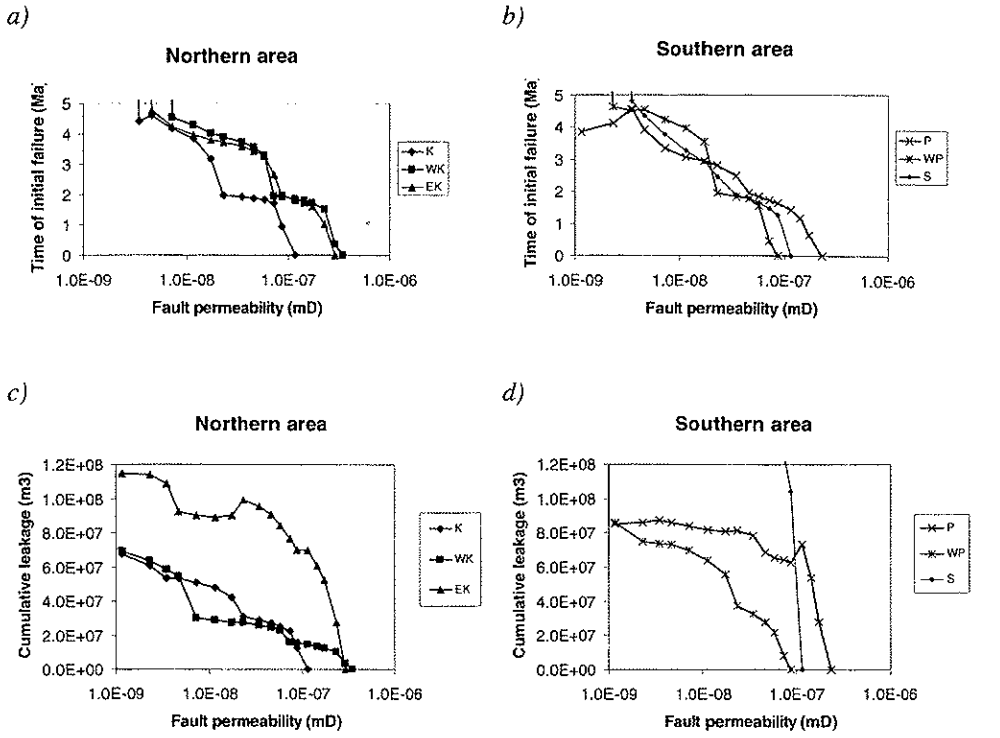

Figure 18 *Timing of hydraulic fracturing versus permeability across faults in a) northern study area and b) southern study area. Cumulative leakage versus fault permeability in c) the northern and d) southern area. The largest amounts of leakage are simulated for EK and S.*

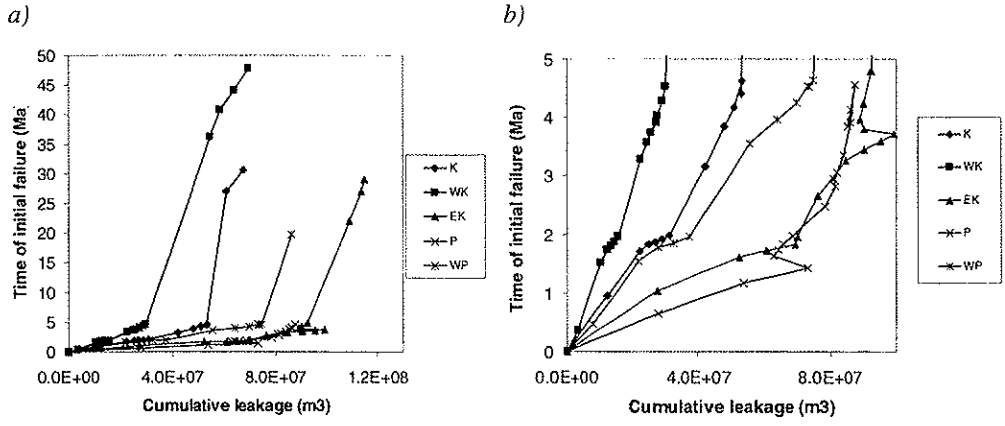

Figure 19 *Time of hydraulic failure versus cumulative leakage for all the compartments during a) the last 50 Ma and b) the last 5 Ma. The smallest compartments (WK, K and EK) show a linear relationship in the last 5 Ma.*

Discussion

Uncertainty is an important issue to address in order to evaluate the quality of the simulations. Therefore, well measurements of present reservoir pressure were used to calibrate the simulations. Unfortunately pressure data are not available for the caprock. Furthermore, not only the pressure measurement would be of interest to estimate, but also the possibilities for hydrocarbon shows. However, many of the highly overpressured compartments that have been simulated in this study, have not yet been drilled and calibration is therefore not possible. Using the predictions from the present simulations, however, better estimates may be obtained.

We start out assuming that hydrocarbons have accumulated in the highly overpressured compartments. The preferred situation from an exploration point of view would be that the caprocks for these compartments did not fail. However, if one or more of the compartments did fail, the timing and the amount of leakage are important factors to evaluate. One scenario is that the pressure build-up may have lead to very early fracturing, but that the caprock subsequently became chemically healed, and the compartment could be refilled. This, however, does not appear to be the case in the study area, because hydraulic fracturing and leakage is predicted during the last 5 Ma. Late leakage may be optimal for accumulations of hydrocarbons, since only small amounts of fluid would have time to escape.

To rank the possibilities of hydraulic fracturing and leakage in the compartments we have studied three important factors; the timing, the amount of leakage and the size of the accumulation. As an example we can compare the timing and amount of leakage in compartments WP and WK (Figure 16). In this dataset, WP is the first compartment that does not go to fail when the permeability is increased in the simulations (Figure 16). However, by using lower permeabilities, the cumulative leakage for compartment WP increases rapidly due to earlier failure (Figure 17). Compartment WK may therefore contain a more preferable prospect for hydrocarbon exploration, even though modelling suggests leakage at high permeabilities (Figure 16). More important perhaps, is that the cumulative leakage in compartment WK seems to be small when low permeabilities are used (Figure 17). In such a case, the size of the field will be the controlling factor: for a large field it would be best for the hydrocarbon accumulation that a low, but steady leakage occurs. As seen directly from the cumulative leakage versus permeability plot (Figure 17), the large compartments, in this case EK and P, would have too large cumulative leakages to be good exploration targets. Thus, the smaller compartments with either late fracturing or early, but low leakage rates are more favourable.

The uncertainty assessment can be used to evaluate the predictability of the simulations. In Figures 16 and 17 show the mean deviation between measured and simulated pressures in all compartments where wells exists calculated. Large mean deviations are observed when very high or low fault permeabilities are used in the simulations. If one define a mean deviation of 13 bars to be acceptable, then the uncertainties in the simulations of the timing and cumulative leakage for one compartment like K can be considered. If a mean deviation of 13 bars is acceptable, then late leakage from compartment K is predicted from 1.9 Ma to Present day. The cumulative leakage is estimated not to exceed $29 \cdot 10^6$ m^3. The runs with lower deviations do not fail (Figure 16). Compartment P most likely fails, except using high permeability values. The timing of the failure in compartment P is simulated between 2.5 to 0.6 Ma, with cumulative leakage in the scale of $280 \cdot 10^6$ m^3 to $78 \cdot 10^6$ m^3, respectively. An uncertainty limit of 15 bar, gives more or less the same results for most compartments (Figure 17). Differences are observed when low permeabilities are used and the rate of leakage

increases rapidly. A relatively large change in the modelled timing of hydraulic leakage and cumulative leakage is seen for compartments K and WP, when changing the "acceptable" deviation from 13 to 15 bars. Both fail from 1 to 1.5 Ma earlier, with higher leakage rates resulting (Figure 16 & 17).

Effects on hydrocarbon migration

Different effects have to be taken into account when the probability of hydrocarbon leakage is evaluated. In the simulations, we assume leakage from the highest point in the structure, with less or no leakage down dip. Still, hydrocarbons may be trapped down dip in compartments that have expired hydraulic leakage at the crest. To be able to evaluate the probability for hydrocarbon reserves, more detailed studies of smaller areas, incorporating more faults, need to be carried out. The presence of internal minor faults in the compartments will influence fluid flow. Furthermore, assuming leakage from the highest point of the structure, time-delays in the leakage should be taken into account.

Comparison of permeabilities used in modelling with measured permeabilities

Faults in clastic sequences often represent significant barriers to fluid flow. Fisher & Knipe (2001) measured the permeability of faults within siliciclastic rocks in the North Sea and the Norwegian Continental Shelf. Faults typical in impure sandstones (vshale 15-40%) have a permeability of ~0.001 mD at depths > 4 km. While, clay-rich sediments (vshale >40%) deform to produce clay smears with very low permeability (< 0.001 mD; Fisher & Knipe 2001). Sperrevik et al. (2002) observed a relationship between the permeability and the mineralogical composition of the faulted rock, the effective stress conditions, and the history of the reservoir prior to, during and after deformation. They measured very low permeabilities ($< 10^{-7}$ mD) in faults with clay smears at depths (> 3.5 km). This is in accordance with the permeability values used in our simulations, which resulted in hydraulic failure in the simulations (Figure 20). With less clay content in the fault zones, the data from Sperrevik et al. (2002) gave too high permeabilities in the fault, and the pressure barriers are not effective enough to simulate hydraulic fracturing. According to this data set, lower permeabilities should be used when simulating the shallow part of the faults. However, since overpressure is unlikely to occur at this shallow depth of burial, this is probably not critical for the timing and amount of hydraulic leakage modelled. On the other hand, clay smear is probably not the controlling sealing factor in all the faults with deeper burial depths in the study area. Diagenesis and quartz cementation in the fault zones are processes that contribute to fault sealing at large depths. Therefore, better control on the lateral leakage would be gained by integrating the clay content of the faults during subsidence into the simulator.

In addition to the initiation of hydraulic fracturing, the continuation of fluid flow and leakage should be considered. Gutierrez et al. (2000) presents results from laboratory tests of extensional fractures in shales. The tests show a decrease in permeability during increasing normal stress across the fracture and after shearing of the fracture under constant high normal stress. However, the fractures never completely closed. This indicates that fractures once created are difficult to close by mechanical loading. Then, as long as sufficient hydraulic gradients are obtained, fluid can still flow along fractures even in the absence of large overpressures. The results from Gutierrez et al. (2000) are in accordance with the simulation of continuous leakage done by us, as long as the pressure compartment is fractured and is at the leakage pressure gradient.

In this article we have presented a type of analysis that can be carried out using a coupled pressure and stress simulator to evaluate hydraulic fracturing and leakage. The simulator itself

is described in Borge (2002), Borge & Sylta (1998) and Lothe et al. (in press). Other input parameters than the ones discussed by us can influence the timing of fracturing. Lothe et al. (in press) shows a large influence of the geo-mechanical parameters used for the caprock (Poisson's ratio and Young's modulus). The handling of stresses in the simulator has room for significant improvements. Nevertheless, by varying the input parameters in different runs, the uncertainty in the simulations can be found with a larger confidence than we could before.

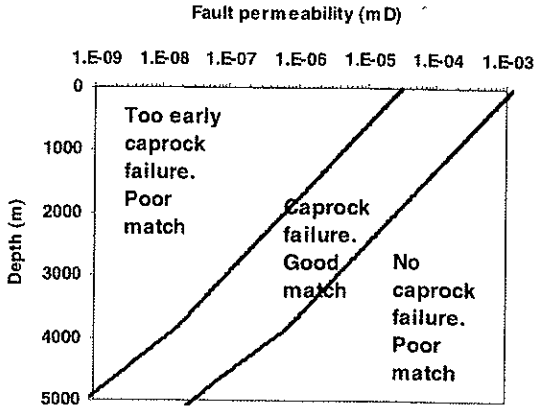

Figure 20 *Variations in fault permeability used in the simulations giving hydraulic fracturing and leakage. Matches to the pressure measurements with wells outlined.*

Conclusions

The main conclusion from this work is that the transmissibilites across faults between overpressured compartments will have a major impact on the timing and amount of hydraulic fracturing and leakage and this can be simulated. Low fault permeabilities cause restricted lateral flow, overpressure build-up and early hydraulic fracturing, and the resultant simulated pressures, give then large deviations compared to the measured pressures in wells. High permeabilities give later failure and in some cases no failure in some compartments. The hydraulic leakage in one compartment will influence the amount and timing of leakage in the neighbouring pressure compartments. The largest compartments in an area will control the timing and amount of leakage in the smaller ones. The uncertainty in the simulations can be estimated by comparing the simulated pressures with the measured pressures in the wells, and thereby be able to improve risk prediction of hydrocarbon shows in undrilled traps.

Acknowledgement

We would like to thank Norsk Hydro ASA for their funding to Lothe's PhD thesis on hydraulic fracturing, providing data, and giving permission to publish. Colleagues at SINTEF Petroleum Research are thanked for useful discussions. Roy H. Gabrielsen has kindly corrected an early version of the manuscript.

References

Berg, T., Berge, K., Cecchi, M. Ekeli, C, Hansen, L., Norvik, O., Waters, D. 2000. Fault seal and overpressure analysis of Halten Terrace. *Hydrocarbon Seal Quantification,* Norwegian Petroleum Society. Extended abstract only.

Blystad, P., Færseth, R. B., Larsen, B. T., Skogseid, J. & Tørudbakken, B. 1995. Structural elements of the Norwegian continental shelf, Part II. The Norwegian Sea Region. Norwegian Petroleum Directorate Bulletin, **8**.

Borge, H. 2000. Fault controlled pressure modelling in sedimentary basins, *An thesis for the degree of Doktor Ingenør of the Norwegian University of Science and Technology*, 148 pp.

Borge, H. 2002. Modelling generation and dissipation of overpressure in sedimentary basins: an example from the Halten Terrace, offshore Norway. *Marine and Petroleum Geology*, **19**, 377-388.

Borge, H. & Sylta, Ø. 1998. 3D modelling of fault bounded pressure compartments in the North Viking Graben. *Energy, Exploration and Exploitation*, **16**, 301-323.

Bour, O., Lerche, I & Grauls, D. 1995. Quantitative models of very high fluid pressures: The possible role of lateral stresses. *Terra Nova*, 7, 68-79.

Chapman, R. E. 1980. Mechanical versus thermal causes of abnormally high pore pressures in shales. *AAPG Bulletin*, **64**, 2, 179-183.

Cosgrove, J. W. 1998. The role of structural geology in reservoir characterization. *In:* Coward, M. P., Daltaban, T. S. & Johnson, H. (eds) *Structural Geology in Reservoir Characterization*. Geological Society Special Publications, London, **127**, 1-13.

Darby, D. Haszeldine, R. S. & Couples, G. D. 1996: Pressure cells and pressure seals in the UK Central Graben. *Marine and Petroleum Geology*, **13**, 865-878.

Dalland, A. G., Worsley, D. & Ofstad, K. 1988. A lithostratigraphic scheme for the Mesozoic and Cenozoic succession offshore mid- and northern Norway. Norwegian Petroleum Directory.

Fisher, Q. & Knipe, R. J. 2001. The permeability of faults within siliciclastic petroleum reservoirs of the North Sea and Norwegian Continental Shelf. *Marine and Petroleum Geology*, **18**, 1063-1081.

Grauls, D. 1996. Minimum Principal Stress as a Control of Overpressures in Sedimentary Basins. *Proceeding of the8th Conference on Exploration and Production*. IFP Report No43313, IFP Ruil-Malmaison.

Gauls, D. 1998. Overpressure assessment using minimum principal stress approach. *Overpressure in Petroleum Exploration*, Proc. Workshop, Bull. Centre Rech. Elf Explor. Prod., Pau, France, **22**, 137-147.

Gutierrez, M., Øino, L. E. & Nygård, R. 2000. Stress-dependent permeability of a de-mineralised fracture in shale. *Marine and Petroleum Geology*, **17**, 895-907.

Hermanrud, C. & Bolås, H. M. N. 2002. Leakage from overpressured hydrocarbon reservoirs at Haltenbanken and in the northern North Sea. *In:* Koestler, A. G. & Hunsdale, R. (eds) *Hydrocarbon Seal Quantification*. NPF Special Publication **11**. Elsevier Science, Amsterdam, 221-231.

Horsrud, P, Sønstebø, E.F. & Bøe, R. 1998. Mechanical and Petrophysical Properties of North Sea Shales. *International Journal of Rock Mechanical Mining Science*, **35**, 1009-1020.

Hunt, J.M. 1990. Generation and Migration of Petroleum from abnormally pressured fluid compartments. *AAPG Bulletin*, **78**, 12, 1811-1819.

Koch, J.-O. & Heum, O. R. 1995. Exploration trends of the Halten Terrace. *In:* Hanslien, S. (ed) *Petroleum Exploration and Exploitation in Norway*. NPF Special Publication. Elsevier, Amsterdam, **4**, 235-251.

Lothe, A. E., Borge, H. & Gabrielsen, R. H. in press. Modelling of hydraulic leakage by pressure and stress simulations and implications for Biot's constant: An example from the Halten Terrace area, offshore Norway. *Accepted for publication in Petroleum Geoscience*.

Loosveld, R. J. H. & Franssen, R. C. M. W. 1992. Extensional vs. Shear Fractures: Implications for Reservoir Characterisation. *SPE 25017*.

Miller, T.W. & Luk, C.H. 1993: Contributions of compaction and aquathermal pressuring to geopressure and the influence of environmental conditions: Discussion. *AAPG Bulletin*, **77**, 2 6-10.

Morrow, C. A., Shi, L. Q. & Byerlee, J. D. 1984. Permeability of fault gouge under confining pressure and shear stress. *Journal of Geophysical Research*, **89**, 3193-3200.

Revil, A. & Cathles, L. M. 1999. Permeability of shaly sands. *Water Resources Research*, **35**, 651-662.

Skar, T., Balen, R. T. v., Arnesen, L. & Cloetingh, S. 1999. Origin of overpressures on the Halten Terrace, offshore mid-Norway: the potential role of mechanical compaction, pressure transfer and stress. *In:* Aplin, A. C., Fleet, A. J. & Macquaker, J. H. (eds) *Mud & Mudstones: Physical and Fluid Flow Properties.* Geological Society of London, London, **158,** 137-156.

Sperrevik, S., Gillespie, P. A., Fisher, Q. J. & Knipe, R. J. 2002. Empirical estimation of fault rock properties. *In:* Koestler, A. G. & Hunsdale, R. (eds) *Hydrocarbon Seal Quantification.* NPF Special Publication. Elsevier Science B.V., Amsterdam, **11,** 109-125.

Swarbrick, R. E. & Osborne, M. J. 1998. Mechanisms that generate abnormal pressures: an overview. *In:* Law, B. E., Ulmishek, G. F. & Slavin, V. I (eds) *Abnormal Pressures in Hydrocarbon Environments*, AAPG Memoir, **70**, 13-34.

Teige, G. M. G., Hermanrud, C., Wensaas, L. & Bolås, H. M. N. 1999. The lack of relationship between overpressure and porosity in North Sea and Haltenbanken shales. *Marine and Petroleum Geology*, **16**, 321-335.

Verbeek, E. R. & Grout, M. A. 1993. Geometry and structural evolution of gilsonite dikes in the eastern Uinta basin, Utah. *U.S. Geological Survey Bulletin*, **1787**, 42.

Walderhaug, O. 1996. Kinetic modelling of quartz cementation and porosity loss in deeply buried sandstone reservoirs. *AAPG Bulletin*, **80**(5), 731-745.

Wiprut, D. & Zoback, M. D. 2002. Fault reactivation, leakage potential, and hydrocarbon column heights in the northern North Sea. *In:* Koestler, A. G. & Hundale, R. (eds) *Hydrocarbon Seal Quantification.* NPF Special Publication. Elsevier Science B.V., Amsterdam, **11,** 203-219.

Zhang, S., Tullis, T. E. & Scruggs, V. J. 2001. Implications of permeability and its anisotropy in a mica gouge for pore pressures in fault zones. *Tectonophysics*, **335**, 37-50.

Appendix A Values of parameters used in the simulations (see Borge (2000) for explanation of parameters and nomenclature)

Description	Symbol	Value	Unit
Pressure generation and accumulation			
Accumulating depth	z_A	2500	m
Generating depth	z_S	4100.0	m
Salinity	s	50000	ppm
Accumulating exponent	A	3.45	
Shale drainage thickness	γ	100.0	m
Minimum reservoir thickness	z_{min}	0.10	m
Minimum net/gross ratio	N/G_{min}	0.050	
Maximum shale compaction depth	z_{shale}	10000.0	m
Hydrostatic gradient	$\rho_w g$	0.1030	bar/m
Lithostatic gradient	$\bar{\rho} g$	0.220	bar/m
Time step	Δt	10000	years
Diameter of quartz grain size	D	0.0003	m
Fraction of detrital quartz	f	0.65	

Molar mass of quartz	M	0.06009	kg/mole
Density of quartz	ρ_{quartz}	2650.0	$kg \cdot m^{-3}$
Temperature at which quartz cementation starts	T_{C0}	80.0	°C
Temperature at which quartz cementation is completed	T_{C1}	175.0	°C
Quartz precipitation rate factor	r_1	1.98e-18	$mole/m^2s$
Quartz precipitation rate exponent	r_2	0.022	$°C^{-1}$
Sand porosity at seabed	ϕ_{S0}	0.45	
Sand porosity constant 1	η_1	2400	m
Sand porosity constant 2	η_2	0.50	
Temperature at seabed	T_0	4.0	°C
Temperature gradient	$\partial T / \partial z$	0.035	$°Cm^{-1}$
Irredusible water saturation (Garn Formation)	ϕ_{C1}	0.040	
Clay coating factor (Garn Formation)	C	0.50	
Minimum dissipation volume	V_{min}	1.0e+06	m^3
Hydraulic leakage			
Poisson's ratio (shales) at surface	ν_{z_0}	0.40	
Poisson's ratio (shales) at accumulating depth	ν_{z_A}	0.27	
Poisson's ratio (shales) at sealing depth	ν_{z_S}	0.20	
Poisson's ratio (shales) at max. shale comp. depth	$\nu_{z_{shale}}$	0.02	
Young's modulus (shales) at surface	E_{z_0}	600	bar
Young's modulus (shales) at accumulating depth	E_{z_A}	20000	bar
Young's modulus (shales) at sealing depth	E_{z_S}	40000	bar
Young's modulus (shales) at max. shale comp depth	$E_{z_{shale}}$	90000	bar
Coefficient of thermal expansion	α_T	1.00e-05	
Bulk modulus (shale)	K_s	170000.0	bar
Coefficient of internal friction	μ	0.6	
Coefficient of sliding friction	μ'	0.7	
Lateral transmissibility			
Lateral transmissibility		0.00069	
Percent transmissibility remaining at no overlap	p	0.05	
Width of fault blocks	b	20.0	m
Porosity at seabed	ϕ_0	0.45	
Rate of change in porosity versus depth	c	0.00039	m^{-1}
Porosity where the K - ϕ curve changes between deep and shallow relationships	ϕ_b	0.1	
Permeability where the K - ϕ curve changes between deep and shallow relationships	K_b	0.00001	mD
Rate of change in fault zone permeability (log) versus depth (log) for shallow faults	δ_{sh}	5.0	mDm^{-1}
Rate of change in fault zone permeability (log) versus depth (log) for deep faults	δ_{de}	7.0	mDm^{-1}

Chapter 13 is not included due to copyright.

CHAPTER 14

14. Structural restoration techniques in 3D basin modelling: Implications for hydrocarbon migration and accumulation.

Structural Restoration Techniques in 3D Basin Modelling: Implications for hydrocarbon migration and accumulation

Paul Huggins[1now5], Stuart D. Burley[1and 6], Oyvind Sylta[2], Are Tommeras[2], Stuart Bland[3], Stephanie Kape[3] and Nick Kusznir[4]

1. Subsurface Technology, BG Group plc, 100 Thames Valley park Drive, Reading, RG6 1PT, U.K.
2. SINTEF Petroleum Research, Trondheim, Norway
3. Midland Valley Exploration Ltd, Glasgow, U.K.
4. Department of Earth Sciences , University of Liverpool, Brownlow Street, Liverpool, L69 3BX U.K.
5. BP Exploration Ltd, Dyce, Aberdeen AB21 7PB
6. Basin Dynamics Research Group, Department of Earth Sciences, University of Keele, Keele, ST5 5BG

Abstract

The effects of structural restoration on hydrocarbon migration pathways in extensional basins are evaluated at two scales using two different structural restoration techniques. Both restoration techniques are integrated with a ray-trace secondary hydrocarbon migration simulator. A regional basin example investigates the effects on migration of restoring a post-rift basin succession employing 3D flexural backstripping. The effects of fault displacement and associated horizon deformation restoration on synchronous hydrocarbon migration are examined in a prospect-scale example.

Geohistory restoration of basin subsidence and fault architecture is shown to influence hydrocarbon drainage areas, trap geometries and volumetrics, migration pathways, accumulation distributions and fill-spill paths. Migration flowpath histories for structurally restored horizon surfaces exhibit significant changes in migration pathways due to spilling from temporary traps and sealing faults, as well as re-migration concomitant with trap destruction during restoration.

In ray-tracing models, fluid flow responds to the smallest of structural features creating a dip change. Modelled results are therefore sensitive to the method and algorithm used in the structural restoration. Additionally, inaccurate fault closure and fault cut-off drag/reverse drag artifacts may channel flow along fault strike, so that the hydrocarbons fail to enter the fault zone, making open faults appear as sealing faults.

Basin restoration and geohistory are two critical inputs to basin modelling, differences in which can have profound effects on simulation results and thus risk analysis. Changing migration pathways may critically affect the modelled hydrocarbon potential of key prospects in a basin. Incorporating appropriate quality structural restorations of basin geohistory into basin simulators is essential for accurately predicting hydrocarbon accumulations in basin and prospect evaluations. The integration method discussed here is feasible for exploration risk assessments.

Introduction

Basin modelling is a powerful tool for predicting the timing of petroleum generation and the distribution of hydrocarbon phase and volumetrics in sub-surface plays – source, carrier and trap systems - to reduce exploration risk (Iliffe and Dawson, 1996; Krokstad and Sylta, 1996; Burley et al., 2000). Basin architecture its evolution are some of the critical inputs to building a basin model. Basin geohistory influences the sediment infill, thermal history and evolving fluid conduit geometries, controlling potential hydrocarbon migration pathways and thus hydrocarbon accumulations.

Commercial and research basin modelling tools already enable most petroleum system processes to be simulated and predicted with considerable sophistication, including subsidence, compaction, pressure, organic matter maturation, three phase hydrocarbon expulsion, secondary migration, trapped hydrocarbon phase and volumes, and losses (Sylta, 1991; Schneider et al., 1996; Mann et al., 1997; Wendebourg, 2000). These processes are dynamic, evolving through time and occurring in different areas of a basin at the same time. Fluid flow conduits, and potential migration along them, are also 3D networks throughout the basin. Accurate prediction of hydrocarbon accumulations therefore requires modelling in 3D. Incorporation of basin architecture and its evolution into 3D basin models is, however, still relatively simplistic in its approach. Commercial 3-D secondary migration simulators do not directly incorporate structural restoration beyond vertical decompaction and backstripping, whilst structural restoration techniques do not simulate secondary hydrocarbon migration processes.

The importance of structural restoration in determining basin geohistory for incorporation into basin simulations and its effects upon modelled secondary hydrocarbon migration and accumulation are considered in this paper. Initial results of a new integrated modelling methodology linking structural restoration software with a hydrocarbon fluid flow/migration simulator are presented. Accurate restoration of a basin geohistory is demonstrated to be critical to the modelling of hydrocarbon migration, and thus for exploration prospect analysis.

The approach adopted herein is to use sequential time-step output from structural restoration techniques as input to a horizon-based, ray-trace, secondary hydrocarbon migration simulator. Two structural scenarios are presented, handled by the same modelling methodology: (1) Incorporation of crustal flexural isostatic response into basin subsidence, which is then normally simply backstripped; (2) A new ability to handle fluid flow with synchronous faulting. Detailed physics and techniques of the structural modelling and fluid simulation or the modelling processes are not described. These can be found in the literature on the individual modelling techniques of fault restoration (Williams et al., 1999), flexural modelling (Kusznir et al, 1995) and ray trace migration (Sylta, 1991; Hindle, 1997). The modelling integration techniques and methodology are proprietary and currently in early development, and are only discussed briefly. Comparison is made between new models integrating structural modelling and 'normal' backstripped models. Full sensitivities of the structural models have yet to be completed. Large differences between models highlight that sensitivity within the structural modelling is probably a secondary factor.

Background to Migration and Restoration in Basin Modelling

Structural restoration and basin modelling have traditionally addressed specialist problems within their own fields of structural validation and hydrocarbon generation. Appropriate tools for each approach has have evolved in isolation from each other, with separate requirements, assumptions and data structures. Advances in computing power, visualization technology and the development of 3D modelling capability now enable the production of high spatial and temporal resolution 3D models. Significant improvements to hydrocarbon accumulation predictions can be made by the integration of improved basin geometries and their evolution (geohistories) from structural modelling to form a more realistic geological framework for basin simulators.

Concepts of secondary migration and accumulation

Secondary hydrocarbon migration is a multi-phase, water-oil-gas process (Schowalter, 1979) driven by buoyancy forces and pressure gradients, the latter a function of compaction and hydrodynamic flow (Hubbert, 1953; Berg, 1975; Dahlberg, 1982; Hindle, 1997). Current understanding of the petroleum system indicates that hydrocarbons migrate in focused stringers of small size (less than a few metres high, few 10's of metres wide and up to many kilometres long), at moderate saturations (10-40%) (Selle et al, 1993, Sylta, 2002). Hydrocarbons move vertically under buoyancy until they encounter a permeability barrier, at which point they migrate laterally or accumulate until the buoyancy pressure of the accumulation exceeds the capillary entry pressure of the confining barrier (Thomas & Clouse, 1995). Faults are modelled as possible permeability barriers between grid-nodes. It is all these aspects of the petroleum system that basin scale migration models try to reproduce.

Basin architecture and its evolution

The overall configuration of a sedimentary basin, reflecting basement movement due to its tectonic style and mode of formation, and the internal stratigraphy and structure of the basin infill define basin architecture. The evolution of basin architecture is described as the basin geohistory – incorporating tectonic subsidence and isostatic loading, sediment deposition and compaction, palaeogeography (including palaeobathymetry, uplift & erosion), and both tectonic and synsedimentary structuration (faulting, folding, diapirism). Horizon geometries evolve as a result of the interplay of all of these processes.

Restoration of the basin architecture

The geohistory of a basin is determined by reverse modelling of the Present-Day stratigraphic and structural architectures to restore palaeogeometries. Sediment layers are sequentially backstripped and the remaining sediments decompacted (Van Hinte, 1978; Sclater and Christie, 1980; Bond and Kominz, 1984). Differential compaction of layers, with highly variable thicknesses, or which are laterally discontinuous, has a major impact upon restored horizon palaeogeometries (Figure 1). Horizon dip and structural closure can be altered by variations in modelled burial history. Different compaction porosity-depth functions also affect restored palaeogeometries (Giles et. al. 1998), though changes in structural amplitude rather than shape most commonly result. Differential compaction

of homogenous sequences of variable thickness, i.e. over structural highs, or constant thickness sequences of variable composition, i.e. channels, commonly result in dip changes but rarely dip direction reversals or location of dip closures.

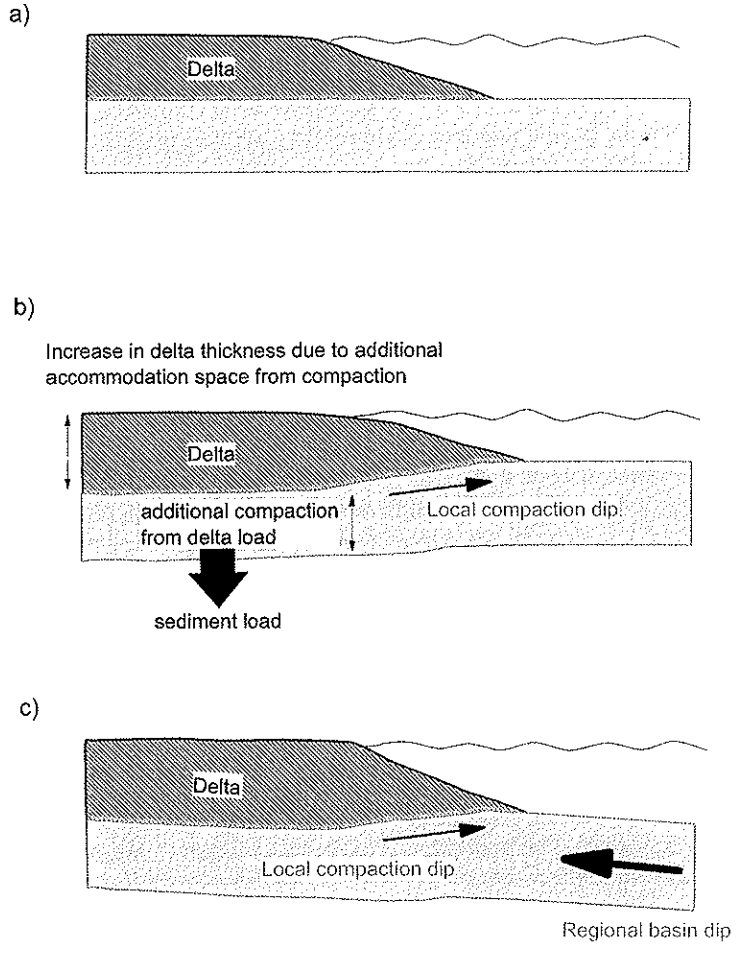

Figure 1: Effect of sediment loading, resulting from a sediment pile, on lower horizon geometries due to differential compaction.
a) Sediment pile on horizontal non-compacting basement
b) Sediment pile on horizontal compactable basement - induces local horizon dip
c) Sediment pile on dipping compactable basement - induces local horizon dip reversal

Backstripping can be purely geometric, restoring horizons to a depositional template, or process-based, using mechnanical models of the lithosphere to predict palaeogeometries. The simplest backstripping procedure restores the sediment depositional surface to a horizontal datum of a specified bathymetry, usually sea-level (Roberts et al., 1998). Such backstripping can be enhanced by restoring the depositional surface to a

palaeobathymetric template, defined from the internal stratigraphic architecture and biostratigraphy of the layer (Van Hinte, 1978). Mechanical models predict basement geometry based upon lithospheric deformation and its isostatic response to basin infilling (Mckenzie, 1978; Beaumont et al., 1982; Watts et al., 1982; Kusznir et al., 1995), defining the evolving horizon geometries and palaeobathymetry. Figure 2 illustrates the loading of an elastic crust by a sediment pile. The effect of the load is to suppress the crust with a wavelength and amplitude greater than that of the load, leading to the development of additional sediment accommodation space and palaeobathymetry (Turcotte and Schubert, 1982). Such techniques are useful in areas with little palaeobathymetric control and where sedimentation is highly variable laterally. Subsidence from isostatic loading can induce horizon dips in the sediment pile not modelled by geometric restoration with no control. Differences in horizon dip between these restoration methods may be significant, with the possibility of opposite, counter regional dips being developed (Figure 2). Using either an incorrect palaeobathymetry or no palaeobathymetry at all, i.e. a simple burial history, can result in an erroneous restoration of horizon geometry and may even reverse the direction of horizon dip and thus fluid flow direction (Figure 3). Such errors are propagated down through the model, from the currently restored layer, affecting all underlying layers.

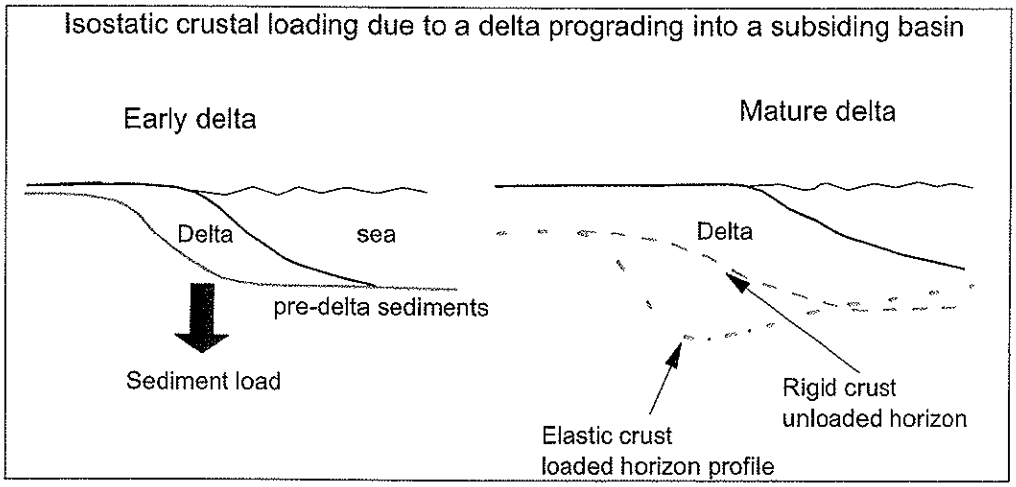

Figure 2: Effect of flexural isostatic loading by a sediment pile on an elastic crust on lower horizon geometries. Early sediment deposition (a) loads the crust resulting in local subsidence and the generation of additional sediment accommodation space. Continued sedimentation continues this process depressing the underlying horizons (b). It is possible to change the dip direction of the lower horizons below the sediment pile.

Structuration of the basin sediment infill by tectonic and syn-sedimentary processes modifies the overall depositional geometries, influencing horizon geometries at the sub-basin and local scales. Faulting affects horizon geometry in relation to the scale of faulting and fault throw, different processes causing footwall and hangingwall deformation. At the basin scale crustal, isostatic forces are predominant whilst at the intra-hydrocarbon field scale elastic dislocation forces are prevalent. Fault growth,

evolving fault tip position and interaction between faults modifies horizon geometry. The horizon geometries around faults and flow properties of the fault zone will define possible flow paths along, across or around faults (Figure 4).

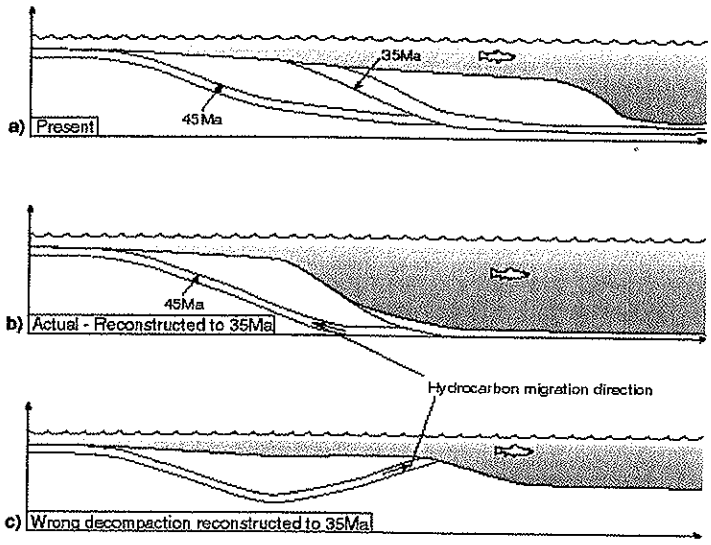

Figure 3 : Decompaction and backstripping of a prograding delta.
a) Present-Day geometries
b) Correct reconstructed to 35Ma using palaeobathymetry
c) Incorrect reconstruction using wrong palaeobathymetry (none over delta foreslope). Resulting in erroneous restored horizon dips which are reversed from the true restoration. (Figure from Semi webpage, SINTEF, see also Kjennerud and Sylta, 2001)

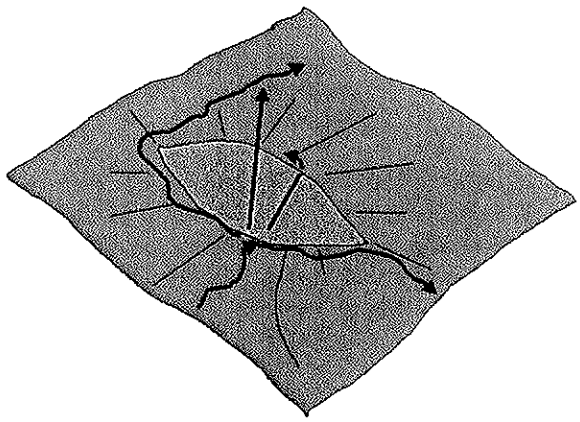

Figure 4: Horizon geometry deformation associated with a fault showing possible migration pathways along, across and around the fault.

Structural validation and modelling tools are based upon geometric algorithms that describe observed rock deformation, preserving area and/or volumes. Several approaches have been developed, including strain trajectories (Cobbold, 1979), iterative finite element methods (Gratier et al., 1991) and jigsaw fitting (Williams et al., 1997) all enable the restoration of complex faulted and folded structures. New algorithms, such as flexural flow, have been developed that handle out-of-plane movement of material for true 3D modelling (Kane, 1999; Gibbs & Kape, 1999, Williams *et al.*, 1999). These techniques enable the kinematic evolution of structures to be modelled. Handling of complex geometries and deformations in 3D requires a flexible model representation in the form of irregular triangulated meshes which change topology (node pattern and connectivity) between modelling steps (Mello and Henderson, 1997; see Figure 5).

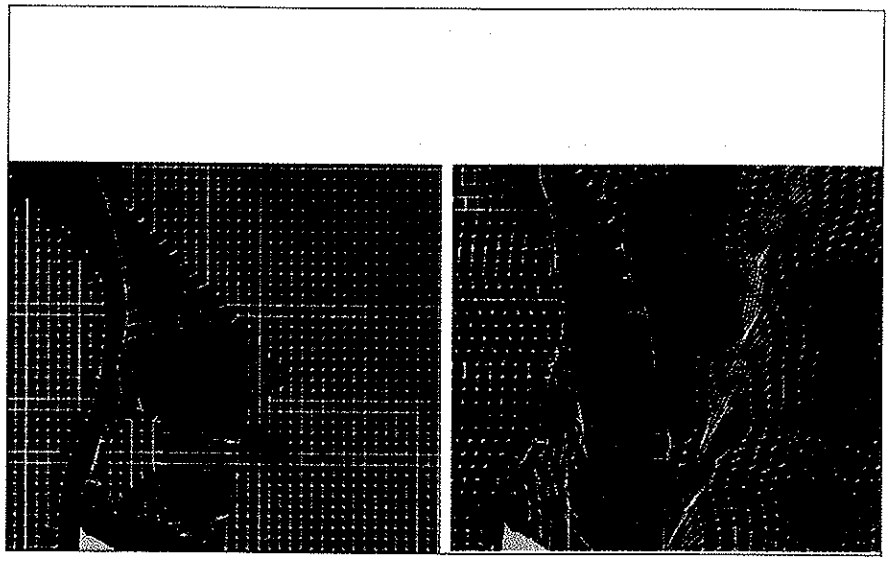

Figure 5: Data structures representing surfaces in different basin modelling software. (a) regular grid from a basin simulator imported into a structural modelling package, which has converted the grid into a regular triangulated mesh. Two horizon segments (different colours) are separated by a fault heave polygon (area of no data). An area of no data in the original interpretation has been infilled in the structural model by triangulation (area of large irregular triangles). (b) Irregular triangulated mesh from the structural model following restorationof the fault and associated horizon deformation. Restoration involved removing the fault throw, closing of the fault heave polygon, and flattening the horizon. Restoration resulted in disruption to the surface data structure with areas where surface data nodes converge and diverge.

Incorporating structural modelling into basin restoration

Conventional, commercial hydrocarbon system simulators are based on finite difference or finite element numerical techniques (Wangen, 1997). Models are constructed from stacked horizon surface grids in which data nodes are vertically aligned so that decompaction and backstripping are incorporated. Simple fault geometries and their

evolution are present in basin simulators but are handled in a relatively simplistic manner without discrete discontinuities in the grids, and do not incorporate the geometries that can be derived from specialist structural techniques.

Initial links for integrated structural and fluid flow models have been developed in 2D for modelling the architecture and thermal evolution of basins (Fjeldskaar et al., 1993; Schneider, et al., 1999). Fully integrated 3D finite element models, not constrained by vertical grid alignment, are in research development (Mello and Henderson, 1997; Cathles, *et al.* 1999; Orteleva, *et al.* 1999; Welte et al., 2000). One possible solution to full process-based integration in 3D is to capture the geometries from structural models and use them to build the finite element mesh framework of the basin simulator. These frameworks can then be populated with properties to model the hydrocarbon system. However, full 3D physics models must be mass balanced through time. The problem remaining for this approach is how to make the structural model, basin model and the processes that are common to both and different between them consistent to enable integration.

Horizon-based ray-trace models of hydrocarbon migration provide an alternative, computationally fast representation of the petroleum system that is able to reproduce hydrocarbon distributions and volumetrics with accuracy (Sylta, 1991). Descriptions of the physical processes of the modeling and applications of the methodology are described in Sylta (1993), Sylta et al. (1998), Skjervøy et al (2000) and Borge and Sylta (1998). Ray-trace models assume hydrocarbon migration is buoyancy driven (Sylta, 1993), although the effect of fluid pressure compartments can be incorporated into the models (Borge and Sylta, 1998). Migration is modelled to be controlled by bed dip rather than pressure gradient, removing the need for full physics pressure analysis. Only the rock properties relevant to fluid flow are considered in detail, namely those of the hydrocarbon source unit and key high permeable units along which hydrocarbons are thought to migrate – carrier beds. Rays therefore represent the migration pathways from the source location to the trap location. The rays are deflected in the direction of maximum dip of the carrier. Barriers to migration can be faults, salt or pinchouts. These barriers can deflect migration away from the steepest dip. Fault properties can be defined from fault juxtapositions using clay-smear concepts (Childs et al, 2002). The user can also manually defined each fault as sealing or open according to knowledge from fault seal studies in the area. Secondary hydrocarbon migration losses are calculated within thin migration stringers (Sylta et al, 1998). Migration between carrier beds through seals is approximated as a leakage term (see e.g. Sylta, 1993), similar to transmissibility modifiers for faults, based on capillary pressure (column height) limits. Simulated migration patterns mimic the perceived nature of hydrocarbon migration as thin focused stringers at the top of carrier surfaces.Ray-trace migration is very sensitive to the geometry of the carrier surface, flow being controlled by topographic features of only a few metres in height. Modelled hydrocarbon masses are balanced between time steps whilst water is not, being assumed to flow into and out of the model area. Similarly, carrier bedrock masses are conserved but inter-surface rock volumes are not considered.

Although these are major simplifications to the rock and hydrocarbon system in nature, they can be justified in many geological settings and such models are able to capture the key aspects of the petroleum system. The flexibility of ray-trace modelling in terms of

material balance is the feature that enables a consistent integration between model parameters derived from structural models and migration simulation. This approach thus offers a working solution to investigate the effects and sensitivities of structural restoration in basin geohistories on hydrocarbon migration and accumulation.

INTEGRATION METHODS

The hydrocarbon migration simulator uses an orthogonal grid data structure. The workflow can be tailored to the modeling problem. This has the advantage that the modeling process can be accessed at a number of stages and parts of the workflow or particular data inputs to be replaced by external software and their outputs. For example, independently derived quantitative palaeobathymetric data can be input to the model (Kjennerud et al, 2000, Kjennerud & Sylta 2001).

In this study we have developed a methodology to integrate structural restorations into the horizon-based ray-trace hydrocarbon migration simulator. The effect of structural restoration on hydrocarbon migration and accumulation patterns is illustrated by two investigations. A comparison of backstripping methods is illustrated with an example of a regional basin whilst a fault restoration is shown for a prospect evaluation-scale area. Both examples are for basins in extensional rift settings. Structural restorations generated independently of the basin simulator have been used as input for migration modelling in the ray-trace basin simulator in both cases. The most important aim of this paper is to demonstrate that the integration of these methods can indeed be accomplished.

Regional backstripping

A 3D flexural isostatic basin model (Norris and Kusznir, 1993) was used to structurally restore the thermal subsidence post-rift sequence of a regional basin area. Details of the flexural modeling technique are given in Roberts *et al.* (1993) and Kusznir *et al.* (1995) and are only briefly summarized here. The flexural model incorporates the strength of the lithosphere and its response to gravity. Output from the model is a sequence back through time of palinspastic surfaces, isostatically balanced, with progressively more of the stratigraphic units removed. The data structure in the structural software is based upon orthogonal grids, enabling direct integration of restored horizon output data with the basin simulator. Horizon geometry and rock property grids, e.g. depth, porosity, temperature, were exported from the structural package. These grids were then imported into the ray-trace simulator and additional model parameters, such as source rock properties, seal effectiveness and carrier bed permeabilities, were calculated and used as model input.

Fault restoration

Structural restoration of both faulting and folding was undertaken of a prospect-scale area to restore the complex geometries and deformation relevant to detailed prospect evaluation. Following backstripping of the overburdon, the faulted carrier horizon was restored in several steps by inclined shear and fault block translation to produce a 'jigsaw fit' matched surface. Horizon and fault surfaces are represented in the structural model as irregular triangulated meshes, able to handle complex geometrical changes and record surface topology information, the latter being important for changes in the position of fault tips.

The locations of data nodes in the surface triangular meshes are tracked between restoration time steps. For use in the basin simulator, these surface mesh nodes need to be translated back to a regular, orthogonal grid and modeled parameters interpolated to the restored grid node positions. The results of each simulation time step were linked using node tracking between each time step. The associated parameter fields, i.e. temperature, fluid saturations, were also mapped and interpolated onto the surface grids. The node-tracking procedure allows the simulator to dynamically move solid mass (source rocks and carriers) and hydrocarbons (oil and gas) laterally from one time step to another according to the translation vectors that the structural reconstruction describes. Node-tracking thus relies on a movement matrix in the three space dimensions created from the restored horizon surfaces. Basin geohistories can be improved by interpolating time steps, in addition to those of the structural restoration, using the node tracking information.

Results of Migration Studies

Both models are actual field study datasets, derived from seismic interpretation surfaces. However, they were chosen for their qualities as prototype datasets for software design and not geological realism in this study, i.e their range of structural features and interpretation quality (artefacts) - data gaps, irregular boundaries, and fault interpretation, were less than perfect. The structural modelling is geologically correct. However, in the fault model the hydrocarbon system was forced to produce optimum visual results (the thermal gradient was modified for maximum hydrocarbon generation/flow at the time of fault growth. This approach is valid here because the aim is to demonstrate the feasibility of the methodology, not to show that it can reproduce the geological history of any particular area.

The simulation results presented here have been chosen to highlight the migration patterns across the whole basin in both studies, reflecting only the influence of differences in the horizon geometry due to restoration. The hydrocarbon systems have been artificially forced by increasing temperature gradients to produce the best visual results and are thus not calibrated to the basin geology. Both models use laterally continuous carrier/reservoir horizons and constant parameter values (source rock, heat flow and seal) for both the structural restorations and the basin simulations. Faults in both studies are considered as being open to lateral fluid flow in areas of horizon juxtaposition.

Geologically realistic models with temporally and laterally varying parameters should be expected to show more complex interactions between hydrocarbon generation, volumes and flow patterns with the horizon geometry.

Regional backstripping

Model results reported here are for the same horizon at a single time step, comparing the migration patterns from different restorations. The regional basin used in the flexural backstripping covers an area of the Moray Firth, UKCS, of approximately 250 by 150km. The basin comprises a Jurassic rift system with several sub-basins overlain a Tertiary thermal subsidence sequence. The basin is split into two sub-basins, north and south,

separated by a central ridge, and has a regional dip to the east. Uplift to the west of the basin resulted in erosion of much of the post-rift sequence. A known hydrocarbon fairway traverses the basin from east to west through the basal post-rift sequence. For this restoration, eight horizons were interpreted over the whole basin and average rock properties derived for the study sequence. The horizon data were generated by merging detailed 2D and 3D seismic mapping with digitized regional published data. Post-rift thermal subsidence sediment sequences were backstripped using the flexural isostatic method (Roberts et al., 1993; Nadin and Kusnir, 1998). As a condition of the 3D flexural backstripping areas of horizon erosion in the basin were infilled with values that result in zero thickness of the missing horizons in eroded areas.

Hydrocarbons were generated from the syn-rift sequences in different sub-basins at varying times, and migrated vertically into the base of the post-rift sequence. Differences in hydrocarbon generation in the different sub-basins resulted in different compositions and volumes of hydrocarbons being supplied along the post-rift carrier system. Comparison is made between the modelled hydrocarbon migration and accumulation patterns using the standard backstripped burial history and the flexurally backstripped geohistory. The effect of incorporating an erosion event is also illustrated. Analysis of the migration patterns and distances is used to identify individual play fairways, changes in hydrocarbon composition along fairways and confluences of migration pathways along fairways.

Two backstripped models of an east-west cross-section through the center of the basin are illustrated by Figure 6 The standard backstripped model (Figure 6a) shows Horizon A restored to a geometric template with a horizontal datum at sea level. The flexurally restored model for the same time step (Figure 6b) incorporates the modelled palaeobathymetry. Horizon dip maps for Horizon B in the standard and flexural backstripped models are shown in Figure 7a&b. In the horizon dip maps, faults are delineated by dips of greater than ca. 5° (red zones). At the basin scale, away from large sub-basin defining faults, horizon relief is uniformly low. Large areas of low horizon dip are present, with dips usually less than 4° and commonly less than 2°. The difference in horizon dip between the two restoration models is equivalent to the dip of the seabed modelled by the flexural restoration (Figure 7c).

Structural closures in the horizon are created by faulting and differential compaction of underlying sediments. Closure is strongly influenced by horizon tilting through time, a consequence of either regional basin subsidence or local faulting. Such tilting may be amplified by the flexural response of the basin upon loading, regionally by prograding sediment wedges or locally by differential sedimentation across syn-sedimentary faults. The flexural tilting effects are reflected in the predicted palaeobathymetry (Figure 7c). Footwall uplift to large faults is clearly defined in the seabed topography. These effects are incorporated into the basin model by including the palaeobathymetry into the basin burial history to generate a full geohistory. Depth maps for Horizon B restored to the time of deposition of Horizon A, are shown in Figure 8a & b, for the standard and flexural backstripped models respectively.

Thermal subsidence induced a regional tilt to the east across the basin, creating accommodation space which was partially infilled by subsequent sediments. The regional

tilt is recorded in two components by a combination of the sediment thickness profile and palaeobathymetry. The standard backstripped model, restored to a horizontal datum recreates only the dip component recorded by the sediment thickness profile. The restored horizon dip underestimates the true dip, equivalent to the palaeobathymetric profile. The flexural model also incorporates local fault footwall uplift, creating or amplifying footwall closure for accumulations, and hangingwall subsidence, which increase the local horizon dips compared with the standard backstripped model.

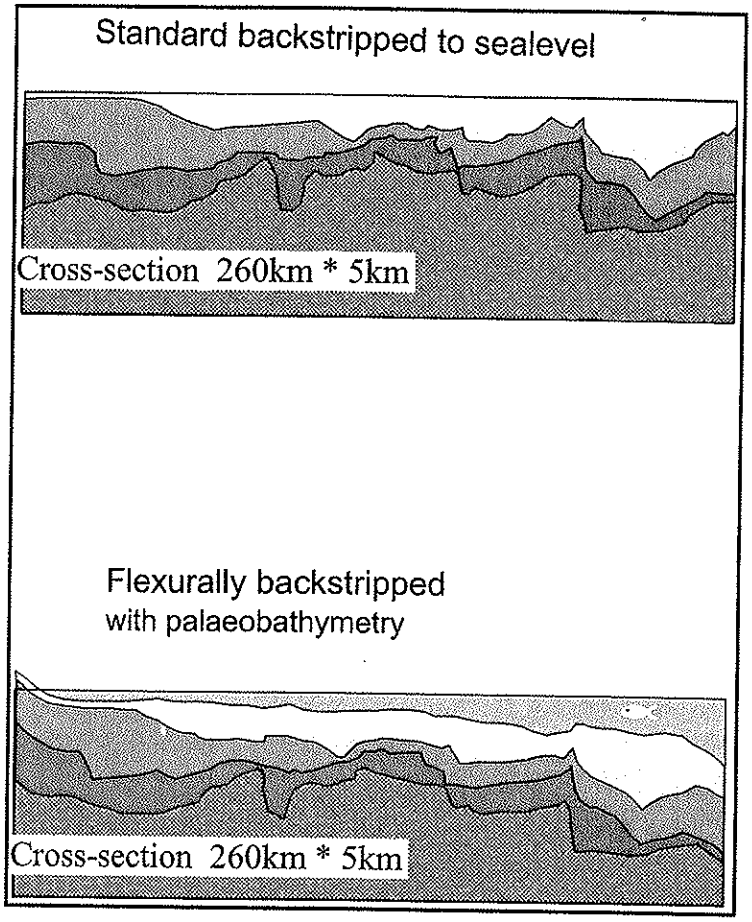

Figure 6: Restored cross-sections across basin

- *Restored to the time of deposition of Horizon A, by standard backstripping, restoring to a horizontal datum at sea-level.*
- *Restored to the time of deposition of Horizon A, by flexural backstripping, incorporating predicted palaeobathymetry.*

Differences in horizon structure between the two models are highlighted by a comparison of their drainage and trap areas, and fill-spill pathways between traps (Figure 9). Some

drainage areas merge into elongate catchments, parallel to the tilting direction and develop new fill-spill pathways, reflecting regional subsidence. Linkage occurs through a combination of the different restorations resulting in different structural configurations, and horizon rotation of similar structures converting drainage boundaries into fill-spill pathways and vice versa. Differences in drainage areas between the models indicate that the hydrocarbon volumes available to charge given prospects will also change.

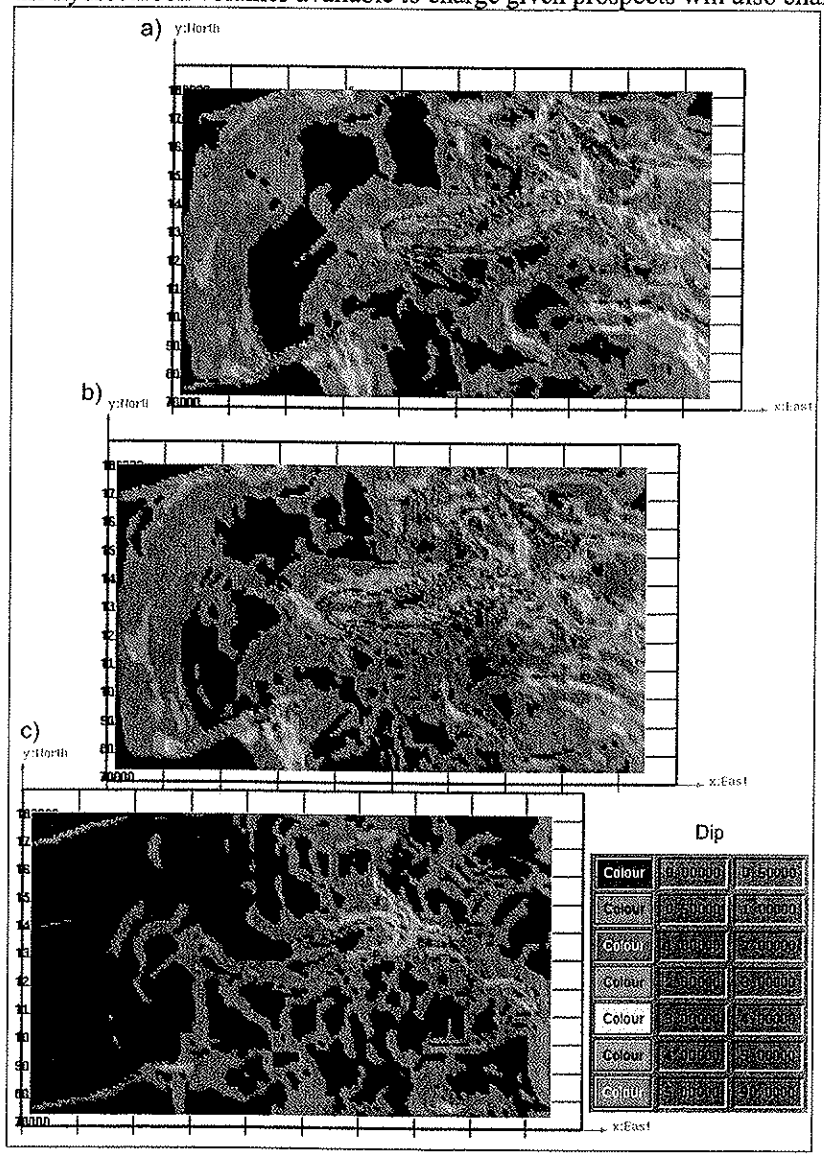

Figure 7: Palaeo horizon dip maps
(a) Horizon B restored to the time of deposition of Horizon A, by flexural backstripping.
(b) Horizon B restored to the time of deposition of Horizon A, by standard backstripping
(c) Seabed (Horizon A) at the time of deposition of Horizon A

standard

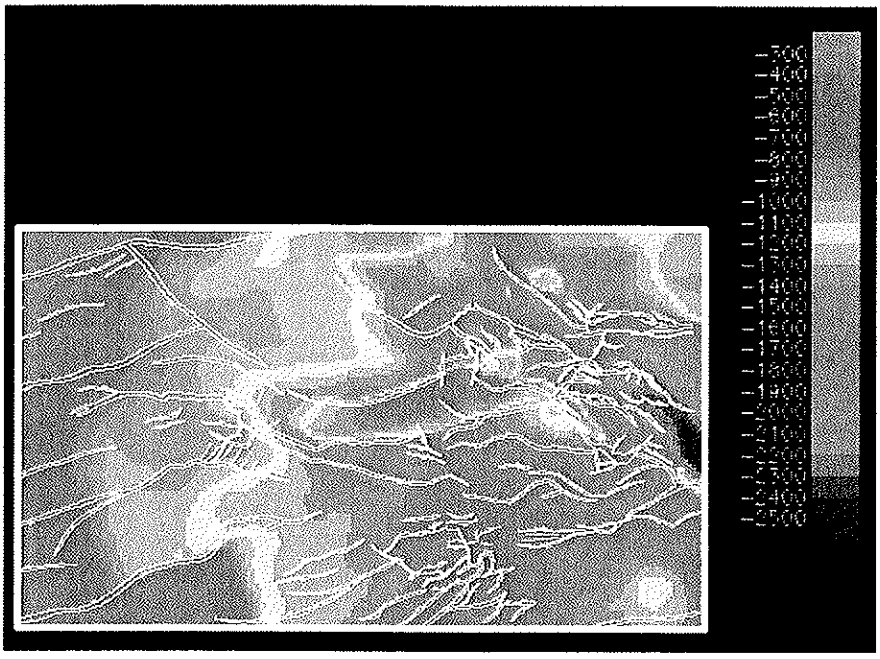

Figure 8: Palaeo horizon depth maps
(a) Horizon B restored to the time of deposition of Horizon A, by standard backstripping
(b) Horizon B restored to the time of deposition of Horizon A, by flexural backstripping.

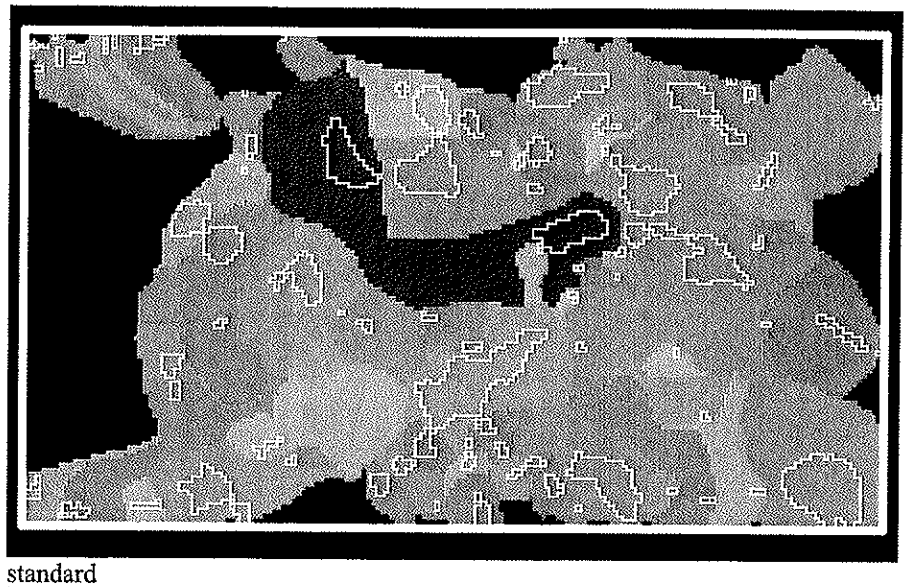

standard

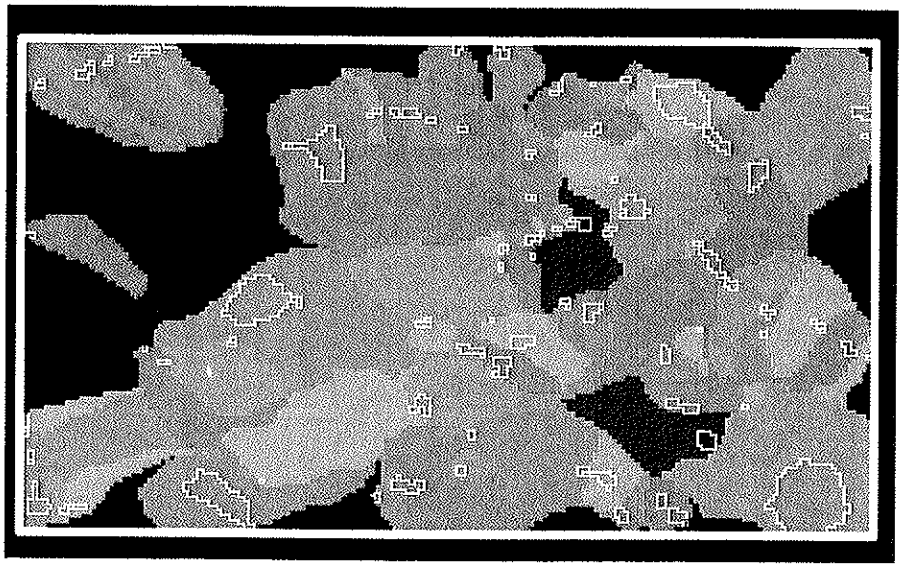

Figure 9: Palaeo drainage area maps. Drainage areas are coloured, and their traps are outlined by white lines.
(a) Horizon B restored to the time of deposition of Horizon A, by standard backstripping
(b) Horizon B restored to the time of deposition of Horizon A, by flexural backstripping.

The effects of these differences in horizon structure are reflected in the modelled migration and accumulation patterns (Figure 10). The figure shows modelled oil filled traps (blue), together with rates of oil flow. Red colours show areas of large flow, and focused migration resulting from spill out of traps (A in Figure 10b) or flow along sharp ridges in the carrier (B in Figure 10b) are typically modelled with only a single grid node

width. As the depth of burial, and thus temperature history, is identical in both models, the timing and volume of hydrocarbon generation is also the same. Changes in the migration and accumulation patterns occur where the horizon geometry and or its relationship to the volume of hydrocarbons has changed. At a given location, horizon dips may change orientation or even reverse direction, redirecting flow (Compare A in Figure 10a and b). Alternatively the shape and size of horizon closures may change (compare C in Figure 10a and b), resulting in trap volume differences, leading to structures not filling, or filling and spilling. Additionally, structures may or may not be present (Compare B in Figure 10a and b) or destroyed through time in either model.

standard

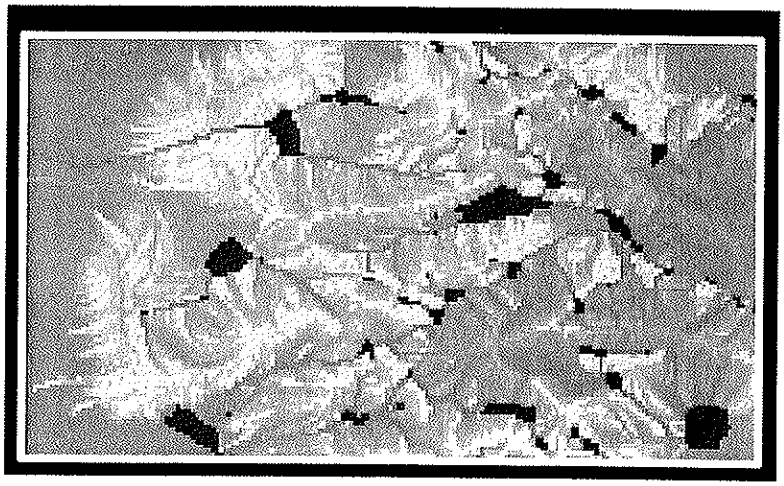

Figure 10: Palaeo hydrocarbon migration maps. Migration fluid flow rates are indicated by the colour spectrum, low flow rates – green, through yellow – orange,to high flow rates – red. Oil accumulations are shown in blue and gas accumulations in pink.
(a) Horizon B restored to the time of deposition of Horizon A, by standard backstripping
(b) Horizon B restored to the time of deposition of Horizon A, by flexural backstripping.

Horizon A is an unconformity surface in the west of the basin with an interpreted linear erosion pattern of 1.5km in the west decreasing to 0km in the east. The effect of incorporating this erosion into the flexural isostatic restored basin model is illustrated in Figure 11. Erosion has a similar effect to that of the regional trend of the palaeobathymetry, inducing a regional tilt, this time to the west, that results in horizon closure and drainage area changes (Figure 11a&b). Additionally, the erosion has changed the depth of burial of Horizon B, resulting in an increase in carrier bed dips, temperature and hydrocarbon generation in the west, indicated by the resulting high flow rates (Figure 11c).

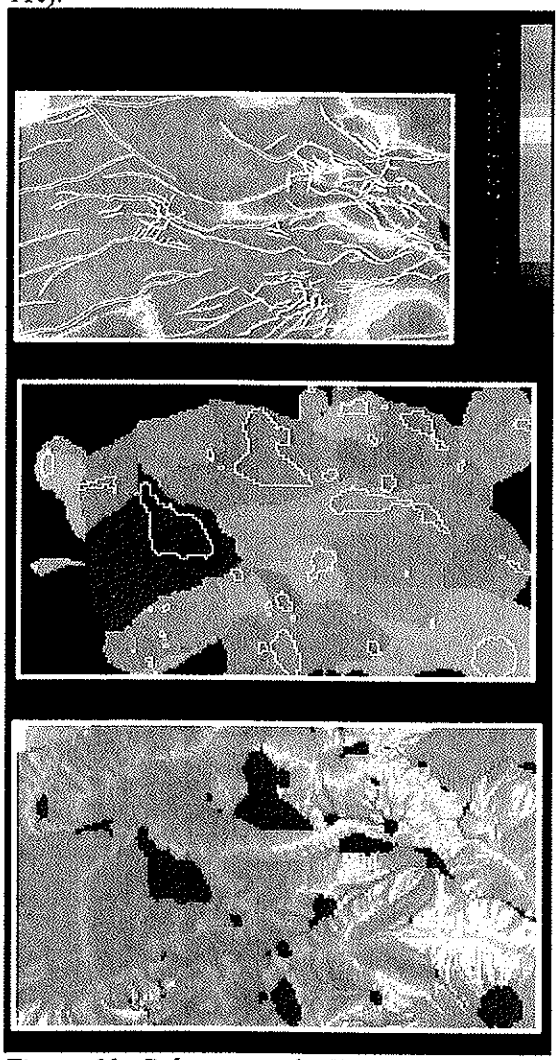

Figure 11: Palaeo maps for Horizon B at the time of deposition of Horizon A, including an erosion event restored by flexural isostatic backstripping
(a) Palaeo depth map (b) Palaeo drainage are map
(c) Palaeo migration map (see fig 10 for legend).

Fault restoration

Model results reported compare migration simulations for successive time steps in the same surface. Structural restoration of faulting and folding was undertaken of a prospect-scale area in an extensional basin of the Central North Sea, UKCS, covering an area of approximately 30 by 40km using a 3D structural modelling package (Gibbs and Kape, 1999). The area comprises a series of fault block terraces, culminating in a central, broadly linear, crestal ridge, adjacent to a major hydrocarbon source kitchen to the east and a shallower source basin to the west (Figure 12a). A carrier system was mapped as a horizon across the study area. The model was sequentially decompacted and backstripped from the Present Day sea bed datum to the faulted reservoir horizon. The decompaction used was based on the Sclater and Christie (1980) method of exponential decrease in porosity with increasing depth. Blanket values were used for surface porosity (normalised to 1) of 0.56 and depth coefficient (porosity decay rate with depth) of 0.36 per km. Vertical shear unfolding was then used to flatten the decompacted horizon onto a zero elevation datum. The reservoir horizon was exported after each decompaction calculation and structural unfolding. The faulted reservoir horizon was kinematically restored in four time steps using an inclined shear algorithm. The algorithm geometrically models the deformation in the hangingwall resulting from the fault geometry, shear orientation and displacement amount and direction. The inclined shear algorithm is applicable to extensional tectonic regimes which exhibit non-planar normal faults. Variable displacement along strike of the fault was accounted for in the restoration workflow. When throw reduces to zero at restored fault tip zones, horizon connectivity across faults produces new cross-fault flow pathways. Incorporating the fault restoration results in significant changes in the horizon geometry compared to a burial restoration without faulting.

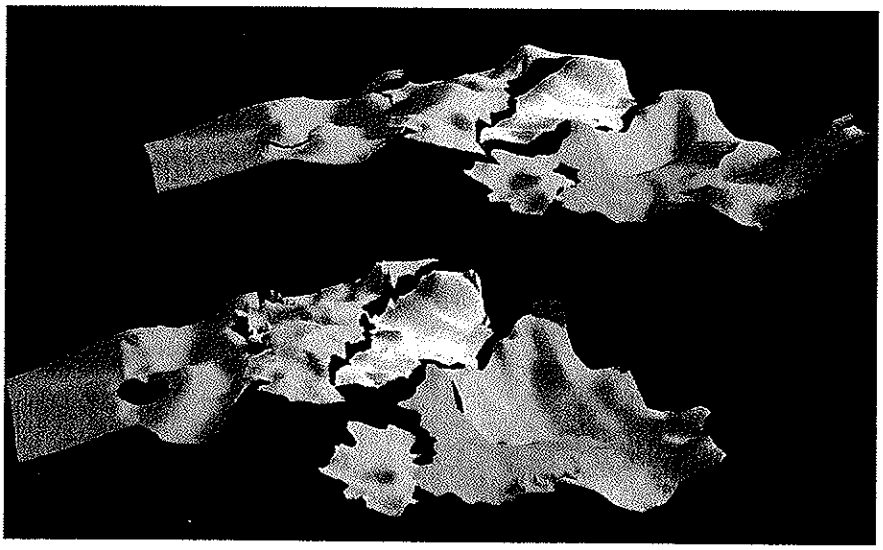

Figure 12: Prospect scale model
(a) Partially restored model
(b) Present Day geometries

In the migration simulation results, the effect of fault restoration on simulated migration patterns is illustrated by hydrocarbon flow rate maps for two sequential time steps (Figure 13). Hydrocarbon charging is critically dependant upon the potential migration routes across the fault terraces and the faults themselves. Generally, hydrocarbon generation from the basin areas on either side of the ridge charges prospects along the central ridge. In the first time step, (Figure 13a) faulting along the eastern margin of the ridge and terraces is well established. However, the fault defining the western edge of the ridge has only just formed and has a small, discontinuous throw along its strike. The eastern basin is overmature, with east-west migration along the basin margins and gas accumulations in the basin centre. Gas generated from the eastern basin in earlier time steps has migrated to charge a large structure on the central ridge in the south. The western basin is just beginning to generate small volumes of oil, which are migrating up-dip onto the central ridge.

In the second time step, the western fault has developed in the south into a major structure with significant and continuous throw, but has not yet developed in the north. Significant volumes of oil from the west basin now migrate onto the ridge in the north of the area. The structural high along, and in the immediate footwall to, the western fault, channels migration along the ridge to south. This oil then charges new structures along the ridge. Modification to the large early gas accumulation has resulted in this gas being displaced. Further burial of the basin has resulting in hydrocarbon generation progressing onto the central high in the north and south. Low volumes of local sourced early mature oil are charging local structures in the north and contributing to the more mature oil accumulations in the south. Restoration has caused the destruction of the main trap and gas accumulation in the eastern basin. The 'spilled' gas re-migrates along north-south pathways.

Implications of restoration methodology for migration

Hydrocarbon migration and accumulation

Hydrocarbon generation is largely controlled by the basin burial history and associated temperature evolution of the sediments. The interpretation of periods of basin evolution recorded by missing stratigraphic section, as erosion, deposition and erosion or non-deposition, strongly affects the burial history. Major periods of erosion reflect tectonic events which may have associated heat flow changes which must be considered (Schegg & Leu, 1998). Incorporating laterally variable erosion will alter the depth and geometry of a horizon, affecting both the generation (Archard *et al.,* 1998) and migration of hydrocarbons.

Modelled thermal and porosity properties of sediments and their thickness (depth) are related to the compaction porosity-depth algorithm used (Ungerer *et al.*, 1990; Giles *et al.,* 1998). Consequently, the sediment temperature profile and fluid flow properties of a model are influenced by this relationship. These property differences are amplified by modelling differences in 1D, 2D and 3D, where simulated pressure effects the porosity-depth relationship (Giles *et al.*, 1999; Throndsen & Wangen, 1998). The choice of porosity-depth function for a model can, therefore, have a significant effect upon the thermal and hydrocarbon generation results. However, providing the same burial history

and compaction algorithms are used in the models, the thermal and fluid flow properties of the sediments are independent of structural restoration methodology.

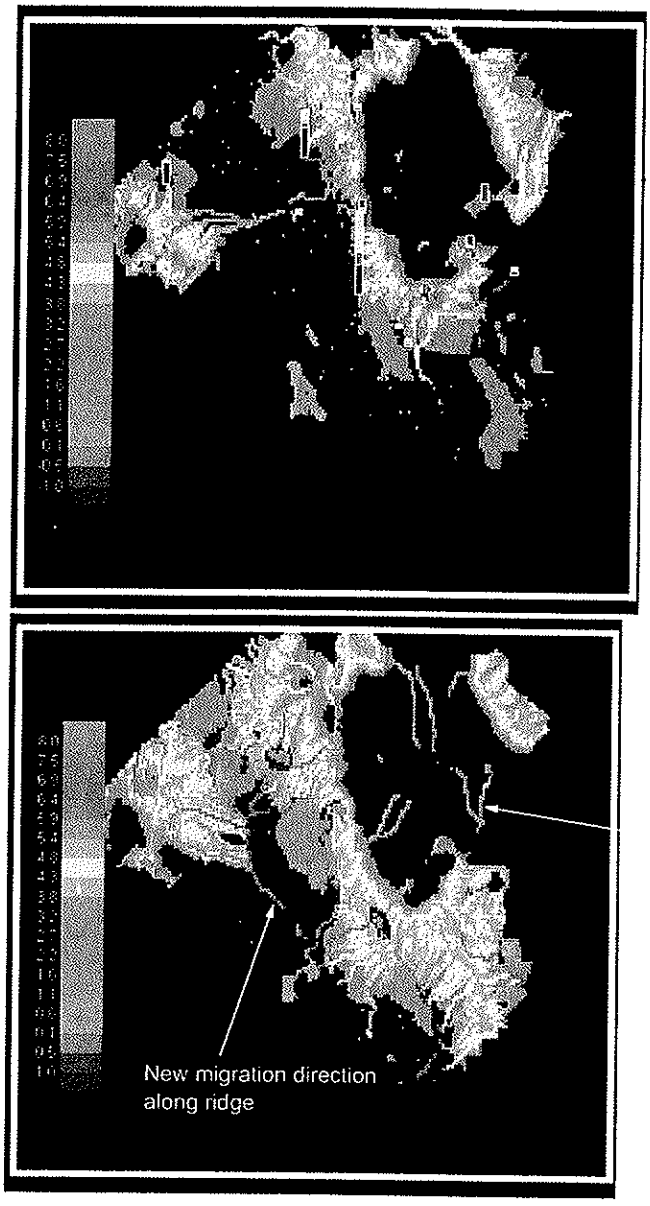

a) Time step 1

b)Time step 2

Figure 13: Hydrocarbon migration simulation results for two time steps from the restoration.

Regional horizon dips across basins are low, typically only a few degrees. Small differences in the restoration of the Present-Day basin horizon geometries can result in significant changes to the horizon palaeogeometries, and thus upon hydrocarbon migration patterns. Differences in restoration can occur either through initial errors in the interpretation or parameter changes in the restoration model. Geometry differences are most likely in areas where layer thicknesses change rapidly, altering the compaction pattern. In standard backstripping the sediment sequence above the horizon of interest is the most important, as decompaction is tied to the geometric template with the basement being a free boundary. In mechanical backstripping the sequence below the horizon of interest is most important as decompaction is tied to the basement with the seabed being a free boundary. Sensitivities of the horizon geometry to restoration model parameters, such as compaction are probably high, implying a high risk to migration patterns in areas of low dip and high stratigraphic compexity.

Differences in modelled horizon palaeogeometries for the standard and flexural backstripped methods reflect the incorporation of the predicted palaeobathymetry into the flexurally restored model. At the basin scale, the main structural features of the basin are the same in both restored models. However, shape, size and amplitude details of the structures do change in response to the method of restoration used. Structural restoration affects trap histories, their size, shape and volume, and their creation and destruction, changing the timing relationship between traps and hydrocarbon generation, migration and remigration. Drainage areas also change between restored models, affecting hydrocarbon volumes available to given traps. At the prospect scale, migration pathways respond to the development of faults, the propagation of fault tips and horizon deformation associated with the increase of fault throw.

In addition to migration pathways, migration rates, and commonly distances, are related to burial rate and carrier-bed dip. Trapped fluid phase and GOR distribution along migration fairways are an integrated function of the timing of hydrocarbon generation and migration rate. Model results predict that late generated hydrocarbons may mix with earlier trapped fluids or by-pass accumulations, migrating further updip. Moreover, trap fluid phase changes through time as a function of both charging history and changing PVT conditions, as a consequence of basin subsidence and uplift (Heum et al., 1996). Significant phase changes can result from small but sudden burial history events, not recorded with low resolution stratigraphic burial history input (Cowan et al., 1999).

Geohistory data in basin models

A major limitation to basin modelling is the detail of the geohistory/burial history interpreted from the available data. In many cases the geohistory available for a basin is limited in its stratigraphical resolution, particularly in frontier exploration areas. Structural restoration for input into basin simulators requires the structural evolution to be dated. The timing of structural events are recorded by stratigraphic relationships within the basin fill. A restoration therefore requires a detailed stratigraphic interpretation of the basin fill, defining palaeobathymetry and tectonic interactions to date structures and quantify uplift and erosion events. Interpretation below the base of the hydrocarbon system (source/carrier) should be considered as restored horizon structure can be significantly influenced by decompaction of the underlying sequence.

Uncertainty and risk

3D modelling provides more accurate hydrocarbon migration simulation results than 2D modelling and thus better predictions of accumulations. Volumetric estimates can only be obtained with 3D models. However, the additional lateral dimension adds a further source of error in the model. Restorations become more uncertain back in time and spatial and temporal resolution usually decreases. If restorations are undertaken by geometrical or mechanical structural models then these also introduce an additional set of parameters and thus uncertainties. Ray-trace simulation of hydrocarbons is very sensitive to the topography and dip of a carrier surface. Hydrocarbon accumulation and particularly migration can therefore be highly sensitive to small changes or errors in the model input data (i.e. depth conversion or mispicks) or restoration model parameters. The accuracy of a restoration and model artifacts of a restoration methodology, which are not important from a structural point, thus become very significant for fluid flow. This effect is much less important in cellular models which have more dispersed migration triggered by cell saturation threshholds. These uncertainties and sensitivities have yet to be quantified, or even fully qualified in order to assess the related risks to the model predictions.

Modelling procedures

Undertaking a structural restoration of a basin and the interpretation of a suitable database is resource intensive. The level of structural restoration undertaken, and resulting model accuracy, therefore, needs to be weighed against the effect of uncertainty and risk associated with the basin geohistory on model hydrocarbon predictions. This question is largely dependent upon issues including but not limited to; the exploration problem to be resolved, the level of detail in the basin interpretation and how well a geohistory can be constrained, the scale of the structural features within the basin, the resolution of the input carrier surfaces, the scale of investigation, and the scale of the area to be modelled.

Future structural development

Modelling techniques are being developed to address handling and restoration of many of the structures and issues discussed, including basin formation, tectonics, faulting and salt tectonics (Mello and Henderson, 1997; Wei & Lerche, 1988; Cathles *et al.*, 1999). Assigning dynamic fluid flow properties to faults from seal analysis will improve migration pathway prediction (Sylta, et al., 1999). New techniques in gridding are improving the handling of faults zones (Cathles, *et al.*, 1999), and manipulation of separate fault blocks (Mello & Cavalcanti, 1999; Schneider et al., 1999). Developments are also being made in basin models capable of modelling overthrust terranes, involving the lateral transfer of mass and associated heat and fluid transport (Schneider *et al.*, 1999).

Integrated 'Earth models' will incorporate mechanical process-driven (rather than existing geometrical) numerical techniques, modelling both crustal and internal basin scale tectonic processes and structures (Cathles *et al.*, 1999; Mello & Cavalcanti, 1999; Ortoleva *et al.*, 1999). Modelling of 3D rock strain and its interaction with an applied stress field is a potential tool for incorporating fracture distribution and their properties into models for fluid flow prediction (Larson *et al.*, 1993; Gibbs & Kape, 1999; Ortoleva *et al.*, 1999). Mechanical modelling requires mass balance to be maintained for complex geometries and deformation. Calling for advanced model data structures such as, non-

orthogonal, non-regular meshes (Mello & Cavalcanti, 1999), and even non-grid methods such as flexural and particle flow. Advanced gridding solutions will also open up the modelling of overthrust structures. The long term aim is to see geohistories incorporating structural restoration embedded in 3D volume basin modelling.

CONCLUSIONS

The geohistory of a basin with its evolving horizon and fault geometries is a critical input to basin models for hydrocarbon migration simulation. Fluid conduits, such as sand rich carriers and faults, form evolving 3D networks through a basin and define potential hydrocarbon migration pathways. Restoration of these carriers effects drainage areas, trap closures, migration pathways, accumulation distributions and fill-spill paths between accumulations. It also influences hydrocarbon generation and the properties of trapped fluids under changing PVT conditions. Restorations used in basin simulators need to be full geohistories rather than simple burial histories. Geohistories should include burial history with palaeobathymetries, stratigraphic structuration and faulting with associated horizon deformation.

Restorations from structural models can be integrated with horizon-based ray-trace migration simulators to investigate the effect of restorations upon migration and accumulation predictions. The resulting restoration of basin geometry and evolution can significantly improve basin geohistory compared with that currently obtainable from hydrocarbon migration simulators.

Ray-trace migration simulation is sensitive to small topographic relief of carrier surfaces. The sensitivity of surface topography, and thus migration, to uncertainties in input data, model restoration method and algorithms, and model artifacts has not yet been well defined. There is, therefore, a related risk in the model predictions. Sensitivity tests should be designed and implemented for each restoration study to assess the risks associated with the restoration modelling and implemented geohistory.

Changing migration pathways may critically affect the hydrocarbon potential of key prospects in a basin. Incorporating appropriate quality structural restorations of basin geohistories into basin simulators is thus an important requirement for accurately predicting hydrocarbon accumulations in basin and prospect evaluations.

References

Andrews, I.J. et al., 1990 The Geology of the Moray Firth, United Kingdom Offshore Report, British Geological Survey, HMSO.

Archard, G., J. Stafford, K. Bardwell and M. Bagge, 1998, A review of techniques used to determine geological and thermal history in the Southern North Sea, *in*: Duppenbecker, S.J. and J.E. Iliffe, ed., 1998, Basin modelling: practice and progress. Geological Society of London Special Publication 141, p. 117-136.

Beaumont, C., Keen,, C.E. and Boutilier, R. 1982. On the evolution of rifted continental margins; comparison of models and observations for Nova Scotian margin. Geophys. J. R. Astr. Soc., V. 70, p667-715.

Berg, R. R., 1975, Capillary pressures in stratigraphic traps, AAPG Bulletin, Vol. 59, P. 939-956.

Bond, G.C. and Kominz, M.A. 1984. Construction of tectonic subsidence curves for the early Paleozoic miogeocline, southern Canadian Pocky Mountains: implications for subsidence mechanisms, age of breakup, and crustal thinning. Bull. Geol. Soc. Am., V.95, p155-173.

Burley, S.D., Clarke, S., Dodds, A., Frielingsdorf, J., Huggins, P., Richards, A., Warburton, I.C. and Williams, G.D. 2000 New insights on petroleum migration from the application of 4D basin modeling in oil and gas exploration. Jl Geochem. Exploration, 70, 465-470.

Cathles, L. M., E. L. Colling and A. Erendi, 1999, 3D basin modeling developments with applications from the Gulf of Mexico and offshore Niger Delta, AAPG Hedberg Conference, Multi-Dimensional basin modeling, *Abs.*

Childs, C., Sylta, Ø., Moriya, S., Walsh, J.J., Manzocchi, T., 2002. A method for including the capillary properties of faults in hydrocarbon migration models. NPF, Special publication no 11. p127-140. Elsevier.

Cobbold-Together, P.R. 1979 Removal of finite strain using strain trajectories. Jl Struct. Geol., 1, 67-72

Cowan, G., S. D. Burley, A. N. Hoey, P. Holloway, P. Bermingham, N. Beveridge, M. Hambourg and O. Sylta, 1999, Oil and gas migration in the Sherwood Sandstone of the East Irish Sea Basin, *in* Fleet, A. J. and S. A. Boldy Petroeum Geology of Northwest Europe, Proceedings of the 5th Conference, Geological Society, London, p. 1383-1398.

Dahlberg, E. C., 1982, Applied hydrodynamics in petroleum exploration, Springer-Verlag, New York.

England, W. A., 1994, Secondary migration and accumulation of hydrocarbons, *in* Magoon, L.B. and W. G. Dow, eds, The Petroleum System. AAPG Memoir 60.

Gibbs, A. and S. Kape, 1999, Advances in and the future of 3D structural modeling, AAPG Hedberg Conference, Multi-Dimensional basin modeling, *Abs.*

Giles, M. R., S. L. Indrelid, and D. M. D. James, 1998, Compaction – the great unknown in basin modelling, *in*: Duppenbecker, S. J. and J. E. Iliffe, ed., 1998, Basin modelling: practice and progress, Geological Society of London Special Publication 141, p.15-43.

Giles, M. R., S. L. Indelid, N. J. Kusznir, A. Loopik, J. A. Meijerink, J. McNutt, P. Dijkstra, W. Heidug, J. Toth, M. Willis, K. Rutten, B. Elsinga, P. Huysse, P. Riviere, H. Burgisser and E. Rowley, 1999, Charge and overpressure modelling in

the North Sea: multi-dimensional modelling and uncertainty analysis, *in* Fleet, A. J. and S. A. Boldy Petroeum Geology of Northwest Europe, Proceedings of the 5th Conference, Geological Society, London, p. 1313-1324.

Gratier, J.P., Guillier, B. and Delorme, A. 1991 Restoration and balance of a folded and faulted surface by best fitting of finite elements: principles and applications. Jl Struct. Geol., 13, 111-115

Heum, O. R., A. Dalland and K. K. Meisingset, 1986, Habitat of hydrocarbons at Haltenbanken (PVT-modelling as a predictive tool in hydrocarbon exploration), *in* Spencer, A. M., *et al.*, ed, Habitat of hydrocarbons on the Norwegian continental shelf, Graham and Trotman, London, p. 259-274.

Hindle, A. D., 1997, Petroleum migration pathways and charge concentration: a 3D model, AAPG Bulletin, Vol. 81, p. 1451-1481.

Hooper, E. C. D., 1991, Fluid migration along along growth faults in compacting sediments. J. Petol. Geol., Vol. 14, p. 161-180.

Hubbert, M. K., 1953, Entrapment of petroleum under hydrodynamic conditions. AAPG Bulletin, Vol. 37, p. 1954-2026.

Illfe, J.E. and Dawson, M.R. 1996 Basin modeling history and predictions. In: Glennie, K. and Hurst, A. (eds) AD1995: NW Europes Hydrocarbon Industry. Geol. Soc. Lond., pp 83-105.

Kjennerud, T., Faleide, J.I., Gabrielsen, R.H. Gillmore, G.K. Kyrkjebo, R., Lippard, S.J. and Loseth, H. 2001 Structural reconstruction of Cretaceous-Cenozoic palaeobathymetry in the Northern North Sea. In: Martinsen, O.J. and Dreyer, T. (Eds) Seimentary environment offshore Norway – Palaeozoic to Recent. Norwegian Pet. Soc. Spec. Pub. (NPF) 10, 347-364.

Kjennerud, T. and Sylta, O. 2001. Application of quantitative palaeobathymetry in basin modeling, with reference to the northern North Sea. Petroleum Geoscience, V.7, No. 4, p. 331-342.

Krokstad, W and Sylta, O. 1996 Risk assessment using volumetrics and secondary migration modeling.

Kusznir, N. J., A. M. Roberts and C. Morley, 1995, Forward and reverse modelling of rift basin formation, in Lambaise J., ed., The hydrocarbon habitat of rift basins, Geological Society of London, Special Publication 88, 3-56.

Larson, K. W., D. W Waples, Han Fu, and K. Kodama, 1993, Predicting tectonic fractures and fluid flow through fractures in basin modeling, *in* Dore, A. G. *et al.*, eds, Basin modelling: Advances and applications, Norwegian Petroleum Society (NPF), Special Publication 3, Elsevier, Amsterdam, p. 385-398.

Larter, S. P. Taylor, M. Chen, B. Bowler, P. Ringrose, and I. Horstaad, 1996, Secondary migration - visualising the invisible - what can geochemistry do? *in* Glennie, K. and A. R. Hurst, NW Europes Hydrocarbon Industry, Geological Society of London, p. 137-143.

Mann, U., Hantschel, T. Schaefer, R.G., Kroos, B., Leythaeuser, D., Littke, R. and Sachsenhofer, R.F. 1997. Petroleum migration: mechanisms, pathways, efficiencies and numerical simulations., p403-509. In: Welte, D.H., Horsfield, B. and Baker, D.R. (eds) Petroleum and Basin Evolution. Springer. 535pp.

Mckenzie, D.P. Some remarks on the development of sedimentary basins. Earth Planetry Sci. Letters, 40, 25-32.

Mello, U.T. and Henderson, M.E. 1997. Techniques for including large deformations associated with salt and fault motion in basin modeling. Marine and Petroleum Geology, V.14, p551-564.

Mello, U. T. and P. R. Cavalcanti, 1999. A topologically-based framework for simulating complex geological processes, AAPG Hedberg Conference, Multi-Dimensional basin modeling, *Abs*.

Norris, S. and Kusnir, N.J. 1993. 3D reverse modelling of post rift extensional basins. Terra Nova, 5, 173-174.

Ortoleva, P., A. Park, D. Payne, K. Tuncay and X. Zhan, 1999, Comprehensive 3D RTM modeling:from fractured reservoirs to salt tectonics, AAPG Hedberg Conference, Multi-Dimensional basin modeling, *Abs*.

Roberts, A. M., G. Yielding, N. J. Kusznir, I. Walker and D. Dorn-Lopez, 1993, Mesozoic extension in the North Sea: constraints from flexural backstripping, forward modelling and fault populations, *in* Parker, J. R., ed., on the petroleum geology of NW Europe: proceedings of the 4th conference, Geological Society, London, p. 1123-1136.

Roberts, A. M.,. Kusznir, N.J., Yielding, G., and Styles, P. 1998 2D flexural backstripping of extensional basins: the need for a sideways glance. Pet. Geoscience, 4, 327-338.

Schegg, R. and W. Leu, 1998, Analysis of erosion events and palaeogeothermal gradients in the North Alpine Foreland Basin of Switzerland, *in*: Duppenbecker, S. J. and J. E. Iliffe, ed., 1998, Basin modelling: practice and progress, Geological Society of London Special Publication 141, p. 137-155.

Sclater, J.G. and Christie, P.A.F., 1980, Continental stretching: an explanation of the post-mid-Cretaceous subsidence of the Central North Sea Basin, Journal of Geophysical Research, vol. 85, No. B7, p. 3711-3739.

Schneider, F., H. Devoitine, I. Faile, E. Flauraut, F. Willien and S. Wolf, 1999 A new 2D basin modeling tool for HC potential evaluation in faulted area. Application to the Congo offshore and to the Bolivian sub Andian zone, AAPG Hedberg Conference, Multi-Dimensional basin modeling, *Abs*.

Schneider, F., Potdevin, J.L., Wolf, S. and Faile, I. 1996 Mechanical and chemical compaction model for sedimentary basin simulators. Tectonophysics, 263, 307-317.

Schowalter, T. T., 1979, Mechanics of secondary hydrocarbon migration and entrapment, AAPG Bulletin, Vol. 63, p. 723-760.

Selle, O. M., J.I. Jenson, O. Sylta, T. Anderson, B. Nyland and T. M. Broks, 1993, Experimental verification of low dip, low rate two-phase (secondary) migration by means of y-ray absorption, Geolfluids '93 Conference, U.K., extended abstract, p. 72-75.

Sylta, O.,1991, Modelling of secondary migration and entrapment of a multicomponent hydrocarbon mixture using equation of state and ray-tracing modelling techniques, *in* England, W. A. and A. J. Fleet, eds, Petroleum migration, Geological Society, London, Special Publication 59, p. 111-122.

Sylta, O., 1993, New techniques and their applications in the analysis of secondary migration, *in* Dore, A. G. *et al.*, eds, Basin modelling: Advances and applications, Norwegian Petroleum Society (NPF), Special Publication 3, Elsevier, Amsterdam, p. 385-398.

Sylta, O., H. Borge, C. Childs, J. Walsh, and T. Manzocchi, 1999, On the use of fault seal methodologies in hydrocarbon migration modeling, AAPG Hedberg Conference, Multi-Dimensional basin modeling, *Abs.*

Sylta, Ø., 2002, Quantifying secondary migration efficiencies. Geofluids (2002) 2, 285-298.

Thomas, M. M. and J. A. Clouse, 1995, Scaled physical model of secondary oil migration, AAPG Bulletin, Vol. 79, p. 19-2.

Throndsen, T. and M. Wangen, 1998, A comparison between 1-D, 2-D and 3-D basin simulations of compaction; water flow and temperature evolution, *in*: Duppenbecker, S. J. and J. E. Iliffe, ed., 1998, Basin modelling: practice and progress: Geological Society of London Special Publication 141, p. 109-116.

Turcotte, D.L. and Schubert, G. 1982. Geodynamics: Applications of Continuum Mechanics to Geologica Problems. Wiley, New York, 450pp.

Ungerer P., J. Burrus, B Doligez, P. Y. Chenet and F. Bessis, 1990, Basin evaluation by integrated two-dimensional modeling of heat transfer, fluid flow, hydrocarbon generation, and migration, AAPG Bulletin, Vol. 74,

Van Hinte, J.E. 1978. Geohistory analysis-application of micropalaeontology in exploration geology. Bull. Am. Assoc. Petrol. Geol., V.62, p201-222.

Wangen, M. 1997 Two phase oil migration in compacting sedimentary basins modeled by the finite element method. Int. Jl Num. Analytical Methods in geomechanics, 21, 91-120.

Watts, A.B., Karner, G.D. and Steckler, M.S. 1982. Lithospheric flexure and evolution of sedimentary basins. Phil. Trans. R. Soc. London, A305, p249-281.

Wei, Z. P. and I. Lerche, 1988, Quantitative dynamical geology of the Pinedale Anticline, Wyoming, U.S.A.: An application of a two-dimensional simulation model. Appl. Geochem., Vol. 3, p. 423-440.

Welte, D.H., Hantschel., T., Wygrala, B.P., Weissenburger, K.S. and Carruthers, D. 2000 Aspects of petroleum migration modelling. Jl Geochem. Exploration, 70, 711-714.

Wendebourg. J. 2000 Modelling multicomponent petroleum migration in sedimentary basins. Jl Geochem. Exploration, 70, 651-656.

Williams, G., S. Kane, Buddin, T.S. and Richards, A. 1999, Restoration and balance of complex folded and faulted rock volumes: flexural flattening, jigsaw fitting and decompaction in three dimensions. Tectonophysics, 273, 203-218

Williams, G., S. Kane, A. Richards, A. Dodds and S. Clarke, 1999, 3D structural geology: restoration algorithms for basin modelling, AAPG Hedberg Conference, Multi-Dimensional basin modeling, *Abs.*

Chapters 15, 16, 17, 18, 19, 20, 21, and 22 are not included due to copyright.

CHAPTER 23

23. Conclusions.

Conclusions

This thesis has investigated hydrocarbon migration modelling for use in quantitative prospect risk assessment. Migration process descriptions have been analyzed and applicable modelling techniques have been tested. The effects of overpressures, hydraulic leakage, fault clay-smear sealing, palaeo water-depths and structural restorations have been investigated. The overall conclusion is that the use of migration modelling to perform quantitative prospect risk assessments is feasible. Volumetric estimates of the amounts of oil and gas in undrilled traps can be obtained by using the migration modelling techniques. This conclusion is arrived at through a series of investigations of the different aspects of migration modelling. Models can be confirmed by demonstration of agreement with observation and prediction, but confirmation is inherently partial. Thus, alternative explanations to geologic observations can be put forward and confirmed by other authors. Several case studies have therefore been used to corroborate the experimental and analytical findings.

The overall conclusion is supported by the following:

- Experimental verification of low-dip, low-rate two-phase secondary migration has shown that the process is vertically focused.
- Analytical and numerical analysis suggests that secondary migration of oil and gas will be focused within a thin zone below vertical barriers. The hydrocarbon saturated zone will typically be less than 1m thick.
- Secondary migration saturations and relative permeabilities of most hydrocarbon flow-paths within carrier rocks will be low, while migration velocities will be very high, typically approaching 1000 km/My.
- There are inherent problems in modelling the secondary hydrocarbon migration process using full Darcy flow numerical schemes with constant saturations within each computing node, mostly due to a lack of resolution.
- Vertical capillary leakage out of a trap has been observed by a visual 2D laboratory model. The leakage process is dynamic, with maximum column heights that exceed the column height defined by the cap-rock entry pressures (h_{Pc}), reducing slowly to a snap-off pressure when supply is stopped.
- The measured experimental snap-off pressure was 35% of the cap-rock entry pressure, and cap-rock snap-off pressures above real traps may therefore also be lower than their cap-rock entry pressures (h_{Pc}).
- The efficiency of capillary gas leakage through cap-rocks is low, and dynamic columns may result when gas input to traps exceed gas leakage. When gas supply stops, or is reduced, the reduction in the dynamic column may take millions of years, thus maintaining a rate of gas leakage long after source rocks have stopped expelling hydrocarbons.
- Vertical capillary leakage through cap-rocks can, in general, not be modelled with percolation methods, because the flow-paths within the cap-rocks are not focused and migration occurs at low saturations.
- Fault property descriptions can be combined with a pressure compartment formulation into a method that effectively can simulate single phase fluid flow between compartments using averaged fault transmissibilities. Pressure histories of compartments can then be estimated.

- Estimated pressures in compartments can be combined with effective stress considerations to study the sensitivity of hydraulic leakage with respect to timing of leakage events and the influence upon pressures in neighbouring compartments. The timing of hydraulic leakage will have major impacts on hydrocarbon trapping.
- Secondary migration can be modelled efficiently by a ray-tracing technique where migration losses are calculated as properties of the flow-paths.
- Multicomponent hydrocarbon mixtures can be simulated during secondary migration and trapping. The difference in mixture patterns between traps may be used to estimate migration properties.
- The effects of structural restoration can be accounted for in hydrocarbon migration modelling. Hydrocarbon accumulations may be modelled to be created, moved and/or destroyed through geologic time. The present day pool contents may change as a result of applying these techniques.
- A method of incorporating clay-smear in estimating the hydrocarbon sealing properties of faults has been incorporated into a hydrocarbon secondary migration simulator. The sensitivity of migration and trapping to clay-smear fault sealing can be studied with this approach.
- A method of determining palaeo water-depths through time has been used in the construction of carrier bed burial histories. It is shown that often, the modelled hydrocarbon migration is not influenced to any significant degree by the proper inclusion of palaeo water-depths. For some traps, however, the modelled volumes of trapped oil and gas are severely affected, and the modelled hydrocarbon phases and volumes can be very different. Only migration modelling can elucidate whether this is an important effect at the present time.
- Hydrocarbon migration simulators can be used to estimate the present day volumes of oil and gas in prospects and fields, but only after calibration of the model to observed well data. Calibration may use estimated oil and gas volumes in drilled traps or observed oil and gas columns in drilled wells.
- Case studies have documented that basin scale hydrocarbon migration modelling can be used to understand the petroleum system and to make quantitative predictions about the amounts of oil and gas in undrilled prospects. Simulation results can be used to assess uncertainties of the predictions.
- Monte Carlo simulations can make use of basin scale migration simulations and thereby provide probabilistic estimates of the amounts of oil and gas in prospects.
- A misfit calculation can weigh the results from each simulation run within the Monte Carlo simulation loop by the difference between modelled and measured oil and gas column heights in wells or trapped oil and gas volumes in fields.
- The Monte Carlo simulation results can be used to study not only probabilities of trapped oil and gas as independent probability distributions, but also the combined probability of the two phases, P(oil-volume, gas-volume).
- The oil and gas probability distributions can be constructed from a total of approximately 1000 simulation runs, while a-posteriori probability distributions of the geological (input) variables require 1 to 2 orders of more simulation runs in order to cover the non-linear parameter space.
- The Monte Carlo approach combined with 3D basin scale hydrocarbon migration simulations may later be developed into a continuously improving

description of the geological model: as more and more simulation runs are completed, the probability distributions of the geological variables become better defined because high misfit simulations will have less influence when more low-misfit simulation runs are sampled.

- A screening filter may be constructed using statistical data fitting to e.g. the first 10.000 simulation runs. A (careful) application of such a filter may increase the efficiency of the Monte Carlo simulation technique by discarding input variable combinations that will produce high misfit results.

Hydrocarbon migration and prospect risking is a complex and challenging area of research. We have investigated a number of effects here. There are, however, many more effects that need to be investigated by further research. Each oil and gas migration topic that can be properly described and understood will contribute to an improved understanding of the risks involved in drilling for new prospects. Some, but not all, of the results from further research will reduce the risk of drilling dry wells. Most importantly however, is that all results may contribute to improving the description of the uncertainties, and therefore allow for more realistic decision processes by oil companies. This, in turn, will lead to a higher utilization of existing resources in the exploration for oil and gas, it is hoped.